HEINRICH HEINE
UNIVERSITÄT DÜSSELDORF

Technology
Arts Sciences
TH Köln

Pharmacological characterization of pseudopterosin, azaphilone and teleocidin as novel drug candidates for the treatment of triple negative breast cancer

Inaugural-Dissertation

zur Erlangung des Doktorgrades
der Mathematisch-Naturwissenschaftlichen Fakultät
der Heinrich-Heine-Universität Düsseldorf

vorgelegt von

Julia Sperlich
aus Karlsruhe

Köln, August 2018

aus dem Institut für Pharmakologische Biologie und Biotechnologie
der Heinrich-Heine-Universität Düsseldorf

durchgeführt an der Fakultät für Angewandte Naturwissenschaften,
Arbeitsgruppe „Bio-Pharmazeutische Chemie & Molekulare Pharmakologie“
der Technischen Hochschule Köln

Gedruckt mit der Genehmigung der
Mathematisch-Naturwissenschaftlichen Fakultät der
Heinrich-Heine-Universität Düsseldorf

Referent: Herr Prof. Dr. Peter Proksch

Korreferent: Frau Prof. Dr. Nicole Teusch (Technische Hochschule Köln)

Tag der mündlichen Prüfung: 17.12.2018

Table of Contents

Index of Figures

Index of Tables and Schemes

1 Abstract

Triple negative breast cancer (TNBC) is a breast cancer subtype with a particularly large size, high grade and lymph node involvement that increases the aggressiveness, the invasiveness and migratory potential of TNBC cells. It is a disease with a high unmet medical need and, to date, no available targeted therapy. A successful treatment is often hampered by high proliferation rates and metastasis to other organs.

Nature represents a vast source of highly diverse bioactive compounds, with undiscovered huge potentials in aiding to cure numerous diseases. To uncover the full potential of natural compounds in *in vivo* pharmacological tests, their underlying *in vitro* mechanism of action has to be unraveled first. Therefore, this study aimed to characterize three natural products in their ability to reduce TNBC characteristics: 1) pseudopterosin isolated from *Antillogorgia elisabethae*, 2) azaphilone isolated from *Coniella fragariae* and 3) teleocidin isolated from *Streptomyces mediocidius*.

Pseudopterosin possesses a variety of promising biological activities including anti-inflammatory effects, but its role in TNBC therapy has not been investigated. This study shows that pseudopterosin significantly reduces NF-κB as well as NF-κB target genes, disrupts the inter-cell communication of TNBC and immune cells and inhibits invasion and proliferation of TNBC cells. The mode of action of pseudopterosin was identified: the natural product activated the glucocorticoid receptor alpha (GRα) and its translocation into the nucleus.

Azaphilones are currently studied as anti-cancer agents due to their diverse biological activities. Novel azaphilone derivatives were isolated and characterized regarding NF-κB inhibition and cytotoxicity against TNBC cells. One derivative inhibited NF-κB activation at low micromolar concentrations as well as reduced migration and invasion.

Teleocidin A2 derivatives have been known as tumor-promoting agents due to activation of protein kinase C (PKC). However, new findings also identified anti-cancer abilities. In this study, we characterized novel teleocidin derivatives using SAR analysis. One derivative was identified as a novel lead compound for the specific inhibition of cancer-related protease activated receptor 2 (PAR2)-dependent calcium mobilization without displaying activation of the “off-targets” PKC or PAR1.

In summary, pseudopterosin, azaphilone and teleocidin hold great potential in reducing the aggressive nature of the breast cancer subtype TNBC by disrupting NF-κB signaling, PAR2 signaling, migration, proliferation as well as invasion. Thus, these classes of natural products provide promising characteristics to develop novel, more effective approaches in TNBC therapy.

1 Zusammenfassung

Triple negativer Brustkrebs (TNBC) ist eine Unterart von Brustkrebs mit speziellen Merkmalen wie zum Beispiel besonderer Größe des Tumors, niedrigem Differenzierungsgrad und einer Involvierung der Lymphknoten, was zu erhöhter Invasivität und zu erhöhtem migratorischem Verhalten dieser Tumorart führt. Zielgerichtete Therapien können bei dieser Krankheit nicht angewendet werden, weshalb ein bis heute jedoch nicht abgedeckter, hoher Bedarf an neuen und innovativen Arzneistoffen besteht. Eine erfolgreiche Behandlung wird zusätzlich durch hohe Proliferationsraten und Metastasen in anderen Organen erschwert.

Die Natur bietet eine unerschöpfliche Quelle an diversen bioaktiven Stoffen, mit einem unentdeckten Potential zur Heilung von zahlreichen Krankheiten. Um das volle pharmakologische Potential dieser Naturstoffe für medizinische Anwendungen nutzen zu können, muss zuerst der Wirkungsmechanismus auf molekularer Ebene aufgeklärt werden. Diese Arbeit hat das Ziel drei verschiedene Naturstoffe auf ihre Fähigkeit zur Hemmung von TNBC-Charakteristika hin zu untersuchen: 1) Pseudopterosin isoliert aus *Antillogorgia elisabethae*, 2) Azaphilon aus *Coniella fragariae* und 3) Teleocidin aus *Streptomyces mediocidius*.

Pseudopterosin besitzt einige vielversprechende biologische Aktivitäten, unter anderem anti-inflammatorische Effekte, wobei seine Rolle in TNBC bislang noch nicht untersucht wurde. Diese Arbeit zeigt erstmals, dass Pseudopterosin das NF-κB und seine Zielgene signifikant reduziert, die interzelluläre Kommunikation zwischen Tumor- und Immunzellen unterbricht und die Invasion sowie die Proliferation blockiert. Auch der molekulare Wirkmechanismus von Pseudopterosin konnte in dieser Arbeit aufgeklärt werden: Der Naturstoff aktiviert den Glukokortikoid Rezeptor alpha (GRα) und dessen Translokation in den Nukleus.

Azaphilone werden aufgrund ihrer diversen biologischen Aktivitäten als mögliche Krebsmittel diskutiert. In dieser Arbeit wurden neue und unbekannte Azaphilon-Derivate auf ihre NF-κB-Hemmung sowie auf ihre zytotoxischen Fähigkeiten hin charakterisiert. Ein Derivat zeigt eine signifikante Inhibition von NF-κB im niedrigen mikromolaren Konzentrationsbereich sowie reduziert die Migration und die Invasion bei TNBC Zellen.

Teleocidin-Derivate sind bekannt dafür, das Tumorwachstum aufgrund der Aktivierung der Proteinkinase C (PKC) zu fördern, neue Erkenntnisse haben jedoch auch krebsreduzierende Eigenschaften gezeigt. Unter Verwendung einer SAR-Analyse konnte in dieser Arbeit ein Teleocidin-Derivat als neue Leitstruktur identifiziert werden. Diese Derivat zeigte eine signifikante Reduzierung der Protease aktivierende Rezeptor (PAR2)-abhängige Kalzium-Mobilisierung im nanomolaren Konzentrationsbereich sowie eine Reduktion der Migration und der Invasion von TNBC-Zellen ohne die Aktivierung der “Off-Targets” PKC oder PAR1.

Zusammenfassend kann gesagt werden, dass Pseudopterosin, Azaphilon und Teleocidin großes Potential haben die aggressive Natur des Brustkrebstyps TNBC zu reduzieren und den NF-κB Signalweg, den PAR2 Signalweg, die Migration, die Proliferation sowie die Invasion zu stören. Diese drei Naturstoffklassen besitzen vielversprechende Charakteristika, um neue und effektivere Ansätze in der Therapie gegen TNBC zu entwickeln.

2 Introduction

2.1 Triple Negative Breast Cancer (TNBC)

Breast cancer is the most common malignancy and the most prevalent cancer in woman worldwide, even considering both sexes. In 2012, 1.7 million new cases, representing 25% of all cancer cases in woman, and 0.5 million cancer deaths were attributed to breast cancer [1]. In Europe however, an increase to 27.7% of new breast cancer cases where predicted (proportions divided into major world regions in Chart 2.1-1) [1]. In the U.S., between 2015 and 2017 estimates of new cases of breast cancer increased from 234.000 to 255.000 and estimates of deaths rates increased from 40.730 and 41.000 deaths [2,3].

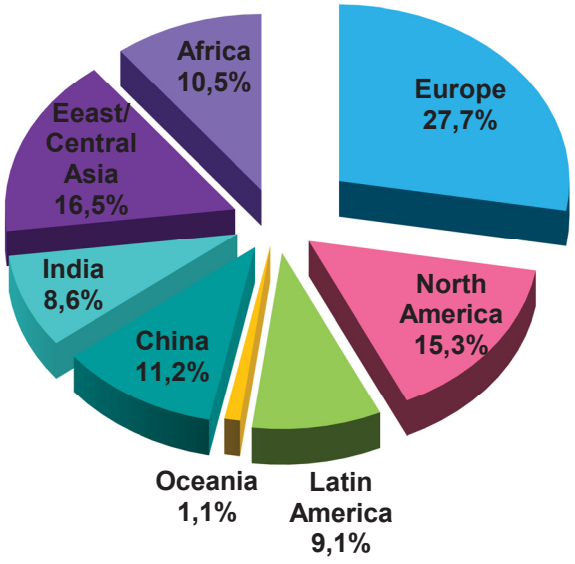

Chart 2.1-1. Estimated global number of new breast cancer cases in 2012 (modified chart from [1]).

Breast cancer is an extremely heterogeneous disease with high variances in hormone receptor expression and high genetic alterations [4]. A thorough assessment of breast cancer histology, using morphological and immunohistochemical analysis, is critical for a correct classification and for effective prognosis and treatment of the malignancy [5]. Limitations in qualitative versus quantitative assessment of specific criteria, however, can cause misclassifications and therefore variations in the response to therapy [6]. Breast tumor cells have unique features that are characteristic to cancer stem cells, including the ability of self-renewal, differentiation and the resistance against chemotherapeutics [7]. Gene expression profiling divides breast cancer into

five molecular subgroups: luminal A/B, HER2-enriched, basal-like, claudin-low and normal-breast-like [8]. Alternatively, a faster assessment in the clinics uses the expression of three hormone receptors: ‘estrogen receptor’ (ER), ‘progesterone receptor’ (PR) and ‘human epidermal growth factor receptor-2’ (HER2). The expression of the hormone receptors differs greatly, whereby 80% of all breast cancer patients express ER^+ [9], in contrast to 15% that are categorized as triple negative as they do not express any of the three receptors [5]. The categorization of breast cancer into these subtypes remains challenging. For instance, 75% of ‘triple negative breast cancers’ (TNBCs) inhere features of the basal-like subtype, but also express genes associated with normal-breast-like tumors [5,6]. TNBC can be further subdivided into inflammatory and non-inflammatory subtypes, with survival rates of 26% compared to 46%, respectively [10]. Furthermore, tumors with mutations in the tumor suppressor gene BRCA1 share characteristics with aggressive features of TNBC [11]. Despite the challenges and problems related to the heterogeneity of breast cancer, the identification of hormone receptor subtypes in breast tumors remains the only existing routine in the clinics [5].

Three different medical treatments are distinguished in TNBC therapy despite the lack of standardized approaches: the classic chemotherapy, consisting of taxanes or platinum-based agents; the neoadjuvant therapy, an administration of a drug before a main chemotherapeutic treatment; or the adjuvant therapy, given in addition of the primary or the initial therapy. For patients with hormone receptor-positive tumors, such as HER2, the anti-HER2 monoclonal antibody trastuzumab increases the success of therapeutic treatment compared to common therapies [12,13]. However, a drawback of endocrine therapies is the lack of efficiency in TNBC patients, leaving cytotoxic chemotherapy as the only treatment option resulting in worse prognosis than in patients with non-TNBC [5,12]. Chemotherapeutics, for example platinum-based compounds or taxanes, target DNA-repair mechanisms or the proliferation of cancer cells [14]. Neoadjuvant chemotherapies show improved prognosis in breast cancer patients compared to classic chemotherapy [14–16]. Combinatorial treatments of known chemotherapeutics benefit even more compared to single-agent therapies: paclitaxel followed by fluorouracil, doxorubicin and cyclophosphamide showed a better therapy outcome compared to neoadjuvant cisplatin therapy [17,18]. Nevertheless, chemotherapeutic treatments have no specific target in breast cancer tumors and thus destroy healthy and malignant cells alike [19]. Moreover, TNBC tumors develop resistances to chemotherapeutic treatments especially in subtypes harboring mutations in p53 [20] or BRCA1 [21–23]. Doxorubicin is often used as a first line treatment, but limitations such as recurrence and high metastasis rates lower the therapeutic success [24]. The average survival rates of breast cancer patients differs greatly dependent on the applied therapy ranging from 30 to 74% in TNBC and from 87 to 93% in non-TNBC patients [13,25]. A dramatic reduction of survival in TNBC patients to only 7-13 month is

observed, which is caused by high visceral metastases [14]. Thus, finding the optimal therapy in TNBC is a difficult task due to the variety of combinatorial treatments reflected by the wide range in clinical outcome and contradicting results in the response of the same agents.

Targeted therapy does not exist for TNBC patients. The heterogeneous nature of TNBC explains the low success of therapeutic treatments and thus the low survival rates. New drugs are required to fulfill the high unmet medical need for novel, innovative therapies to increase the response and survival rates of TNBC patients. This study focuses on the characterization of novel compounds on inhibiting important regulatory signaling pathways which drive cancer progression.

2.2 The Tumor Microenvironment (TME) in Breast Carcinogenesis

To better understand the heterogeneity of breast cancer, the composition of a tumor and the diverse signaling in the 'tumor microenvironment' (TME) needs to be illuminated. Normal breast tissue consists of myoepithelial cells, surrounding luminal epithelial cells, playing an essential role in assembling the basement membrane and in the lactation process resulting from high collagen IV levels [26,27]. Epithelial cells, myoepithelial cells, fibroblasts, adipocytes and immune cells synthesize 'extracellular matrix' (ECM) proteins and make up the breast microenvironment, thereby assembling the mammary gland as a complex organ. Distinct functional groups of the ECM – the basal-lamina, the intra-, the interlobular stroma and the fibrous connective tissue – provide physical support for the tissue architecture. Second messengers, such as growth factors and cytokines, play an important role in the ECM in regulating mammary morphogenesis by activating their respective signaling pathways. ECM can be described as an interconnected network of secreted proteins interacting with cells and starting specific signaling pathways [26,28,29]. However, these components of the breast microenvironment are increasingly recognized as cause of advanced carcinogenesis, invasive behavior, advanced differentiation as well as tumor growth and together with the surrounding blood vessels make up the TME [28,30]. A macrophage-rich TME, for example, is correlated with an increased aggressive behavior of the tumor with high metastatic potential [31].

The TME differs from patient to patient and its establishment is a complex process. At the beginning of tumor emergence, immune cells, for example peripheral blood mononuclear cells (PBMC), release chemotactic factors to infiltrate and destroy tumor cells analogous to the wound-healing process [32]. These immune cells immediately detect malignant cells and interfere with tumor progression, a process referred to as immune surveillance [33]. At the

beginning of progression, tumors can stay for a long time in an ‘angiogenic dormancy’, where the tumor does not grow beyond 1-2 mm^2 due to limit of oxygen and nutrients, thereby staying in a balance of proliferation and apoptosis [34]. 36-56% of breast cancer patients show dormant, non-proliferative tumor cells, which later can be a signal for higher metastasis and a lower survival rate. [34]. At a critical point of tumor progression, the tumor evades immune infiltrates and creates a microenvironment that is favorable for further tumor growth [35]. When proliferation rates rise compared to apoptosis and the tumor grows beyond 2 mm^2 due to vascular infiltration, its state is called ‘angiogenic switch’ (see Scheme 2.3-1) [34]. At this state, the initial inflammatory response of immune cells is followed by an influx of anti-tumor effector cells and afterwards by a downregulation of anti-tumor signals [35]. At a critical size of tumor growth, *de novo* angiogenesis, initiated by increased levels of ‘vascular endothelial growth factor’ (VEGF), is important for the supply of higher amounts of nutrients and oxygen [28,36].

Tumor progression is not only a result of uncontrollably proliferating colonies of cancer cells, but also of a heterogeneous co-evolving microenvironment, where tumor cells and immune cells communicate within the microenvironment in paracrine manner [37]. Macrophage and lymphocyte infiltration into the TME of the breast, for example, characterizes an increased invasive phenotype leading to the intravasation of carcinoma cells into the blood vessel [27,38]. ‘Tumor associated macrophages’ (TAM), originating from blood monocytes [39], are the major inflammatory infiltrating cells in the breast tumor [40]. Different subpopulations of macrophages fulfill distinct functions in the innate immune response dependent on their polarization status known as classical-activated (M1), alternatively activated (M2) and regulatory macrophages (Mregs) [38]. M1 macrophages secrete high levels of pro-inflammatory cytokines [31]. M2 macrophages secrete anti-inflammatory cytokines resulting in immunosuppression and wound-healing, but in the periphery of cancer cells they secrete proteases stimulating pro-oncogenic functions including angiogenesis, matrix remodeling, tumor cell migration and invasion [31]. Mregs arise in response to stress and secrete anti-inflammatory cytokines, but unlike M2 macrophages, do not contribute in producing ECM proteins [41]. Macrophages are able to exert both pro-tumorigenic as well as anti-tumorigenic signals at the same time to either promote tumor cell proliferation, angiogenesis, immunosuppression as well as tissue expansion or inversely to suppress tumor growth, tissue remodeling and prevent differentiation and maturation of malignant cells [31,37,38]. The upregulation of pro-inflammatory signals in the immune response is regulated through activation of the transcription factor ‘nuclear factor kappa-light-chain-enhancer of activated B-cells’ (NF-κB). In the TME however, NF-κB signaling creates a paracrine signaling loop driving an invasive phenotype [35]. The dynamic process of the bidirectional communication of tumor and tumor-associated immune cells and their

interaction with the ECM is necessary for adhesion, survival, proliferation as well as differentiation of the tumor [42].

In summary, the tumor microenvironment plays a critical role in the invasiveness and aggressiveness of breast cancer, consisting of a complex network of different cell types and signals, where the composition of the microenvironment exerts a vast influence on the related therapy.

2.3 Signaling Pathways Responsible for Breast Cancer Progression

2.3.1 NF-κB Signaling

The function of NF-κB signaling is the regulation of innate immunity and anti-inflammatory response. However, constitutive activation of NF-κB can lead to chronic inflammation and subsequent tumor progression. In carcinomas, high NF-κB expression is associated with increased aggressiveness and high metastatic potential. NF-κB regulates markers of 'epithelial-to-mesenchymal transition' (EMT) as well as the self-renewal of breast cancer stem cells and plays an important role specifically in initiation and progression of breast cancer [43–45]. Thus, the NF-κB pathway is the key to better understand inflammatory processes in the breast cancer microenvironment.

NF-κB shows immediate responses to several triggers such as 'pathogen-associated molecular patterns' (PAMPs), pro-inflammatory cytokines including 'tumor necrosis factor alpha' (TNFα), growth factors, hormones, oxidative stress, viral infections or DNA-damaging agents [46–49]. The main function of NF-κB is the recruitment of macrophages to the inflammatory site to eliminate pathogens through increased secretion of its target genes, the cytokines [50]. In mammalian cells, the NF-κB family consists of five functionally conserved members: p50 (also known as c-Rel or NF-κB1), p52 (or NF-κB2), p60 (or RelB) and p65 (also known as RelA or NF-κB3) [51,52]. The transcription of target genes is triggered by different members of the Rel family, but the most common dimer consists of the p50 and p65 subunits (NF-κB subsequently refers to the p65/p50 dimer).

All members are equipped with an N-terminal Rel domain, responsible for DNA binding and dimerization. Transcriptional activation is triggered via the C-terminal domain found in p65, p50 and p60. The Rel homology domain, which contains a 'nuclear localization sequence' (NLS), is responsible for the translocation of NF-κB. Additionally, the Rel domain is necessary to form

homo- and heterodimers of different members of the Rel family to regulate distinct signaling pathways of immunity, inflammation, anti-apoptosis, proliferation and stress responses [53].

In unstimulated cells, NF-κB remains in an inactive form in the cytoplasm due to the interaction with the family members of the 'inhibitors of κB' (IκB). The IκB family consists of four members, IκBα, IκBβ, IκBε, IκBγ, which interact with the NF-κB dimer through five to seven ankyrin repeats [54], thereby preventing its translocation into the nucleus and subsequent gene expression by masking the nuclear localization sequence [55,56]. Ligand binding to the 'Toll-like receptor' (TLR)-family or 'tumor necrosis factor alpha receptor 1' (TNFR1) leads to activation of a complex consisting of three different kinases - IKKα, IKKβ and IKKγ – named the IKK complex [57]. The IKK complex phosphorylates IκBα, which follows polyubiquitination and degradation of IκBα through the 26S proteasome. With the now exposed NLS sequence, the phosphorylated NF-κB is able to translocate into the nucleus and bind to response elements triggering expression of target genes (see NF-κB signaling in Figure 2.3-1) [51].

The transcription factor Toll, first discovered in *Drosophila*, belongs to a highly conserved family of receptors, consisting of 10 different members in humans, each detecting specific PAMPs [58,59]. TLRs are localized either in intracellular compartments such as endosomes (TLR3, 7, 8, and 9) or on the cell surface (TLR1, 2, 4, 5, and 6) [59]. They belong to the type I integral membrane receptors with a horseshoe-shaped extracellular domain responsible for recognizing structural patterns, a transmembrane helix as anchor and an intracellular signaling domain where adaptor proteins can bind and pass on the signal [60]. The TLR receptor family recognizes a large variety of signals. TLR4 for instance binds a divergent set of ligands such as lipopolysaccharide (LPS), paclitaxel, fibronectin or 'heat shock proteins' (HSPs) [59]. This receptor is the only member of the family where ligand-binding leads to conformational changes followed by a homo-dimerization [61]. Additional modulatory proteins such as 'Toll/IL-1 receptor' (TIR), the 'myeloid differentiation primary response gene 88' (MyD88) [62] and the co-receptor protein MD-2 – a glycoprotein important for the direct binding of LPS [63] – form hemophilic interactions with TLR4 and are important in the recognition of different pathogenic particles. Another receptor which triggers NF-κB activation is TNRF1. Its adapter proteins 'TNF receptor-associated protein with a death domain' (TRADD) and 'receptor-interacting protein 1' (RIP1) together with TNFR1 trigger NF-κB signaling after the binding of TNFα [61]. The interplay of every single signal component in this pathway is important in the course of the inflammatory response, because its deregulation leads to constitutive activation of NF-κB and thus cancer progression. Therefore, NF-κB is an essential actor in the link between inflammation as well as initiation of oncogenesis and progression [43].

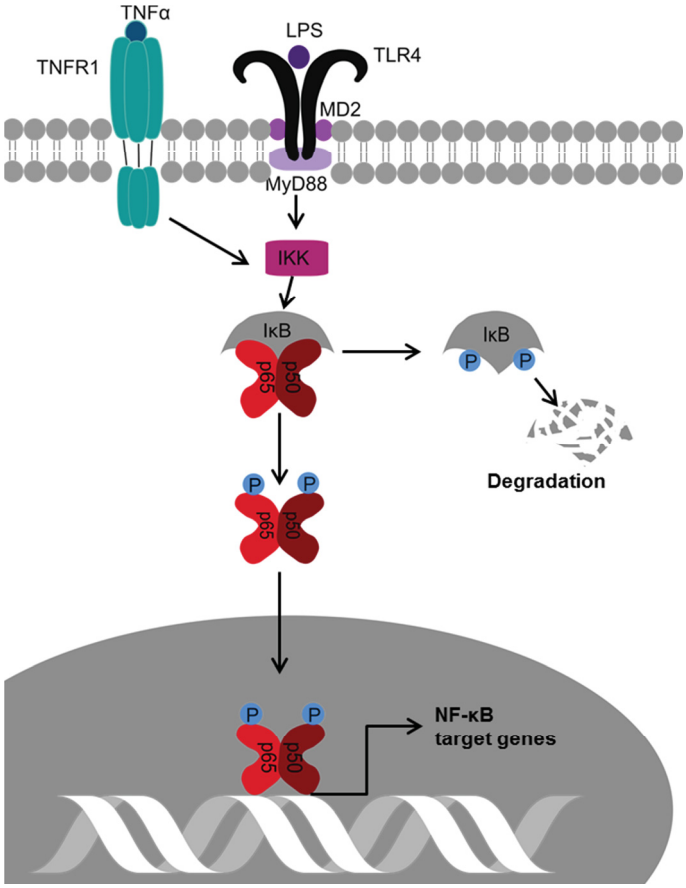

Figure 2.3-1. Stimulation of TNFR1 or TLR4 leads to the translocation of the p65/p50 dimer into the nucleus, activating subsequent target gene expression.

Constitutive activation of NF-κB signaling and subsequent target gene expression is responsible for cancer progression in various tumor types, especially in early stages of transformation of mammary cells [64]. NF-κB has thus been proposed to be a hallmark of cancer progression, as increasing evidence in research correlates the NF-κB signaling with characteristics of cancer: IKKα plays an important role in the self-renewal of tumor-initiating cells [43]; NF-κB plays a key role in tissue organization, disrupting important signals in the microenvironment [65]; NF-κB activation correlates with expansion of cancer stem cell populations [8]; activation of NF-κB is associated with poor prognosis in breast cancer patients [66]; increased NF-κB activity correlates with higher aggressiveness [9], initiation and progression of breast cancer [45]. Other more indirect observations point towards a correlation of breast cancer progression and inhibition of NF-κB or NF-κB signaling components: increased apoptosis in cancer cells as well as reduced tumor formation [67], proliferation, cytokine production [68], metastasis [69], invasiveness and migration [44]. Overexpression of NF-κB signaling in non-malignant breast cancer cells results in an imitation of constitutive activation and thus to the process of EMT by suppressing epithelial markers, simultaneously inducing mesenchymal markers thereby driving metastasis of epithelial cells [70,71].

Chromosomal translocations of the NF-κB2 locus may be the result of NF-κB constitutive activation [72]. However, elevated NF-κB activation and secretion of pro-inflammatory cytokines in the tumor microenvironment may also result from increased mutations of upstream signaling components [73]. In breast cancer, specifically basal-like, TNBC [74], but also $HER2^+$ subtypes harbor activated NF-κB levels [67]. Numerous small molecule inhibitors of NF-κB signaling are published, 130 patents targeting IKK, but only few have advanced into clinical stages due to high toxicity issues [75]. Although two compounds entered phase I clinical trials against dermatitis and solid tumors, none are tested against breast cancer [75]. This underlines the high medical need for targeted therapy against TNBC to fill the gap of potent active drugs with reduced cytotoxicity and increased specificity. Thus, NF-κB and its signaling components might be possible therapeutic targets in TNBC.

In conclusion, increase in the expression of NF-κB target genes in healthy breast tissue drives breast cancer progression and NF-κB overexpression is strongly associated with poor prognosis in TNBC patients.

2.3.1.1 Cytokines Involved in the Bidirectional Communication of the Tumor microenvironment

NF-κB activation in tumor cells and tumor-associated immune cells leads to secretion of a diverse group of cytokines and chemokines – including interleukins, interferons, growth factors and necrosis factors – to communicate with each other, thereby regulating for instance angiogenesis and metastasis [76,77]. At the beginning of tumor assembling, cancer cells secrete cytokines into the surrounding tumor microenvironment to initiate recruitment and reprogramming of immune cells, whereas in later stages, cytokines maintain the inflammatory milieu and support tumor growth and progression [68,78]. In the next sections, four different cytokines are described, each with a distinct role in supporting the growth and the progression of breast cancer.

Interleukin 6 (IL-6) is a monomeric polypeptide of the hematopoietin family containing four alpha helical regions [79]. The binding of IL-6 to its receptor follows a co-precipitation of a glycoprotein and dimerization to initiate downstream activation of kinase activity [80]. IL-6 responds to the presence of pathogens such as viruses and bacteria [81] and activates different immune cells [82]. TAMs, fibroblasts or endothelial cells in turn produce IL-6 to intensify the inflammatory response [79]. However, overproduction of IL-6 is associated with autoimmune diseases [83,84] and increases cell motility [85], invasiveness as well as acquisition of EMT markers in TNBC [85,86]. In breast cancer, elevated IL-6 levels correlated with ER^- hormone status but not with ER^+ [87], the latter showing low proliferation rates [88]. Breast cancer patients with high IL-6 serum levels have reduced responsiveness to chemo-endocrine treatment and a bad prognosis,

especially in cases with higher disease recurrence and visceral metastasis [88–90]. In the clinics, a monoclonal antibody targeting the IL-6 receptor – tocilizumab –is approved to treat patients suffering from rheumatoid arthritis, but not to treat breast cancer, yet [91]. In summary, IL-6 has a primary role as a major mediator of the inflammatory response in the pathophysiology and aggressiveness of breast cancer [92].

Interleukin 8 (IL-8), also known as CXCL-8, is a member of secreted α-chemokines or CXCs, originally found to be secreted by monocytes to attract neutrophils [77]. However, endothelial cells, fibroblasts and cancer cells also secrete IL-8 [93]. IL-8 is strongly associated with tumor progression, as cancer cells with elevated IL-8 levels show a high metastatic potential [94]. In breast carcinoma, epigenetic modifications on the IL-8 gene in undifferentiated cells increase ectopic IL-8 expression and thus the metastatic potential [95]. High expression of IL-8 results in poor prognosis especially in TNBC patients [96]. Interestingly, ER status and IL-8 both are inversely correlated: ER^+ cancer cells show low migration rates as a cause of ERα-dependent downregulation of IL-8 expression. In contrast, IL-8 induces migration in TNBC cells harboring low ERα expression [85]. IL-8 is involved in breast cancer cell invasion and angiogenesis [97], possibly by stimulating VEGF [93] and vimentin [97]. As IL-8 increases the formation of mammospheres and promotes the self-renewal of breast cancer stem cells [98], this cytokine may be a marker for breast cancer and its receptor an indicator for tamoxifen resistance [93]. Combinatorial administration of IL-8 and ‘epidermal growth factor’ (EGF) antibodies significantly reduces metastasis in TNBC xenografts [99]. In conclusion, IL-8 has been described as a major driver of breast cancer progression and targeting IL-8 might be a successful approach in TNBC therapy.

Tumor necrosis factor alpha (TNFα) is released by a set of immune cells, including macrophages, T-, B-cells as well as natural killer cells in response to endotoxin and other bacterial particles, playing a key role in the innate immune response of NF-κB [100]. After the binding of TNFα to its corresponding receptor, TNF receptor 1 (TNFR1), IKK is subsequently activated and initiates NF-κB translocation into the nucleus as described in chapter 2.3.1. In this manner, TNFα is an inducer of other cytokines, including IL-6, IL-8 [101] and MCP-1 [102,103]. The functions of TNFα are either tumor suppressive by inducing necrosis, apoptosis and sensitizing cells to chemotherapy, or tumor supportive by promoting proliferation, angiogenesis, metastasis [104,105] and invasiveness in breast carcinomas [106]. Furthermore, increased TNFα levels in the serum of breast cancer patients has been linked to lymph node metastasis, tumor stage [107] and micropapillary carcinoma [108]. TNFα up-regulates matrix metalloproteinases resulting in increased motility as well as invasion [109]. The development of resistance to chemotherapeutic drugs in ER^+ cells is ascribed to TNFα affecting the expression

of ATP binding-cassette (ABC) transporters [110]. In the clinics, TNFα inhibitors are used against inflammatory diseases [111] and one inhibitor, etanercept, is also tested in phase II clinical trials against breast cancer [112]. However, another TNFα inhibitor, infliximab, is ineffective in breast cancer [113,114]. In summary, TNFα is a regulator of NF-κB signaling, contributing to tumor progression and intensifying the amount of inflammatory signals in the breast cancer microenvironment and thus TNFα inhibitors might be possible agents in TNBC therapy.

'Monocyte chemoattractant protein 1' (MCP-1), also known as CCL2, belongs to the glycosylated C-C chemokine subfamily containing conserved cysteine residues [77]. MCP-1 is the major driver of recruiting TAMs to the tumor as a result of tumor cell and macrophage interaction [115]. The cytokine is produced both by tumor cells and macrophages alike and correlates with an increased number of TAMs in the TME resulting in poor prognosis of patients [31]. 'Cancer-associated fibroblasts' (CAFs), residing in the proximity of cancer cells, also secrete MCP-1 and thus maintain the inflammatory milieu in the TME [103]. Low levels of MCP-1 in non-melanoma cells are sufficient for the accumulation of TAMs to initiate tumor formation, however, high levels of MCP-1 lead to macrophage infiltration into the tumor followed by its destruction [116]. Therefore, it is not surprising that MCP-1 can be detected in the medium of TNBC cells, but also in immortalized healthy breast cells [117]. MCP-1 overexpression in TNBC correlates with invasion into lymph nodes and blood vessels [118], increases metastasis [119], tumor progression and angiogenesis in mammary tumor cells [120], but not proliferation [121]. In summary, MCP-1 is a key molecule in recruiting macrophages to the tumor site and modulating angiogenesis in the TME.

In summary, the interplay of tumor cells with tumor-associated immune cells using the pro-inflammatory cytokines IL-6, IL-8, TNFα and MCP-1, regulated by NF-κB signaling, is important in the process of angiogenic switch, the development of a TME and the progression of tumor growth (see Scheme 2.3-1). Thus, combinatorial inhibition of these pro-inflammatory cytokines may be a new, innovative approach in TNBC therapy.

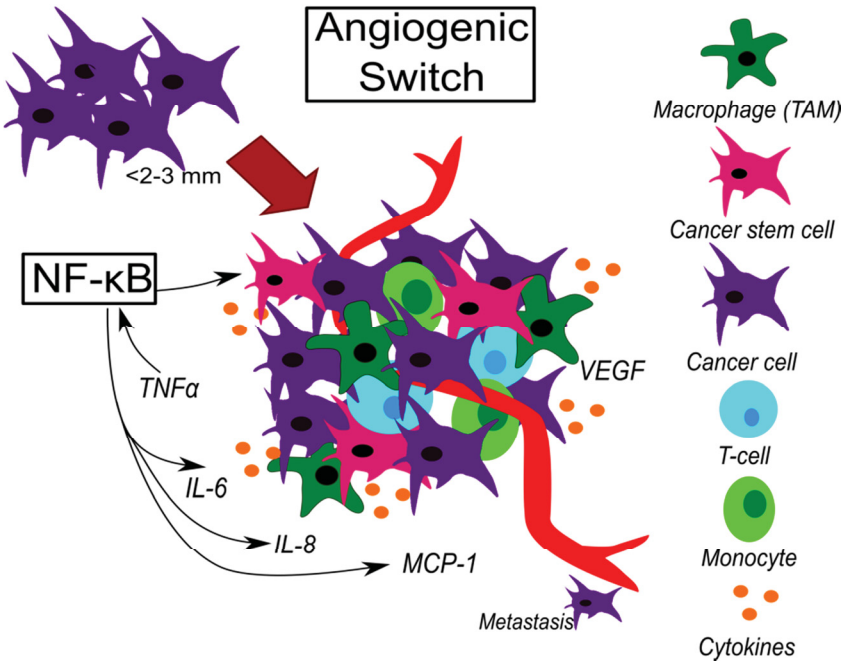

Scheme 2.3-1. Constitutive NF-κB activation can lead to increased secretion of cytokines and thus to tumor development and the establishment of an own tumor microenvironment (TME).

2.3.2 Glucocorticoid Receptor Alpha (GRα) Signaling

In the clinics, the anti-inflammatory signaling and immunosuppressive effect of the 'glucocorticoid receptor alpha' (GRα) is used to reduce side effects of chemotherapeutic treatments, such as nausea and vomiting [122–124]. However, the development of venous thromboembolism, avascular necrosis, as well as chronic diseases such as diabetes mellitus or osteoporosis led to controversial discussions and a reduction of corticosteroid prescriptions [125,126]. Glucocorticoids (GCs) activate GRα, but administration correlates with poor prognosis of patients due to suppression of chemotherapy induced apoptosis [127,128]. However, other studies report an increase in response rates and improved survival after GC administration combined with chemotherapy, not affecting the survival of breast cancer patients [122,129].

The natural GC cortisol is an important messenger, which is synthesized in the adrenal cortex and delivered through the circulating system. The concentration is raised daily in the mornings, up-regulating the process of gluconeogenesis to maintain the metabolism, but an increase is also a response to stress. GCs are able to freely diffuse into cells and interact with, as well as activate, GRα – a member of the nuclear receptor superfamily. This family shares a variable N-terminal transactivation domain, a central DNA binding domain and a C-terminal domain responsible for ligand binding [130]. In the inactive state, GRα resides in the cytoplasm bound to the regulatory 'heat shock proteins' (HSPs) 90, 70 and 56 [131]. Upon ligand-binding, the HSPs dissociate, GRα then is hyperphosphorylated, translocates into the nucleus and binds to its

response elements as a dimer [132,133]. By binding positive 'glucocorticoid response elements' (GREs), GRα activates subsequent target gene transcription, whereas by binding negative GREs (nGREs), GRα downregulates transcription in GC-responsive genes [130,134]. Interestingly, nGREs cannot be found in promotors of cytokine genes, suggesting a distinct transcriptional regulatory mechanism [135]. GRα can interact with co-factors, chromatin-modulators and modifying enzymes which enable or prevent the transcription of target genes [136]. As a monomer, GRα binds to transcription factors such as NF-κB downregulating the inflammatory response and suppressing subsequent expression of pro-inflammatory cytokines [130,137]. In breast cancer, 20-50% of invasive and ductal lobular cells express GRα [137,138]. Malignant mammary epithelium expresses higher amounts of GRα than normal or lactational epithelium, which is correlated with HER2-negativity [139]. In breast cancer patients, immunosuppressive properties of GCs can increase the response rates after chemotherapy [122]. In contrast, GCs also increase the survival of tumor cells [138]. Continuative research is needed to better understand the mechanisms of GRα signaling in the breast cancer microenvironment. In the next section, the correlation of GRα activation with ER status is discussed to distinguish beneficial versus harmful effects of GC administration in the progression of breast cancer.

Studies that report a harmful outcome after GC treatment show reduced apoptosis in ER^- and ER^+ breast cancer cells in the context of chemotherapeutic treatment [140,141]. Administration of the synthetic GC dexamethasone (Dex) in ER^- is associated with a greater ER^- tumor growth [142] and increased drug resistance as a result of driving pro-tumorigenic genes [143]. High GRα expression correlates with increased activation of EMT pathways leading to a shorter survival of ER^- patients [142]. High ER^+ expression is correlated with low GRα expression resulting in longer relapse free survival, whereas high GRα expression in ER^- patients is associated with shorter relapse free survival [142].

Studies that report a beneficial outcome after GC treatment show an induction of apoptosis in lymphoid cancer and in ER^+ breast cancer cells [127,144]. Anti-proliferative effects are correlated with high expression of GRα, suggesting a tumor suppressor role in ER^+ breast cancer cells [123]. Dex treatment is correlated with transcriptional repression of a gene responsible for resistance in ER^+ and ER^- breast cancer [145]. A specific gene, which is associated with reduced proliferation and invasiveness, is transcriptional activated after Dex treatment in ER^- cells [146]. In the absence of ER, GRα significantly inhibits migration [147], upregulates metastasis-suppressor genes as well as represses VEGF and thus reduces angiogenesis [148,149]. Dex is also described to potentiate the anti-tumor effects and can act as a chemosensitizer and chemoprotectant at the same time [150]. In breast carcinoma, GCs

can also display tumor suppressor roles by maintaining the accuracy of chromosome segregation during mitosis [151].

To conclude a correlation of GRα expression and ER status in breast cancer, additional studies are necessary and further investigations of the highly dynamic nature of GRα signaling are needed. A possible approach in TNBC therapy may be the activation of GRα-dependent inhibition of NF-κB signaling and pro-inflammatory cytokines in parallel with a reduction of the GRα-mediated side effects.

2.3.3 PAR2 Signaling

'Protease-activated receptor 2' (PAR2) belongs to a superfamily of G protein-coupled receptors. To date, four different PAR receptors are known, that share 7 transmembrane domains, connected by three extracellular as well as three intracellular loops, an intracellular C-terminus and an extracellular N-terminus. The activation of PAR2 is independent of an endogenous ligand, instead the N-terminal domain is irreversibly cleaved and the then liberated amino acid sequence SLIGKV serves as ligand [152–155]. The cleavage is executed by trypsin and trypsin-like proteases, such as tryptase, thrombin and coagulation proteases [152,156]. Upon receptor activation, PAR2 interacts with three different G-proteins followed by receptor internalization and activation of downstream signaling [157,158]. The G-proteins activate inositol triphosphate production and subsequently lead to protein kinase C (PKC) activation as well as mobilization of calcium ions. Different G-proteins can regulate either migratory, differentiation and proliferation processes [159]. PAR2 is crucial for the modulation of actin cytoskeleton reorganization, where β-arrestin plays a major role in PAR2-stimulated immune-cell migration [158]. Internalization of PAR2 and formation of a complex consisting of β-arrestin, raf-1 and activated 'extracellular-regulated kinases' (ERK) is required for the phosphorylation of ERK1/2, an important regulator of proliferation [157]. Numerous cells express PAR2, including immune cells, inflammatory cells, endothelial cells and epithelial cells, leading to a broad spectrum of PAR2-regulated processes [159]. In the cardiovascular system, the PAR family regulates relaxation and the aggregation of thrombocytes, whereas PAR2 plays a crucial role in the response to vessel injury [160,161]. PAR2-expressing monocytes secrete increased levels of inflammatory cytokines such as IL-6 and IL-8 [162]. However, PAR2 activation also results in multiple diseases and metabolic dysfunctions and is associated with cancer progression [159]. Paradoxically, in certain disease settings, PAR2 executes protective effects, for example by the contribution to wound-healing [163].

In the context of breast cancer, PAR2 increases motility, cancer cell proliferation as well as invasion and is associated with bad prognosis [164–167]. In clinical studies, PAR2

overexpression is not only correlated with increased malignancy in the breast but also of other entities, for example lung or esophagus [159]. Co-expression of PAR2, PAR2-associated tissue factors as well as VEGF results in high recurrence rates and treatment with PAR2 agonists increases the aggressiveness of breast cancer [167,168]. Furthermore, PAR2 is involved in inducing migration and formation of actin stress fibers in TNBC cells [169]. The majority of PAR-related antagonists on the market are based on inhibition of PAR1, for instance vorapaxar [170]. Other compounds inhibiting PAR2 show activities only at low mircomolar concentrations due to low receptor specificity or agonistic activities on related receptors, for example PAR1 [171]. In a recent study, a new class of compounds is described as PAR2-antagonists with activities at nanomolar concentrations, however also activating PKC [169]. A high medical need for effective therapeutic strategies in TNBC supports the development of new and selective PAR2-antagonists and the investigation of their underlying mechanism of action.

2.4 Natural Products as Sources of Novel Drug Leads

Organic compounds, isolated from natural sources have not only played a central role in recent medicinal chemistry, but have also demonstrated health benefits in the entire human history. Resveratrol or flavonoids for example, have been used as dietary supplements due to their anti-oxidative effects [172]. Phytochemicals can contain disease-preventing compounds and might even benefit against cancer [173]. The modern medicinal science has since explored a wide range of compounds isolated from plants, marine organisms, bacteria or fungi and developed potent drugs based on their lead structures. An increasing amount of anti-cancer drugs was derived from natural products, raising from 62% in the years 1981-2002 [174] to 75% till 2010 [175]. Higher plants and microorganisms were long the richest source for natural products [176] and long known anti-cancer agents: Paclitaxel, for example, was discovered in the seventies (taxol) in the bark of the tree *Taxus brevifolia* [175,177]; epipodophyllotoxin is produced in the roots of the plant *Podophyllum peltatum* and was the archetype for etoposide and teniposide [175]; doxorubicin and bleomycin are produced by different *Streptomyces* species [176].

Natural products from marine sources came into focus of research in the 1960s, with the emergence of scuba diving. Marine approved drugs are, for example, cytarabine (Cytosar-U), vidarabine (Vira-A), and zyconotide (Prialt) [178]. To date, the only marine-derived drug approved for treatment of metastatic breast cancer is eribulin mesylate, extracted from the family *Halichondriidae* [179,180]. To date, spongistatin is the most active marine anti-tumor compound in 60 different human cancer cell lines with an average IC_{50} value of 0.12 nM [181]. Limited supply and cultivation difficulties, however, limit further development of anti-cancer

drugs from marine sources. In part, this is because low concentrations of the critical organic compounds demand high amounts of the marine organism for its isolation. For example, 1 ton of the associated tunicate had to be collected for the isolation of one gram of the anti-cancer agent ET-743 [176]. Other problems are the complexity of the chemical structures with no syntheses routes available, rare species or negative side effects in advanced animal or human testing [181]. The high competition among marine organisms in the reefs explains the diversity in natural compounds to survive in the limited habitat. Corals can thus be a particularly rich source of natural products also in breast cancer research.

Three natural products where investigated in this thesis in the context of TNBC for the first time: 1) pseudopterosin as a promising anti-inflammatory compound from marine sources, 2) azaphilone inhering cytotoxic abilities against tumor cells isolated from fungus and 3) teleocidin a promising anti-tumor agent isolated from bacteria.

2.4.1 Pseudopterosin

Pseudopterosins are a class of diterpene glucosides with 31 known derivatives today [182] produced by the soft coral *Antillogorgia elisabethae* (formerly named *Pseudopterogorgia e.*) growing in the Carribean Sea. The soft coral belongs to the family of *Gorgoniidae* (*Octocorals*), representing the most important octocoral in the reefs with high production levels of terpenoids and secosterols [183]. Between 1986 and 2004, several pseudopterosins were isolated: Pseudopterosins A, B, C and D contain β-D-xylose as a sugar moiety [183], E to L contain either α-L-fucose or α-D-arabinose [184] and P to Z contain either β-D-arabinose or α-L-fucose [185].

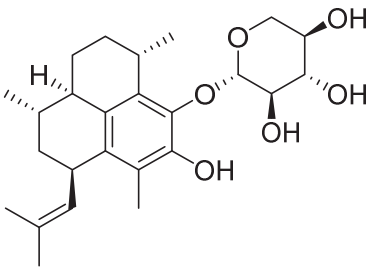

Figure 2.4-1. Pseudopterosin A (PsA) structure.

Pseudopterosin A (PsA) has a tricarbocyclic core with four stereocenters. The β-D-xylose glycosylation resides on C-9 of the catechol unit.

‘Pseudopterosin A’ (PsA) and E (PsE) demonstrated superior anti-inflammatory potency compared to the conventional marketed, ‘non-steroidal anti-inflammatory drug’ (NSAID) indomethacin. Although the mechanism of action of indomethacin is the inhibition of

cyclooxygenase, the pharmacological mechanism of action of pseudopterosin has not been discovered yet [186,187]. In experiments with mice, PsE showed low toxicity at a concentration of 300 mg/kg, whereas the mixture of PsA-D showed elevated toxicity at a concentration of 50 mg/kg [184]. PsA in particular demonstrated significant biological activities inhibiting phagocytic activity, increasing intracellular calcium concentrations [188], inhibiting activity on pancreatic phospholipase A2 [186] and modulating neurological activity during phases of oxidative stress [189]. *In vivo* pharmacokinetic parameters revealed a rapid distribution and elimination of PsA in mice, showing a half-life of 3-4 hours in the brain, the liver and the kidney [189]. The striking properties of PsA listed above are thus evaluated in phase II clinical trials as a wound healing agent [178,181]. In summary, pseudopterosin exhibits a wide range of anti-inflammatory properties that have been used in skin care products [181].

Despite the published *in vivo* pharmacological actions of pseudopterosin, the *in vitro* mechanism of action remains unknown, as yet. In this thesis, anti-inflammatory effects of pseudopterosins A, B, C and D (PsA-D) were investigated in the context of NF-κB signaling as well as inhibitory activity on TNBC characteristics such as migration, proliferation and invasion. Furthermore, inhibitory activities on the bidirectional communication of immune and TNBC cells were investigated [190,191].

2.4.2 Azaphilone

Azaphilones are secondary metabolites mainly produced by fungi. They are characterized by a highly oxygenated pyrano-quinone bicyclic core [192]. The production of the azaphilones might result from a gene cluster called *'aza',* which was discovered in *Aspergillus niger* [192]. Various species of *Monascus* (for example *Monascus purpureus*) or other molds like *Chaetomium* [193], *Penicillium* [194], *Aspergillus*, *Bulgaria* [195] or *Talaromyces* [196] produce azaphilone derivatives, which are commonly used as natural pigment food additives [193]. Commercially available pigment mixtures of azaphilones range from yellow to orange to purple-red [194,197]. A steadily increasing number of compounds with an azaphilone core-structure (see Figure 2.4-2), produced from 23 different fungal genera, have been identified so far [196,198].

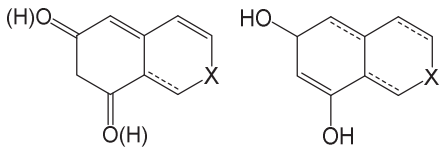

Figure 2.4-2. Azaphilone core structure (X = O, N) (adapted from [196]**).**

Azaphilone and azaphilone-derivatives exhibit diverse biological activities, such as telomerase inhibition [199], induction of Epstein-Barr virus [200], anti-microbial activity [201,202],

lipooxigenase inhibition [203], inhibition of nitric oxide [204], or inhibition of PMA-induced inflammation [193]. In the context of cancer, azaphilone derivatives inhibit tumor promotion in a two-stage carcinogenesis [193], proliferation [205,206] or inhibit a RNA-binding protein that stabilizes oncogenic mRNA, cytokine mRNA or growth factor mRNA [207]. Cytotoxic activity against A549 lung carcinoma cells [208], HL-60 acute leukemia cells [209,210], HepG2 liver cancer cells [211], HeLa cervical cancer cells [212] and additional 39 human cancer cell lines, including MDA-MB-231 breast cancer cells, are described [196,210].

Azaphilones show a broad spectrum of potent anti-cancer properties. In this thesis, new azaphilone derivatives were investigated regarding NF-κB inhibition, anti-migratory and anti-invasive effects on MDA-MB-231 breast cancer cells [213].

2.4.3 Teleocidin

Teleocidins biosynthetically derive from indolactam V and are a class of natural compounds, which were first isolated from *Streptomyces mediocidius* in 1960 [214]. Teleocidin showed toxic properties to the teleost fish *Oryzias latipes*, but no toxicity to bacteria or molds [215]. The class of teleocidins belongs to the indole alkaloids derived from the natural product indolactam V, which is produced from *Streptoverticillium blastmyceticum* [216] and include the isoforms teleocidins A1-2 and teleocidins B1-4 [215,217,218]. *Lyngbya* algae, such as the marine cyanobacterium *Moorea producens* (originally *Lyngbya majuscula*), produce the teleocidin derivatives teleocidin B [219] and lyngbyatoxine A, which is structurally identical to teleocidin A1 [217,220]. Today, several compounds belong to the teleocidins and they are produced by different *Streptomyces* strains, for example olivoretine [221], blastmycetine [222] or dihydroteleocidin B [217]. Although some natural products have beneficial effects such as anti-inflammation, the major effect of teleocidins is the activation of the protein kinase C (PKC) similar to phorbol esters. Teleocidins activate PKC and promote tumor growth as a result of increased calcium levels [156]. Activation of PKC results in secretion of high amounts of inflammatory signals [217,223,224], increase of tumor proliferation in lung cancer and increase of cell growth as well as secretion of pro-survival factors in breast cancer [225]. Additionally, lyngbyatoxine A together with teleocidin B induce lethality in mice [220], epidermal hyperplasia and promote skin tumors [226].

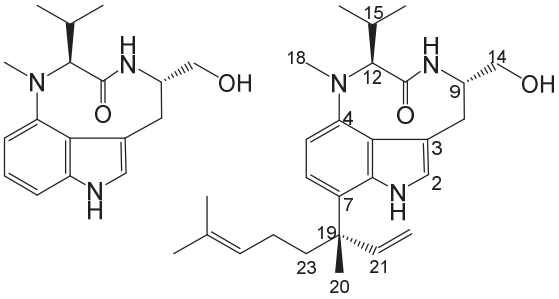

Figure 2.4-3. Chemical structure of indolactam V (left) and teleocidin A2 (right).

However, the teleocidin-aglycon indolactam V is also reported to downregulate some PKC isoforms, in contrast showing anti-tumor properties for the first time [227]. By analyzing PAR2-dependent calcium release, teleocidin A2 demonstrates inhibitory abilities in MDA-MB-231, A549 cells as well as human umbilical vein endothelial cells (HUVEC) and displays anti-migratory potential in MDA-MB-231 cells at nanomolar concentrations. The anti-migratory effect is independent of actin rearrangement, but may be a result from Rac1 inhibition, a small signaling G-Protein regulating cytoskeletal reorganization. The analysis of inhibitory abilities on related receptors, such as PAR1 or the ubiquitously expressed G-protein coupled receptor P2Y, reveals less specificity of teleocidin A2 compared to PAR2. However, teleocidin A2 also activates phosphorylation of PKC [169].

In this thesis, the focus was on the improvement of the indolactam/teleocidin aglycon structure and the investigation of different teleocidin-derivatives on inhibition of calcium-dependent PAR2 signaling. Hence, the aim was to identify a compound with similar PAR2 inhibiting activity like teleocidin A2, a low ability to modulate PAR1 and no “off-target” effects, such as PKC activation. [126].

2.5 Aims

The main aim of this thesis was to elucidate the role of three natural products as putative agents against high inflammatory signals and aggressive features of the breast cancer subtype named triple negative and thus provide a novel approach in the TNBC therapy.

The first chapter gives a short abstract of the capabilities of three natural products investigated in this thesis and their correlation in TNBC. The introduction in chapter 2 provides an overview in the general topics of breast cancer subtypes and related chemotherapeutic treatments, the role of the tumor microenvironment as well as signaling pathways that are upregulated in cancer and thus promote tumor progression. Chapter 3.1 and 3.2 illuminate the mechanism of action of the marine natural product pseudopterosin in the context of TNBC. The chapter 3.3 portrays azaphilone isolated from a fungus and chapter 3.4 teleocidin isolated from bacteria and their

abilities to inhibit features of TNBC. Chapter 4 illustrates the conclusions of the investigated natural products as putative anti-cancer agents.

Objective 1 (Chapter 3.1)

Tumor development, progression and growth are often the result of deregulated signaling, for example constitutive activation of NF-κB. Therefore, I aimed to characterize pseudopterosin as a putative anti-cancer agent and evaluated its ability to inhibit specific attributes of triple negative breast cancer. The main aims in this chapter were: (1) to investigate the influence on the NF-κB pathway as a potential basis for the anti-inflammatory abilities of pseudopterosin, (2) to investigate whether the anti-inflammatory abilities of pseduopterosin are transferable to the breast microenvironment, where inflammatory signals are the communicating devices of tumor and tumor-associated immune cells (3) and to elucidate the mode of action of pseudopterosin by identifying a possible interaction partner.

Objective 2 (Chapter 3.2)

This chapter complements chapter 3.1 in characterizing the inhibitory abilities of pseudopterosin on the so-called hallmarks of cancer defined by Hanahan and Weinberg [28]: (1) uncontrolled proliferation and growth, (2) the potential to invade blood vessels and migrate to distant organs and (3) the development of a microenvironment maintaining and supporting tumor growth. (4) Additionally, I aimed to verify the mode of action of pseudopterosin and fortify the target structure I identified as interacting partner.

Objective 3 (Chapter 3.3)

Fungi are able to produce a variety of compounds differing in their structure and their bioactivity. In chapter 3.3, the aim of the study was to identify novel bioactive compounds isolated from *Coniella fragariae,* a fungus infesting plants, such as the garden strawberry, to analyze their structure and to investigate their potential to block the pro-inflammatory signaling pathway NF-κB. Additionally, I aimed to further investigate the compounds with the best capabilities on processes in cancer that depend on NF-κB activation such as migration and invasion.

Objective 4 (Chapter 3.4)

The class of teleocidins, natural products mainly produced by bacteria, aberrantly activates signals that lead to the promotion of tumor progression. However, tumor suppressing abilities in aggressive lung and breast cancer cells were also attributed to this class. The aim in chapter 3.4 was to analyze the structure-activity-relationship of teleocidin/indolactam and improve its biological activities by reducing the ability to promote cancer progression and at the same time enhancing the ability to suppress PAR2-dependent calcium mobilization and migration of TNBC cells.

3 Publications

3.1 The Marine Natural Product Pseudopterosin Blocks Cytokine Release of Triple-Negative Breast Cancer and Monocytic Leukemia Cells by inhibiting NF-κB Signaling

Julia Sperlich[1], Russell Kerr[2] and Nicole Teusch[1]

[1] Bio-Pharmaceutical Chemistry & Molecular Pharmacology, Faculty of Applied Natural Sciences, Technische Hochschule Koeln, 51373 Leverkusen, Germany;

[2] Department of Chemistry, and Department of Biomedical Sciences, Atlantic Veterinary College, University of Prince Edward Island, Charlottetown, PE C1A 4P3, Canada;

ABSTRACT

Pseudopterosins are a group of marine diterpene glycosides which possess an array of biological activities including anti-inflammatory effects. However, despite the striking *in vivo* anti-inflammatory potential, the underlying *in vitro* molecular mode of action remains elusive. To date, few studies have examined pseudopterosin effects on cancer cells. However, to our knowledge, no studies have explored their ability to block cytokine release in breast cancer cells and the respective bidirectional communication with associated immune cells. The present work demonstrates that pseudopterosins have the ability to block the key inflammatory signaling pathway nuclear factor κB (NF-κB) by inhibiting the phosphorylation of p65 and IκB (nuclear factor of kappa light polypeptide gene enhancer in B-cells inhibitor) in leukemia and in breast cancer cells, respectively. Blockade of NF-κB leads to subsequent reduction of the production of the pro-inflammatory cytokines interleukin-6 (IL-6), tumor necrosis factor alpha (TNFα) and monocyte chemotactic protein-1 (MCP-1). Furthermore, pseudopterosin treatment reduces cytokine expression induced by conditioned media in both cell lines investigated. Interestingly, the presence of pseudopterosins induces a nuclear translocation of the glucocorticoid receptor. When knocking down the glucocorticoid receptor, the natural product loses the ability to block cytokine expression. Thus, we hypothesize that pseudopterosins inhibit NF-κB through activation of the glucocorticoid receptor in triple negative breast cancer.

INTRODUCTION

Cancer represents one of the diseases with the highest unmet medical need, causing the second highest incidence of death after cardiovascular diseases in industrialized countries. Among the different types of malignant tumors, breast cancer is the leading cause of cancer mortalities in women worldwide [1]. Classification of breast cancer subtypes is based on the expression of progesterone receptor (PR), estrogen receptor (ER) and/or human epidermal growth factor receptor (HER2). Accordingly, the breast cancer subtype expressing none of these three receptors, the so-called triple-negative breast cancer (TNBC), represents the most aggressive form with currently no targeted therapy available and a significantly reduced overall survival rate [2,3]. Thus, development of innovative and more effective therapies is urgently needed. Marine organisms represent a vast source of biologically active compounds with a highly unexploited potential for innovative drug development [4]. For instance, the soft coral *Antillogorgia elisabethae* (formerly *Pseudopterogorgia elisabethae*) has been reported to produce at least 31 different secondary metabolites, most of which have been pharmacologically unexplored [5]. Amongst others, the pseudopterosin family displays a broad spectrum of biological activities, including anti-inflammatory [6–8], analgesic [6,9,10], wound-healing [7,8] and neuromodulatory [11] activity. Moreover, pseudopterosins have shown anti-inflammatory efficacy in phase II clinical trials [12,13] and represent the first commercially licensed marine natural product for use in cosmetic skin care [7,11]. Intriguingly, *in vivo* assays revealed a higher efficacy of pseudopterosins against topically induced inflammation than the marketed drug indomethacin [6]. Despite the striking *in vivo* pharmacological effect [6,10,14] and the application in cosmetic products [7,11] the underlying *in vitro* mechanism of action of the anti-inflammatory potential of pseudopterosins remains elusive. The potential of pseudopterosin A (PsA) has been described as spreading across different intracellular mechanisms ranging from inhibition of phospholipase A2 [10], altering calcium release [15], and inducing cytotoxicity in cancer cells [16]. To our knowledge, no studies have explored the potential of pseudopterosins as a novel immune modulatory agent in breast cancer. A key factor in regulating inflammatory responses is the transcription factor nuclear factor κB (NF-κB) that acts by controlling expression of cytokines and chemokines. Activation can be triggered by various factors including pro-inflammatory cytokines, growth factors, hormones, oxidative stress, viral infections or DNA-damaging agents [17–20]. Pathogen-associated-molecular-patterns (PAMPs) such as lipopolysaccharides (LPS) and tumor necrosis factor alpha (TNFα) are ligands of different receptors, both triggering activation of the NF-κB-controlled immune response [21–23]. The NF-κB family consists of five functionally conserved members in mammalian cells, including RelA (nuclear factor NF-kappa-B subunit p65), RelB (nuclear factor NF-kappa-B subunit p60), c-Rel, NF-κB1 (p105 and p50) and NF-κB2 (p100 and p52) [24]. The specific activation of NF-κB in the innate and adaptive immune defense is opposed by constitutive NF-

κB expression in various tumor types. Constitutive activation of NF-κB could be confirmed in cancer in general, and in breast cancer in particular, supporting overall tumor progression, drug resistance, invasiveness, epithelial-to-mesenchymal-transition (EMT) and the promotion of hormone-independent growth [17,25–28]. Elevated NF-κB activity has been observed in both primary human breast cancer tissues and breast cancer cell lines. Furthermore, a recent study assigned a key role of NF-κB in disrupting important microenvironmental cues necessary for tissue organization [29]. The tumor microenvironment (TME) encompasses a complex interplay between tumor cells and tumor associated immune cells. Tumor associated macrophages (TAM) play a crucial role in cancer progression [30]. TAMs produce high amounts of cytokines such as interleukin-6 (IL-6), interleukin-8 (IL-8), monocyte chemotactic protein 1 (MCP-1) and tumor necrosis factor alpha (TNFα) to alter the tumor progression in different ways. IL-6 promotes tumor proliferation, IL-8 leads to neovascularization, growth, angiogenesis and metastasis, and TNFα affects necrosis, invasion and metastasis [26,27]. Moreover, MCP-1 overexpression correlates with histological grade and low level differentiation in breast tumors [31]. The glucocorticoid receptor alpha (GRα) has been investigated in different clinical studies as a putative pharmacological target for the treatment of breast cancer [32–34]. Interestingly, there is evidence that NF-κB and GRα can physically interact and heterodimerize in breast cancer [35]. By binding other transcription factors such as NF-κB or AP-1, GRα can either transactivate or suppress its target genes [1]. Agonism of glucocorticoids (GC) can block migration, invasion and angiogenesis via down-regulation of IL-6 and IL-8 and has been reported to induce drug sensitivity. Furthermore, GC activation induces apoptosis in lymphoid cancer and MCF-7 breast cancer cells [36–38]. However, due to high variability in its expression frequency, divergent cellular functions of GRα have been described [2]. Herein, we describe inhibitory capabilities of a mixture of pseudopterosins on the NF-κB signaling pathway and its target genes, the cytokines, in monocytic leukemia and in triple negative breast cancer cells (TNBC) presumably by agonizing the glucocorticoid receptor α. Moreover, our study ascribes the efficient cytokine blockade in the context of bidirectional tumor-immune-cell communication to pseudopterosin treatment.

RESULTS

Pseudopterosin Reduces Cytokine Release by Inhibition of NF-κB Signaling

Pseudopterosins have been described as anti-inflammatory agents with an *unknown in vitro* mechanism of action. To explore intracellular signaling pathways following pseudopterosin treatment, we investigated the influence of an extract mixture containing four different pseudopterosin derivatives (PsA-D) on the key inflammatory signaling pathway NF-κB. For this

purpose, we generated a stable cell line based on the triple negative breast cancer cell line MDA-MB-231 (subsequently named NF-κB-MDA-MB-231) (see Section 'Stable Cell Line Generation'). MDA-MB-231 cells display a high level of toll-like-receptor 4 (TLR4) [39] which can activate NF-κB signaling via its ligand LPS [40]. Interestingly, increasing amounts of pseudopterosin inhibited LPS-induced NF-κB activation in NF-κB-MDA-MB-231 breast cancer cells in a concentration-dependent manner (Figure 3.1-1A) with an IC_{50} value of 24.4 µM. Additional studies revealed that pseudopterosin also reduced NF-κB activation initiated by other stimuli including TNFα (Supplemental Figure 3.1-1). Moreover, addition of 30 µM of pseudopterosin in monocytic THP-1 cells led to a 1.65-fold inhibition of NF-κB-dependent luciferase activity (Figure 3.1-1B).

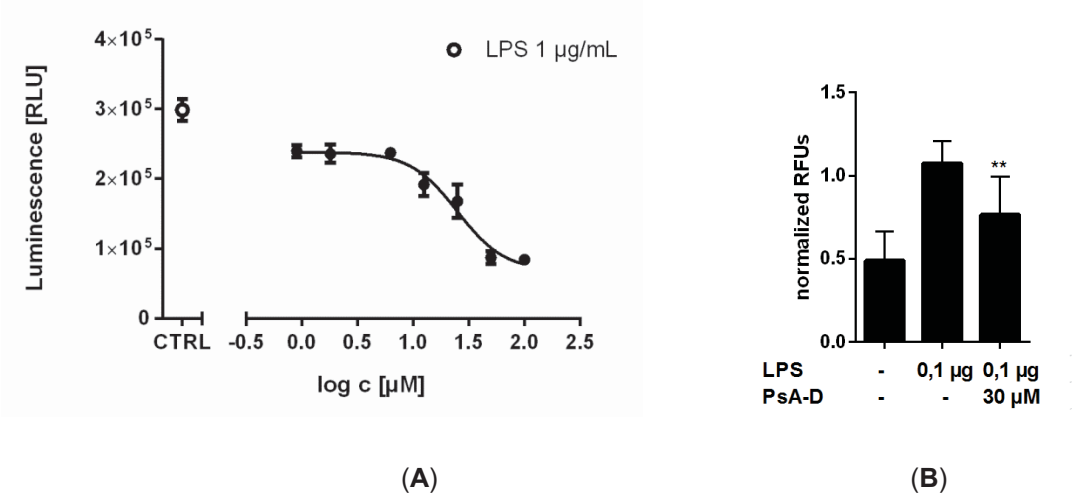

Figure 3.1-1. Nuclear factor κB (NF-κB) inhibition in lipopolysaccharide (LPS)-stimulated stable NF-κB-MDA-MB-231 and THP-1 monocytic leukemia cells.

(**A**) Dose–response curve of pseudopterosin (PsA-D) on LPS stimulated NF-κB-MDA-MB-231 cells expressing a luciferase reporter gene which is under the control of a NF-κB CMV (cytomegalovirus) promotor. Luminescence intensity correlates proportionally with NF-κB activation. The solid circle represents NF-κB induction in the presence of 1 µg/mL LPS (positive control). PsA-D treatment was performed for 20 min in a bisecting titration followed by 1 µg/mL LPS for 1 h. IC50 value of 24.4 µM of pseudopterosin was calculated from three independent experiments; (**B**) Inhibition of NF-κB upon pseudopterosin treatment in THP-1 monocytic leukemia cells (ELISA). Cells were incubated with PsA-D for 20 min followed by LPS treatment. Pseudopterosin decreased NF-κB activation significantly. RLU = relative luminescence units; RFU = relative fluorescence units. Two stars represent a significance of $\rho < 0.05$. Error bars were calculated using standard error of the mean (+SEM); n = 3.

As multiple pro-inflammatory cytokines such as IL-1, IL-6 and TNFα represent target genes of NF-κB [41–43], we investigated the effect of PsA-D on pro-inflammatory cytokine release. Analyzing a subset of six different cytokines simultaneously, in THP-1 cells incubated with 1 µg/mL LPS led to a significant secretion of IL-6, TNFα and MCP-1 compared with unstimulated control (23-fold induction of IL-6, 33-fold induction of TNFα and 24-fold increase of MCP-1;

Table 6.1-1), but not IL-1β, IL-12 or IL-4 (data not shown). Compared to THP-1 cells, MDA-MB-231 breast cancer cells displayed a higher basic level of IL-6 and MCP-1. Upon LPS stimulation, we confirmed a 3-fold increase of IL-6, a 15-fold induction of TNFα and a 5-fold increase of MCP- 1 in MDA-MB-231 cells (Table 3.1-1). In contrast, no induction of IL-1β or IL-4 could be observed in the triple negative breast cancer cells (data not shown). In both cell lines investigated, PsA-D incubation was able to induce a significant blockade of cytokine secretion: In THP-1 monocytic leukemia cells pseudopterosin reduced TNFα release by at least 47%, blocked IL-6 release by 50% and MCP-1 release by 73%. In MDA-MB-231 breast cancer cells incubated with PsA-D led to a reduction of MCP-1 by 85%, a decrease of TNFα release by 75%, and a decrease of IL-6 by 38%.

Table 3.1-1. Inhibition of cytokine release in THP-1 monocytic leukemia and MDA-MB-231 triple negative breast cancer.

THP-1 cells were treated with 10 ng PMA for 24 hours to induce differentiation. Cytokine amounts were analyzed in supernatants after 24 hours incubation time. Total amounts of cytokines (pg/mL) were calculated according to a standard concentration curve. No treatment serves as a control. '%'-inhibition reflects the percentage of the amount of cytokines reduced by PsA-D treatment. Standard deviation was calculated for amounts of cytokines (±SD); n=3.

MDA-MB-231	**Control (pg/ml)**	**+LPS 1 µg/mL**	**+PsA-D 30 µM µM**	***P*-value**	**%**
IL-6	1626.3 (±144)	4666.7 (±307)	2874.8 (±610)	<0.0002	38.3
TNFα	1.9 (±0.6)	29.1 (±5.5)	7.17 (±3.4)	<0.0005	75.3
MCP-1	325.3 (±260)	1625.6 (±540.6)	241.3 (±100.9)	0.0082	85.2
THP-1	**Control (pg/ml)**	**+LPS 1 µg/mL**	**+PsA-D 30 µM**	***P*-value**	**%**
IL-6	2.8 (±1)	66.7 (±9.8)	33 (±2.0)	0.0089	50.0
TNFα	13.4 (±4.5)	439.4 (±28)	232.0 (±100)	0.1138	47.2
MCP-1	182.9 (±65.3)	4436.7 (±2098)	1208.9 (±762.3)	0.0552	72.8

As the NF-κB signaling pathway can be activated with different stimuli including LPS, TNFα or pathogen-associated molecular patterns (PAMPs) [18,44,45], we utilized TNFα, the ligand of the TNFα receptor 1 (TNFR1) [23,46], to induce NF-κB signaling independent of TLR4. As expected, stimulation with TNFα increased the expression levels of the investigated cytokines in MDA-MB-231 breast cancer cells significantly compared to unstimulated control (IL-6 4-fold, IL-8 6-fold, MCP-1 5-fold) (Figure 3.1-2A). It is noteworthy that pseudopterosin blocked the expression of all cytokines investigated; however, statistical significance was only noted for IL-6 and MCP-1 (IL-6 2.7-fold induction, MCP-1 3.7-fold induction).

Secretion of cytokines is stimulated after TNFα treatment (IL-6 4540 ±329 pg/mL, IL-8 4047 ±196 pg/mL, MCP-1 4048 ±18 pg/mL) (Figure 3.1-2B). Cytokine amounts declined in the triple negative breast cancer cells in a concentration-dependent manner upon pseudopterosin treatment (at a PsA-D concentration of 30 µM: 18-fold decrease of IL-6, 12-fold reduction of IL-8 and a 26-fold decrease of MCP-1). Significant inhibition at a concentration of 10 µM of PsA-D could be achieved for MCP-1 (6-fold decrease of MCP-1 release compared to untreated control).

It is noteworthy that irrespective of exogenous cytokine stimulation via LPS or TNFα, pseudopterosins are able to significantly reduce endogenous release of at least two cytokines in the MDA-MB-231 triple negative breast cancer cells (IL-6 1.2-fold, IL-8 1.4-fold, MCP-1 1.4-fold) (Figure 3.1-2C). Moreover, additional investigation demonstrates that the reported inhibitory effect of PsA-D on cytokine release can be assigned to other triple negative cell lines (Supplemental Table 3.1-1).

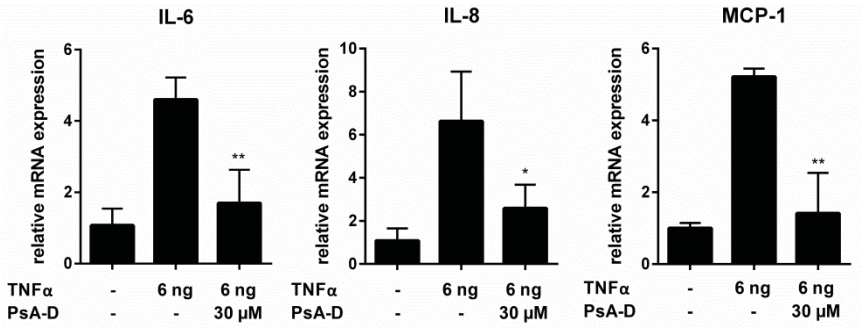

(**A**)

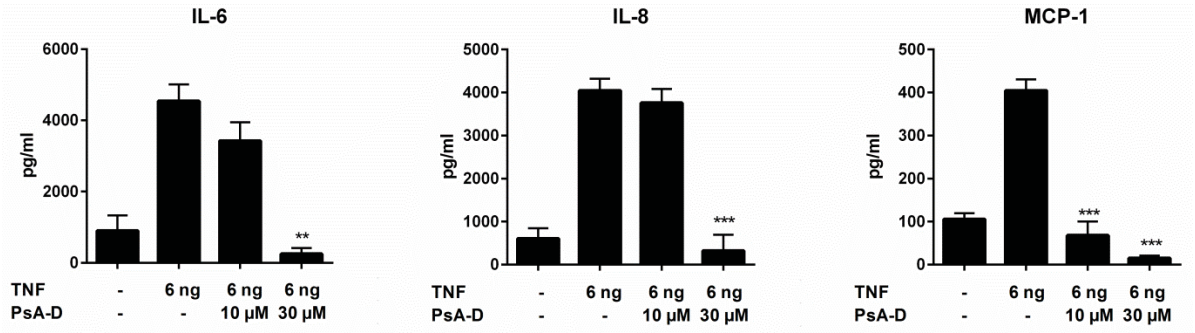

(**B**)

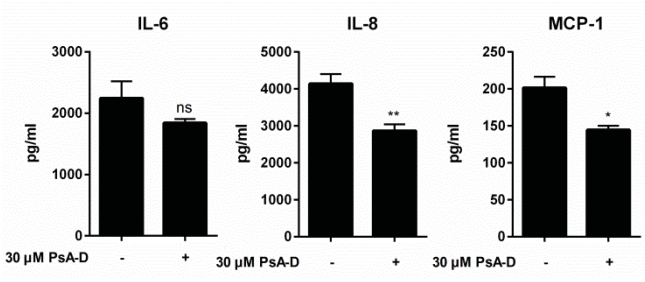

(**C**)

Figure 3.1-2. Inhibition of cytokine expression (A) and secretion (B) after TNFα stimulation and inhibition of endogenous cytokine secretion (C) in MDA-MB-231 triple-negative breast cancer (TNBC).

(**A**) MDA-MB-231 cells were treated with 30 µM of PsA-D for 20 min followed by 6 ng/mL of TNFα for 5 h; (**B**) Various concentrations of PsA-D were incubated for 20 min followed by TNFα treatment for 24 h; (**C**) MDA-MB-231 cells were treated with 30 µM of PsA-D and cytokine secretion was measured 24 h thereafter. Error bars were calculated using +SEM; n = 3. *P*-values are calculated against TNFα. Three stars represent a significance of $\rho < 0.001$, two stars $\rho < 0.01$, one star $\rho < 0.05$ and "ns." means not significant.

Pseudopterosin Blocks Bidirectional Communication

To explore whether pseudopterosins have the ability to inhibit the bidirectional communication between immune cells and tumor cells, we designed an experimental set-up imitating inter-cell communication within the tumor microenvironment (Figure 3.1-3A). As shown, stimulation by LPS leads to the production of secondary metabolites including cytokines and the subsequent secretion into the surrounding "conditioned medium" (CM). Medium containing cytokines released by MDA-MB-231 cells represents the so called "MDA-MB-231 conditioned medium" (M-CM; Figure 3.1-3B), whereas medium encompassing cytokines secreted by THP-1 cells referred to as "THP-1 conditioned medium" (THP-CM; Figure 3.1-3C). Both conditioned media were used in independent experiments to stimulate the respective opposite cell line. Treatment with unstimulated conditioned medium did not influence cytokine expression in any of the investigated cell lines. However, incubation of THP-1 leukemia cells with stimulated M-CM induced a significant cytokine expression in THP-1 cells (8-fold increase of IL-6, 18-fold induction of TNFα and nearly 13-fold in MCP-1 expression). Furthermore, the triple negative breast cancer cell line MDA-MB-231 induced expression of IL-6, TNFα and MCP-1 in the presence of stimulated THP-CM (IL-6 induction 177-fold, TNFα induction nearly 10-fold and MCP-1 induction nearly 19-fold). Notably, pseudopterosin treatment was able to block cytokine expression induced by conditioned media in both leukemia cells and in triple negative breast cancer cells. In THP-1 cells stimulated with M-CM, a 2-fold reduction of IL-6 expression and a 3-fold reduction of MCP-1 expression were noted following pseudopterosin treatment. Also, MDA-MB-231 cells stimulated with THP-CM displayed a 4-fold increase in IL-6 and a 2.5-fold increase in MCP-1 expression. In conclusion, our data demonstrate that PsA-D is able to significantly decrease expression of the cytokines IL-6 and MCP-1 after stimulation with pre-conditioned medium in monocytes and breast cancer cells, respectively.

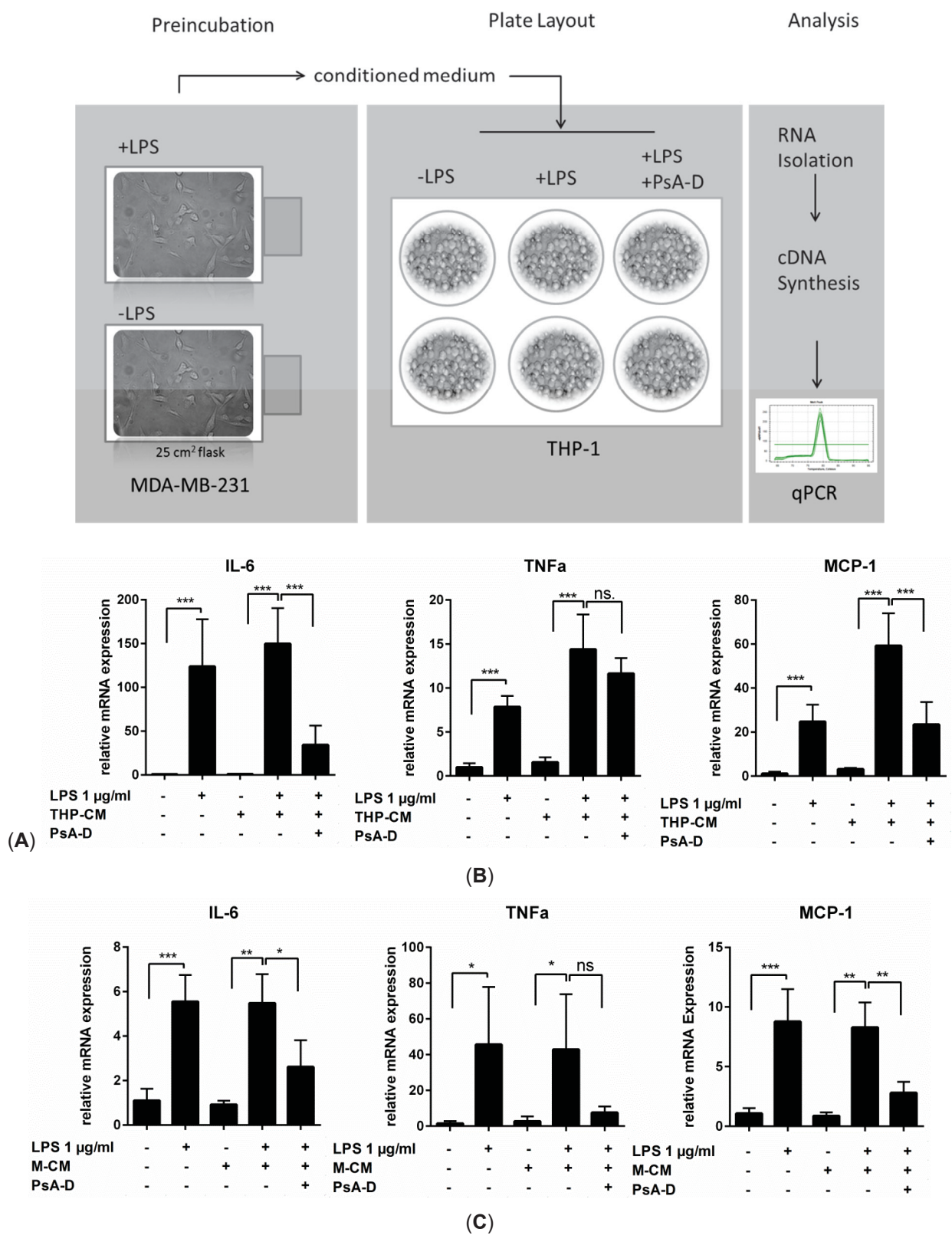

Figure 3.1-3. Blockage of bidirectional communication between THP-1 monocytic leukemia and MDA-MB-231 TNBC.

(**A**) Process scheme of producing tumor conditioned medium. THP-1 or MDA-MB-231 cells were cultured in 25 cm^2 flasks and treated with 1 µg/mL LPS for 24 h. Medium was collected and centrifuged. After sterile filtration, tumor conditioned medium was added to seeded cells in 6-well plates. (**B**) MDA-MB-231 conditioned

medium (M-CM) or (**C**) THP-1 conditioned medium (THP-CM) was added to the adversary cells. RNA was isolated for further analysis in real-time PCR. Error bars were calculated using +SEM. *P*-values of three stars represent a significance of $\rho < 0.001$, two stars $\rho < 0.01$, one star $\rho < 0.05$ and "ns." means not significant.

To exclusively ascribe the demonstrated cytokine expression patterns to the pre-treatment with the respective conditioned medium, we subjected MDA-MB-231 cells to a knock-down of the TLR4 receptor (siRNA-TLR4 (siTLR4) transfected cells) (Figure 3.1-4A). As a control, we transfected non-coding silencing RNA (nc siRNA). A 50% TLR4 knockdown was achieved. Compared to a nc siRNA control, siTLR4 transfection did not influence TNFα expression level upon pseudopterosin treatment. Monitoring the p65 phosphorylation with TNFα and LPS in parallel experiments we confirmed a 2-fold reduction of phosphorylation after pseudopterosin treatment independent of the stimulus (Figure 3.1-4B). In conclusion, PsA-D induced cytokine blockade and p65 phosphorylation in triple negative breast cancer cells does not dependent on TLR4.

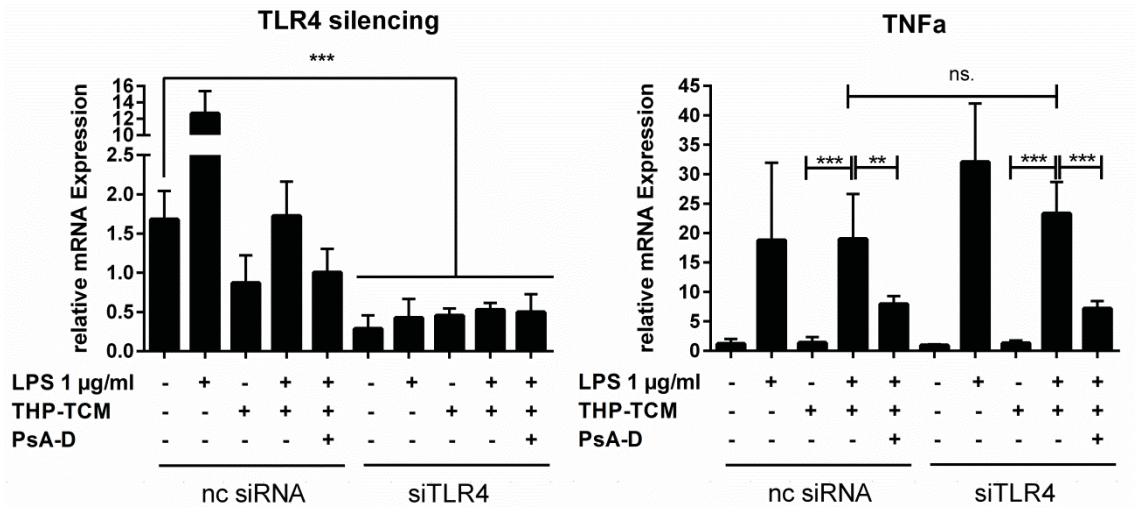

(**A**)

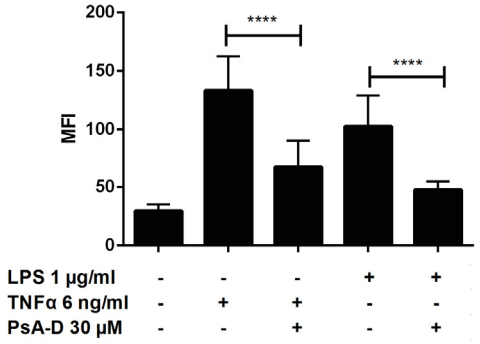

(**B**)

Figure 3.1-4. PsA-D-induced NF-κB inhibition is toll-like-receptor-4 (TLR4)-independent.

(**A**) MDA-MB-231 cells were seeded in 6-well plates and incubated for 24 h. Transfection with 2 µM siRNA was done with Lipofectamine3000 following the manufacturer's protocol. After 24 h, cells were first treated

with 30 µM PsA-D before and following treatment with THP-CM for 5 h. After another 24 h of incubation, cells were harvested and lysed for RNA isolation in preparation for realtime PCR. Knock-down efficiency of TLR4 was about 50%. PsA-D blocked TNFα expression independent of TLR4 expression; (**B**) MDA-MB-231 cells were stimulated either with 1 µg/mL LPS or with 6 ng/mL TNFα following 20 min treatment of PsA-D. P65 phosphorylation was measured after 24 h of treatment. Error bars were calculated using +SEM. *P*-values of four stars show a significance of $\rho < 0.0001$, three stars $\rho < 0.001$, two stars $p < 0.01$ and "ns." means not significant.

Pseudopterosin Inhibits NF-κB through Activation of the Glucocorticoid Receptor

Our data show for the first time that the underlying *in vitro* mechanism of the well described anti-inflammatory response of pseudopterosin might be ascribed to inhibition of the NF-κB pathway. To further explore putative molecular pharmacological targets of pseudopterosins, we started to investigate the influence of the natural product on glucocorticoid signaling. NF-κB and glucocorticoid receptor α (GRα) display opposed functions in regulating immune and inflammatory responses. Moreover, both transcription factors have been described as transcriptional antagonists [36]. Thus, we investigated the interaction of pseudopterosin with GRα. To evaluate transactivation of GRα in the presence of PsA-D on the whole cell level, we used immunofluorescent staining of GRα in MDA-MB-231 cells incubating the cells with dexamethasone, serving as a positive control, or PsA-D (Figure 3.1-5A). Untreated cells displayed an even GRα distribution within the cytosol, whereas the nucleus did not show any GRα localization. As expected, upon dexamethasone treatment the GRα staining revealed a complete translocation of the receptor to the nucleus in breast cancer cells. Interestingly, the presence of pseudopterosin induced a comparable nuclear translocation of the GRα. Quantification of the respective fluorescence intensities using the software ImageJ confirmed a significant GRα translocation to the nucleus after dexamethasone treatment (4.5-fold reduction of cytoplasmic total corrected cell fluorescence (TCCF) compared to control) and pseudopterosin treatment (2.5-fold reduction of cytoplasmic total corrected cell fluorescence (TCCF) compared to control, Figure 3.1-5B). Accordingly, PsA-D inhibited phosphorylation of p65 and IκBα significantly compared to LPS stimulation (Figure 3.1-5C) or compared to stimulation with TNFα (Supplemental Figure 3.1-2) (2-fold inhibition, respectively). Moreover, to confirm GRα as a putative pharmacological target of pseudopterosin we performed a glucocorticoid receptor α knock-down in MDA-MB-231 cells. In this context, we transfected cells with siRNA of GRα (siGR, Figure 3.1-6A) with non-coding siRNA (nc siRNA) serving as a negative control. A 60% knock-down of GRα was achieved. Treatment with negative control nc siRNA revealed that unaltered GRα expression resulted in cytokine expression level after LPS stimulation comparable to previous results (Table 3.1-1). Furthermore, as demonstrated earlier, pseudopterosin inhibited IL-6 (3-fold) and MCP-1 (nearly 4-fold) significantly in the presence of

GRα. However, when knocking down GRα, pseudopterosin lost the ability to block IL-6 or MCP-1 expression, respectively. To finally confirm glucocorticoid receptor α as a potential pharmaceutical target for pseudopterosin, we used a reporter gene assay expressing a luciferase under the control of a human GRα promotor (Figure 3.1-6B). In line with our previous findings, pseudopterosin induced a significant increase in expression of human GRα. In conclusion, the described inhibitory effect of pseudopterosin on cytokine expression and release in triple negative breast cancer is putatively ascribed to agonism of glucocorticoid receptor α.

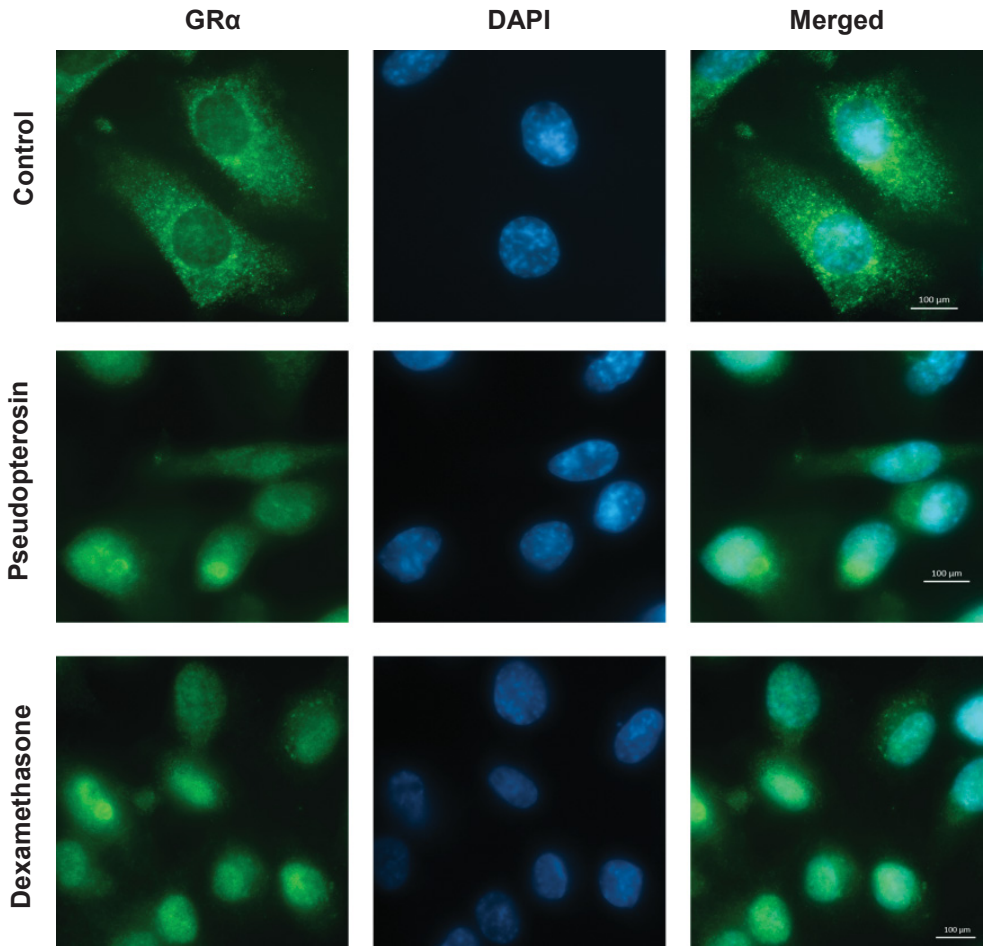

(**A**)

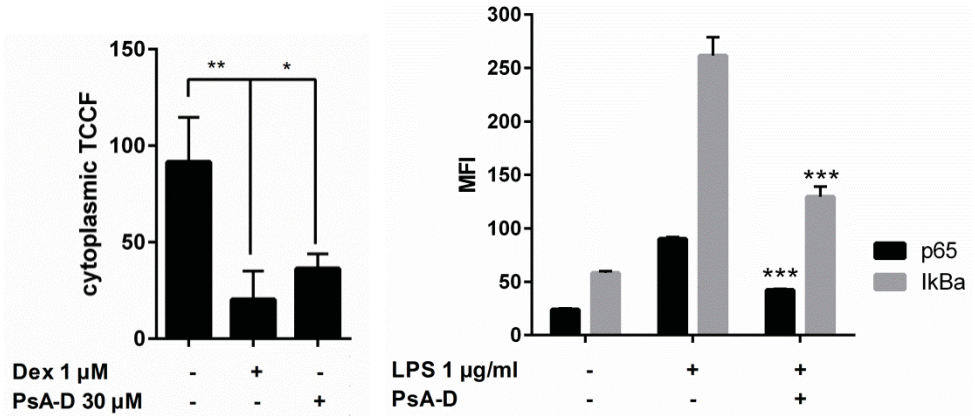

(**B**) (**C**)

Figure 3.1-5. Pseudopterosin-induced activation of glucocorticoid receptor alpha (GRα) translocation into the nucleus is accompanied by inhibition of phosphorylation of p65.

(**A**) PsA-D was added at a concentration of 30 µM and dexamethasone at 1 µM in MDA-MB-231 cells. Cell nuclei were stained with 3 µM 4′,6-Diamidin-2-phenylindol (DAPI; blue channel). GRα is shown in green. The right column shows merged channels; (**B**) Quantification of immunofluorescence staining shows cytoplasmic total corrected cell fluorescence (TCCF). TCCF was calculated as described in methods section. Cytoplasmic TCCF was calculated after following formula: TCCF GFP–TCCF DAPI. Cytoplasmic staining reduced significantly after dexamethasone (Dex) or PsA-D treatment; (**C**) Phosphorylation of p65 and IκBα induced by LPS were investigated in the absence or presence of PsA-D with an incubation time of 20 min on MDA-MB-231 breast cancer cells. *P*-values of three stars show a significance of $\rho < 0.001$, two stars of $\rho < 0.01$ and one star of $\rho < 0.05$; +SEM; n = 30. MFI = median fluorescence intensity.

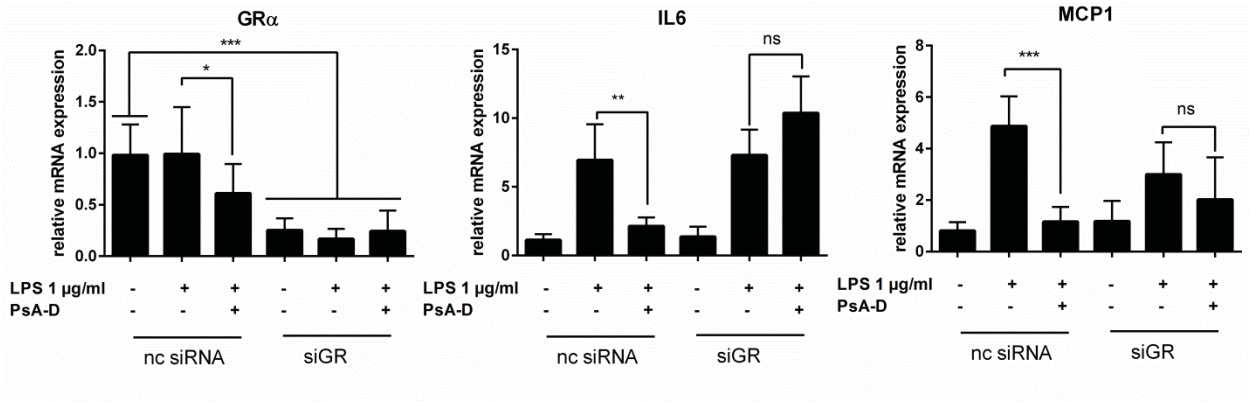

(**A**)

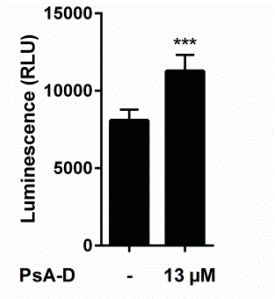

(**B**)

Figure 3.1-6. Pseudopterosin as a low molecular weight agonist of GRα.

(**A**) MDA-MB-231 cells were seeded in 6-well plates and transfected with 2 µM siRNA with the Nucleofector® 2b device using the manufacturer's protocol. After 24 h, cells first were treated with 30 µM PsA-D for 20 min and subsequently with 1 µg/mL LPS for 24 h. After another 24 h of incubation, cells were harvested and lysed for RNA isolation as preparation for further real-time PCR analysis; (**B**) Cells were seeded following manufacturer's instructions. Reporter cells stably expressing a luciferase under the control of a human GRα promotor were activated upon pseudopterosin treatment. Error bars were calculated using +SEM; (A) n = 3; (B) n = 2. *P*-values of three stars show a significance of $\rho < 0.001$, two stars $\rho < 0.01$, one star $\rho < 0.05$ and "ns." means not significant.

DISCUSSION

Though their mechanism of action remains unknown, pseudopterosins have been demonstrated as anti-inflammatory [6–8], analgesic [6,9,10], wound-healing [7,8], anti-microbial [47,48], and anti-cancer agents [16]. In our work we were able to illuminate a novel molecular mechanism of the broadly described anti-inflammatory activity of pseudopterosin by demonstrating a concentration-dependent inhibition of the NF-κB pathway based on inhibition of p65 and IκB phosphorylation.

NF-κB overexpression maintains cancer stem cell populations in the basal-subtype of breast cancer and plays a crucial role in overall cancer progression [29,49–51]. NF-κB activity is involved in epithelial-to-mesenchymal transition (EMT) [52]. Thus, previous studies have approached the inhibition of NF-κB activity in several ways: Gordon et al. suppressed NF-κB transcription in MDA-MB-231 breast cancer cells resulting in reduced osteolysis after tumor cell injection in mice combined with decreased cytokine expression [53]. Furthermore, inhibition of NF-κB activity in human breast cancer cells (MDA-MB-231 and HCC1954) reduced invasiveness and migration [52]. In conclusion, NF-κB activation blockade demonstrates effective reduction in tumor growth and progression. Our study revealed pseudopterosin to efficaciously inhibit NF-κB signaling and subsequent cytokine release in both THP-1 monocytic leukemia cells and MDA-MB-231 breast cancer cells. Furthermore, pseudopterosin has demonstrated the ability to block the inter-cell communication between immune cells and MDA-MB-231 breast cancer cells, a complex interplay presumably important within the tumor microenvironmental set-up.

Nuclear receptors like the glucocorticoid receptor α (GRα) translocate into the nucleus upon activation and bind the glucocorticoid response element (GRE) enabling the transcription of target genes ultimately resulting in immune suppression. Thus, GRα and NF-κB are transcription factors with opposing functions in regulating inflammatory responses. In cancer therapy glucocorticoids are used as a pre-treatment combined with chemotherapy to prevent vomiting and allergic reactions [32,38,54]. However, due to high variability in its expression frequency, divergent cellular functions of GRα have been described [2]. For instance, high expression levels not only lead to poor prognosis for ER^- breast cancer patients, but are also associated with better outcomes in patients with ER^+ breast cancer [55]. Suppression of chemotherapy induced apoptosis for example is correlated with high GRα expression and poor prognosis [37,55,56]. On the other hand, glucocorticoids can suppress migration, invasion and angiogenesis via down-regulation of IL-6 and IL-8. Furthermore, GRα agonism has been shown to induce drug sensitivity and apoptosis in lymphoid cancer and breast cancer [36–38].

Interestingly, there is evidence that expression of both transcription factors, NF-κB and GRα, are correlated in the context of breast cancer. While NF-κB is up-regulated [25,57], GRα over-expression could be confirmed for breast cancer, however, in contrast to NF-κB, GRα levels decreased during cancer progression [58]. Furthermore, there is evidence that NF-κB and GRα can even physically interact by hetero-dimerization [35,51]. Glucocorticoids regulate target genes by either positive or negative regulatory mechanisms. Anti-inflammatory effects are mediated via a transcription repressive function (so called transrepressive action) of GRα, whereas activation of gene transcription (namely transactivation) results in an undesirable side effect of glucocorticoids including chemoresistance, impaired wound-healing, and skin and muscle atrophy [59–61]. A previous study revealed that NF-κB inhibition is likely based on the transrepressive function of GRα [1]. Our study confirms GRα as putative pharmacological target of pseudopterosins. In conclusion, we hypothesize that the induction of GRα activation upon pseudopterosin treatment might be based on GRα acting as transrepressive on NF-κB.

As triple-negative breast cancer represents one of the diseases with a high unmet medical need resulting in a low overall survival rate, there is a need for efficacious drug treatment regimens. Our study contributes by elucidating the molecular mode of action of the striking anti-inflammatory effect of the marine diterpene glycosides PsA-D in the context of breast cancer. Thus, we demonstrate the mostly unexplored pharmaceutical potential of pseudopterosins as a promising basis for developing novel cancer treatment strategies. Future studies may include a medicinal chemistry approach to design simplified derivatives of pseudopterosin with improved potency.

MATERIALS AND METHODS

Cell Culture and Commercially Available Reagents

TNFα was purchased from Peprotech (Rocky Hill, NJ, USA). MDA-MB-231 breast cancer cells were obtained from European Collection of Authenticated Cell Cultures (Salisbury, UK) and grown in humidified atmosphere containing no CO_2 in Leibovitz's L15 medium. Medium was supplemented with 15% FCS (fetal calf serum), 2 mM glutamine, 100 units·mL^{-1} penicillin and 100 µg·mL^{-1} units streptomycin. THP-1 acute monocytic leukemia cells were purchased from the German Collection of Microorganisms and Cell Culture (Braunschweig, Germany) and cultured in the presence of 5% CO_2 in RPMI along with 10% FCS, penicillin and streptomycin. This cell line was used as a model for cells derived from the immune system. Medium and antibiotics were purchased from Gibco (Life Technologies, Carlsbad, CA, USA).

Stable Cell Line Generation

MDA-MB-231 breast cancer cells were used to create a stable cell line subsequently named NF-κB-MDA-MB-231 where the expression of a Luciferase reporter gene is under the control of a NF-κB CMV promoter. The vector was purchased from Promega (Madison, WI, USA): pNL3.2.NF-κB-RE[NlucP/NF-κB-RE/Hygro]. Cells were transfected with the nucleofector 2b device from Lonza Group AG (Basel, Switzerland) and the corresponding RCT Cell Line Kit V according to the manufacturer's protocol. Cells were cultured in DMEM supplemented with 10% FCS, 100 units·mL^{-1} penicillin and 100 units·mL^{-1} streptomycin. After transfection cells were diluted serially to obtain monoclonal cells. After colony formation hygromycin (Sigma, Munich, Germany) clones were cultivated in the presence of hygromycin.

NF-κB Reportergene Assay

To determine NF-κB activation, cells were seeded with a density of 5×10^5 cells per mL in 384-well plates using the CyBio® pipetting robot (Analytic Jens AG; Jena, Germany). After 24 h of incubation, cells were treated with different concentrations of PsA-D for 20 min. Afterwards, cells were treated with 1 µg/mL LPS or 6 ng/mL TNFα for 1 h, respectively. Luciferase activity was detected with the NanoGlo Luciferase Assay from Promega. NanoGlo Substrate and buffer were pre-mixed in 1:50 ratio and reagent was added to the wells in a 1:1 ratio and luminescence was determined immediately.

NF-κB and Human Cytokine Magnetic Bead Kit

MDA-MB-231 breast cancer cells were cultured in 10 cm dishes in 1.8×10^6 cells per mL and incubated for 24 hours at 37 °C. Before compound treatment medium was changed to serum-free medium. Cells were treated with PsA-D for 15 min, followed by incubation with 1 µg/mL LPS. Afterwards, cells were lysed with the lysis buffer provided in the NF-κB magnetic bead kit from Merck Millipore (Darmstadt, Germany) to obtain phosphorylated proteins from the nucleus. Protein concentration was determined with Bradford reagent (Roth, Karlsruhe; Germany). Samples were diluted to achieve a concentration of 0.8 mg/mL of total proteins. The subsequent protocol was according to manufacturer's instructions. MDA-MB-231 breast cancer cells and were seeded in 96-well plates in 4×10^5 cells per mL and MDA-MB-453 in 6×10^5 cells per mL and incubated for 24 hours at 37 °C. THP-1 cells were seeded in 4×10^5 cells per mL and after 1 h of incubation differentiated with 10 ng/mL PMA for 24 hours. Cells were treated with PsA-D for 20 minutes and afterwards with 1 µg/mL LPS for 24 hours. Supernatant was harvested and stored at −20 °C until measurement of cytokines. The subsequent protocol was performed according to the manufacturer's instructions with the MAGPIX® Multiplexing System from Merck Millipore (Darmstadt, Germany).

Quantitative Real-Time PCR

To determine cytokine expression levels after PsA-D treatment, the following primers were used (purchased from Eurofins, Ebersberg): IL-6 forward (GGCACTGGCAGAAAACAACC), IL-6 reverse (GCAAGTCTCCTCATTGAATCC) IL-8 forward: (ACTGAGAGTGATTGAGAGTGGAC), IL-8 reverse: (AACCCTCTGCACCCAGTTTTC), TNFα forward: (GCCTGCTGCACTTTGGAGTG), TNFα reverse: (TCGGGGTTCGAGAAGATGAT), MCP-1 forward: (CCCCAGTCACCTGCTGTTAT), MCP-1 reverse: (TGGAATCCTGAACCCACTTC), GAPDH forward: (TGCACCACCAACTGCTTAGC), GAPDH reverse: (GGCATGGACTGTGGTCATGAG), GRα forward: (AAAAGAGCAGTGGAAGGACAGCAC) GRα reverse: (GGTAGGGGTGAGTTGTGGTAACG). Total RNA was isolated with QIAGEN (Hilden, Germany) RNA Isolation Kit according to manufacturer's instructions and reverse transcriptase PCR were performed with iScript RT cDNAse Kit from BioRad (Munich, Germany). Real-time PCR was conducted with QuantiTect SYBR Green from QIAGEN (Hilden, Germany) based on the following protocol: pre-incubation at 95 °C for 900 s, amplification was performed over 45 cycles (95 °C for 15 s, 55 °C for 25 s and 72 °C for 10 s). No-template controls served as negative control. CT values were calculated according to the $2^{-\Delta\Delta}{}_{CT}$ method [62]. Sample values were normalized to the house-keeping gene GAPDH (glyceraldehyde 3-phosphate dehydrogenase).

Immunofluorecent Staining

MDA-MB-231 breast cancer cells were seeded in 1×10^5 cells per mL and incubated for 24 hours. PsA-D or dexamethasone treatment comprised 30 minutes. Cells were fixed afterwards with -10 °C cold methanol. Cells were made permeable using 0.1% Triton™ X-100. Antibodies were purchased from Santa Cruz Biotechnology (Dallas, TX, USA): primary antibody (sc-8992 GRα (H-300)) incubated 1:50 for 24 hours overnight at 4 °C and secondary antibody (sc-2012 IgG-FITC (fluorescein isothiocyanate)) was incubated 1:100 for 2.5 hours at room temperature. Cells were washed three times with PBS following each incubation step. For staining, cell nuclei 4′,6-Diamidin-2-phenylindol (DAPI, Sigma) was incubated for 5 minutes at room temperature at a concentration of 3 µM and washed three times with PBS for 5 minutes. Quantification of immunofluorescence intensity was achieved with ImageJ (v1.51k). The shape of the cells was outlined and the area, mean gray fluorescence value and integrated density measured. Several background readings were also measured. The "total corrected cellular fluorescence" (=TCCF) was calculated according to following formula: integrated density - (area of selected cell x mean fluorescence of background readings) [63]. Values of GFP staining were subtracted by values of DAPI staining to obtain cytoplasmic TCCF.

Conditioned Medium (CM) from Tumor Cells

MDA-MB-231 of THP-1 cells were cultured until 70-90% confluency. 1×10^6 cells were counted and transferred into a 25 cm^2 flask. Cells were either stimulated with 1 µg/mL LPS or without LPS as a negative control. Supernatant was collected after 24 hours, centrifuged and sterile filtered. Conditioned medium was stored at -80 °C. MDA-MB-231 or THP-1 cells were seeded at 1×10^6 cells per mL in 6-well plates and incubated for 24 hours. PsA-D was added at a concentration of 30 µM for 20 minutes followed by 25 volume percentage of tumor-conditioned medium for 5 hours. Cells were then harvested and RNA isolated for further analysis in real-time PCR.

Knock-Down Studies

TLR4 siRNA s14194 and Silencer® Select Negative Control No. 2 siRNA was purchased from Life Technologies (Darmstadt, Germany). Glucocorticoid receptor (GRα) siRNA was purchased from Santa Cruz Biotechnology (Dallas, TX, USA). SiRNA transfection (2 µM of siRNA) was performed using Lipofectamine3000 from Invitrogen (Carlsbad, CA, USA) according to manufacturer's protocol.

GRα Reportergene Assay

Reportergene assay based on non-human stable cells containing constitutive high-level expression of full-length human GRα (NR3C1) were purchased from Indigo Biosciences (State College, PA, USA). Assay was performed according to manufacturer's instructions. PsA-D was added to cells according to the agonist assay described in the protocol and incubated for 24 h at 37 °C.

Preparation of PsA-D Mixture

A. elisabethae was collected from South Bimini Island, The Bahamas, was dried and extracted in EtOAc/MeOH (1:1) for 48 h. The crude extract was subjected to silica gel chromatography eluting with hexanes and EtOAc to afford a mixture of PsA-D. The ratio was determined to be 85:5:5:5 (PsA:B:C:D) by LC-MS analysis.

Statistical Analysis

Obtained data represent at least three independent experiments. Error bars show ±SEM of the means of triplicate values. Statistical analysis was calculated using one-way-ANOVA followed by Dunnett's multiple comparisons test. When groups were compared with a control and/or comparison of mean values of only two groups, an unpaired student's t-Test was applied.

P<0.05 was chosen to define statistically significant difference. Figures and data analysis were generated with Graphpad Prism v. 6.07 (Graphpad Software, San Diego, CA, USA).

Supplementary Materials: The following are available online at www.mdpi.com/1660-3397/15/9/262/s1, Figure S1: Pseudopterosin inhibits activation of NF-κB after two different stimuli, Figure S2: Pseudopterosin blocked phosphorylation of p65 and IkBα after TNFα stimulation; Table S1: Inhibition of cytokine release in MDA-MB-453 triple negative breast cancer cells.

Acknowledgments: The research project is financed by a grant of Nicole Teusch provided by the Ministry of Innovation, Science and Research of the federal state of North Rhine-Westphalia, Germany. Furthermore, the Ph.D. training of Julia Sperlich is financed by the graduate program in Pharmacology and Experimental Therapeutics at the University of Cologne which is financially and scientifically supported by Bayer. Russel Kerr would like to thank the Government of The Bahamas for permission to collect *Antillogorgia elisabethae*.

Author Contributions: Nicole Teusch and Julia Sperlich developed the scientific concept and designed the experiments. Julia Sperlich performed the experiments and analyzed the data. Russell Kerr provided the pseudopterosin extract and reviewed the manuscript. Nicole Teusch and Julia Sperlich wrote the manuscript.

REFERENCES

1. P. Moutsatsou, A. G. Papavassiliou, *J. Cell. Mol. Med.* **2008**, *12*, 145–63.
2. L. Belova, B. Delgado, M. Kocherginsky, A. Melhem, O. Olopade, S. Conzen, *Breast Cancer Res. Treat.* **2015**, *116*, 441–447.
3. S. K. Pal, B. H. Childs, M. Pegram, *Breast Cancer Res. Treat.* **2011**, *125*, 627–636.
4. M. J. Abad, P. Bermejo, *Stud. Nat. Prod. Chem.* **2001**, *25*, 683–755.
5. F. Berrué, M. W. B. McCulloch, R. G. Kerr, *Bioorganic Med. Chem.* **2011**, *19*, 6702–6719.
6. A M. Mayer, P. B. Jacobson, W. Fenical, R. S. Jacobs, K. B. Glaser, *Elsevier Sci.* **1998**, *62*, PL401-L407.
7. H. Correa, A. L. Valenzuela, L. F. Ospina, C. Duque, *J. Inflamm. (Lond).* **2009**, *6*, 5.
8. A. Ata, R. G. Kerr, C. E. Moya, R. S. Jacobs, *Tetrahedron* **2003**, *59*, 4215–4222.
9. S. a. Look, W. Fenical, G. K. Matsumoto, J. Clardy, *J. Org. Chem.* **1986**, *51*, 5140–5145.
10. S. A. Look, W. Fenical, R. S. Jacobst, J. O. N. Clardyt, R. S. Jacobs, J. Clardy, R. S. Jacobst, J. O. N. Clardyt, *Proc. Natl. Acad. Sci* **1986**, *83*, 6238–6240.
11. S. L. Caplan, B. Zheng, K. Dawson-Scully, C. A. White, L. M. West, *Mar. Drugs* **2016**, *14*, 1–14.
12. D. J. Newman, G. M. Cragg, *J. Nat. Prod.* **2004**, *67*, 1216–1238.
13. A. M. S. Mayer, K. B. Glaser, C. Cuevas, R. S. Jacobs, W. Kem, R. D. Little, J. M. Mcintosh, D. J. Newman, B. C. Potts, D. E. Shuster, *Trends Pharmacol. Sci.* **2010**, *31*, 255–265.
14. A. M. S. Mayer, A. D. Rodriguez, R. G. S. Berlinck, M. T. Hamann, *Comp. Biochem. Physiol. - Part C Toxicol. Pharmakology* **2008**, *145*, 553–581.
15. C. E. Moya, R. S. Jacobs, *Comp. Biochem. Physiol. - C Toxicol. Pharmacol.* **2006**, *143*, 436–443.
16. I. I. Rodríguez, Y. P. Shi, O. J. García, A. D. Rodríguez, A. M. S. Mayer, J. a. Sánchez, E. Ortega-Barria, J. González, *J. Nat. Prod.* **2004**, *67*, 1672–1680.

17. C. Badr, J. M. Niers, L.-A. Tjon-Kon-Fat, D. P. Noske, T. Wurdinger, B. Tannous, *Mol Imaging* **2009**, *8*, 278–290.
18. T. Kawai, S. Akira, *Nat. Immunol.* **2010**, *11*, 373–384.
19. L. Ramage, Expression of Pro-Inflammatory Proteins in the Lung Epithelial Cell Line A549, in Response to Cytokine, and Environmental Particle Exposure., Edinburgh Napier University, **2003**.
20. V. Blank, P. Kourilsky, A. Israel, E. S. Publishers, *Elsevier Sci. Publ.* **1992**, 135–140.
21. P. a Baeuerle, D. Baltimore, *Cell* **1988**, *53*, 211–217.
22. F. Balkwill, *Cancer Metastasis Rev.* **2006**, *25*, 409–16.
23. L. Zhang, K. Blackwell, A. Altaeva, Z. Shi, H. Habelhah, *Mol. Biol. Cell* **2010**, *22*, 128–140.
24. N. D. Perkins, *Nat. Rev. Mol. Cell Biol.* **2007**, *8*, 49–62.
25. C. Cai, Z. Yao, *Chinese J. Clin. Oncol.* **2006**, *3*, 5–10.
26. X. Zhao, X. Sun, F. Gao, J. Luo, Z. Sun, *J. Exp. Clin. Cancer Res.* **2011**, *30*, 22.
27. M. Park, J. Hong, *Cells* **2016**, *5*, 15.
28. K. Shostak, A. Chariot, *Breast Cancer Res.* **2011**, *13*, 214.
29. S. Becker-Weimann, G. Xiong, S. Furuta, J. Han, I. Kuhn, U.-D. Akavia, D. Pe'er, M. J. Bissell, R. Xu, *Oncotarget* **2013**, *4*, 2010–2020.
30. M. J. Bissell, D. Radisky, *Nat. Rev. Cancer* **2001**, *1*, 46–54.
31. M. Mestdagt, M. Polette, G. Buttice, A. Noël, A. Ueda, J. Foidart, *Int. J. Cancer* **2006**, *118*, 35–42.
32. B. D. Keith, *BMC Cancer* **2008**, *8*, 84.
33. M. Skor, E. Wonder, M. Kocherginsky, A. Goyal, B. Hall, Y. Cai, S. Conzen, *Clin. Cancer Res.* **2012**, *100*, 130–134.
34. I. B. Mitre-Aguilar, A. J. Cabrera-Quintero, A. Zentella-Dehesa, *Int. J. Clin. Exp. Pathol.* **2015**, *8*, 1–10.
35. L. I. McKay, J. A. Cidlowski, *Endocr. Rev.* **1999**, *20*, 435–459.
36. S. Schmidt, J. Rainer, C. Ploner, E. Presul, S. Riml, R. Kofler, *Cell Death Differ.* **2004**, *11*, 45–55.
37. K. T. Lin, L. H. Wang, *Steroids* **2016**, *111*, 84–88.
38. F. Buxant, N. Kindt, G. Laurent, J. Noel, S. Saussez, *Mol. Med. Rep.* **2015**, 4051–4054.
39. M. Mehmeti, R. Allaoui, C. Bergenfelz, L. H. Saal, S. P. Ethier, M. E. Johansson, K. Jirström, K. Leandersson, *Breast Cancer Res.* **2015**, *17*, 130.
40. S. Akira, S. Uematsu, O. Takeuchi, *Cell* **2006**, *124*, 783–801.
41. P. P. Tak, G. S. Firestein, *J. Clin. Invest.* **2001**, *107*, 7–11.
42. H. L. Pahl, *Oncogene* **1999**, *18*, 6853–6866.
43. A. Kumar, Y. Takada, A. Boriek, B. Aggarwal, *J. Mol. Med.* **2004**, *82*, 434–448.
44. S. Schütze, K. Potthoff, T. Machleidt, *Cell* **1992**, *71*, 765–776.
45. K. Miyake, *Trends Microbiol.* **2004**, *12*, 186–192.
46. H. Wajant, P. Scheurich, *FEBS J.* **2011**, *278*, 862–876.
47. H. Correa, F. Aristizabal, C. Duque, R. Kerr, *Mar. Drugs* **2011**, *9*, 334–344.
48. A. Ata, H. Y. Win, D. Holt, P. Holloway, E. P. Segstro, G. S. Jayatilake, *Helv. Chim. Acta* **2004**, *87*, 1090–1098.
49. M. Yamamoto, Y. Taguchi, T. Ito-kureha, K. Semba, N. Yamaguchi, J. Inoue, *Nat. Commun.* **2013**, *4*, 1–13.
50. N. Yamaguchi, T. Ito, S. Azuma, E. Ito, R. Honma, Y. Yanagisawa, A. Nishikawa, M. Kawamura, J. ichi Imai, S. Watanabe, et al., *Cancer Sci.* **2009**, *100*, 1668–1674.
51. J. Ling, R. Kumar, *Cancer Lett.* **2012**, *322*, 119–126.
52. B. R. B. Pires, A. L. Mencalha, G. M. Ferreira, W. F. de Souza, J. A. Morgado-Díaz, A. M. Maia, S. Corrêa, E. S. F. W. Abdelhay, *PLoS One* **2017**, *12*, e0169622.
53. A. H. Gordon, R. J. O'Keefe, E. M. Schwarz, R. N. Rosier, J. E. Puzas, *Am. Assoc. Cancer Res.* **2005**, *65*, 3209–3218.
54. H. P. Rutz, *Lancet* **2002**, *360*, 1969–1970.
55. D. Pan, M. Kocherginsky, S. D. Conzen, *Cancer Res.* **2011**, *71*, 6360–6370.

56. S. K. Mondal, S. Jinka, K. Pal, S. Nelli, S. K. Dutta, E. Wang, A. Ahmad, K. M. AlKharfy, D. Mukhopadhyay, R. Banerjee, *Mol. Pharm.* **2016**, *13*, 2507–2523.
57. D. C. Radisky, M. J. Bissell, *Nat. Cell Biol.* **2007**, *9*, 361–363.
58. R. Abduljabbar, O. H. Negm, C.-F. Lai, D. A. Jerjees, M. Al-Kaabi, M. R. Hamed, P. J. Tighe, L. Buluwela, A. Mukherjee, A. R. Green, et al., *Breast Cancer Res. Treat.* **2015**, *150*, 335–346.
59. G. P. Chrousos, T. Kino, *Sci. Signal.* **2005**, *2005*, pe48-pe48.
60. K. De Bosscher, W. Vanden Berghe, G. Haegeman, *Endocr. Rev.* **2003**, *24*, 488–522.
61. T. Kino, M. U. De Martino, E. Charmandari, M. Mirani, G. P. Chrousos, *J. Steroid Biochem. Mol. Biol.* **2003**, *85*, 457–467.
62. K. J. Livak, T. D. Schmittgen, *Methods* **2001**, *25*, 402–408.
63. R. A. McCloy, S. Rogers, C. E. Caldon, T. Lorca, A. Castro, A. Burgess, *Cell Cycle* **2014**, *13*, 1400–1412.

3.1.1 Supplemental Material

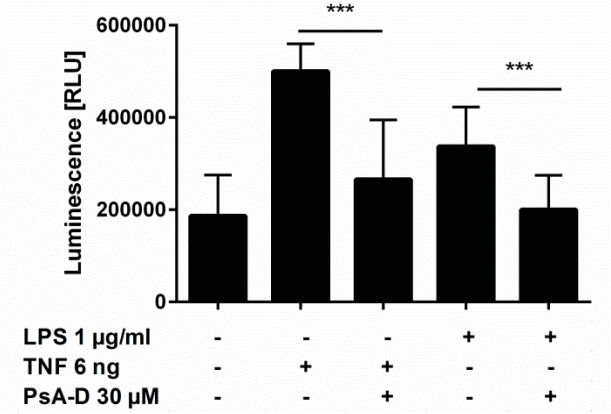

Supplemental Figure 3.1-1. PsA-D inhibited activation of NF-κB in the presence of two different stimuli.

Cells are stably transfected with a NF-κB-Luc reporter gene. PsA-D treatment was performed for 20 minutes following 1 µg/mL LPS incubation for 1 hour. Error bars were calculated using +SEM; n=3. Three stars show a significance of ρ<0.001.

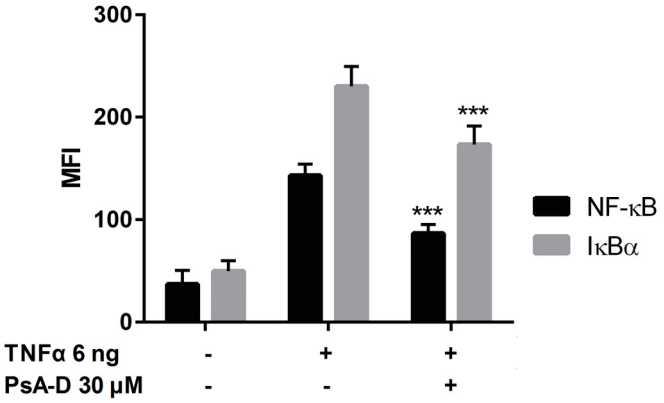

Supplemental Figure 3.1-2. PsA-D blocked phosphorylation of NF-κB/p65 and IκBa.

MDA-MB-231 cells were seeded in a 10 cm dish. Cells were incubated with 30 µM PsA-D for 15 minutes followed by a treatment with 1 µg/mL TNFα for 15 minutes. Cells were lysed and protein concentration was measured with Bradford Reagent. A total protein amount of 0.8 mg/mL was used. Control cells were treated

with DMSO in the same amounts as PsA-D. Error bars were calculated using +SEM; n=3. *P*-values of three stars show a significance of ρ<0,001.

Supplemental Table 3.1-1. Inhibition of cytokine release in MDA-MB-453 triple negative breast cancer cells.

MDA-MB-453 cells were seeded at a density of 6×10^6 cells per mL. 30 µM PsA-D was incubated for 20 minutes followed by incubation with 20 ng/mL TNFα. Cytokine amounts were analyzed in supernatants after 24 hours incubation time. No treatment serves as a control. Values were normalized to TNFα treatment and set to 100 % ±SD. % inhibition reflects the percentage of the amount of cytokines reduced by PsA-D treatment compared to TNFα. *P*-values were analyzed according to student's t-test; n=3.

MDA-MB-453	Control %	+TNFα %	+PsA-D %	*P*-values	% Inhibition
IL-8	4,7 (±5,5)	100.5 (±24,9)	51,7 (±14,0)	0,012	48.9
MCP-1	17.3 (±11.6)	97.4 (±7.9)	87.2 (±14.1)	0.43	10.2

3.1.2 Appendix to Supplemental Material

Supplemental Table 3.1-2. Pseudopterosin inhibited cytokine release more effectively than indomethacin in MDA-MB-231 cells.

Cells were seeded at a density of 4×10^5 cells per mL in 96-well plates. After 24 hours, the cells were incubated with either 30 µM of PsA-D or 30 µM of indomethacin for 20 minutes followed by treatment of 50 ng/mL LPS for 24 hours. Cytokine content was analyzed in the supernatant on the basis of a standard curve with the MAGPIX multiplexing system from Merck after manufacturers' protocol. IL-4 and IL-1β could not be detected in the supernatant. PsA-D showed a more effective inhibition (IL-6 38.3 %, IL-8 40.8 %, MCP-1 85.2 %, TNFα 75.3 %) of at least three cytokines compared to indomethacin treatment (IL-6 44.3 %, IL-8 29.7 %, MCP-1 40.6 %, TNFα 60.7 %). *P*-values were calculated compared to LPS using one-way-ANOVA followed by Dunnett's multiple comparisons test. Data represent means of triplicates of three independent experiments ±SEM.

	Control (pg/mL)	50 ng/mL LPS	30 µM PsA-D	30 µM Indomethacin	*P*-values PsA-D	Indom.
IL-6	1626 (±144)	4662 (±307)	2875 (±611)	2595 (±483)	0.0001	0.0001
IL-8	2791(±1442)	15.180 (±592)	8976 (±2411)	10.672 (±1324)	0.0002	0.0016
MCP-1	325 (±260)	1626 (±541)	241 (±101)	966 (±449)	0.008	0.169
TNFα	1.9 (±0.6)	29.1(±5.5)	7.2 (±3.4)	11.4 (±1.7)	0.0001	0.0004

Supplemental Table 3.1-3. Pseudopterosin inhibited cytokine release in A549 small lung cancer cells.

Cells were seeded at a density of 4×10^5 cells per mL in 96-well plates. After 24 hours, the cells were incubated with either 30 µM of PsA-D or 30 µM of indomethacin for 20 minutes followed by treatment of 50 ng/mL LPS for 24 hours. Cytokine content was analyzed in the supernatant on the basis of a standard curve with the MAGPIX multiplexing system from Merck after manufacturers' protocol. TNFα, IL-4 and IL-1β could not be detected in the supernatant. *P*-values were calculated compared to LPS treatment using one-way-

ANOVA followed by Dunnett's multiple comparisons test. PsA-D and indomethacin inhibit IL-8 and MCP-1 significantly. PsA-D showed a more effective inhibition of at least two cytokines (IL-6 by 5.8%, IL-8 by 46.5% and MCP-1 by 26.9%) compared to indomethacin (IL-6 by 0%, IL-8 by 33.3% and MCP-1 by 46.3%). 'Indom.' represents indomethacin. Data represent means of triplicates of three independent experiments ±SEM.

	Control (pg/mL)	**50 ng/mL LPS**	**30 µM PsA-D**	**30 µM Indomethacin**	***P*-values PsA-D**	**Indom.**
IL-6	11.7 (±2.7)	14.8 (±2.9)	13.9 (±3.0)	16.0 (±4.7)	0.98	0.93
IL-8	1913 (±377)	3433 (±769)	1838 (±509)	2289 (±222)	0.0088	0.015
MCP-1	6710 (±268)	8020 (±994)	5864 (±1048)	4308 (±891)	0.0021	0.0001

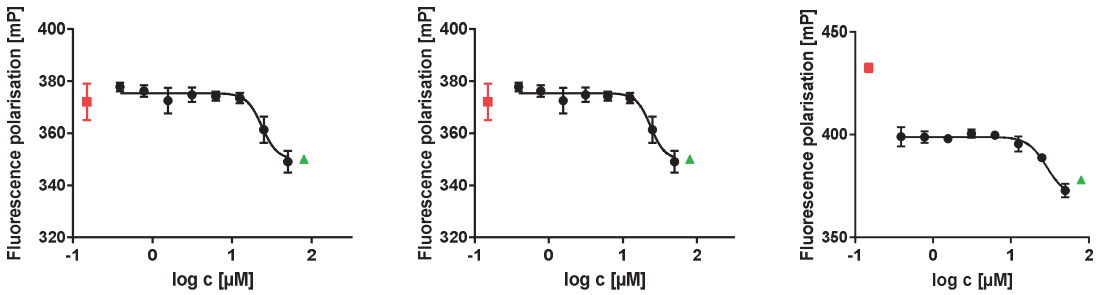

Supplemental Figure 3.1-3. *In vitro* binding study of pseudopterosin to GRα reveals dose-dependency.

Increasing doses of pseudopterosin, starting at 50 µM, shows a binding to GRα in a PolarScreen *in vitro* assay. Using a gain of 1.598 we calculated an IC_{50} value of 25.5 µM out of three independent measurements. First, second and third measurements with single IC_{50} values of 24.0, 23.6 and 28.8 µM are shown separately. Red square shows maximal and green triangle minimal possible fluorescence polarization.

molecules

MDPI

3.2 Pseudopterosin Inhibits Proliferation and 3D Invasion in Triple Negative Breast Cancer by Agonizing Glucocorticoid Receptor Alpha

Julia Sperlich and Nicole Teusch

Bio-Pharmaceutical Chemistry & Molecular Pharmacology, Faculty of Applied Natural Sciences, Technische Hochschule Köln, 51373 Leverkusen, Germany;

ABSTRACT

Pseudopterosin, produced by the sea whip of the genus *Antillogorgia*, possesses a variety of promising biological activities including potent anti-inflammatory effects. However, few studies examined pseudopterosin in the treatment of cancer cells and, to our knowledge, the ability to inhibit triple negative breast cancer (TNBC) proliferation or invasion have not been explored. Thus, we evaluated the as yet unknown mechanism of action of pseudopterosin: Pseudopterosin was able to inhibit proliferation of TNBC. Interestingly, analyzing breast cancer cell proliferation after knocking down glucocorticoid receptor α (GRα) revealed that anti-proliferative effects of pseudopterosin were significantly inhibited when GRα expression was reduced. Furthermore, pseudopterosin inhibited invasion of MDA-MB-231 3D tumor spheroids embedded in an extracellular-like matrix. Remarkably, the knockdown of GRα in 3D tumor spheroids revealed increased ability of cells to invade the surrounding matrix. In a co-culture, encompassing peripheral blood mononuclear cells (PBMC) and MDA-MB-231 cells, production of interleukin 6 (IL-6) and interleukin 8 (IL-8) significantly increased compared to monoculture. Notably, pseudopterosin indicated to block cytokine elevation, representing key players in tumor progression, in the co-culture. Thus, our results reveal pseudopterosin treatment as a potential novel approach in TNBC therapy.

INTRODUCTION

Breast cancer is still the most common malignancy in woman with one million cases annually worldwide [1]. Of these, approximately 15% belongs to the triple-negative ($ER^-/PR^-/HER2^-$) breast cancer (TNBC). TNBC represents the most aggressive breast cancer type, characterized by high proliferation rate, a pronounced potential to metastasize and a shorter survival rate [2-4]. Furthermore, TNBC lacks effective therapies available for other breast cancer subtypes

underlining the significant unmet medical need for identifying novel targets and developing innovative drugs.

The tumor microenvironment is increasingly recognized as a major regulator of carcinogenesis. In breast cancer, tumor associated macrophages (TAMs) enhance proliferation and metastasis as well as resistance to chemotherapy by activation of the transcription factor nuclear factor κB (NF-κB), a key factor in regulating inflammatory responses [5,6]. High expression levels of the NF-κB target genes interleukin 6 (IL-6) or interleukin 8 (IL-8) secreted by macrophages can be correlated with advanced growth of TNBC and poor prognosis [7]. The pseudopterosins, a family of 31 known related diterpene glycosides, are produced by the sea whip *Antillogorgia elisabethae* (formerly named *Pseudopterosin e.*) [8]. Striking biological activities have been described ranging from anti-inflammation [9-11], wound-healing [10,11], analgesia-reducing [9,12,13] to neuromodulation [14]. In contrast, to date, little is known regarding anti-tumor effects of pseudopterosin, where only one derivative showed moderate cytotoxic effects on ER^+ breast cancer cells and non-small-cell lung cancer cells [15].

Previously, we have described the potential of pseudopterosin as a novel immune modulator in TNBC acting via NF-κB inhibition and subsequent blockade of cytokine secretion [16]. Moreover, we identified inhibitory capabilities of pseudopterosin on the NF-κB signaling pathway by agonizing the glucocorticoid receptor α (GRα) [16]. Accordingly, there is evidence that NF-κB and GRα can physically interact and hetero-dimerize in breast cancer [17]. By binding other transcription factors such as NF-κB, GRα can either transactivate or -suppress its target genes [18]. Although glucocorticoids (GCs) are frequently used to relieve symptoms of cancer treatment related side effects, contradictory effects on breast cancer progression upon GC treatment and with respect to GRα expression have been described [19–21]. High expression levels of GRα in ER^- breast cancer might be associated with drug resistance resulting in an unfavorable clinical outcome [22–24]. In contrast, a recent analysis demonstrates improved survival independent of the ER status in breast cancer patients receiving GC combined with adjuvant anthracycline-based chemotherapy [25]. Thus, in the current study we further elucidated the role of GRα in TNBC progression, thereby focusing on pseudopterosin as a novel agent for breast cancer therapy.

RESULTS

Pseudopterosin Inhibited Proliferation of Triple Negative Breast Cancer Cells

In our previous work we identified the natural product pseudopterosin as a novel inhibitor of NF-κB signaling [16], one key pathway in controlling progression of TNBC. As NF-κB is known to

regulate various processes in cancer progression such as proliferation, angiogenesis or invasion [26–28], the aim of the current study was to further characterize the pharmacological properties of pseudopterosin. First, we investigated a pseudopterosin extract (PsA-D) regarding its effect on breast cancer cell proliferation in MDA-MB-231 cells. To remain within a non-toxic concentration range of PsA-D (IC_{50} values of cell viability for PsA-D after 24 hours or 48 hours of treatment were 31.4 µM and 32.2 µM, respectively; Supplemental Figure 3.2-1A/B), 7.5 and 15 µM of PsA-D were chosen to evaluate anti-proliferative effects (Figure 3.2-1A). As expected, MDA-MB-231 cells treated with DMSO showed a high proliferation rate, represented by a confluency of 78% after 48 hours (Figure 3.2-1A). Notably, a concentration of 15 µM of PsA-D was able to reduce proliferation significantly after 24 hours by 1.9 fold and after 48 hours by 1.6 fold compared to DMSO control (Figure 3.2-1B and Figure 3.2-1C). Furthermore, preliminary data indicate that pseudopterosin-induced reduction of proliferation is not pERK dependent (Supplemental Figure 3.2-3), which is a key regulator for cell proliferation in principle [29].

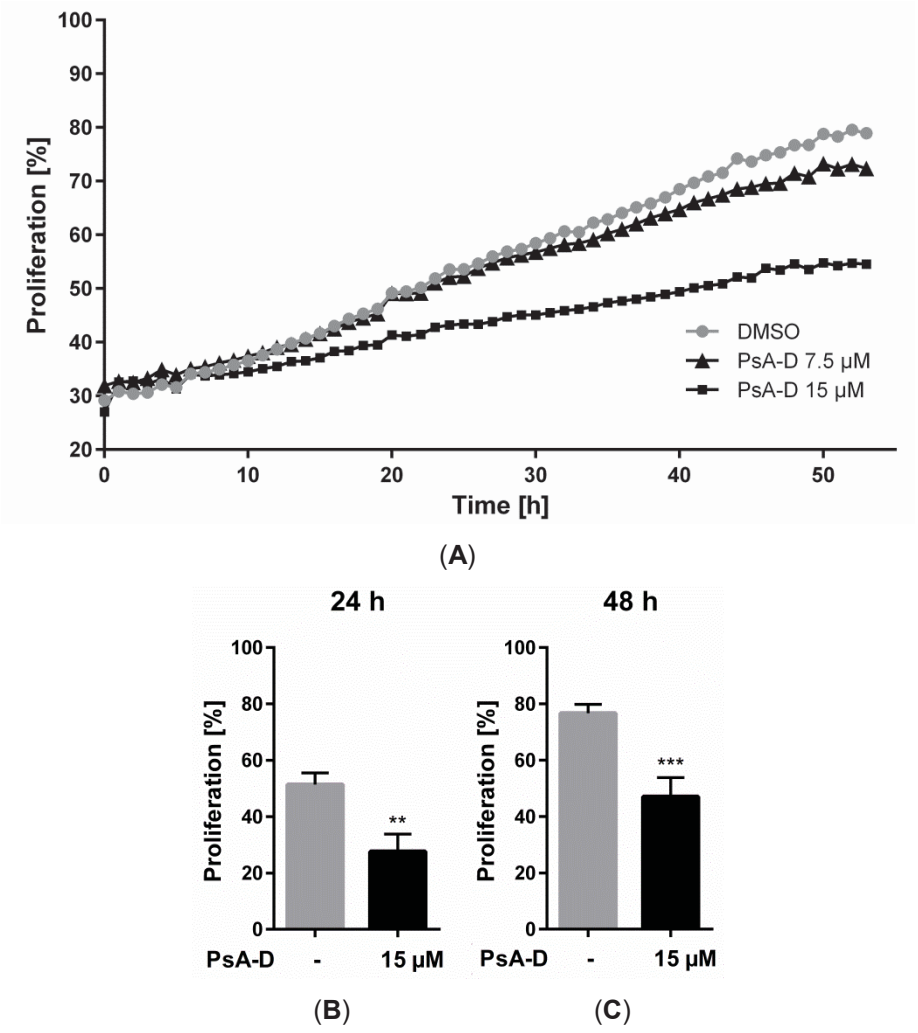

Figure 3.2-1. Pseudopterosin inhibited proliferation in triple negative breast cancer cells.

(**A**) Proliferating cells were imaged every hour over a time range of 50 hours with the IncuCyte® ZOOM. Confluency of cells was determined with IncuCyte® software indicated as proliferation in percentage. Cells were treated with either 7.5 µM (triangle) or 15 µM (square) of PsA-D. (**B-C**) Inhibition of proliferation is shown at selected time points of 24 and 48 hours compared to DMSO control, respectively. The data represent means of three independent experiments. Error bars were calculated using ±SEM. *P*-values were calculated against DMSO control. Two stars represent a significance of $\rho<0.01$ and three stars represent a significance of $\rho<0.001$.

Glucocorticoid Receptor Alpha Expression is Essential for Anti-Proliferative Effects of Pseudopterosin

In our previous work we hypothesized pseudopterosin to act as an agonist of the glucocorticoid receptor alpha (GRα) [16]. Subsequently, when downregulating GRα, pseudopterosin failed to inhibit NF-κB target gene expression. Thus, to further explore the role of GRα in the mode-of-action of pseudopterosin, we analyzed the effect of a GRα knockdown on breast cancer cell proliferation. After 72 and 85 hours, treatment with PsA-D inhibited proliferation in non-coding siRNA (nc siRNA) transfected cells by 2 fold, respectively (Figure 3.2-2A and Supplemental Figure 3.2-4). Importantly, in siGRα transfected cells, PsA-D lost its anti-proliferative effect (Figure 3.2-2A). Efficiency of the GRα knockdown using realtime qPCR (up to 88%) is exemplified in Figure 3.2-2B and depicted on the protein level via immunofluorescence analysis in Figure 3.2-2C. In conclusion, our data suggests that GRα expression might be crucial for the anti-proliferative effects of PsA-D. Notably, treatment with the marked GRα ligand dexamethasone showed less potency in reducing proliferation: after 48 hours, PsA-D resulted in a 21% proliferation decrease, whereas 100 nM dexamethasone reduced proliferation by 15% compared to DMSO, respectively (Figure 3.2-2C). After 72 hours, PsA-D treatment diminished proliferation by 20%, whereas treatment with 100 nM dexamethasone reduced the proliferation rate by only 9% (Figure 3.2-2D).

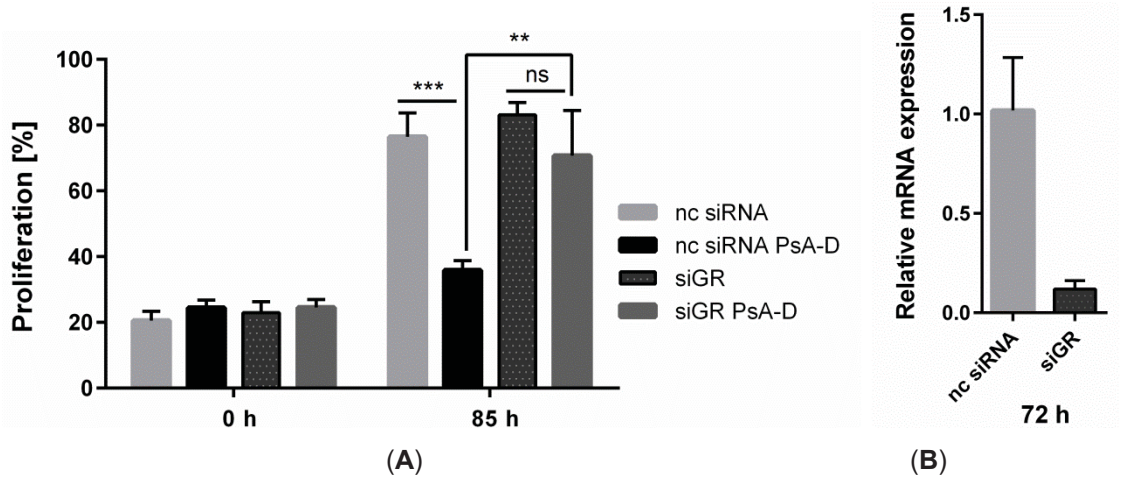

(**A**) (**B**)

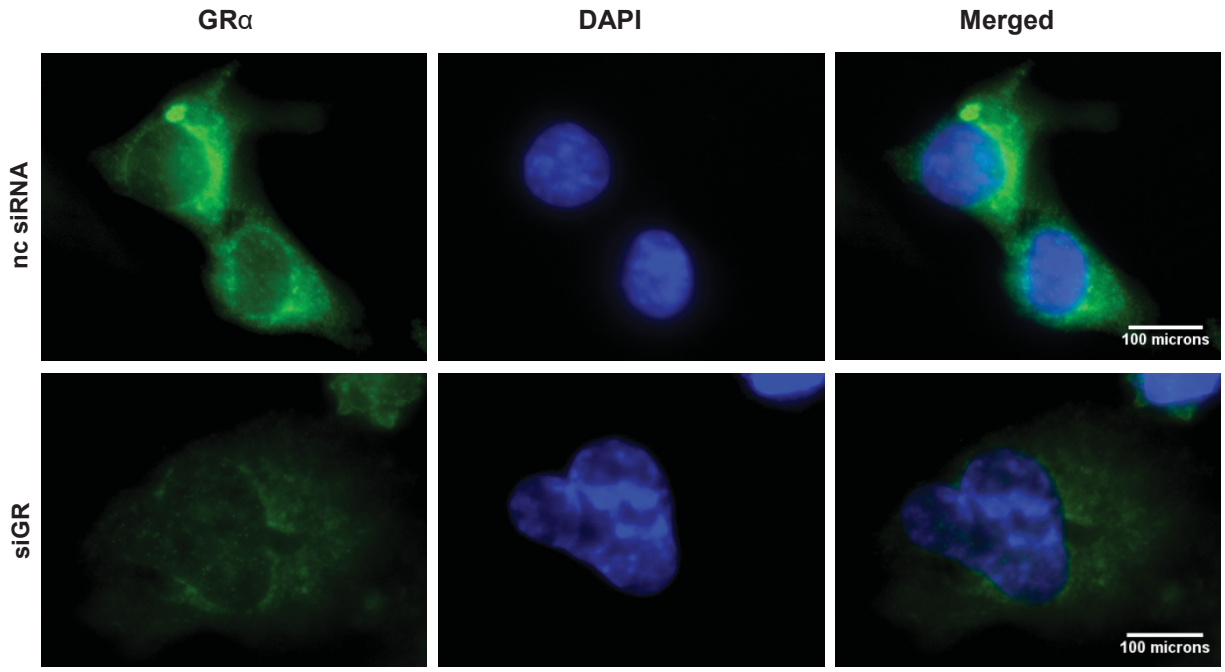

(**C**)

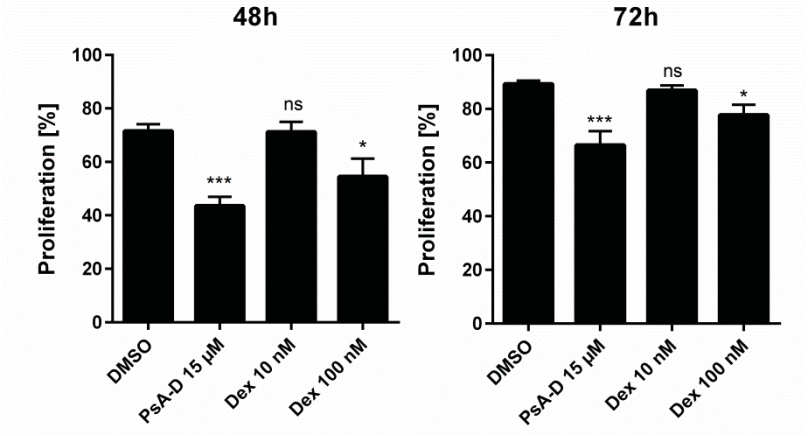

(**D**) (**E**)

Figure 3.2-2. Pseudopterosin failed to inhibit breast cancer cell proliferation after knockdown of the glucocorticoid receptor alpha (GRα) and inhibited proliferation of MDA-MB-231 more efficaciously than dexamethasone (Dex).

(**A**) Knockdown of GRα was done with the Lonza Nucleofector 2b device on day one. On day two, the cells were seeded and proliferating cells were imaged with the IncuCyte® ZOOM every hour over a time range of five days. Cell proliferation was determined with IncuCyte® software indicated in percentage. Cells were treated with a concentration of 15 µM of PsA-D. (**B**) After knockdown of GRα, expression of GRα reduced up to 88.3%, which was confirmed by qPCR analysis at 72 hours. (**C**) Immunofluorescent analysis of GRα knockdown after 72 hours. Scale bars in white show 100 microns in length. (**D-E**) PsA-D inhibited proliferation after 48 and 72 hours more efficaciously than dexamethasone. The data represent means of three independent experiments. Error bars were calculated using ±SEM. Three stars represent a significance of $\rho<0.001$ and two stars of $\rho<0.01$.

Pseudopterosin Inhibited Invasion into 3D Matrix

Breast tumors harbor many devastating characteristics resulting in poor prognosis of patients: high proliferation rate and high histological grade. Furthermore, genetic and epigenetic alterations enable breast cancer cells to migrate and invade the surrounding tissue via a process known as epithelial-to-mesenchymal transition (EMT) [30]. To explore the effects of pseudopterosin on the invasiveness of MDA-MB-231 cells, we developed a 3D invasion assay, where the cancer cells form a micro-tumor spheroid embedded in extracellular matrix. In the presence of DMSO, the cells immediately started to invade into the 3D matrix by partly disassembling the spheroid core (Figure 3.2-3A). In contrast, treatment with PsA-D significantly inhibited the invasion of single cells into the matrix. After 24 hours, the invasive area was reduced significantly by 59%, after 48 hours by 53% and after 72 hours by 73% (Figure 3.2-3B-D). Importantly, spheroid growth did not change after PsA-D treatment (Supplemental Figure 3.2-5). Thus, in our experiment we verified the inhibitory properties of pseudopterosin in a 3D assay on TNBC progression, thereby hinting at a better prediction for future *in vivo* tumor models with this natural product.

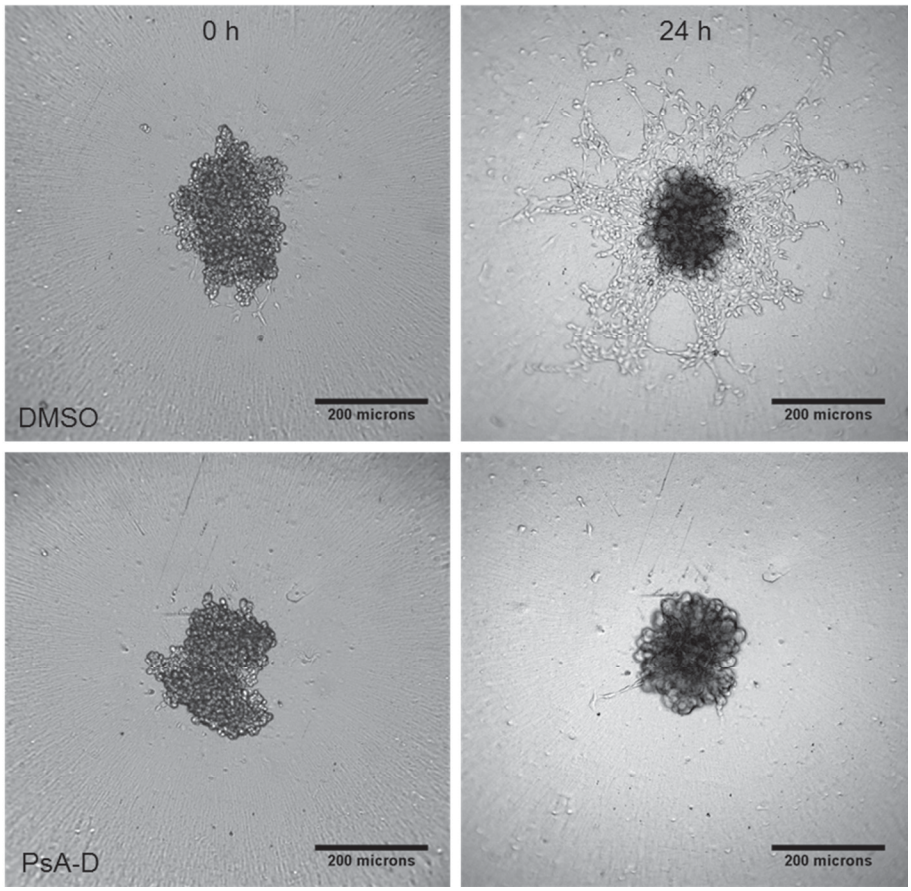

(**A**)

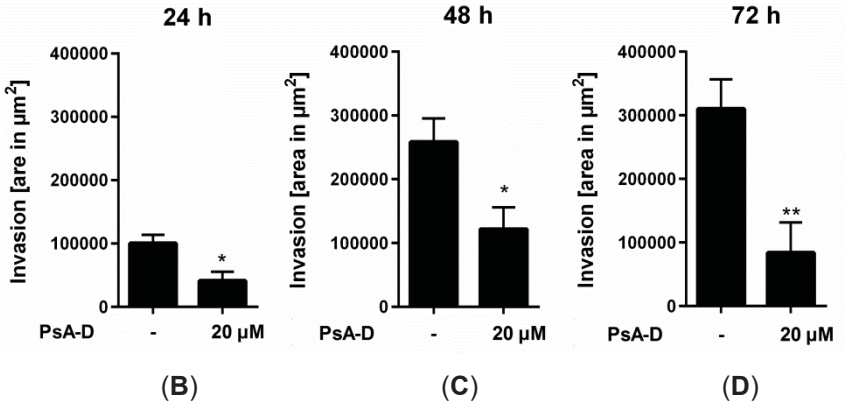

Figure 3.2-3. Pseudopterosin inhibited invasion into a 3D matrix.

(**A**) Representative images of invasion of cells into a 3D matrix at 24 hours' time point. Cells were imaged with IncuCyte® ZOOM over a time range of three days. 3×10^3 cells per well were seeded into ULA round bottom plates and spheroids were formed for 72 hours. Scale bars in black show 200 microns in length. (**B-D**) The bar diagrams show three different time points representing six independent experiments. Spheroids were treated with a concentration of 20 µM of PsA-D. Error bars were calculated using ±SEM. *P*-values were calculated against DMSO. Two stars represent a significance of $\rho<0.01$ and one star represents a significance of $\rho<0.05$.

Down-Regulation of Glucocorticoid Receptor Alpha Expression Increased Invasiveness in TNBC

The clinical use of glucocorticoids (GC) is discussed controversially, due to extensive side effects, chemotherapy resistance and survival of cancer cells [21,23,31]. However, recent literature indicates the beneficial effects of GCs to be strongly dependent on the tumor entity: survival in patients receiving GC combined with anthracycline-based chemotherapy was improved [25]. In this context, we further investigated the role of GRα in the invasiveness of MDA-MB-231 micro-tumor spheroids (Figure 3.2-4A). The efficiency in GRα knockdown is represented by a reduction of 94% (Figure 3.2-4C). After 72 hours, the spheroids transfected with siGRα showed a significant increase in invasion by 27% compared to nc siRNA (Figure 3.2-4B). In conclusion, the knockdown of GRα led to an elevation of invasiveness in MDA-MB-231 cells, suggesting a potential of GRα agonists like pseudopterosin in diminishing TNBC progression.

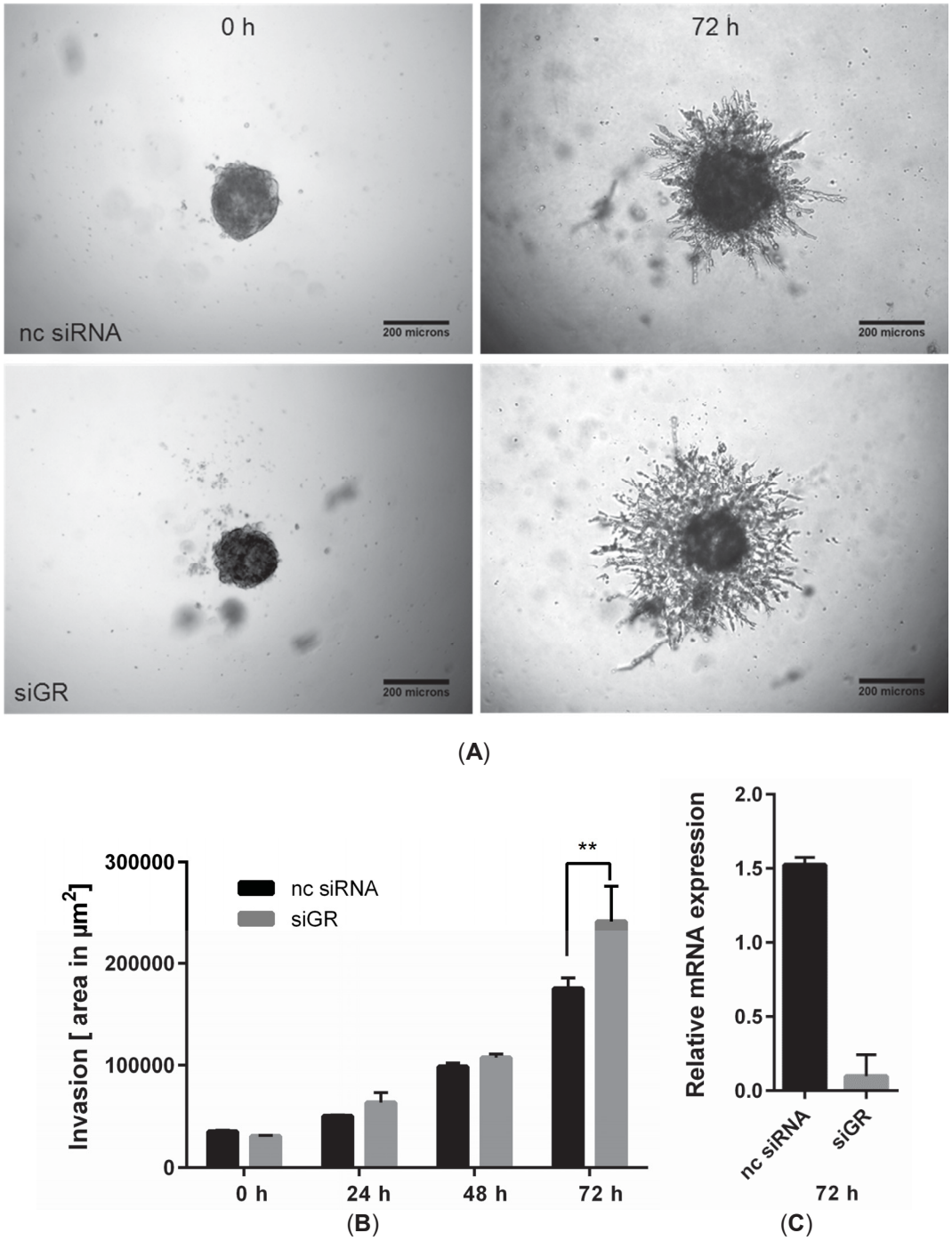

Figure 3.2-4. Knockdown of the glucocorticoid receptor alpha (GRα) increased invasiveness of triple negative breast cancer.

(**A**) Representative images of tumor cell invasion into a 3D matrix. Knockdown of GRα was performed with the Lonza Nucleofector 2b device on day one. On day three, 3×10^3 cells per well were seeded into ultra-low-attachment (ULA) round bottom plates. Formation of spheroids was allowed for 72 hours. At t= 0, matrigel was added to the spheroids to start invasion. Scale bars in black show 200 microns in length. (**B**) The invasion is depicted over a time range of three days and the area of invaded cells into matrigel was calculated with imageJ FIJI at the respective time points. (**C**) As confirmed by qPCR analysis, GRα expression is reduced up to 94% after 72 hours. The data represent means of three independent experiments. Error bars were

calculated using ±SEM. *P*-values were calculated against nc siRNA control. Two stars represent a significance of $\rho<0.01$.

Pseudopterosin Inhibited Cytokine Release in a Co-Culture of Primary Blood Mononuclear Cells (PBMC) and Triple Negative Breast Cancer Cells

The microenvironment plays a critical role in breast cancer carcinogenesis [32]. Tumor associated macrophages are the drivers of breast cancer cells invasion [33,34]. A main characteristic of inflammatory breast cancer is the secretion of pro-inflammatory cytokines such as IL-6 or IL-8 by macrophages, regulating angiogenesis and promoting tumor progression [35,36]. Previously, we verified a blockade of NF-κB-dependent cytokine expression and secretion after pseudopterosin treatment in both, MDA-MB-231 and THP-1 cells [16]. In this context, GRα knockdown led to the failure of pseudopterosin to inhibit cytokine expression. Furthermore, as shown previously, stimulation by the TLR4 ligand LPS leads to the production of cytokines and the subsequent secretion into the surrounding “conditioned medium” (CM) [16]. Our current data amend a significant reduction of cytokine expression, such as IL-6, IL-8 and TNFα, after PsA-D treatment in peripheral blood mononuclear cells (PBMC) (Supplemental Figure 3.2-6). Medium containing cytokines released by MDA-MB-231 cells, representing the so called “MDA-MB-231 conditioned medium” (M-CM), induced a significant cytokine expression in PBMC. Notably, pseudopterosin treatment was able to block cytokine expression induced by breast cancer cell conditioned media in PBMC (Supplemental Figure 3.2-6). Thus, to further evaluate the pharmacological effects of pseudopterosin on bidirectional communication, we set up a co-culture encompassing PBMC and MDA-MB-231 cells to analyze the change in IL-6 and IL-8 expression levels. In the co-culture model, PsA-D treatment inhibited IL-6 expression significantly by 52.6% and IL-8 expression by 76.8%, respectively (Table 3.2-1). The fold increase of the IL-6 expression level in co-culture increased by 1.9 compared to mono-culture (Figure 3.2-5). As expected, PsA-D treatment reduced IL-6 expression levels by 3.5 fold (Figure 3.2-5). To further explore the agonism of pseudopterosin and GRα in the context of our co-culture model, the focus in future studies will lay in continuing investigations concerning knockdown studies of GRα. Taking together, our data indicate that pseudopterosin has the potential to inhibit the proliferation, the invasiveness and the communication of PBMC and MDA-MB-231 cells in a co-culture model. Thereby, the inhibitory activity of pseudopterosin seems to depend on GRα expression.

Table 3.2-1. Inhibition of cytokine expression in co-culture of peripheral blood mononuclear cells (PBMC) and MDA-MB-231 cells after pseudopterosin treatment.

	Mono-culture PBMC	Mono-culture MDA*	Co-culture PMBC+MDA +DMSO	Co-culture PBMC+MDA +PsA-D	*P*-values[1]
IL-6[2]	1.09 (±3.2)[1]	31.7 (±20.3)[1]	44.6 (±25.3)[1]	21.2 (±12.7)[1]	0.02
IL-8[2]	27.1 (±36.9)[2]	67.9 (±46.5)[2]	213.9 (±99.6)[2]	49.5 (±13.2)[2]	0.22

[1] *P*-values were calculated with ONE-Way ANOVA between 'co-culture' and 'co-culture + PsA-D'.

[2] The data represent relative mRNA expression values measured with realtime qPCR; * MDA is equivalent for MDA-MB-231 cells.

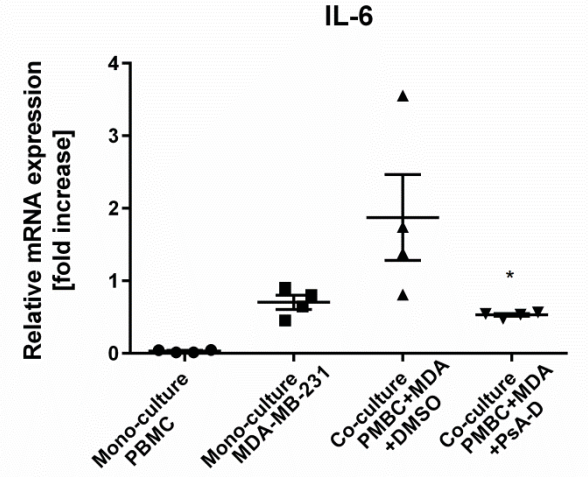

Figure 3.2-5. Pseudopterosin inhibited cytokine expression in a co-culture of PBMC and MDA-MB-231.

Both cell lines were co-cultured at a ratio of 1:1 before treatment with 30 µM PsA-D. Cells were harvested 24 hours after treatment and cytokine expression levels were analyzed with qPCR. Relative mRNA levels were normalized to fold increase. MDA is equivalent for MDA-MB-231 cells. Data represent means of four independent experiments. Standard deviation was calculated using ±SEM. *P*-values were calculated between 'co-culture' and 'co-culture + PsA-D' using Dunnett's multiple comparisons test.

DISCUSSION

For pseudopterosin effective biological activities in various therapeutic areas including anti-inflammatory effects are described [9–11]. This study aimed to explore the inhibitory capabilities of pseudopterosin on distinct features of triple negative breast cancer (TNBC), namely the ability to invade surrounding tissue and the contribution to rapid tumor progression. For TNBC, a disease with a high unmet medical need and a low survival rate, we demonstrated previously a novel potential of pseudopterosin by inhibiting NF-κB signaling and subsequent cytokine secretion [16]. Furthermore, suggested by the translocation of GRα, we revealed a role of GRα activation upon pseudopterosin treatment. In the current study, GRα again indicated to play a role in mediating pseudopterosin induced inhibition of breast cancer cell proliferation.

Among others, NF-κB is an important regulator in the development of the mammary glands [37]. However, chronic inflammation in general and inflammation in the tumor microenvironment in particular, caused by NF-κB up-regulation over a long time range, increases aggressiveness, invasiveness [38,39] and correlates with poor prognosis in breast cancer patients [40]. As our data suggest pseudopterosin to inhibit constitutive NF-κB activity in TNBC cells [16], we further examined effects of pseudopterosin on blocking invasion. Adipocytes in breast tumors are described to secrete high amounts of collagen leading to increased tumor growth [41]. Despite of using equivalently high collagen concentrations, which is known to reduce drug sensitivity [42], pseudopterosin displayed strong anti-invasive properties. Moreover, in a GRα knockdown, invasiveness in breast cancer tumor spheroids increased.

Gene expression analysis of breast tumors revealed a down-regulation of genes involved in cell differentiation, whereas genes promoting tumorigenesis were up-regulated [43]. However, mutations alone cannot explain the high malignancy and the complexity of the tumor. The tumor microenvironment is the most important factor of why immune cells undergo a reprogramming step, thereby promoting tumor progression. The discovery that normal mammary epithelial cells cooperate with innate immune cells for invasive processes, led to the discovery that macrophages are the drivers of intravasation from invasive breast tumors by establishing the tumor microenvironment [33,44]. Thereby, extracellular matrix (ECM), stromal cells such as endothelial and immune cells, fibroblasts and adipocytes are the main components of the microenvironment [45]. Additionally, tumor associated macrophages (TAMs) play a critical role in the tumor microenvironment by secreting second messengers such as IL-8 or IL-6 via NF-κB activation, thus promoting the tumor microenvironment and regulating angiogenesis which in turn correlates with poor outcome and malignant features in breast cancer [35,36,46,47]. Paradoxically, cytotoxic chemotherapy further initiates TAM recruitment into invasive carcinoma [48], where co-culture with breast cancer cells results in high IL-6 levels leading to activation of cancer stem cells [49.] We confirmed elevated IL-6 and IL-8 expression levels as a result of co-cultivating PBMC and MDA-MB-231 cells, where pseudopterosin was able to significantly block cytokine expression and henceforth the communication of both cell types.

In the clinics, glucocorticoids are used to reduce allergic reactions or nausea during chemotherapy due to up-regulation of anti-inflammatory signals [50–52]. On tumor cells, the synthetic GRα ligand dexamethasone (Dex) has been described to reduce cell proliferation by decreasing ERK phosphorylation in ER^+ breast cancer cells, possibly via the mechanism of transactivation [51]. ERK is a key regulator of proliferation and remodels the chromatin structure [29]. To our knowledge, anti-proliferative effects of Dex where as yet not observed in MDA-MB-231 cells. In contrast, Dex was described to increase tumor growth and act pro-proliferative [53].

However, in our study, we not only observed anti-proliferative effects after Dex treatment, but also witnessed improved anti-proliferative effects of pseudopterosin treatment compared to Dex. Interestingly, preliminary data indicate that the mechanism of action of pseudopterosin seems to be distinct from Dex, as the phosphorylation status of ERK did not change in the presence of pseudopterosin.

To date, GRα signaling can be divided into two distinct pathways: the so-called “transactivation”, reflecting target gene expression, and the “transrepression”, representing the downregulation of parallel signaling pathways such as NF-κB activation. Prominent metabolic side effects of glucocorticoid treatment might be ascribed to transactivation of GRα [54]. In contrast, positive effects of glucocorticoids include reduced migration and a reduction in proteins associated with chemotherapy resistance in TNBC cells, which might be explained by transrepression of GRα [55–57]. The mechanism of the transrepressive process of GRα can have different origins: GRα can hetero-dimerize and bind directly to the p65/p50 dimer [58] or GRα recruits histone deacetylases to the promotors of inflammatory genes [59]. GRα transrepression is thereby defined as a direct interaction with transcription factors, for example NF-κB, without binding to DNA response elements and independent of IκB, p50 or p65 regulation of expression [54]. Thus, up-regulation of IκBα expression [60] or repression of IL-8 by transcriptional inhibition of NF-κB are correlated with transactivation of GRα [54]. After GRα knockdown, we observed increased invasiveness in tumor spheroids and a lack of pseudopterosin to inhibit proliferation or invasion. Thus, we suggest the expression of GRα to be beneficial in maintaining a less invasive phenotype in TNBC and propose pseudopterosin to address the mechanism of transrepression by agonizing GRα.

In conclusion, we demonstrated inhibitory effects of pseudopterosin on pronounced characteristics of TNBC including tumor cell proliferation and invasion. Our results imply pseudopterosin as a potential therapeutic basis suitable for targeting TNBC. Future studies will focus on investigating the molecular function including transrepressive effects of GRα in mediating pseudopterosin-dependent pharmacological actions.

MATERIALS AND METHODS

Cell Culture and Reagents

The origin of the extract of pseudopterosin A to D isolated from *A. elisabethae* (subsequently named PsA-D) was kindly provided by Dr. Russell Kerr (University of Prince Edward Island, Marine Natural Products Lab, Canada) as described in our previous work [16]. U0126 inhibitor was purchased from Selleckchem (Houston, U.S.). MDA-MB-231 breast cancer cells were

obtained from European Collection of Authenticated Cell Cultures (ECACC, Salisbury, UK) and grown in humidified atmosphere containing 5% CO_2 in RPMI medium. Medium was supplemented with 15% FCS, 100 units·mL^{-1} penicillin and 100 µg·mL^{-1} units streptomycin. PBMCs were purchased from STEMCELL Technologies (Vancouver, Canada) and cultured in the presence of 5% CO2 in RPMI along with 10% FCS, penicillin and streptomycin. Staurosporine was purchased from Sigma-Aldrich (St. Louis, USA) and medium and antibiotics from Life Technologies (Gibco, Carlsbad, U.S.).

Realtime Cell Proliferation

MDA-MB-231 breast cancer cells were seeded at a density of 1×10^5 cells per mL in 96-well image lock plates (Sartorius, Goettingen, Germany) and images were taken every hour for a time frame of five days with the IncuCyte® Zoom from Sartorius (Goettingen, Germany). Confluency of cells was determined using the software of IncuCyte® Zoom (Version 2016B).

Knockdown Studies

Glucocorticoid receptor alpha (GRα) siRNA (siGR) sc-35505 was purchased from Santa Cruz Biotechnology (Dallas, U.S.). Silencer® Select Negative Control No. 2 siRNA (nc siRNA) was obtained from Life Technologies (Carlsbad, U.S.). 1×10^6 cells were transfected with 300 nM siRNA using the Nucleofector 2b device (Lonza, Basel, Switzerland) using the X-013 protocol for transfection of MDA-MB-231 cells. After different time points, cells were harvested and expression upon knockdown of interest was analyzed using quantitative realtime PCR, respectively.

Quantitative Realtime PCR

To determine cytokine or GRα expression levels after co-culture or knockdown, the following primers were used (purchased from Eurofins, Ebersberg, Germany): IL-6 forward (GGCACTGGCAGAAAACAACC), IL-6 reverse (GCAAGTCTCCTCATTGA-ATCC) IL-8 forward: (ACTGAGAGTGATTGAGAGTGGAC), IL-8 reverse: (AACCCT-CTGCACCCAGTTTTC), GAPDH forward: (TGCACCACCAACTGCTTAGC), GAPDH reverse: (GGCATGGACTGTGGTCATGAG), GRα forward: (AAAAGAGCAGTGG-AAGGACAGCAC), GRα reverse: (GGTAGGGGTGAGTTGTGGTAACG). Total RNA was isolated with “RNase Mini kit” from QIAGEN (Hilden, Germany) according to the manufacturer’s instructions and reverse transcriptase PCR was performed using “Reverse Transcription Kit” from Promega (Darmstadt, Germany). Realtime PCR was conducted with “Quantitect SYBR Green” from QIAGEN based on the following protocol: Pre-incubation at 95° for 900 seconds, amplification was performed over 45 cycles (95° for 15 seconds, 55° for 25 seconds and 72° for 10 seconds). No-template

controls served as negative controls. CT values were calculated according to the $2^{-\Delta\Delta CT}$ method [61]. Sample values were normalized to the house-keeping gene GAPDH (glyceraldehyde 3-phosphate dehydrogenase).

3D Invasion Assay

To study MDA-MB-231 invasion into an extracellular matrix such as matrigel (Corning, New York, U.S.), spheroids of MDA-MB-231 were generated for 72 hours starting with 3×10^3 cells and 0.25% matrigel in an ultra-low-attachment (ULA) plate (Corning, New York, U.S.). Invasion was initiated by addition of matrigel in a ratio of 1:1 volume to the spheroids. Images were taken with the IncuCyte® Zoom (Sartorius, Goettingen, Germany) to create a time lapse movie or the Axio Vert.A1 microscope (Zeiss, Oberkochen, Germany) every 24 hours for a time frame of three days. Image analysis was done with imageJ makro “Analyze Spheroid Cell Invasion in 3D matrix” by Volker Bäcker [62] (FIJI distribution [63]).

Co-culture Studies

Co-culture of PBMC and MDA-MB-231 cells: PBMC were freshly thawed for each experiment. 1×10^6 cells of MDA-MB-231 were seeded on day one and incubated with PsA-D for 20 minutes on day two. Treatment was followed by addition of PBMC cells to the MDA-MB-231 cells at a ratio of 1:1. Finally, cells were harvested at day three and analyzed for cytokine expression by realtime PCR.

Preparation of PsA-D Mixture

A. elisabethae was collected from South Bimini Island, as described in our previous work [16]: the extract was dried and extracted in EtOAc/MeOH (1:1) for 48 hours and subjected to silica gel chromatography eluting with hexanes and EtOAc to afford a mixture of PsA-D. The ratio was determined to be 85:5:5:5 (PsA:B:C:D) by LC-MS analysis.

Immunofluorescent staining

After treatment according to *Knockdown studies*, cells were fixed with -10°C cold methanol for 5 minutes and treated with 0.1% Triton™ X-100 for 15 minutes. Antibodies were purchased from Santa Cruz Biotechnology (Dallas, Texas, USA): primary antibody (sc-8992 GRα (H-300)) incubated 1:50 for 24 hours overnight at 4°C and secondary antibody (sc-2012 IgG-FITC) was incubated 1:100 for 2.5 hours at room temperature For staining the cell nuclei 4′,6-Diamidin-2-phenylindol (DAPI, Sigma Aldrich, St. Louis, USA) was incubated for 5 min at room temperature

at a concentration of 3 µM. Cells were washed three times with PBS following each incubation step.

Statistical Analysis

All data shown represent at least three independent experiments. Error bars show ±SEM of all the means of triplicate values. Figures and statistical analysis were generated with Graphpad Prism v. 6.07 (Graphpad Software, San Diego, USA) using one-way-ANOVA and the underlying Dunnett's multiple comparisons test. $P<0.05$ was chosen to define statistically significant differences.

Supplementary Material: Figure S1: Cell Viability of MDA-MB-231 cells after pseudopterosin treatment. Figure S2: Cell viability assessment of PBMC cells after pseudopterosin treatment. Figure S3: Pseudopterosin did not change ERK phosphorylation status in MDA-MB-231 cells. Figure S4: Pseudopterosin failed to inhibit breast cancer cell proliferation after knockdown of the glucocorticoid receptor alpha (GRα) after 72 hours. Figure S5: Pseudopterosin does not inhibit spheroid growth. Figure S6: Pseudopterosin inhibited bidirectional communication between triple negative breast cancer (TNBC) and peripheral blood mononuclear cells (PBMC).

Acknowledgments: We would like to thank Lars Frangenberg for excellent technical assistance. Russell Kerr, from the University of Prince Edward Island, Canada, has kindly provided the PsA-D extract originating from *A. elisabethae* collected in the Bahamas Islands.

Funding: The research project is financed by a grant to Nicole Teusch provided by the Ministry of Culture and Science of the federal state of North Rhine-Westphalia, Germany. Ph.D. training of Julia Sperlich was financed by the graduate program in Pharmacology and Experimental Therapeutics at the University of Cologne, which is financially.

Author Contributions: Nicole Teusch developed the scientific concept. Julia Sperlich and Nicole Teusch designed the experiments. Julia Sperlich performed the experiments and analyzed the data. Nicole Teusch and Julia Sperlich wrote the manuscript.

REFERENCES

1. C. P. Stewart, B. W., Wild, IARC, I. A. for R. on Cancer, *World Heal. Organ.* **2014**, 1–631.
2. S. K. Pal, B. H. Childs, M. Pegram, *Breast Cancer Res. Treat.* **2011**, *125*, 627–636.
3. T. Biswas, J. T. Efird, S. Prasad, S. E. James, P. R. Walker, T. M. Zagar, *Clin. Breast Cancer* **2016**, *16*, 212–216.
4. H. Matsumoto, S. Koo, R. Dent, P. H. Tan, J. Iqbal, *J. Clin. Pathol.* **2015**, *68*, 506–510.
5. J. W. Pollard, *J. Leukoc. Biol.* **2008**, *84*, 623–630.
6. C. Rolny, M. Mazzone, S. Tugues, D. Laoui, I. Johansson, C. Coulon, M. L. Squadrito, I. Segura, X. Li, E. Knevels, et al., *Cancer Cell* **2011**, *19*, 31–44.
7. Z. C. Hartman, G. M. Poage, P. Den Hollander, A. Tsimelzon, J. Hill, N. Panupinthu, Y. Zhang, A. Mazumdar, S. G. Hilsenbeck, G. B. Mills, et al., *Cancer Res.* **2013**, *73*, 3470–3480.

8. F. Berrué, M. W. B. McCulloch, R. G. Kerr, *Bioorganic Med. Chem.* **2011**, *19*, 6702–6719.
9. A. M. Mayer, P. B. Jacobson, W. Fenical, R. S. Jacobs, K. B. Glaser, *Elsevier Sci.* **1998**, *62*, PL401-L407.
10. A. Ata, R. G. Kerr, C. E. Moya, R. S. Jacobs, *Tetrahedron* **2003**, *59*, 4215–4222.
11. H. Correa, A. L. Valenzuela, L. F. Ospina, C. Duque, *J. Inflamm. (Lond).* **2009**, *6*, 5.
12. S. a. Look, W. Fenical, G. K. Matsumoto, J. Clardy, *J. Org. Chem.* **1986**, *51*, 5140–5145.
13. S. A. Look, W. Fenical, R. S. Jacobst, J. O. N. Clardyt, *Proc. Natl. Acad. Sci* **1986**, *83*, 6238–6240.
14. S. L. Caplan, B. Zheng, K. Dawson-Scully, C. A. White, L. M. West, *Mar. Drugs* **2016**, *14*, 1–14.
15. I. I. Rodríguez, Y. P. Shi, O. J. García, A. D. Rodríguez, A. M. S. Mayer, J. a. Sánchez, E. Ortega-Barria, J. González, *J. Nat. Prod.* **2004**, *67*, 1672–1680.
16. J. Sperlich, R. Kerr, N. Teusch, *Mar. Drugs* **2017**, *15*, 1–16.
17. L. I. McKay, J. A. Cidlowski, *Endocr. Rev.* **1999**, *20*, 435–459.
18. P. Moutsatsou, A. G. Papavassiliou, *J. Cell. Mol. Med.* **2008**, *12*, 145–63.
19. S. D. Conzen, *Mol. Endocrinol.* **2008**, *22*, 2215–28.
20. R. E. Hall, C. S. Lee, I. E. Alexander, J. Shine, C. L. Clarke, R. L. Sutherland, *Int. J. Cancer* **1990**, *46*, 1081–1087.
21. D. Pan, M. Kocherginsky, S. D. Conzen, *Cancer Res.* **2011**, *71*, 6360–6370.
22. Z. Chen, X. Lan, D. Wu, B. Sunkel, Z. Ye, J. Huang, Z. Liu, S. K. Clinton, V. X. Jin, Q. Wang, *Nat. Commun.* **2015**, *6*, 8323.
23. D. C. West, D. Pan, E. Y. Tonsing-Carter, K. M. Hernandez, C. F. Pierce, S. C. Styke, K. R. Bowie, T. I. Garcia, M. Kocherginsky, S. D. Conzen, *Mol. Cancer Res.* **2016**, *14*, 707–19.
24. M. Skor, E. Wonder, M. Kocherginsky, A. Goyal, B. Hall, Y. Cai, S. D. Conzen, *Clin. Cancer Res.* **2013**, *25*, 713–724.
25. C. H. Lin, P. Y. Chuang, S. L. You, C. J. Chiang, C. S. Huang, M. Y. Wang, M. Chao, Y. S. Lu, A. L. Cheng, C. H. Tang, *Breast Cancer Res. Treat.* **2018**, 1–10.
26. C. Cai, Z. Yao, *Chinese J. Clin. Oncol.* **2006**, *3*, 5–10.
27. C. Badr, J. M. Niers, L.-A. Tjon-Kon-Fat, D. P. Noske, T. Wurdinger, B. Tannous, *Mol Imaging* **2009**, *8*, 278–290.
28. S. M. Smith, Y. L. Lyu, L. Cai, *PLoS One* **2014**, *9*, DOI 10.1371/journal.pone.0106966.
29. J. C. Chambard, R. Lefloch, J. Pouysségur, P. Lenormand, *Biochim. Biophys. Acta - Mol. Cell Res.* **2007**, *1773*, 1299–1310.
30. C. Neophytou, P. Boutsikos, P. Papageorgis, *Front. Oncol.* **2018**, *8*, DOI 10.3389/fonc.2018.00031.
31. S. K. Mondal, S. Jinka, K. Pal, S. Nelli, S. K. Dutta, E. Wang, A. Ahmad, K. M. AlKharfy, D. Mukhopadhyay, R. Banerjee, *Mol. Pharm.* **2016**, *13*, 2507–2523.
32. D. Hanahan, R. a. Weinberg, *Cell* **2011**, *144*, 646–674.
33. A. S. Harney, E. N. Arwert, D. Entenberg, Y. Wang, P. Guo, B.-Z. Qian, M. H. Oktay, J. W. Pollard, J. G. Jones, J. S. Condeelis, *Cancer Discov.* **2015**, *5*, 932–943.
34. K. D. Grugan, F. L. McCabe, M. Kinder, A. R. Greenplate, B. C. Harman, J. E. Ekert, N. van Rooijen, G. M. Anderson, J. a Nemeth, W. R. Strohl, et al., *J. Immunol.* **2012**, *189*, 5457–66.
35. M. M. Mohamed, E. A. El-Ghonaimya, M. A. Nouhb, R. J. Schneiderc, B. F. Sloaned, M. El-Shinawie, *Int J Biochem Cell Biol.* **2014**, *46*, 138–147.
36. A. Sanguinetti, D. Santini, M. Bonafè, M. Taffurelli, N. Avenia, *World J. Surg. Oncol.* **2015**, *13*, 4–9.
37. Y. Cao, M. Karin, *J. Mammary Gland Biol. Neoplasia* **2003**, *8*, 215–23.
38. C. Porta, P. Larghi, M. Rimoldi, M. Grazia Totaro, P. Allavena, A. Mantovani, A. Sica, *Immunobiology* **2009**, *214*, 761–777.
39. J. E. Goldberg, K. L. Schwertfeger, *Curr. Drug Targets* **2010**, *11*, 1133–1146.
40. D. G. DeNardo, L. M. Coussens, *Breast Cancer Res.* **2007**, *9*, 1–10.

41. P. Iyengar, V. Espina, T. W. Williams, Y. Lin, D. Berry, L. A. Jelicks, H. Lee, K. Temple, R. Graves, J. Pollard, et al., *J. Clin. Invest.* **2005**, *115*, 1163–1176.
42. T. Armstrong, G. Packham, L. B. Murphy, A. C. Bateman, J. A. Conti, D. R. Fine, C. D. Johnson, R. C. Benyon, J. P. Iredale, *Clin. Cancer Res.* **2004**, *10*, 7427–7437.
43. M. Allinen, L. Cai, C. Brennan, J. Lahti-Domenici, H. Huang, D. Porter, M. Hu, L. Chin, A. Richardson, S. Schnitt, et al., *Cancer Cell* **2004**, *6*, 17–32.
44. A. K. Bonde, V. Tischler, S. Kumar, A. Soltermann, R. A. Schwendener, *BMC Cancer* **2012**, *12*, 35.
45. A. E. Place, S. Jin Huh, K. Polyak, *Breast Cancer Res.* **2011**, *13*, DOI 10.1186/bcr2912.
46. A. K. Agrawal, E. Pielka, A. Lipinski, M. Jelen, W. Kielan, S. Agrawal, *Tumor Biol.* **2018**, *40*, 1–10.
X. Dolcet, D. Llobet, J. Pallares, X. Matias-Guiu, *Virchows Arch.* **2005**, *446*, 475–482.
47. D. G. DeNardo, D. J. Brennan, E. Rexhepaj, B. Ruffell, S. L. Shiao, S. F. Madden, W. M. Gallagher, N. Wadhwani, S. D. Keil, S. A. Junaid, et al., *Cancer Discov.* **2011**, *1*, 54–67.
48. N. Zhou, Y. Zhang, X. Zhang, Z. Lei, R. Hu, H. Li, Y. Mao, X. Wang, D. M. Irwin, G. Niu, et al., *Int. J. Mol. Sci.* **2015**, *16*, 11966–11982.
49. B. D. Keith, *BMC Cancer* **2008**, *8*, 84.
50. F. Buxant, N. Kindt, G. Laurent, J. Noel, S. Saussez, *Mol. Med. Rep.* **2015**, 4051–4054.
51. E. M. King, J. E. Chivers, C. F. Rider, A. Minnich, M. A. Giembycz, R. Newton, *PLoS One* **2013**, *8*, DOI 10.1371/journal.pone.0053936.
52. S. Gündisch, E. Boeckeler, U. Behrends, E. Amtmann, H. Ehrhardt, I. Jeremias, *Anticancer Res.* **2012**, *32*, 4251–4262.
53. R. Newton, N. S. Holden, *Mol. Pharmacol.* **2007**, *72*, 799–809.
54. N. Ferrand, E. Stragier, G. Redeuilh, M. Sabbah, *Biochem. J.* **2012**, *447*, 71–79.
55. M. Honorat, A. Mesnier, A. Di Pietro, V. Lin, P. Cohen, C. Dumontet, L. Payen, *Biochem. Biophys. Res. Commun.* **2008**, *375*, 308–314.
56. E. R. Fietz, C. R. Keenan, G. López-Campos, Y. Tu, C. N. Johnstone, T. Harris, A. G. Stewart, *Sci. Rep.* **2017**, *7*, 1–13.
57. M. O. Altonsy, S. K. Sasse, T. L. Phang, A. N. Gerber, *J. Biol. Chem.* **2014**, *289*, 8231–8239.
58. K. Ito, P. J. Barnes, I. M. Adcock, *Mol. Cell. Biol.* **2000**, *20*, 6891–6903.
59. N. Auphan, J. DiDonato, C. Rosette, A. Helmberg, M. Karin, *Science (80-.).* **1995**, *270*, 286–290.
60. K. J. Livak, T. D. Schmittgen, *Methods* **2001**, *25*, 402–408.
61. V. Baecker, in *ImageJ User Dev. Conf. 2012*, **2012**, pp. 1–6.
62. J. Schindelin, I. Arganda-Carreras, E. Frise, V. Kaynig, M. Longair, T. Pietzsch, S. Preibisch, C. Rueden, S. Saalfeld, B. Schmid, et al., *Nat. Methods* **2012**, *9*, 676.

3.2.1 Supplemental Material

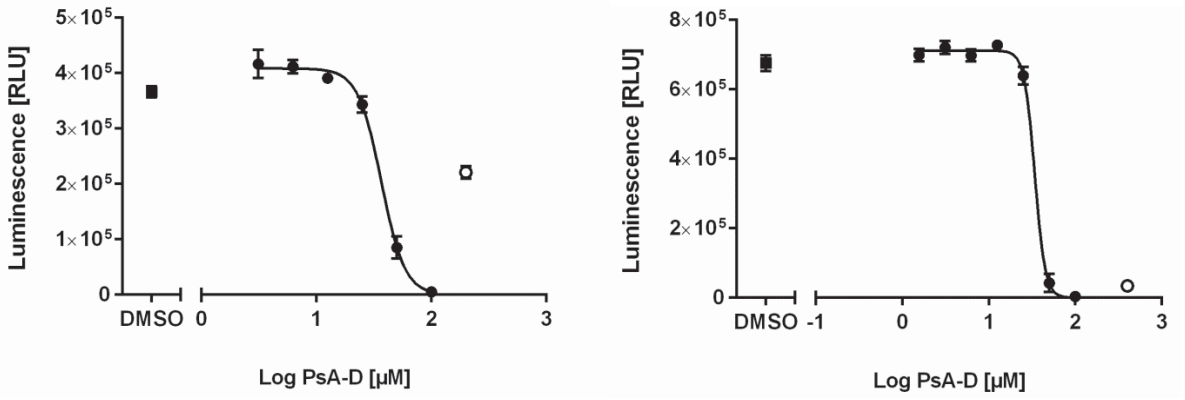

Supplemental Figure 3.2-1. Cell Viability of MDA-MB-231 cells after pseudopterosin treatment.

Increasing amounts of PsA-D were incubated for either 24 hours showing an IC_{50} value of 31.4 µM (**A**) or for 48 hours leading to an IC_{50} value of 32.16 µM (**B**). Staurosporine (white circles) serves as positive control and 1% DMSO as negative control. Error bars were calculated using ±SEM. Graphs represent exemplary data. Means of IC_{50} values were calculated of three independent experiments.

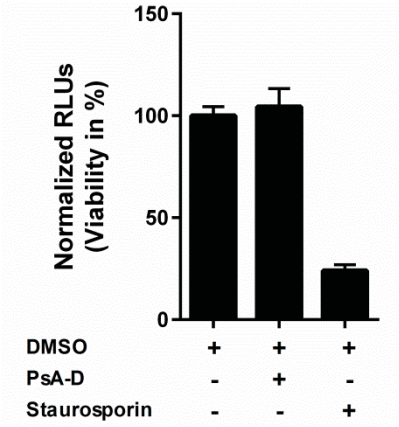

Supplemental Figure 3.2-2. Cell viability assessment of PBMC cells after pseudopterosin treatment.

30 µM of PsA-D were tested for its cytotoxic properties after 24 hours of treatment on PBMC cells. 3 µM staurosporine served as positive control and DMSO as negative control. Error bars were calculated using ±SEM. Graphs represents means of two independent biological repeats. RLU represents "Relative Luminescent Units".

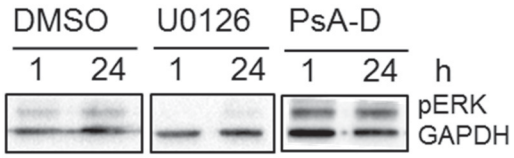

Supplemental Figure 3.2-3. Pseudopterosin did not change ERK phosphorylation status in MDA-MB-231 cells.

Cells were treated with 15 µM of PsA-D and incubated for either 1 or 24 hours. DMSO served as negative control and the MEK inhibitor U0126 at a concentration of 10 µM as positive control. At the indicated time points, cells were harvested and 20 mg of protein were used for a western blot analysis. The house keeping gene GAPDH served as a loading control.

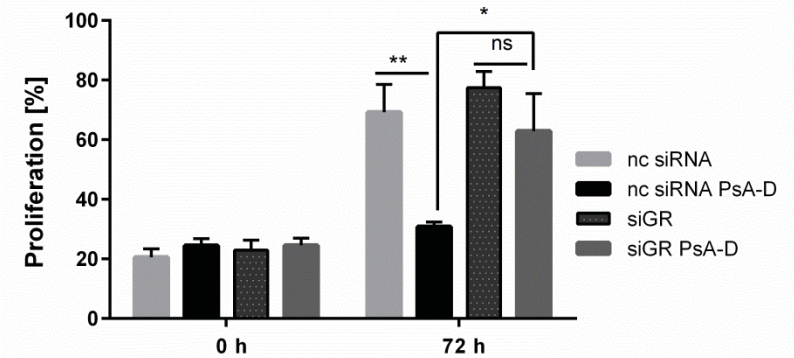

Supplemental Figure 3.2-4. Pseudopterosin failed to inhibit breast cancer cell proliferation after knockdown of the glucocorticoid receptor alpha (GRα) after 72 hours.

Knockdown of GRα was done with the Lonza Nucleofector 2b device. The cells were seeded and proliferating cells were imaged with the IncuCyte® ZOOM every hour. Confluency of cells was determined with IncuCyte® software indicated in proliferation in percent. Cells were treated with a concentration of 15 µM of PsA-D. The bar diagram shows the proliferation rate at time points 0 and 72 hours. The data represent means of three independent experiments. Error bars were calculated using ±SEM. Two stars represent a significance ρ<0.01 and one star of ρ<0.05.

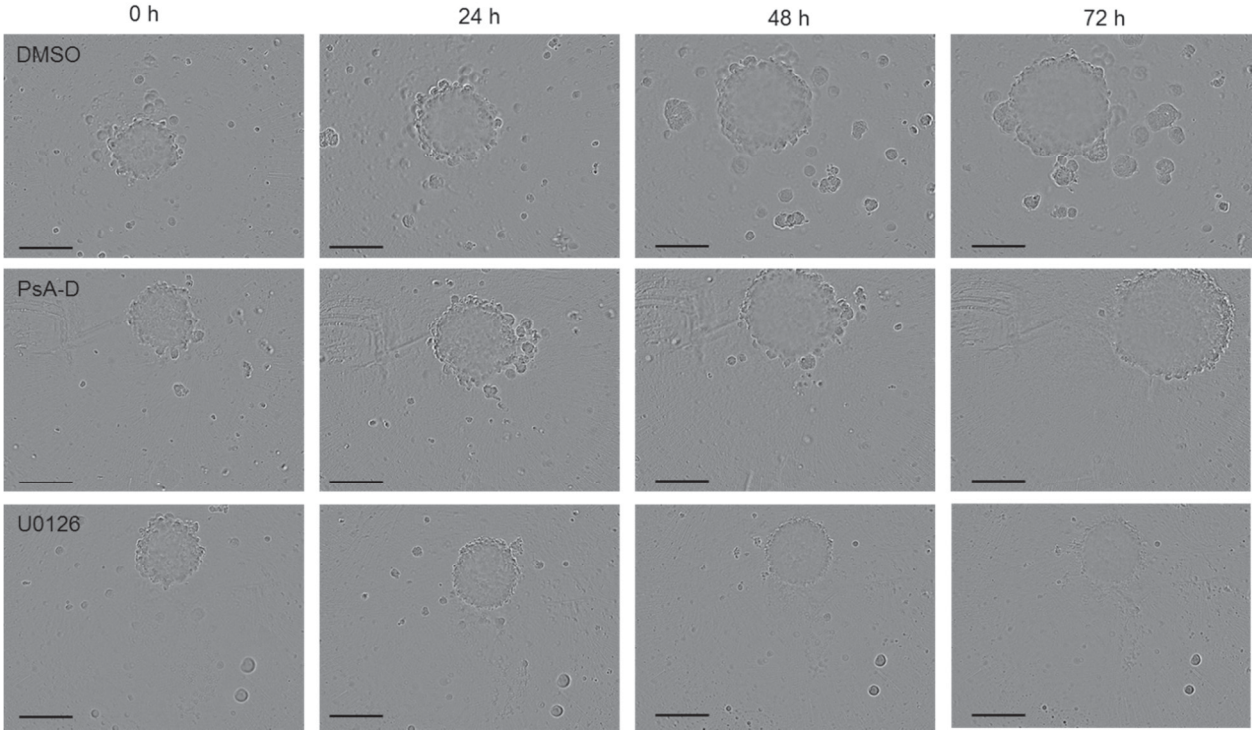

(**A**)

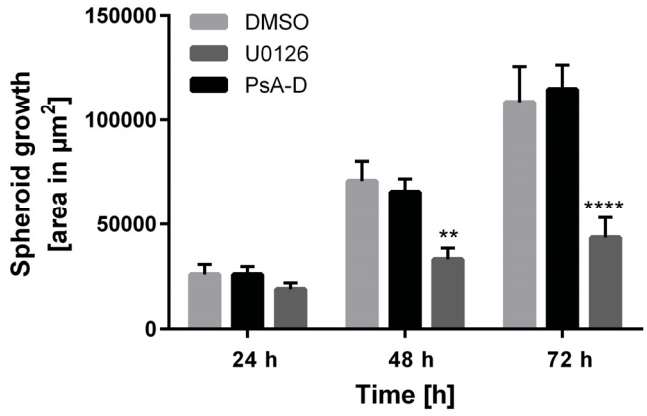

(**B**)

Supplemental Figure 3.2-5. Pseudopterosin did not inhibit spheroid growth.

Spheroids were formed for 72 hours, using 3×10^3 cells and 2.5% matrigel. The spheroids were imaged with the IncuCyte® ZOOM every hour for a time frame of three days. The growth of the spheroids was measured using Fiji ImageJ. As positive control MEK inhibitor U0126 was added at a concentration of 10 µM and DMSO served as a negative control. PsA-D was added at a concentration of 30 µM. The data represent means of six independent experiments. Scale bars in black represent 300 microns. Error bars were calculated using ±SEM. Four stars represent a significance of $\rho<0.0001$ and two stars of $\rho<0.01$.

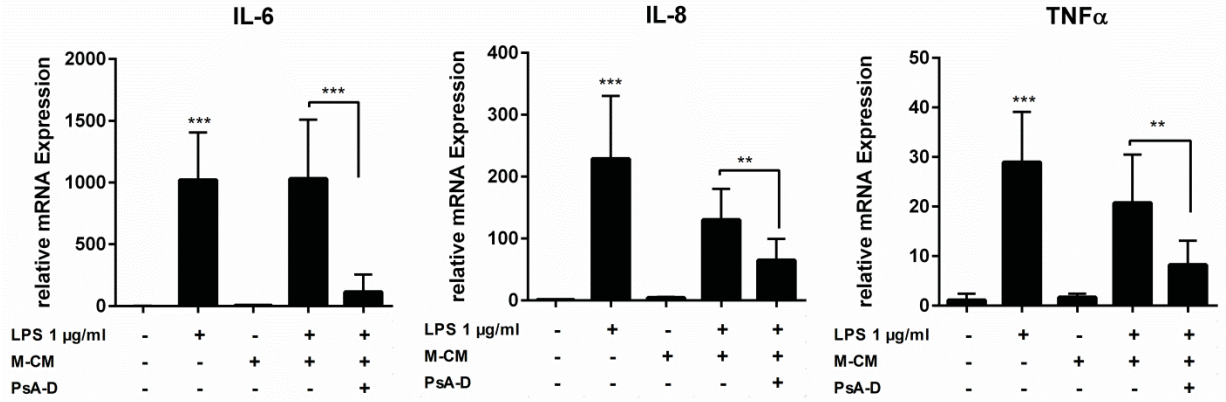

Supplemental Figure 3.2-6. Pseudopterosin inhibited bidirectional communication between triple negative breast cancer (TNBC) and peripheral blood mononuclear cells (PBMC).

Tumor-conditioned medium of MDA-MB-231 cells was produced using 1 µg/mL LPS and 1×10^6 cells per mL. After 24 hours of incubation, tumor conditioned medium (MDA-MB-231-conditioned medium, M-CM) was harvested, centrifuged and sterile filtered. Afterwards, M-CM was added at 25 volume percentages to 1×10^6 cells per mL of PBMC. After 5 hours of incubation, cells were harvested, RNA isolated and analyzed with qPCR.

Supplementary Method 1: Measurement of cell viability: MDA-MB-231 cells were seeded at a density of 2.8×10^5 cells per mL in 384 well plates (Greiner Bio-One, Kremsmuenster, Austria) with the CyBio pipetting robot (Analytic Jena AG, Jena, Germany) and PBMCs were seeded at a density of 1×10^6 cells per mL in 96 well plates (Greiner Bio-One, Kremsmuenster, Austria). MDA-MB-231 cells were incubated for 24 hours at 37°C before treatment and PBMCs for one

hour before treatment. Compounds were added at different concentrations and incubated for 24 or 48 hours, respectively. Measurement of cell viability was performed with CellTiterGlo® from Promega (Darmstadt, Germany) according to the manufacturer's instructions.

Supplementary Method 2: Western blot measurement of phosphorylated ERK in MDA-MB-231 cells: 1×10^6 cells per mL were seeded into 6 well plates (Thermo Fisher Scientific, Waltham, USA) and incubated for 24 hours at 37°C before treatment. After treatment, cells were harvested, lysed (5x Lysis buffer, Promega, Darmstadt, Germany) with a buffer containing protease and phosphatase inhibitors (Roche, Basel, Switzerland) and protein concentration of samples, determined with Roti®-Quant reagent (Roth, Karlsruhe, Germany), was adjusted to 20 mg. Samples were loaded on 12% SDS gels, run at 100 V and afterwards blotted on a PVDF membrane at 25 V using a semi-dry installation (Bio-Rad Laboratories, Hercules, USA). The membrane was blocked with 5% non-fat dry milk (Roth, Karlsruhe, Germany). The housekeeping gene GAPDH was used as a loading control. Primary antibodies (GAPDH rabbit: D16H11; pERK rabbit: D13.14.4E) were purchased from Cell Signaling Technology (Danvers, USA), used at a dilution of 1/1000 in 5% non-fat dry milk and incubated over night at 4°C. The secondary anti-rabbit HRP-linked antibody (Cell Signaling Technology, Danvers, USA) was used at a dilution of 1/2000 and incubated for 2 hours at room temperature.

Supplementary Method 3: Spheroids of MDA-MB-231 cells were generated for 72 hours starting with 3×10^3 cells and 2.5% matrigel (Corning, New York, U.S.) in an ultra-low-attachment (ULA) plate (Corning, New York, U.S.). U0126 MEK inhibitor (Sellekchem, Houston, U.S.) served as positive control. Images were taken with the IncuCyte® Zoom (Sartorius, Goettingen, Germany) every hour for a time frame of three days. Image analysis was done with imageJ, FIJI distribution [63].

Supplementary Method 4: Production of conditioned medium (CM) from MDA-MB-231 cells: MDA-MB-231 cells were seeded at a density of 1×10^6 cells into a 25 cm^2 flask. Cells were either stimulated with 1 µg/mL LPS or without, serving as a negative control. MDA-MB-231 conditioned media (M-CM) was collected after 24 hours, centrifuged and sterile filtered. Peripheral blood mononuclear cells (PBMC) were freshly thawed and seeded at 1×10^6 cells per mL. PsA-D was added at a concentration of 30 µM for 20 minutes followed by addition of 25 volume percentage of M-CM for 5 hours. Cells were then harvested and RNA isolated with RNase Mini Kit (Qiagen, Hilden, Germany) for further quantitative realtime PCR analysis.

JOURNAL OF NATURAL PRODUCTS

3.3 Azaphilone Derivatives from the Fungus Coniella fragariae Inhibit NF-κB Activation and Reduce Tumor Cell Migration

Haiqian Yu,[†] Julia Sperlich,[‡] Attila Mándi,[§] Tibor Kurtán,[§] Haofu Dai,[⊥] Nicole Teusch,[‡] Zhi-Yong Guo,[#] Kun Zou,[#] Zhen Liu,[*] Peter Proksch[*]

[†]Institute of Pharmaceutical Biology and Biotechnology, Heinrich-Heine-Universität Düsseldorf, Universitätsstrasse 1, 40225 Düsseldorf, Germany

[‡]Bio-Pharmaceutical Chemistry and Molecular Pharmacology, Faculty of Applied Natural Sciences, Technische Hochschule Köln, Chempark, 51368 Leverkusen, Germany

[§]Department of Organic Chemistry, University of Debrecen, P.O. Box 400, H-4002 Debrecen, Hungary

[⊥]Key Laboratory of Biology and Genetic Resources of Tropical Crops, Ministry of Agriculture, Institute of Tropical Bioscience and Biotechnology, Chinese Academy of Tropical Agricultural Sciences, Haikou 571101, China

[#]Hubei Key Laboratory of Natural Product Research and Development, College of Biological and Pharmaceutical Sciences, China Three Gorges University, Yichang 443002, China

ABSTRACT

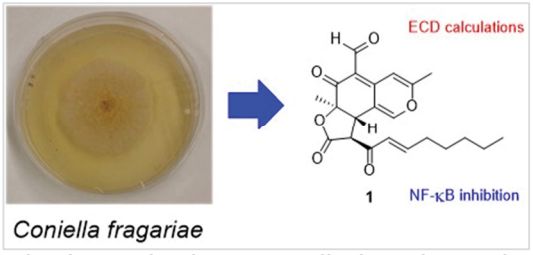

Seven new azaphilones, coniellins A−G (**1**−**7**) were obtained from the fungus *Coniella fragariae* that had been isolated from goose dung. Their structures were elucidated by 1D and 2D NMR as well as by HRESIMS data. TDDFT-ECD calculation was used to determine the absolute configuration of **1**, while Mosher's method was applied to determine the absolute configuration of **5**. While displaying only moderate cytotoxicity, compound **1** exhibited significant inhibition of NF-κB activation in the triple negative breast cancer cell line MDA-MB-231 with an IC_{50} value of 4.4 μM. Moreover, compounds **1**, **4** and **5** clearly reduced tumor cell migration. Compound **1** was the most active derivative tested in this assay and displayed 60% inhibition of tumor cell migration at a dose of 5 μM and 98% inhibition at 10 μM after 24 h.

INTRODUCTION

Fungi are an important source of secondary metabolites with a variety of chemical structures and diverse biological activities [1]. Investigation of fungi from hitherto less investigated habitats

such as animal dung is expected to enhance the discovery rate of new secondary metabolites. Dung-inhabiting fungi, also known as coprophilous fungi, have already been shown to produce an impressive number of bioactive natural products with antibacterial and antifungal activities [2,3]. These fungi and their metabolites play an important ecological role in decomposing and recycling nutrients from animal dung [4].

In our continuous studies on new bioactive fungal natural products [5−7], the fungus *Coniella fragariae* was isolated from goose dung, which was collected near the sea coast in North Germany. Fungi from the genus *Coniella* are generally known as phytopathogens. For example, *C. granati* is the causative agent of pomegranate disease in Greece, Israel, Turkey, and Italy [8−11]. *C. diplodiella* is known to cause white rot in grapes [12] and crown rot in strawberries [13]. In Australia, *C. fragariae* was found to cause foliage blight in *Eucalyptus pellita* [14]. In the present study, plants that had been eaten by geese are expected to be the true source of *C. fragariae*.

No report on natural products from fungi of the genus *Coniella* has been published so far. Investigation of *C. fragariae* now yielded seven new azaphilone derivatives, coniellins A−G (**1**−**7**). The isolation and structure elucidation of the new compounds as well as their cytotoxic and NF-κB inhibitory activities are reported herein.

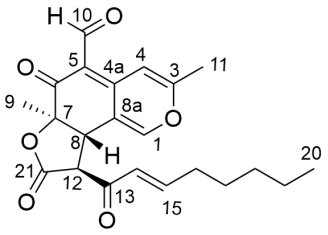

1

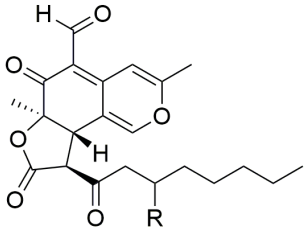

2 R = H
3 R = OMe

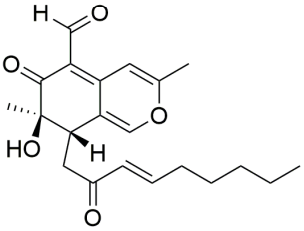

4

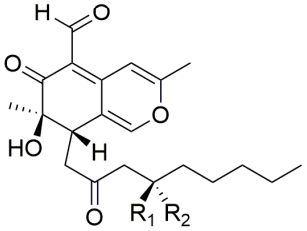

5 R_1 = H, R_2 = OH
6 R_1 = OH, R_2 = H
7 R_1 = H, R_2 = OMe

RESULTS AND DISCUSSION

Compound **1** was isolated as a yellow powder. It had the molecular formula $C_{22}H_{24}O_6$ with 11 degrees of unsaturation as deduced from the HRESIMS data. The ^{13}C NMR data of **1** (Table 3.3-1) showed the presence of three carbonyls at δ_C 191.1 (C-6), 190.2 (C-13) and 190.0 (C-10), an ester carbonyl at δ_C 168.8 (C-21), and eight olefinic carbons at δ_C 165.4 (C-3), 153.0 (C-15), 149.5 (C-4a), 148.5 (C-1), 127.3 (C-14), 117.9 (C-8a), 110.0 (C-5) and 108.0 (C-4), accounting for eight degrees of unsaturation. Thus, compound **1** was suggested to be tricyclic. The ^1H NMR spectrum displayed an aldehyde group at δ_H 10.18 (H-10), two olefinic proton singlets at δ_H 8.40 (H-4) and 7.49 (H-1) and two methyl group singlets at δ_H 2.42 (Me-11) and 1.36 (Me-9). HMBC correlations from H-1 to C-3, C-4a and C-8 (δ_C 43.1), from Me-11 to C-3 and C-4, from H-4 to C-5 and C-8a, from H-10 to C-4a and C-5, from Me-9 to C-6, C-7 (δ_C 81.0) and C-8, and from H-8 (δ_H 3.90) to C-6 established the pyranoquinone bicyclic core with an aldehyde group at C-5 and two methyl groups at C-3 and C-7, respectively (Figure 3.3-1). Apart from these signals, two olefinic protons at δ_H 7.13 (H-15) and 6.58 (H-14), a methyl group at δ_H 0.89 (Me-20), a methine group at δ_H 4.16 (H-12), and four methylene groups were observed in the ^1H NMR data of **1**. The COSY correlations between H-8/H-12, between H-14/H-15/H_2-16 (δ_H 2.31)/H_2-17 (δ_H 1.51)/H_2-18 (δ_H 1.34), and between H_2-19 (δ_H 1.34)/Me-20, together with the HMBC correlations from Me-20 to C-18 (δ_C 31.4) and C-19 (δ_C 22.4), from H-8 to C-13, and from H-12 to C-8a, C-13 and C-21, indicated the presence of an ester bridge between C-7 and C-21 to form the third ring and a 1-oxooct-2-en-1-yl side chain at C-12. Thus, the planar structure of compound **1** was elucidated as shown, representing a new azaphilone derivative, for which the name **coniellin A** is proposed. The double bond at C-14/C-15 was determined to be *E* configurated based on the large coupling constants between H-14 and H-15 (15.6 Hz). In the ROESY spectrum, the NOE relationship between H-12 and Me-9 was observed, suggesting that H-12 and Me-9 were on the same face of the lactone ring, while H-8 was on the opposite face. The chemical shifts of H-8, H-12 and Me-9 of compound **1** also supported this assignment of the relative configuration after comparison with similar tricyclic azaphilones reported in the literature [15]. In addition, cohaerins G and H exhibited similar ECD data (+350, −272 nm) when compared to those of coniellin A (Figure 3.3-2), suggesting they shared the same absolute configuration [15].

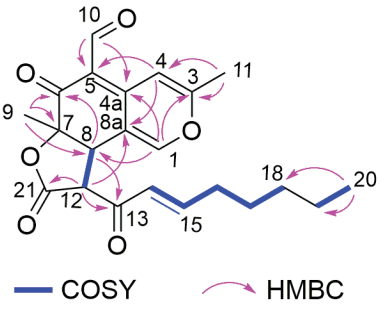

Figure 3.3-1. COSY and key HMBC correlations of compound 1.

To elucidate the absolute configuration of **1**, the solution time-dependent density functional theory/ electronic circular dichroism (TDDFT-ECD) method was applied on the arbitrarily chosen (7*R*,8*S*,12*S*) enantiomer [16,17]. Merck Molecular Force Field (MMFF) conformational search with a 21 kJ/mol energy window resulted in 395 conformers, which were reoptimized at the B3LYP/6-31G(d), the B97D/TZVP [18,19] PCM/MeCN and the CAM-B3LYP/TZVP20 PCM/MeCN levels of theory. To decrease the number of computed conformers, orientation of the last four carbons of the C-12 substituent was neglected by reclustering after DFT optimizations [21]. ECD spectra computed at various levels (B3LYP, BH&HLYP, CAM-B3LYP and PBE0 with the TZVP basis set) for all sets of conformers gave moderate to good agreement suggesting the 7*R*,8*S*,12*S* absolute configuration (Figure 3.3-2). In order to further verify the absolute configuration, specific rotation values were also computed for the (7*R*,8*S*,12*S*) B3LYP conformers resulting in the same positive sign as the experimental value for all the low-energy conformers supporting the ECD results [22,23]. The Boltzmann-averaged values (+373, +350 and +374 at the B3LYP/TZVP, BH&HLYP/TZVP and PBE0/TZVP levels, respectively) are also in good agreement with the experimental specific rotation (+371). Thus, the absolute configuration of **1** was unambiguously elucidated as (7*R*,8*S*,12*S*).

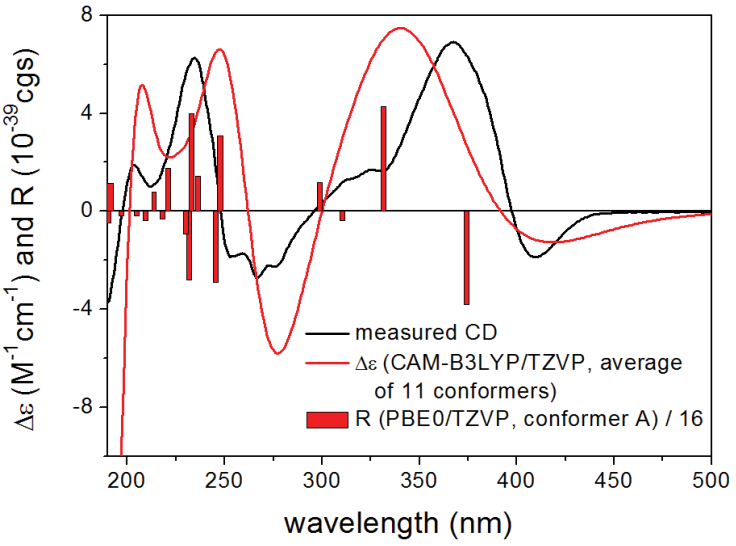

Figure 3.3-2. Experimental ECD spectrum of 1 compared with the Boltzmann-weighted CAM-B3LYP/TZVP (PCM/MeCN) ECD spectrum of (8*S*,9*R*,12*S*)-1.

Level of optimization: B97D/TZVP PCM/MeCN. Bars represent the rotatory strength values of the lowest-energy conformer.

The molecular formula of coniellin B (**2**) was determined to be $C_{22}H_{26}O_6$ by HRESIMS, containing two additional hydrogen atoms compared to **1**. The NMR data of compound **2** (Table 3.3-1) resembled those of **1** except for the replacement of the double bond in the side chain by

two methylene groups at δ_H 3.07 (H_a-14), 2.76 (H_b-14) and 1.65 (H_2-15), which was confirmed by the COSY correlations between H_{ab}-14/H_2-15/H_2-16 (δ_H 1.31) and the HMBC correlations from H-8 (δ_H 3.81), H-12 (δ_H 3.95), H_{ab}-14 and H_2-15 to the downfield shifted C-13 (δ_C 202.3). The remaining substructures and the relative configuration of **2** were determined to be identical to those of **1** by detailed analysis of the 2D NMR spectra of **2**.

Table 3.3-1. ^{1}H and ^{13}C NMR Data of Compounds 1−3.

Position	**1**[a]		**2**[b]		**3**[a]	
	δ_C, type	δ_H (*J* in Hz)	δ_C, type	δ_H (*J* in Hz)	δ_C, type	δ_H (*J* in Hz)
1	148.5, CH	7.49, d (1.5)	148.4, CH	7.46, d (1.7)	148.7, CH	7.44, d (1.7)
3	165.4, C		165.6, C		165.5, C	
4	108.0, CH	8.40, s	108.1, CH	8.41, s	108.1, CH	8.39, s
4a	149.5, C		149.5, C		149.5, C	
5	110.0, C		109.8, C		109.9, C	
6	191.1, C		191.1, C		191.2, C	
7	81.0, C		80.9, C		81.0, C	
8	43.1, CH	3.90, dd (12.7, 1.5)	42.8, CH	3.81, dd (12.8, 1.7)	42.3, CH	3.89, dd (12.7, 1.7)
8a	117.9, C		117.8, C		117.9, C	
9	18.3, CH_3	1.36, s	18.3, CH_3	1.34, s	18.4, CH_3	1.34, s
10	190.0, CH	10.18, s	190.0, CH	10.19, s	190.1, CH	10.19, s
11	20.4, CH_3	2.42, s	20.4, CH_3	2.43, s	20.5, CH_3	2.42, s
12	51.6, CH	4.16, d (12.7)	53.1, CH	3.95, d (12.8)	55.0, CH	4.15, d (12.7)
13	190.2, C		202.3, C		202.1, C	
14	127.3, CH	6.58, d (15.6)	42.2, CH_2	3.07, dt (18.2, 7.2)	46.9, CH_2	3.23, dd (14.4, 10.3)
				2.76, dt (18.2, 7.2)		2.76, dd (14.4, 3.4)
15	153.0, CH	7.13, dt (15.6, 7.0)	23.2, CH_2	1.65, m	79.5, CH	3.78, m
16	32.8, CH_2	2.31, q (7.0)	28.9, CH_2	1.31, m	32.4, CH_2	1.70, m
						1.54, m
17	27.5, CH_2	1.51, m	29.0, CH_2	1.31, m	24.1, CH_2	1.32, m
18	31.4, CH_2	1.34, m	31.6, CH_2	1.27, m	31.8, CH_2	1.31, m
19	22.4, CH_2	1.34, m	22.6, CH_2	1.28, m	22.6, CH_2	1.33, m
20	13.9, CH_3	0.89, t (7.0)	14.0, CH_3	0.88, t (6.9)	14.0, CH_3	0.90, t (6.9)
21	168.8, C		168.7, C		168.7, C	
15-OMe					56.4, CH_3	3.35, s

[a] Recorded at 600 MHz (^{1}H) and 150 MHz (^{13}C) in $CDCl_3$; [b] Recorded at 300 MHz (^{1}H) and 75 MHz (^{13}C) in $CDCl_3$.

Coniellin C (**3**) had the molecular formula $C_{23}H_{28}O_7$ as determined by the HRESIMS data. Comparison of its ^{1}H and ^{13}C NMR data with those of compound **2** showed the presence of an additional methoxy group (δ_H 3.35 and δ_C 56.4) and an additional methine (δ_H 3.78 and δ_C 79.5, CH-15). The attachment of the methoxy group at C-15 was confirmed by the HMBC correlation from the protons of the methoxy group to C-15 and the COSY correlations between H_{ab}-14 (δ_H

3.23 and 2.76)/H-15/H_{ab}-16 (δ_H 1.70 and 1.54). Thus, compound **3** was a 15-methoxy derivative of coniellin B (**2**). The relative configuration of the methoxy group at C-15 could not be assigned.

Coniellin D (**4**) was isolated as a yellow powder. The molecular formula of $C_{21}H_{26}O_5$ was deduced from the HRESIMS data of **4**, differing from **1** by the loss of a carbonyl group and the addition of two extra protons. The NMR data of **4** (Table 3.3-2) were similar to those of **1** including signals of the pyranoquinone bicyclic ring, the aldehyde group and the 1-oxooct-2-en-1-yl side chain. However, an additional methylene group at δ_H 3.50 and 2.82 (H_{ab}-12) was observed in **4** in addition to the absence of the ester carbonyl at C-21. The COSY correlation between H_{ab}-12/H-8 (δ_H 3.33) and the HMBC correlations from H_{ab}-12 and H-8 to C-13 (δ_C 198.7) confirmed the location of the additional methylene at C-12 and the disappearance of the lactone carbonyl group in **4**. The NOE cross-peaks from Me-9 (δ_H 1.11) to H_{ab}-12 suggested a *trans* relationship between Me-9 and H-8, as already confirmed in compounds **1**−**3**. Thus, the structure of compound **4** was elucidated as shown.

The molecular formula of compound **5** was elucidated as $C_{21}H_{28}O_6$ based on the HRESIMS data, containing an additional oxygen atom and two additional protons when compared to **4**. Comparison of the NMR data of **5** with those of **4** revealed the presence of an additional oxygenated methine group at δ_H 4.14 and δ_C 68.5 (CH-15). The attachment of a hydroxy group at C-15 was confirmed by the COSY correlations between H_{ab}-14 (δ_H 2.74 and 2.62)/H-15/H_{ab}-16 (δ_H 1.54 and 1.47) and the HMBC correlations from H_{ab}-14 to C-13 (δ_C 209.3). The remaining structure of **5** was shown to be identical to that of **4** after analysis of the 2D NMR data. The NOE relationships from Me-9 (δ_H 1.09) to H_{ab}-12 (δ_H 3.28 and 2.86) indicated the same *trans* configuration between Me-9 and H-8 as that in **4**. The absolute configuration at C-15 in **5** was determined to be *S* using Mosher's method (Figure 3.3-3).

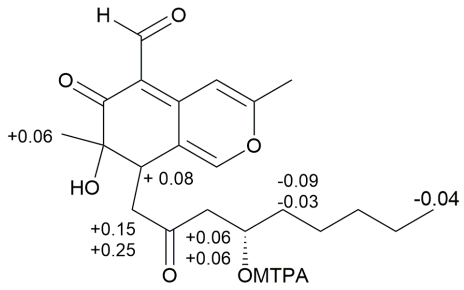

Figure 3.3-3. $\Delta\delta^{SR}$ (δ_S – δ_R) values of (*S*)- and (*R*)-MTPA esters of 5.

Detailed analysis of the HRESIMS and 2D NMR data of coniellin F (**6**) revealed that it shared the same planar structure as that of **5**. In the ROESY spectrum of **6**, Me-9 (δ_H 1.08) showed NOE correlations to H_{ab}-12 (δ_H 3.31 and 2.87) suggesting that the relative configuration at C-7 and C-8 was identical to that of **5**. Meanwhile, the different coupling constants between H-15

and H_{ab}-14 in compounds **5** ($J_{Ha\text{-}14/H\text{-}15}$ = 3.0 Hz, $J_{Hb\text{-}14/H\text{-}15}$= 9.4 Hz) and 6 ($J_{Ha\text{-}14/H\text{-}15}$= 9.9 Hz, $J_{Hb\text{-}14/H\text{-}15}$ = 2.7 Hz) suggested that both compounds are 15-epimers.

The molecular formula of coniellin G (**7**) was determined to be $C_{22}H_{30}O_6$ on the basis of the HRESIMS data. The NMR data of **7** (Table 3.3-2) were similar to those of compounds **5** and **6** except for signals indicating the presence of an additional methoxy group. HMBC correlations from the methoxy singlet to the downfield shifted C-15 (δ_C 77.8) and the COSY correlations between H_{ab}-14 (δ_H 2.68 and 2.66)/H-15/H_{ab}-16 (δ_H 1.62 and 1.48) indicated the methoxy group to be located at C-15. Detailed analysis of the 2D NMR spectra of **7** confirmed the compound to be identical to **5** and **6** with exception to the methoxy substituent at C-15. The chemical shifts and coupling constants of CH_2-14 in **7** ($J_{Ha\text{-}14/H\text{-}15}$= 5.3 Hz, $J_{Hb\text{-}14/H\text{-}15}$= 7.1 Hz) were comparable to those in **5** ($J_{Ha\text{-}14/H\text{-}15}$ = 3.0 Hz, $J_{Hb\text{-}14/H\text{-}15}$ = 9.4 Hz) but differed from those in **6** ($J_{Ha\text{-}14/H\text{-}15}$ = 9.9 Hz, $J_{Hb\text{-}14/H\text{-}15}$= 2.7 Hz), suggesting that **5** and **7** share the same configuration.

Table 3.3-2. ^{1}H and ^{13}C NMR Data for Compounds 4−7.

Position	4[a]		5[b]		6[b]		7[a]	
	δ_C, type	δ_H (*J* in Hz)	δ_C, type	δ_H (*J* in Hz)	δ_C, type	δ_H (*J* in Hz)	δ_C, type	δ_H (*J* in Hz)
1	150.9. CH	7.61. d (1.7)	150.4. CH	7.57. d (1.8)	150.6. CH	7.55. d (1.9)	150.8. CH	7.55. d (1.9)
3	165.1, C		165.0, C		165.0, C		165.1, C	
4	107.7, CH	8.43, s	107.6, CH	8.44, s	107.6, CH	8.44, s	107.7, CH	8.42, s
4a	151.1, C		150.9, C		151.0, C		151.1, C	
5	108.4, C		108.5, C		108.4, C		108.3, C	
6	198.9, C		198.8, C		198.9, C		198.9, C	
7	71.8, C		71.7, C		71.5, C		71.5, C	
8	40.3, CH	3.33, dt (10.2, 1.7)	39.7, CH	3.37, ddd (9.4, 2.6, 1.8)	39.6, CH	3.39, ddd (9.8, 2.1, 1.9)	39.3, CH	3.37, dt (10.0, 1.9)
8a	121.9, C		121.6, C		121.5, C		121.7, C	
9	20.6, CH_3	1.11, s	20.6, CH_3	1.09, s	20.7, CH_3	1.08, s	20.7, CH_3	1.07, s
10	190.2, CH	10.20, s	190.1, CH	10.20, s	190.2, CH	10.20, s	190.2, CH	10.18, s
11	20.2, CH_3	2.38, s	20.1, CH_3	2.39, s	20.1, CH_3	2.38, s	20.1, CH_3	2.38, s
12	36.3, CH_2	3.50, dd (16.7, 1.7)	39.4, CH_2	3.28, dd (17.6, 2.6)	40.7, CH_2	3.31, dd (18.4, 2.1)	39.7, CH_2	3.27, dd (18.0, 1.9)
		2.82, dd (16.7, 10.2)		2.86, dd (17.6, 9.4)		2.87, dd (18.4, 9.8)		2.85, dd (18.0, 10.0)
13	198.7, C		209.3, C		209.4, C		207.9, C	
14	129.4, CH	6.17, dt (15.9, 1.5)	49.7, CH	2.74, dd (16.0, 3.0)	49.3, CH	2.70, dd (15.6, 9.9)	46.9, CH	2.68, dd (14.8, 5.3)
				2.62, dd (16.0, 9.4)		2.61, dd (15.6, 2.7)		2.66, dd (14.8, 7.1)
15	150.1 CH	7.06, dt (15.9, 6.9)	68.5 CH	4.14, m	69.0 CH	4.14, m	77.8 CH	3.74, m
16	32.6, CH_2	2.25, q (7.0)	37.1, CH_2	1.54, m	37.2, CH_2	1.54, m	32.9, CH_2	1.62, m
				1.47, m		1.48, m		1.48, m
17	27.7, CH_2	1.48, m	25.2, CH_2	1.45, m	25.0, CH_2	1.43, m	24.7, CH_2	1.30, m
				1.34, m		1.33, m		
18	31.4, CH_2	1.30, m	31.7, CH_2	1.31, m	31.7, CH_2	1.31, m	31.8, CH_2	1.30, m
19	22.4, CH_2	1.32, m	22.6, CH_2	1.32, m	22.6, CH_2	1.32, m	22.5, CH_2	1.31, m
20	13.9, CH_3	0.90, t (7.0)	14.0, CH_3	0.90, t (7.0)	13.9, CH_3	0.90, t (7.0)	14.0, CH_3	0.89, t (6.9)
15-OMe							56.2, CH_3	3.33, s

[a] Recorded at 300 MHz (^{1}H) and 75 MHz (^{13}C) in $CDCl_3$; [b] Recorded at 600 MHz (^{1}H) and 150 MHz (^{13}C) in $CDCl_3$.

Azaphilones possessing a highly oxygenated bi- or tricyclic core have hitherto mainly been reported from the fungal genera *Penicillium*, *Aspergillus*, *Talaromyces*, *Monascus*, and *Chaetomium* [24]. Some of these compounds may be considered as important taxonomic marker metabolites. Azaphilones are biogenetically derived from the polyketide pathway giving rise to the cyclized core structure and from fatty acid metabolism yielding the side chain. The aldehyde group at C-5 in the azaphilone derivatives isolated in this study is unusual. Few azaphilones with an aliphatic side chain at C-5 have been reported in the literature including austdiol from *Aspergillus ustus* [25] and helotialins A and C from *Helotiales* sp. Due to the deshielding effect of the aldehyde group in coniellins and austdiol or the carboxylic acid group in helotialins A and C, the signals of H-4 of those compounds are around δ_H 8.5, whereas the signals of H-4 of azaphilone derivatives with a proton at C-5 appear at δ_H 5.9–6.5.

Azaphilones were previously reported to possess cytotoxicity against various tumor cell lines [27,28]. However, to date, effects of azaphilones on triple negative breast cancer cell lines have not been evaluated. Noteworthy, triple negative breast cancer (TNBC) represents the most aggressive form of breast cancer with currently no targeted therapy available and a significantly reduced overall survival rate [28]. Thus, the effects on viability of the triple negative breast cancer cell line MDA-MB-231 of compounds **1**−**7** were tested. Among them compounds **1**-**5** and **7** displayed weak cytotoxic activities with IC_{50} values ranging between 18.6 µM (**4**) and 79.3 µM (**5**). Compound **6** displayed no activity (IC_{50} > 100 µM) after 24 h of compound incubation (Table 3.3-3).

Various studies suggested that several azaphilones exhibit anti-inflammatory activity by inhibiting nitric oxide production [30,31]. Furthermore, Youn *et al.* reported inhibition of tumor necrosis factor alpha (TNF-a)-induced nuclear factor-kappa B (NF-κB) in RAW 264.7 cells with IC_{50} values ranging between 0.9 and 11.6 µM [32]. In our study, compounds **1** and **4-7** displayed inhibition of NF-κB, with compound **1** as the most active analogue (IC_{50} value of 4.4 µM). Noteworthy, based on the short compound incubation time of 2 hours used for this assay, NF-κB inhibition effects of azaphilones can be clearly distinguished from their cytotoxicity (Table 3.3-3). NF-κB activity is involved in epithelial-to-mesenchymal transition (EMT) in breast cancer, thereby enhancing invasion and metastasis [32]. Thus, to explore the potential of azaphilone derivatives on tumor cell migration, we further analyzed the NF-κB inhibitor **1** at concentrations of 1, 5 and 10 µM and compounds **4**, **5** and **7** at a concentration of 10 µM each in a 2D scratch wound assay, respectively (Figure 3.2-4 and Figure 3.2-5). Compound **1** displayed 60% inhibition of tumor cell migration at 5 µM and 98% inhibition at 10 µM after 24 h. Furthermore, compounds **4** and **5** blocked migration by 78% and 83% at 10 µM, respectively. In contrast, compounds **6** and **7** did not exhibit significant cell migration inhibition when tested at a

concentration of 10 µM. Furthermore, we evaluated compound **1** in a 3D invasion assay at a concentration of 10 µM. After 24 hours, compound **1** reduced invasion of triple negative breast cancer cells into the surrounding extracellular matrix by 52%.

Comparison of the structure of **1** with those of **2** and **3** indicated that the presence of a double bond at C-14/C-15 is important for NF-κB inhibition. Compared to **1**, the loss of the lactone ring in **4** significantly decreased the inhibitory activity. For the 15-epimers **5** and **6**, the 15*S* isomer **5** was more active than the 15*R* isomer **6**, while methylation at 15-OH (**7** vs. **5**) increased NF-κB inhibitory activity perhaps due to increased lipophilicity and enhanced diffusion across membranes.

Table 3.3-3. Cell viability and NF-κB inhibition assessment of azaphilone derivatives.

Compound	Cell viability[a] IC_{50} (µM)	NF-κB inhibition[b] IC_{50} (µM)
1	21.5 ±9.5	4.4 ±2.3
2	19.6 ±10.0	>100
3	21.0 ±3.7	>100
4	18.6 ±4.7	37.8 ±3.2
5	79.3 ±0.8	29.4 ±2.2
6	>100	70.7 ±7.8
7	21.6 ±3	11.3 ±0.5

[a]Cell Viability of MDA-MB-231 cells was measured 24 hours after compound treatment. As a positive control, cells were incubated with a concentration of 5 µM staurosprorine normalized to 1% DMSO, the latter equaling 100% cell viability; 5 µM staurosporine reduced the cell viability to 10.9%.
[b]To determine NF-κB inhibition, compounds were incubated for 20 minutes followed by treatment with 20 ng/mL TNFα for 2 hours. TNFα alone served as positive control, inducing NF-κB activation by 5.3-fold at a concentration of 20 ng/mL.

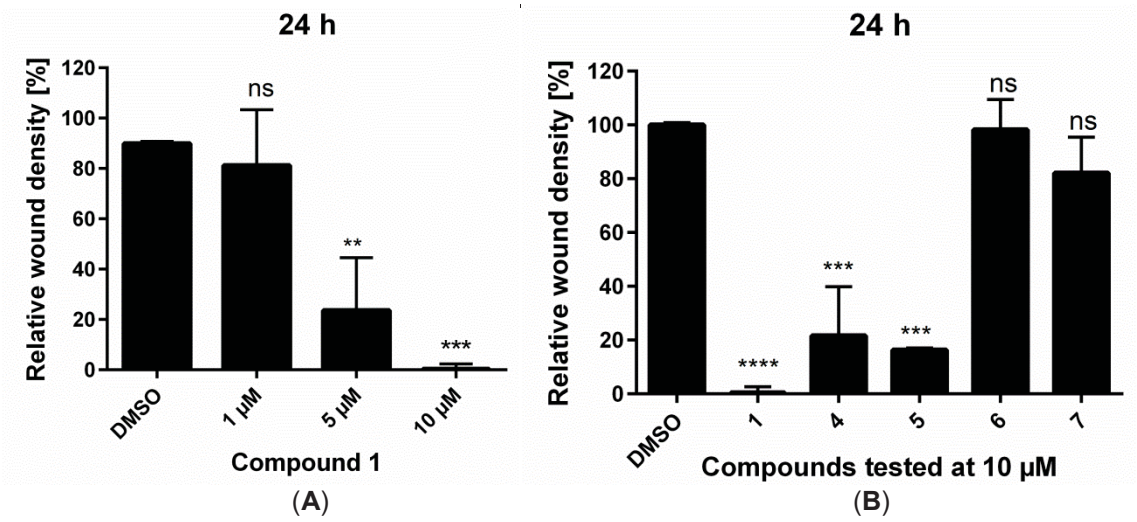

Figure 3.3-4. Inhibition of tumor cell migration in a scratch wound assay.

Compound 1 was (A) tested at the concentrations of 1, 5 and 10 µM, respectively or (B) evaluated at 10 µM in comparison with derivatives 4−7. Data represent increasing relative wound density in percentage calculated with the IncuCyte ZOOM® software. Error bars show ±SEM. Four stars represent a significance of ρ<0.0001, three stars of ρ<0.001 and two stars of ρ<0.01. 'Ns' means not significant.

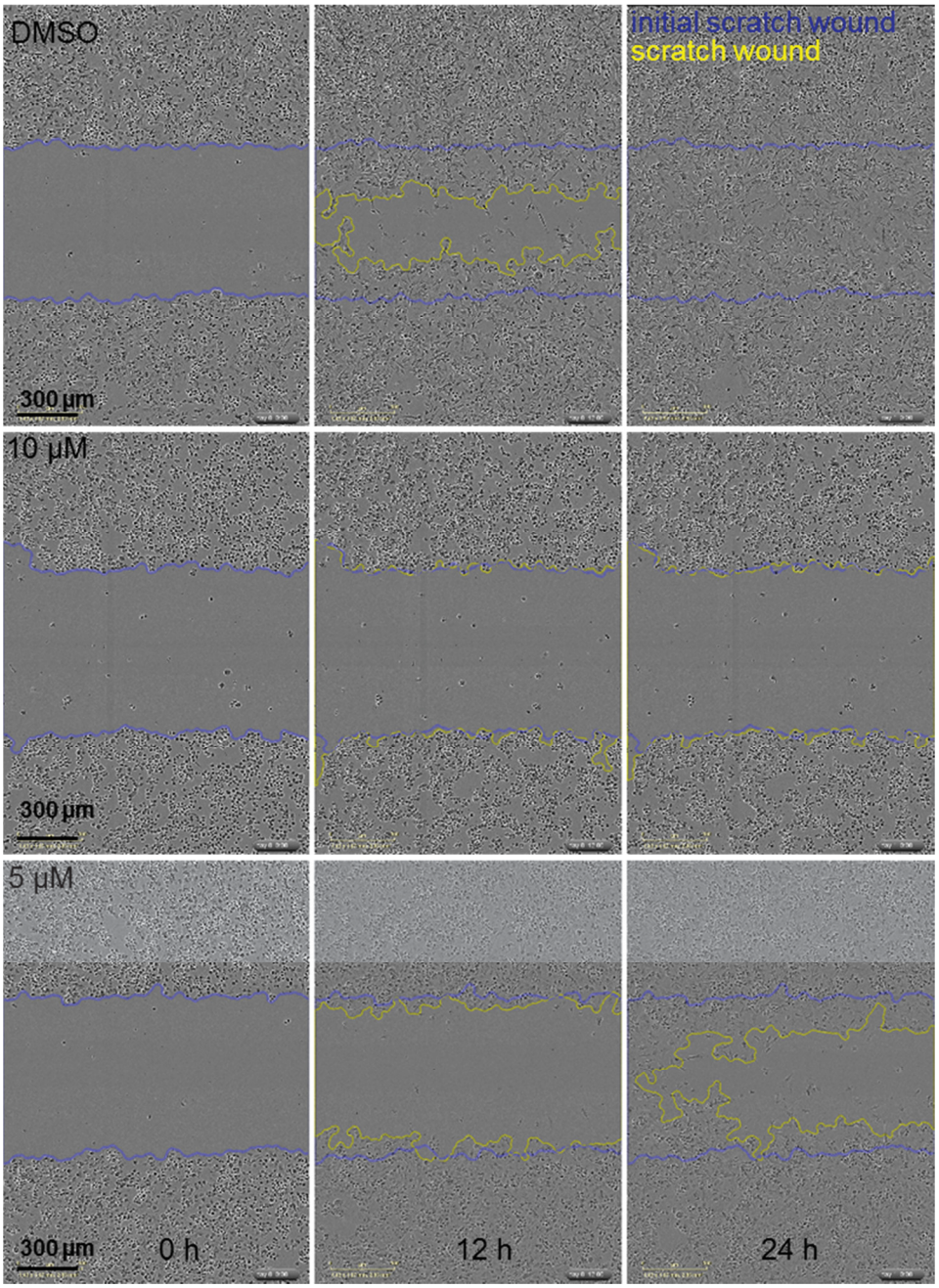

Figure 3.3-5. Images of the scratch wound assay after 0, 12 and 24 hours of incubation with compound 1. Compound 1 was tested at concentrations of 5 and 10 µM, respectively. Whereas the cells in control migrate and cover the clear zone of the scratch wound completely after 24 h, treatment with compound **1** inhibits cell migration.

EXPERIMENTAL SECTION

General Experimental Procedures

NMR spectra were recorded on Bruker Avance III 300 or Bruker Avance III 600 spectrometers. HRESIMS data were obtained on a Bruker Daltonics UHR-QTOF Maxis 4G mass spectrometer. Optical rotations were measured with a JASCO P-2000 polarimeter. ECD spectra were recorded on a J-810 spectropolarimeter. HPLC analysis was carried out using a Dionex UltiMate-3400SD system (an LPG-3400SD pump and a DAD3000RS photodiode array detector) coupled with a Knauer Eurospher C_{18} analytical column (125×4 mm, 5µm). Semi-preparative HPLC was performed on a Lachrom-Merck Hitachi system using a 300×8 mm Knauer Eurospher C_{18} column. For TLC, plates precoated with Merck silica gel F254 were used with detection under 254 and 365 nm or by spraying the plates with anisaldehyde reagent followed by heating.

Fungal Material and Identification

The fungus was isolated from goose (*Anser anser*) dung collected at the North Sea coast close to Garding, Germany in September 2016. The fungus was identified as *C. fragariae* (GenBank accession number KJ710465.1) by DNA amplification and sequencing of ITS region as described before [34].

Fermentation, Extraction, and Isolation

The fungus was cultivated on rice medium in 50 Erlenmeyer flasks (1L each, 100 g of rice and 110 mL demineralized water per flask, autoclaved at 121 °C for 20 min before inoculation). After 14 days fermentation at 20 °C under static conditions, 500 mL EtOAc was added to each flask, followed by shaking at 150 rpm for 8 h. The solvent was evaporated to dryness to give 52 g crude extract. Liquid–liquid separation between *n*-hexane and MeOH was performed. The obtained MeOH soluble fraction (27 g) was separated by vacuum liquid chromatography on a RP-18 column (50×200 mm) using a solvent gradient (from 100% H_2O to 100% MeOH) to give seven fractions (Fr.1 to Fr.7). Fr.5 (1.6 g) was subjected to a Sephadex LH-20 column (20×1000 mm) with MeOH, followed by separation on a silica gel column (30×500 mm) eluted with a gradient of *n*-hexane and EtOAc (from 9:1 to 1:2) to afford five subfractions (Fr.5.1 to Fr.5.5). Fr.5.3 contained compound **1** (1.1 g). Fr.5.4 was separated by semi-preparative HPLC using 60% MeOH-H_2O to give compounds **2** (6.1 mg) and **3** (5.6 mg). Fr.4 (0.9 g) was fractionated on a silica gel column with *n*-hexane and EtOAc as mobile phase to give three subfractions (Fr.4.1 to Fr.4.3). Fr.4.1 and Fr.4.2 were separated by semi-preparative HPLC with 60% MeOH-H_2O to afford compounds **4** (5.5 mg) and **7** (6.9 mg), respectively. Following the same procedure, Fr.3 (0.8 g) was subjected to a silica column (30×300 mm) using a gradient of *n*-hexane and EtOAc,

followed by purification with semipreparative HPLC using 50% MeOH-H_2O to give compounds **5** (3.4 mg) and **6** (2.9 mg).

*Coniellin A (**1**)*: yellow powder; $[\alpha]^{20}_{,D}$ +371 (*c* 0.1, $CHCl_3$); UV (CH_3OH) λ_{max} 255, 382 nm; ECD (MeCN, λ [nm] ($\Delta\varepsilon$), *c* 0.163 mM): 410 (-1.87), 368 (+6.92), 326sh (+1.70), 313sh (+1.30), 276sh (-2.27), 267 (-2.72), 253sh (-1.85), 235 (+6.27), 204sh (+1.88); ^1H and ^{13}C NMR data,; HRESIMS *m/z* 385.1650 $[M+H]^+$ (calcd for $C_{22}H_{25}O_6$, 385.1646).

*Coniellin B (**2**)*: yellow powder; $[\alpha]^{20}_{,D}$ +417 (c 0.1, $CHCl_3$); UV (CH_3OH) λ_{max} 257, 379 nm; ^1H and ^{13}C NMR data,

Table 3.3-1; HRESIMS *m/z* 387.1802 $[M+H]^+$ (calcd for $C_{22}H_{27}O_6$, 387.1802).

*Coniellin C (**3**)*: yellow powder; $[\alpha]^{20}_{,D}$ +400 (c 0.1, $CHCl_3$); UV (CH_3OH) λ_{max} 257, 379 nm; ^1H and ^{13}C NMR data,

Table 3.3-1; HRESIMS *m/z* 417.1903 $[M+H]^+$ (calcd for $C_{23}H_{29}O_7$, 417.1908).

*Coniellin D (**4**)*: yellow powder; $[\alpha]^{20}_{,D}$ +124 (c 0.1, $CHCl_3$); UV (CH_3OH) λ_{max} 271, 379 nm; ^1H and ^{13}C NMR data, Table 3.3-2; HRESIMS *m/z* 359.1853 $[M+H]^+$ (calcd for $C_{21}H_{27}O_5$, 359.1853).

*Coniellin E (**5**)*: yellow powder; $[\alpha]^{20}_{,D}$ +171 (c 0.1, $CHCl_3$); UV (CH_3OH) λ_{max} 258, 378 nm; ^1H and ^{13}C NMR data, Table 3.3-2; HRESIMS *m/z* 377.1957 $[M+H]^+$ (calcd for $C_{21}H_{29}O_6$, 377.1959).

*Coniellin F (**6**)*: yellow powder; $[\alpha]^{20}_{,D}$ +97 (c 0.1, $CHCl_3$); UV (CH_3OH) λ_{max} 252, 377 nm; ^1H and ^{13}C NMR data, Table 3.3-2; HRESIMS *m/z* 377.1959 $[M+H]^+$ (calcd for $C_{21}H_{29}O_6$, 377.1959).

*Coniellin G (**7**)*: yellow powder; $[\alpha]^{20}_{,D}$ +225 (c 0.1, $CHCl_3$); UV (CH_3OH) λ_{max} 269, 379 nm; ^1H and ^{13}C NMR data, Table 3.3-2; HRESIMS *m/z* 391.2111 $[M+H]^+$ (calcd for $C_{22}H_{31}O_6$, 391.2115).

Cell Culture and Reagents

MDA-MB-231 cells, obtained from European Collection of Authenticated Cell Cultures (Salisbury, UK), were cultured in RPMI medium supplemented with 15% fetal calf serum (FCS), 100 $U \cdot mL^{-1}$ penicillin and 100 $U \cdot mL^{-1}$ streptomycin at 37°C in the presence of 5% CO_2. Stable transfected NF-κB-MDA-MB-231 cells were cultured with Dulbecco's modified Eagle's medium supplemented with 10% FCS, 450 µg/mL hygromycin B (Sigma, Munich, Germany), 100 $U \cdot mL^{-1}$ penicillin and 100 $\mu g \cdot mL^{-1}$ streptomycin at 37°C in the presence of 5% CO_2. Media and antibiotics were purchased from Gibco (Life Technologies, Carlsbad, USA). Matrigel was obtained from Corning (New York, USA) and collagen R solution (0.2%) was purchased from Serva Electrophoresis GmbH (Heidelberg, Germany).

Cell Viability Assay

Cytotoxicity of test compounds was determined 24 hours after compound treatment with the CellTiter-Glo Luminescent Cell Viability Assay (Promega, Madison, USA) according to the manufacturer's instructions. 5600 cells/ well were seeded in white 384 well plates using the CyBi-Well 96-channel simultaneous pipettor (Analytic Jena, Jena, Germany) and cultured overnight at 37°C before compound addition.

NF-κB Reporter Gene Assay

Stable NF-κB-MDA-MB-231 cells were generated as described previously [35]. The cells were seeded at a density of 20.000 cells/well in white 96-well plates (Greiner Bio-One, Kremsmuenster, Austria). After 24 hours, cells were treated with indicated compounds for 20 minutes followed by incubation of 20 ng/mL TNFα (Peprotech, Rocky Hill, USA) for 2 h. Luminescence was determined using NanoGlo reagent from Promega (Madison, USA).

2D Scratch Wound Assay

MDA-MB-231 cells were seeded in an ImageLock 96-well plate (Sartorius, Goettingen, Germany) at a density of 50.000 cells/well. After 24 hours a scratch was made with the IncuCyte WoundMaker. Compounds were added at different concentrations and images were taken every 2 h for a time range of 24 h with the IncuCyte ZOOM Imager.

3D Invasion Assay

Spheroids were generated with 3000 cells/well of MDA-MB-231 cells supplemented with 0.25 % matrigel in an ultra-low-attachment (ULA) plate (Corning, New York, USA). The cells were centrifuged for 10 minutes at 1000 rpm at 4°C. After 72 h of spheroid formation, a mixture of matrigel and collagen R solution (ratio of 1:1) was used for embedding the spheroids. Polymerization of matrigel-collagen solution was allowed for 1 h at 37°C. Invasion of cells into the surrounding matrix was recorded every day for a time range of 3 days and analyzed with ImageJ Fiji.

Computational Section

Mixed torsional/low-mode conformational searches were carried out by means of the Macromodel 10.8.011 software [36] using the MMFF with an implicit solvent model for $CHCl_3$ applying a 21 kJ/mol energy window. Geometry reoptimizations of the resultant conformers [B3LYP/6-31G(d) level in vacuo, B97D/TZVP with PCM solvent model for MeCN, and CAM-B3LYP/TZVP with PCM solvent model for MeCN], OR, and ECD calculations were performed

with Gaussian 09 [37]. Chiroptical values were computed using various functionals (B3LYP, BH&HLYP, CAM-B3LYP, PBE0) and the TZVP basis set. ECD spectra were generated as the sum of Gaussians [38] with 3900 cm^{-1} half-height width (corresponding to ca. 28 nm at 270 nm), using dipole-velocity-computed rotational strength values. Boltzmann distributions were estimated from the ZPVE-corrected B3LYP/6-31G(d) energies in the gas-phase calculations and from the B97D/TZVP, and CAM-B3LYP/TZVP energies in the PCM model ones. The MOLEKEL [39] software package was used for visualization of the results.

Chiral Derivatization

Compound **5** (1.0 mg) dissolved in deuterated pyridine (1.5 mL) was added to two dry and clean NMR tubes at equal parts. Then 10 µl (*R*)- or (*S*)-MTPA (α-methoxy-α-(trifluoromethyl)phenylacetyl) chloride were added separately under argon protection. The tubes were shaken to mix the samples and MTPA chloride. After 8 h incubation at room temperature, ^1H NMR spectra were measured in order to detect the reaction products. Then the reaction products were purified by semipreparative HPLC with MeOH–H_2O as mobile phase.

Supporting Information: HRESIMS, UV, and NMR spectra of compounds **1**−**7** as well as ECD calculations, cell viability and NF-κB inhibitory assay for compound **1** (the biological experiments were performed by Julia Sperlich).

Acknowledgments: We thank the DFG (GRK 2158) and the Manchot Foundation for support. The research project was further supported by a grant to N.T. provided by the Ministry of Culture and Science of the federal state of North Rhine-Westphalia, Germany. The research of the Hungarian authors was supported by the EU and co-financed by the European Regional Development Fund under the project GINOP-2.3.2-15-2016-00008. The Governmental Information-Technology Development Agency (KIFÜ) is acknowledged for CPU time.

REFERENCES

1. Bills, G. F.; Gloer, J. B. *Microbiol. Spectrum* **2016**, 4, 1−32.
2. Jayanetti, D. R.; Yue, Q.; Bills, G. F.; Gloer, J. B. *J. Nat. Prod.* **2015**, 78, 396−401.
3. Jayanetti, D. R.; Li, Y.; Bartholomeusz, G. A.; Bills, G. F.; Gloer, J. B. *J. Nat. Prod.* **2017**, 80, 707−712.
4. Sarrocco, S. *Pest Manage. Sci.* **2016**, 72, 643−652.
5. Liu, S.; Dai, H.; Makhloufi, G.; Heering, C.; Janiak, C.; Hartmann, R.; Mándi, A.; Kurtán, T.; Müller, W. E. G.; Kassack, M. U.; Lin, W.; Liu, Z.; Proksch, P. *J. Nat. Prod.* **2016**, 79, 2332−2340.

6. Elnaggar, M. S.; Ebrahim, W.; Mándi, A.; Kurtán, T.; Müller, W. E. G.; Kalscheuer, R.; Singab, A.; Lin, W.; Liu, Z.; Proksch, P. *RSC Adv.* **2017**, 7, 30640−30649.
7. Wang, H.; Eze, P. M.; Hofert, S.-P.; Janiak, C.; Hartmann, R.; Okoye, F. B. C.; Esimone, C. O.; Orfali, R. S.; Dai, H.; Liu, Z.; Proksch, P. *RSC Adv.* **2018**, 8, 7863−7872.
8. Tziros, G. T.; Tzavella-Klonari, K. *Plant Pathol.* **2008**, 57, 783.
9. Levy, E.; Elkind, G.; Ben-Arie, R.; Ben-Ze'ev, I. S. *Phytoparasitica* **2011**, 39, 403−405.
10. Çeliker, N. M.; Uysal, A.; Çetinel, B.; Poyraz, D. *Australas. Plant Dis. Notes* **2012**, 7, 161−162.
11. Pollastro, S.; Dongiovanni, C.; Gerin, D.; Pollastro, P.; Fumarola, G.; De Miccolis Angelini, R. M.; Faretra, F. *Plant Dis.* **2016**, 100, 1498.
12. Han, J.; Chen, D.; Huang, J.; Li, X.; Zhou, W.-W.; Gao, W.; Jia, Y. *Biocontrol Sci. Technol.* **2015**, 25, 1120−1132.
13. Grantina-Ievina, L.; Kalniņa, I. *Environ. Exp. Biol.* **2016**, 14, 51−52.
14. Griffiths, M.; Wylie, R.; Lawson, S.; Pegg, G.; McDonald, J. p. 15. In *Prospects for High-Value Hardwood Timber Plantations in the 'Dry' Tropics of Northern Australia*; Academic Press: Mareeba, Australia, **2004**, p15.
15. Stierle, A. A.; Stierle, D. B.; Girtsman, T.; Mou, T. C.; Antczak, C.; Djaballah, H. *J. Nat. Prod.* **2015**, 78, 2917−2923.
16. Superchi, S.; Scafato, P.; Górecki, M.; Pescitelli, G. *Curr. Med. Chem.* **2017**, *25*, 287−320.
17. Mándi, A.; Mudianta, I. W.; Kurtán, T.; Garson, M. J. *J. Nat. Prod.* **2015**, *78*, 2051−2056.
18. Grimme, S. *J. Comput. Chem.* **2006**, *27*, 1787−1799.
19. Sun, P.; Xu, D. X.; Mándi, A.; Kurtán, T.; Li, T. J.; Schulz, B.; Zhang, W. *J. Org. Chem.* **2013**, *78*, 7030−7047.
20. Yanai, T.; Tew, D. P.; Handy, N. C. *Chem. Phys. Lett.* **2004**, *393*, 51−57.
21. Zhou, Z. F.; Kurtán, T.; Yang, X. H.; Mándi, A.; Geng, M. Y.; Ye, B. P.; Taglialatela-Scafati, O.; Guo, Y. W. *Org. Lett.* **2014**, *16*, 1390−1393.
22. Polavarapu, P. L. *Chirality* **2008**, *20*, 664−672.
23. Sun, P.; Yu, Q.; Li, J.; Riccio, R.; Lauro, G.; Bifulco, G.; Kurtán, T.; Mándi, A.; Tang, H.; Zhuang, C. L.; Gerwick, W. H.; Zhang, W. *J. Nat. Prod.* **2016**, *79*, 2552−2558.
24. Gao, J.-M.; Yang, S.-X.; Qin, J.-C. *Chem. Rev.* **2013**, *113*, 4755−4811.
25. Vleggaar, R.; Steyn, P. S.; Nagel, D. W.; *J. Chem. Soc., Perkin Trans. 1* **1974**, *1, 45−49*.
26. Zou, X.-W.; Sun, B.-D.; Chen, X.-L.; Liu, X.-Z.; Che, Y.-S. *Zhongguo Tianran Yaowu* **2009**, *7, 140−144.*
27. Panthama, N.; Kanokmedhakul, S.; Kanokmedhakul, K.; Soytong, K. *J. Nat. Prod.* **2011**, 74, 2395−2399.
28. Zhou, S.-L.; Wang, M.; Zhao, H.-G.; Huang, Y.-H.; Lin, Y.-Y.; Tan, G.-H.; Chen, S.-L. *Arch. Pharm. Res.* **2016**, 39, 1621−1627.
29. Pal, S. K.; Childs, B. H.; Pegram, M. *Breast Cancer Res. Treat.* **2011**, 125, 627−636.
30. Luo, J.-G.; Xu, Y.-M.; Sandberg, D. C.; Arnold, A. E.; Gunatilaka, A. A. L. *J. Nat. Prod.* **2017**, 80, 76−81.
31. Cheng, M.-J.; Wu, M.-D.; Su, Y.-S.; Yuan, G.-F.; Chen, Y.-L.; Chen, I.-S. *Phytochem. Lett.* **2012**, 5, 262−266.
32. Youn, U. J.; Sripisut, T.; Park, E. J.; Kondratyuk, T. P.; Fatima, N.; Simmons, C. J.; Wall, M. M.; Sun, D.; Pezzuto, J. M.; Chang, L. C. *Bioorg. Med. Chem. Lett.* **2015**, 25, 4719−4723.
33. Pires, B. R. B.; Mencalha, A. L.; Ferreira, G. M.; de Souza, W. F.; Morgado-Díaz, J. A.; Maia, A. M.; Corrêa, S.; Abdelhay, E. S. F. W. *PLoS One* **2017**, 12, e0169622.
34. Kjer, J.; Debbab, A.; Aly, A. H.; Proksch, P. *Nat. Protoc.* **2010**, *5*, 479−490.
35. Sperlich, J.; Kerr, R.; Teusch, N. *Mar. Drugs* **2017**, 15, 262.
36. *MacroModel*; Schrödinger LLC: New York, **2015**, https://www.schrodinger.com/macromodel
37. Frisch, M. J.; Trucks, G. W.; Schlegel, H. B.; Scuseria, G. E.; Robb, M. A.; Cheeseman, J. R.; Scalmani, G.; Barone, V.; Mennucci, B.; Petersson, G. A.; Nakatsuji, H.; Caricato, M.; Li, X.; Hratchian, H. P.; Izmaylov, A. F.; Bloino, J.; Zheng, G.; Sonnenberg, J. L.; Hada,

M.; Ehara, M.; Toyota, K.; Fukuda, R.; Hasegawa, J.; Ishida, M.; Nakajima, T.; Honda, Y.; Kitao, O.; Nakai, H.; Vreven, T.; Montgomery, J. A., Jr.; Peralta, J. E.; Ogliaro, F.; Bearpark, M.; Heyd, J. J.; Brothers, E.; Kudin, K. N.; Staroverov, V. N.; Kobayashi, R.; Normand, J.; Raghavachari, K.; Rendell, A.; Burant, J. C.; Iyengar, S. S.; Tomasi, J.; Cossi, M.; Rega, N.; Millam, J. M.; Klene, M.; Knox, J. E.; Cross, J. B.; Bakken, V.; Adamo, C.; Jaramillo, J.; Gomperts, R.; Stratmann, R. E.; Yazyev, O.; Austin, A. J.; Cammi, R.; Pomelli, C.; Ochterski, J. W.; Martin, R. L.; Morokuma, K.; Zakrzewski, V. G.; Voth, G. A.; Salvador, P.; Dannenberg, J. J.; Dapprich, S.; Daniels, A. D.; Farkas, Ö.; Foresman, J. B.; Ortiz, J. V.; Cioslowski, J.; Fox, D. J.; *Gaussian 09*, Revision E.01; Gaussian, Inc.: Wallingford, CT, **2013**.

38. Stephens, P. J.; Harada, N. *Chirality* **2010**, *22*, 229−233.

39. Varetto, *U. MOLEKEL 5.4*; Swiss National Supercomputing Centre: Manno, Switzerland, **2009**.

3.3.1 Supplemental Material

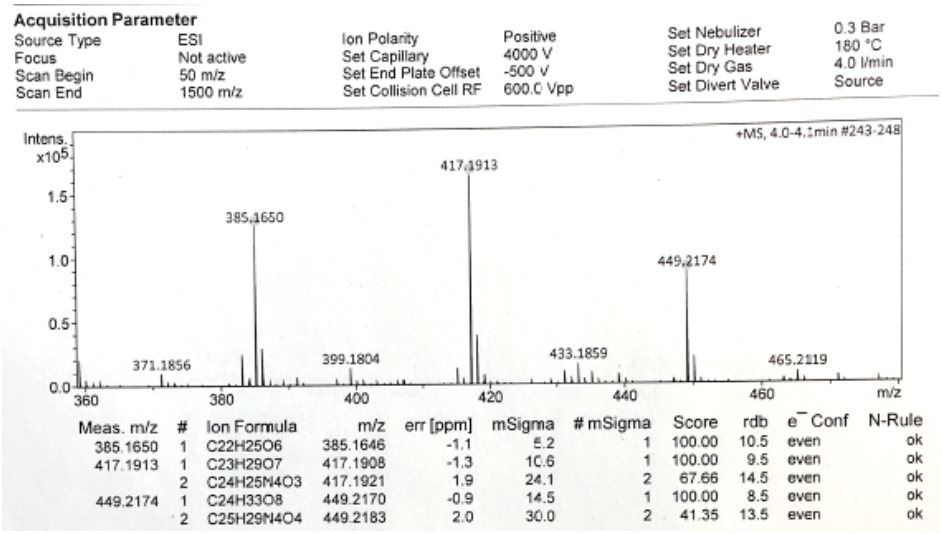

Meas. m/z	#	Ion Formula	m/z	err [ppm]	mSigma	# mSigma	Score	rdb	e⁻ Conf	N-Rule
385.1650	1	C22H25O6	385.1646	-1.1	5.2	1	100.00	10.5	even	ok
417.1913	1	C23H29O7	417.1908	-1.3	10.6	1	100.00	9.5	even	ok
	2	C24H25N4O3	417.1921	1.9	24.1	2	67.66	14.5	even	ok
449.2174	1	C24H33O8	449.2170	-0.9	14.5	1	100.00	8.5	even	ok
	2	C25H29N4O4	449.2183	2.0	30.0	2	41.35	13.5	even	ok

Supplemental Figure 3.3-1. The HRESIMS of compound 1

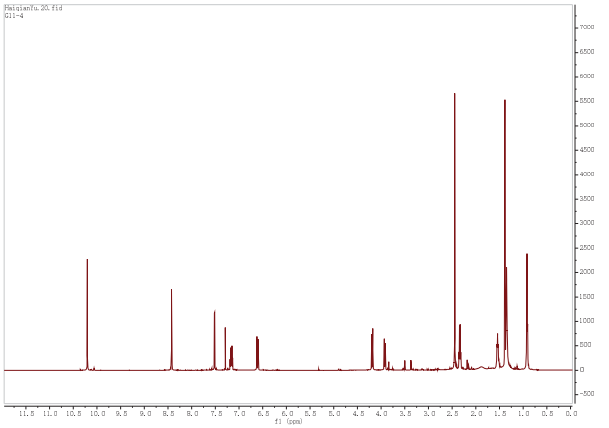

Supplemental Figure 3.3-2. The ^{1}H NMR (600 MHz, $CDCl_3$) spectrum of compound 1.

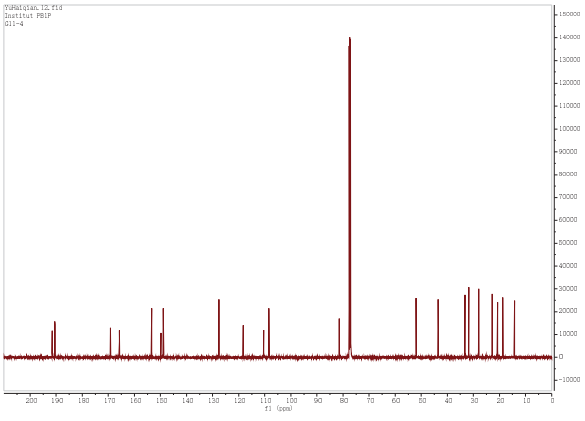

Supplemental Figure 3.3-3. The ^{13}C NMR (150 MHz, $CDCl_3$) spectrum of compound 1.

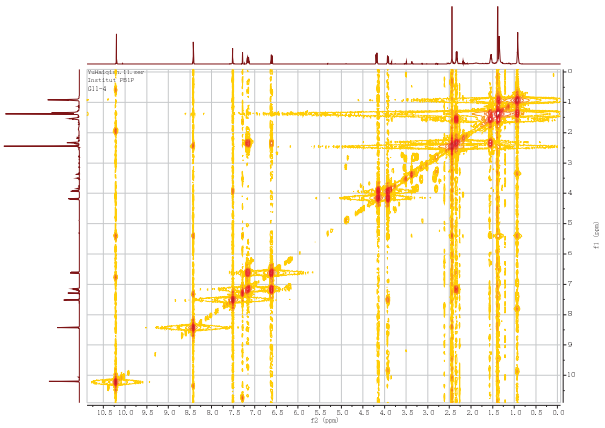

Supplemental Figure 3.3-4. The COSY (600 MHz, $CDCl_3$) spectrum of compound 1.

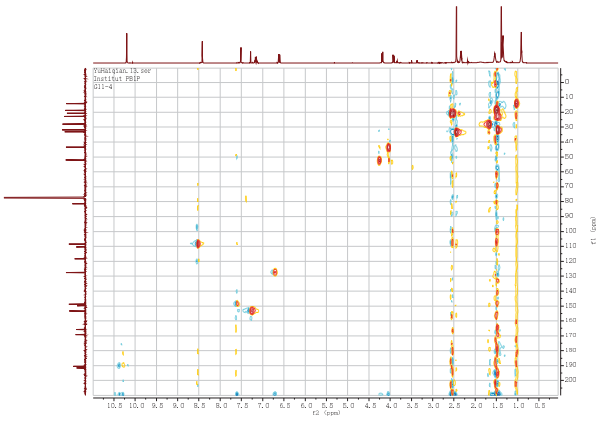

Supplemental Figure 3.3-5. The HSQC (600 MHz, $CDCl_3$) spectrum of compound 1.

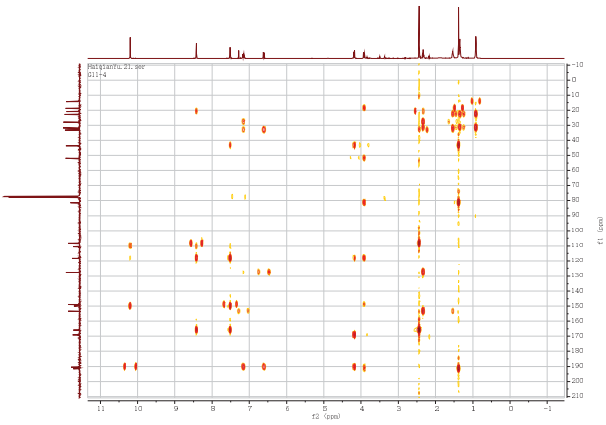

Supplemental Figure 3.3-6. The HMBC (600 MHz, $CDCl_3$) spectrum of compound 1.

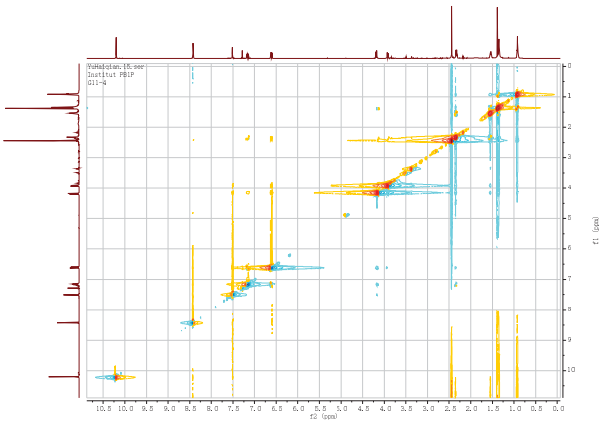

Supplemental Figure 3.3-7. The ROESY (600 MHz, $CDCl_3$) spectrum of compound 1.

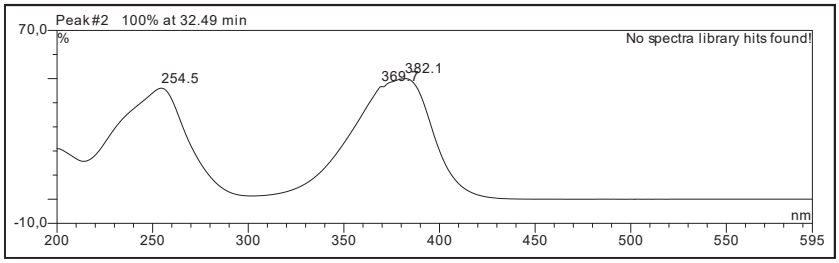

Supplemental Figure 3.3-8. The UV spectrum of compound 1.

Acquisition Parameter

Source Type	ESI	Ion Polarity	Positive	Set Nebulizer	0.3 Bar
Focus	Not active	Set Capillary	4000 V	Set Dry Heater	180 °C
Scan Begin	50 m/z	Set End Plate Offset	-500 V	Set Dry Gas	4.0 l/min
Scan End	1500 m/z	Set Collision Cell RF	600.0 Vpp	Set Divert Valve	Source

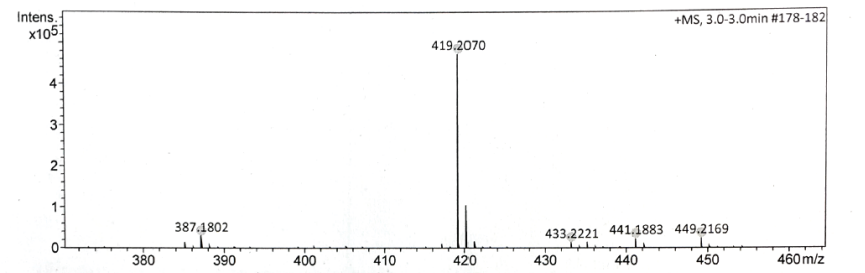

Meas. m/z	#	Ion Formula	m/z	err [ppm]	mSigma	# mSigma	Score	rdb	e¯ Conf	N-Rule
387.1802	1	C22H27O6	387.1802	0.1	23.3	1	100.00	9.5	even	ok
419.2070	1	C23H31O7	419.2064	-1.4	19.9	1	100.00	8.5	even	ok
	2	C24H27N4O3	419.2078	1.8	32.9	2	67.27	13.5	even	ok
433.2221	1	C24H33O7	433.2221	0.1	28.6	1	100.00	8.5	even	ok
441.1883	1	C23H30NaO7	441.1884	0.1	6.1	1	100.00	8.5	even	ok
	2	C21H25N6O5	441.1881	-0.6	6.2	2	91.33	12.5	even	ok
449.2169	1	C24H33O8	449.2170	0.2	14.9	1	100.00	8.5	even	ok
	2	C24H26N8Na	449.2173	0.8	15.1	2	66.37	15.5	even	ok

Supplemental Figure 3.3-9. The HRESIMS of compound 2.

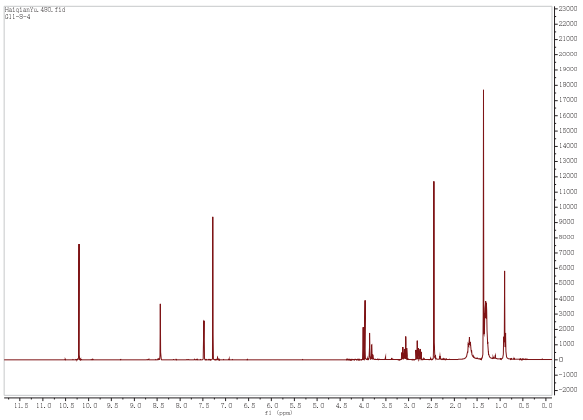

Supplemental Figure 3.3-10. The ^{1}H NMR (300 MHz, $CDCl_3$) spectrum of compound 2.

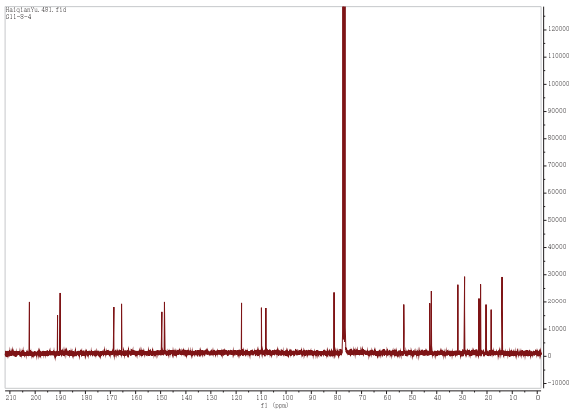

Supplemental Figure 3.3-11. The ^{13}C NMR (75 MHz, $CDCl_3$) spectrum of compound 2.

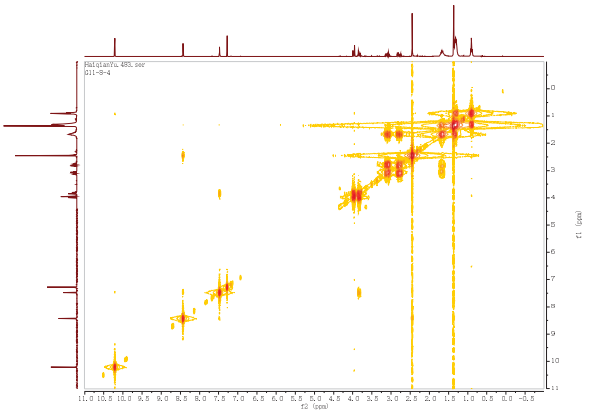

Supplemental Figure 3.3-12. The COSY (300 MHz, $CDCl_3$) spectrum of compound 2.

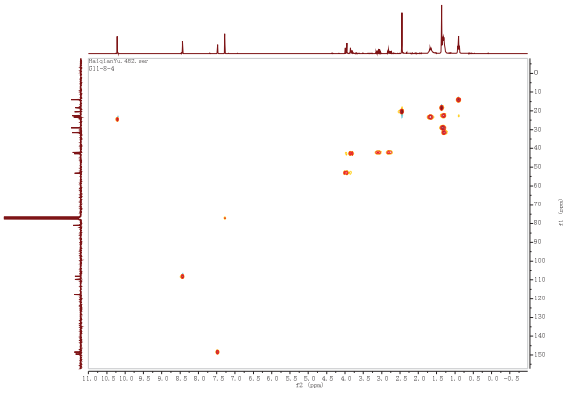

Supplemental Figure 3.3-13. The HSQC (300 MHz, $CDCl_3$) spectrum of compound 2.

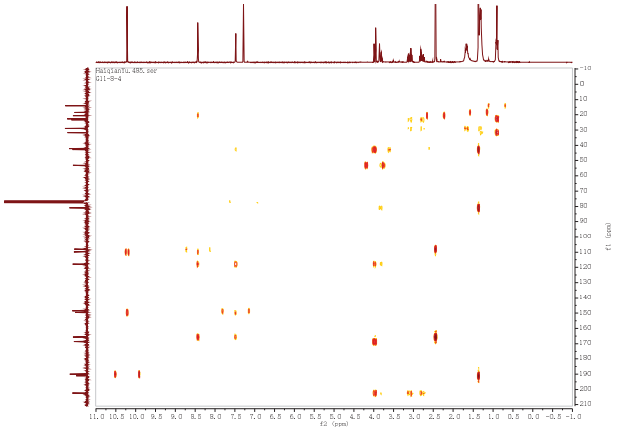

Supplemental Figure 3.3-14. The HMBC (300 MHz, $CDCl_3$) spectrum of compound 2.

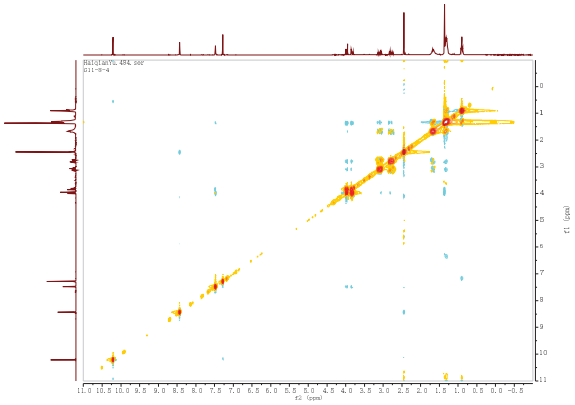

Supplemental Figure 3.3-15. The ROESY (300 MHz, $CDCl_3$) spectrum of compound 2.

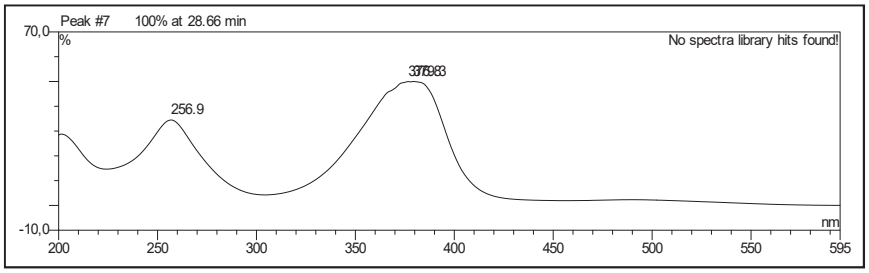

Supplemental Figure 3.3-16. The UV spectrum of compound 2.

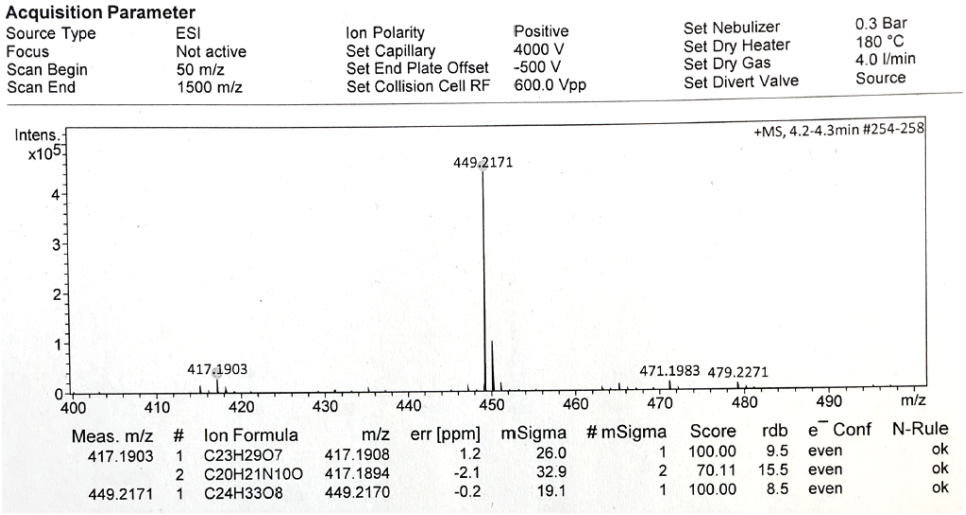

Supplemental Figure 3.3-17. The HRESIMS of compound 3.

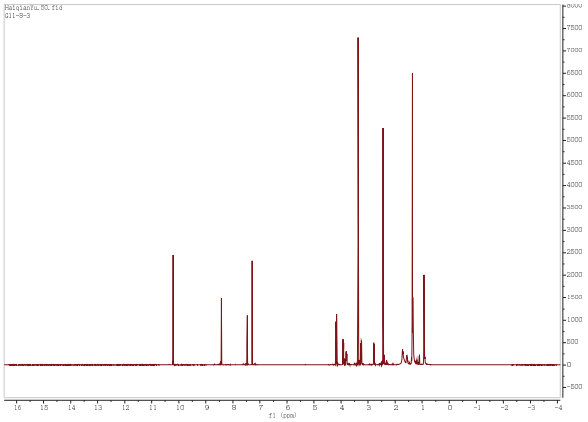

Supplemental Figure 3.3-18. The ^{1}H NMR (600 MHz, $CDCl_3$) spectrum of compound 3.

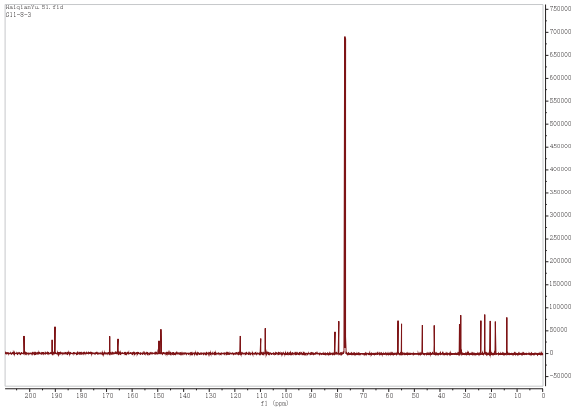

Supplemental Figure 3.3-19. The ^{13}C NMR (150 MHz, $CDCl_3$) spectrum of compound 3.

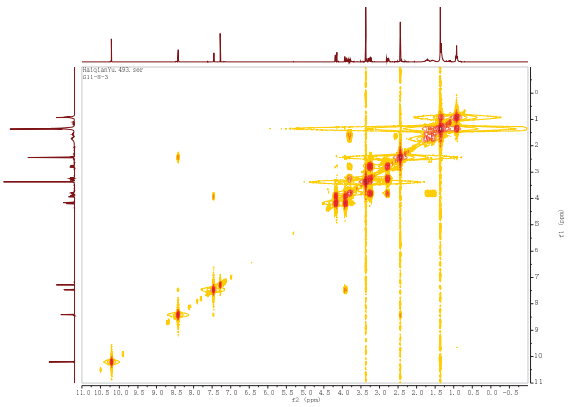

Supplemental Figure 3.3-20. The COSY (600 MHz, $CDCl_3$) spectrum of compound 3.

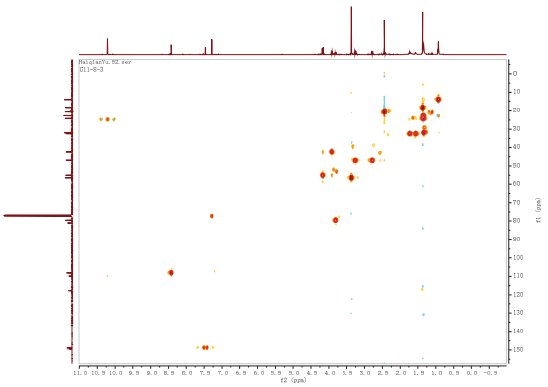

Supplemental Figure 3.3-21. The HSQC (600 MHz, $CDCl_3$) spectrum of compound 3.

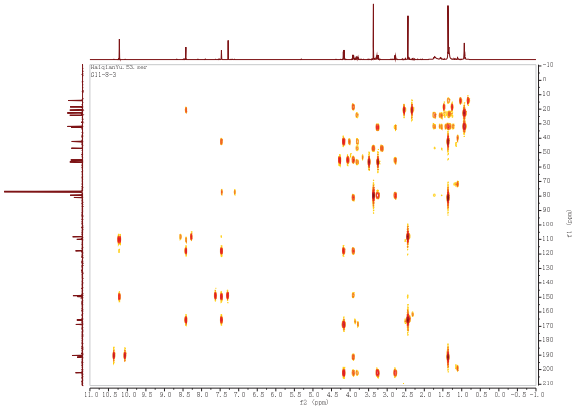

Supplemental Figure 3.3-22. The HMBC (600 MHz, $CDCl_3$) spectrum of compound 3.

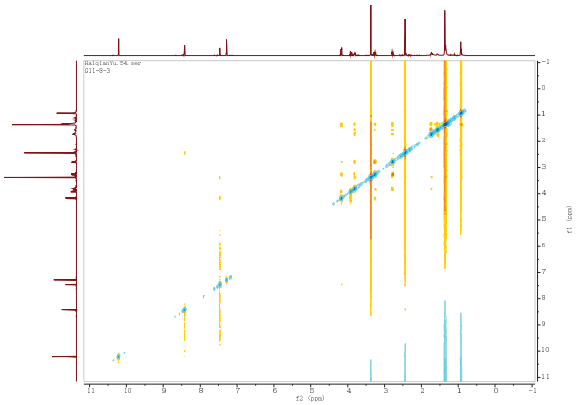

Supplemental Figure 3.3-23. The ROESY (600 MHz, $CDCl_3$) spectrum of compound 3.

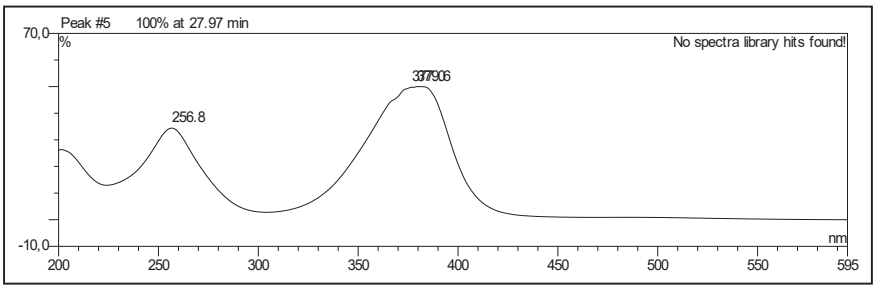

Supplemental Figure 3.3-24. The UV spectrum of compound 3.

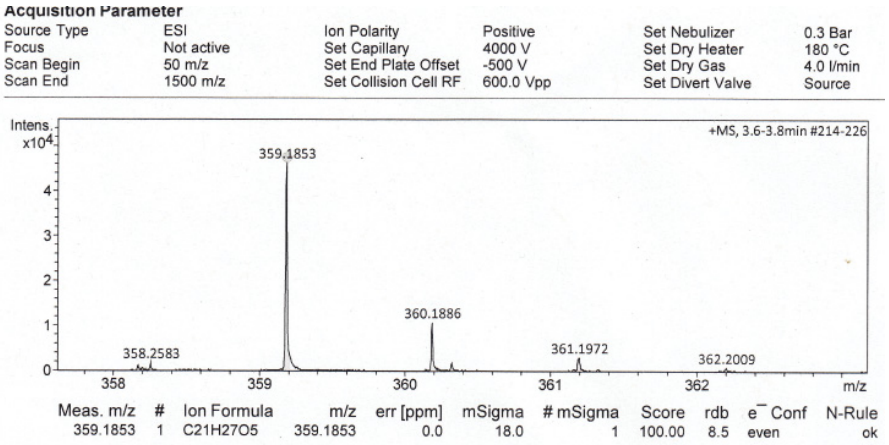

Supplemental Figure 3.3-25. The HRESIMS of compound 4.

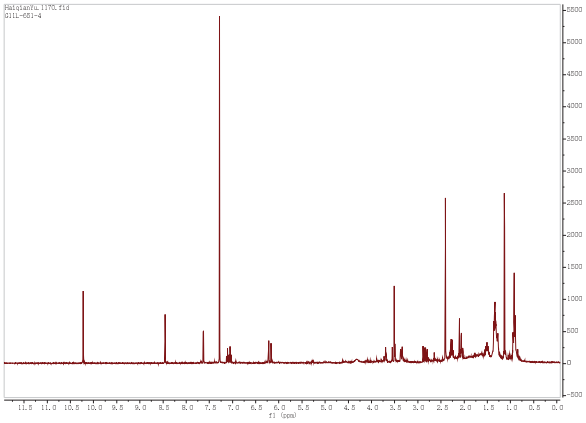

Supplemental Figure 3.3-26. The ^{1}H NMR (300 MHz, $CDCl_3$) spectrum of compound 4.

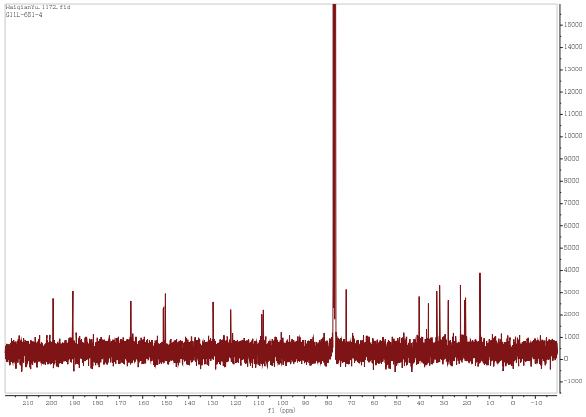

Supplemental Figure 3.3-27. The ^{13}C NMR (75 MHz, $CDCl_3$) spectrum of compound 4.

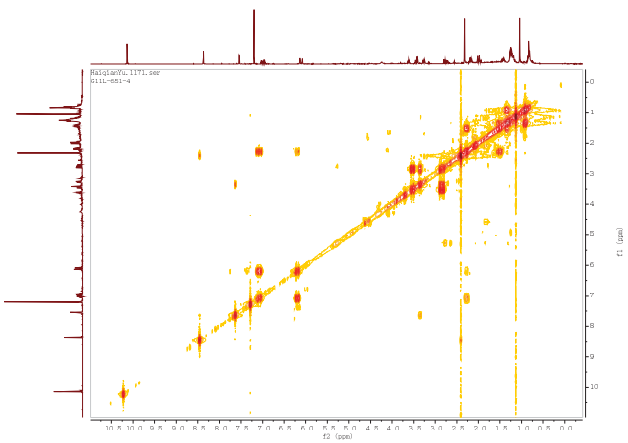

Supplemental Figure 3.3-28. The COSY (300 MHz, $CDCl_3$) spectrum of compound 4.

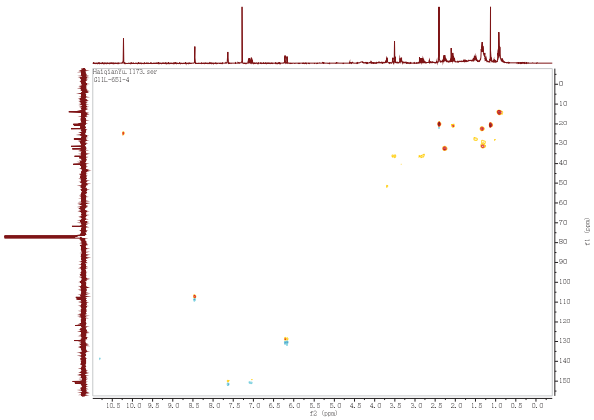

Supplemental Figure 3.3-29. The HSQC (300 MHz, $CDCl_3$) spectrum of compound 4.

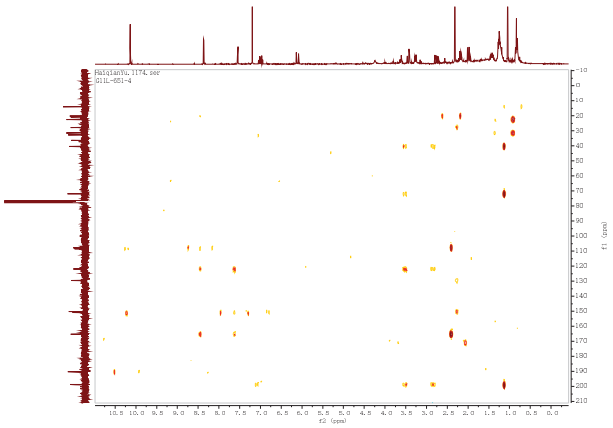

Supplemental Figure 3.3-30. The HMBC (300 MHz, $CDCl_3$) spectrum of compound 4.

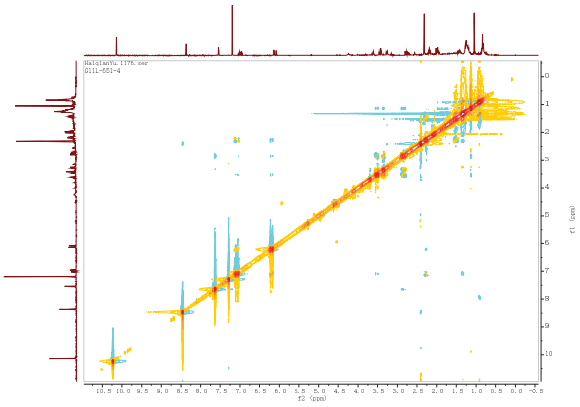

Supplemental Figure 3.3-31. The ROESY (300 MHz, $CDCl_3$) spectrum of compound 4.

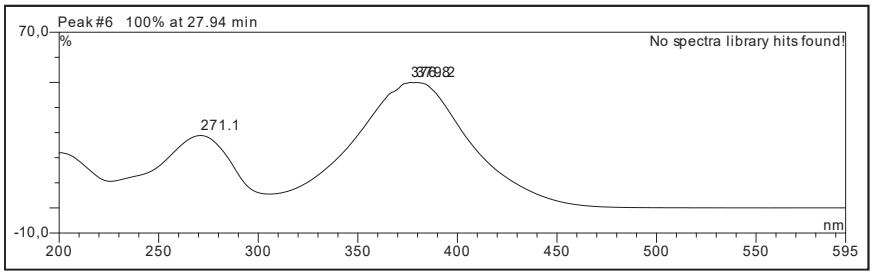

Supplemental Figure 3.3-32. The UV spectrum of compound 4.

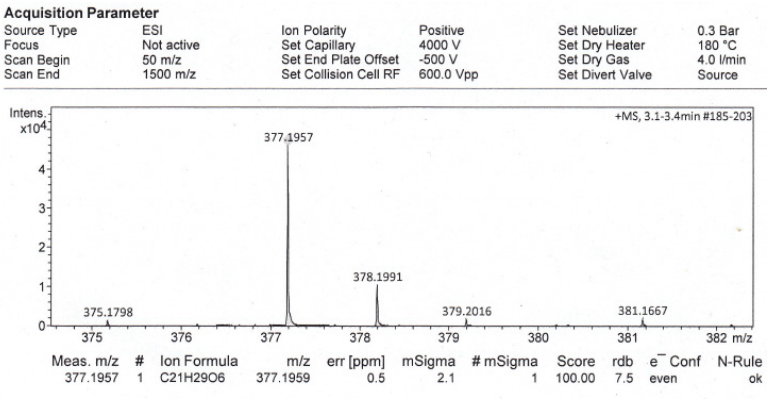

Supplemental Figure 3.3-33. The HRESIMS of compound 5.

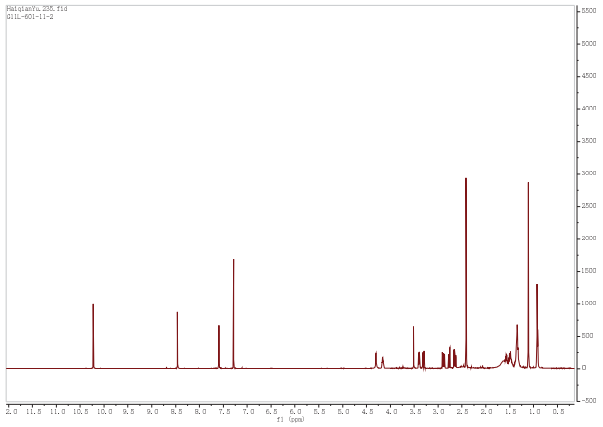

Supplemental Figure 3.3-34. The ^{1}H-NMR (600 MHz, $CDCl_3$) spectrum of compound 5.

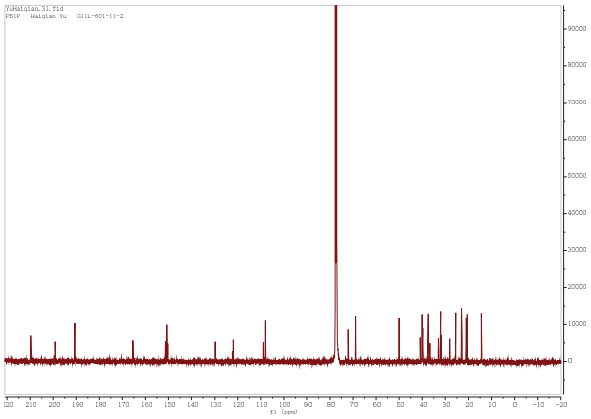

Supplemental Figure 3.3-35. The ^{13}C NMR (150 MHz, $CDCl_3$) spectrum of compound 5.

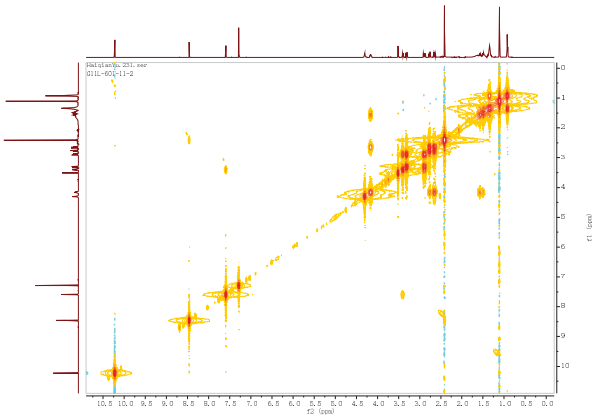

Supplemental Figure 3.3-36. The COSY (600 MHz, $CDCl_3$) spectrum of compound 5.

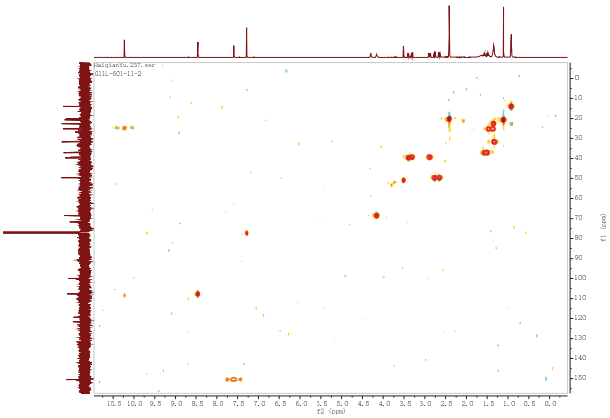

Supplemental Figure 3.3-37. The HSQC (600 MHz, $CDCl_3$) spectrum of compound 5.

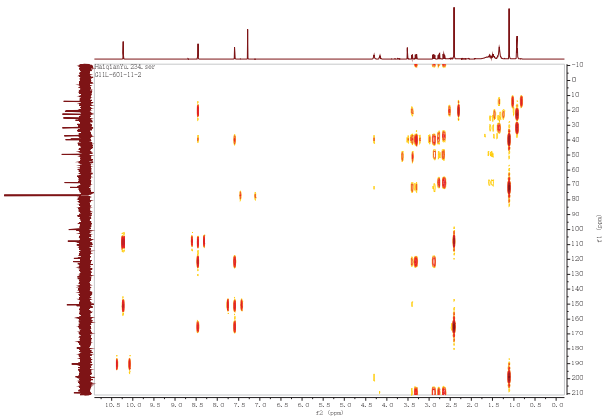

Supplemental Figure 3.3-38. The HMBC (600 MHz, $CDCl_3$) spectrum of compound 5.

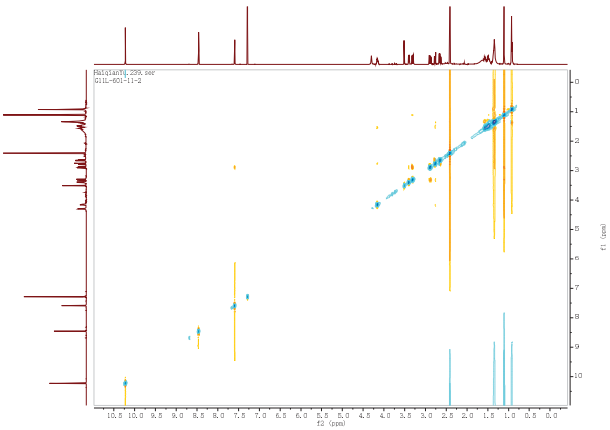

Supplemental Figure 3.3-39. The ROESY (600 MHz, $CDCl_3$) spectrum of compound 5.

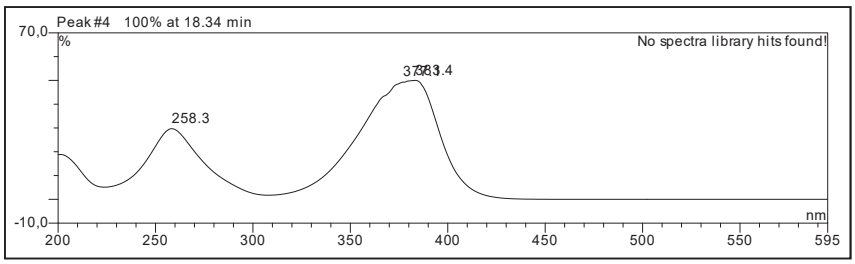

Supplemental Figure 3.3-40. The UV spectrum of compound 5.

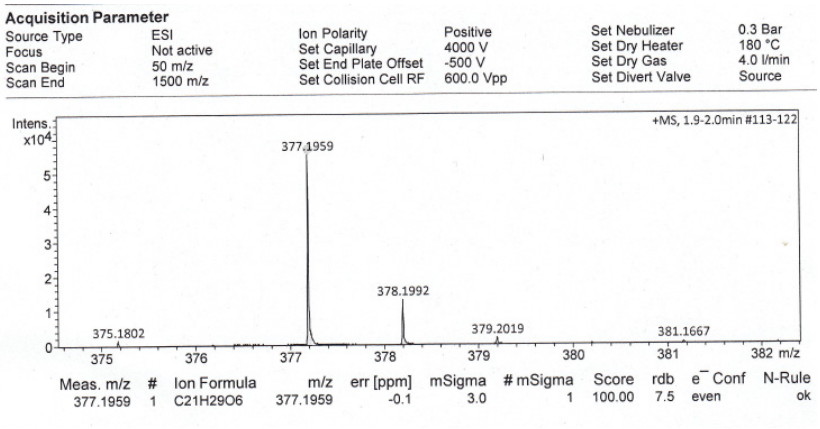

Supplemental Figure 3.3-41. The HRESIMS of compound 6.

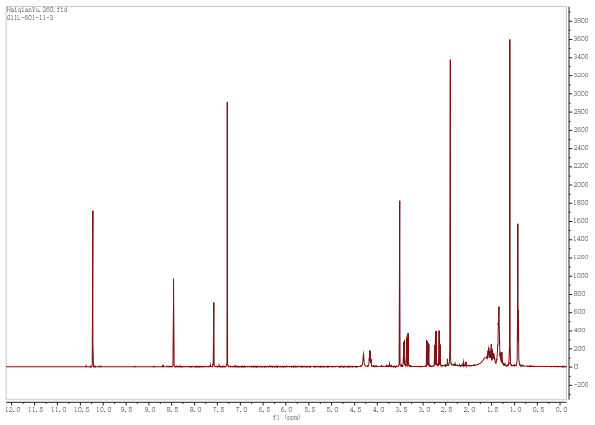

Supplemental Figure 3.3-42. The ^{1}H NMR (600 MHz, $CDCl_3$) spectrum of compound 6.

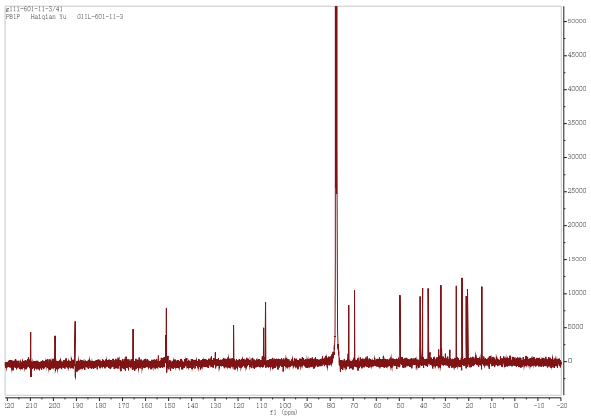

Supplemental Figure 3.3-43. The ^{13}C NMR (150 MHz, $CDCl_3$) spectrum of compound 6.

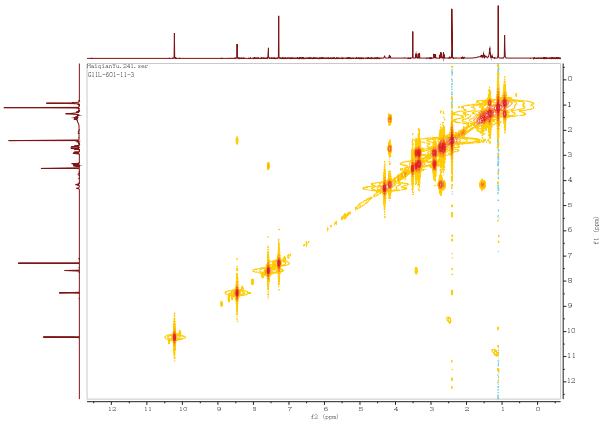

Supplemental Figure 3.3-44. The COSY (600 MHz, $CDCl_3$) spectrum of compound 6.

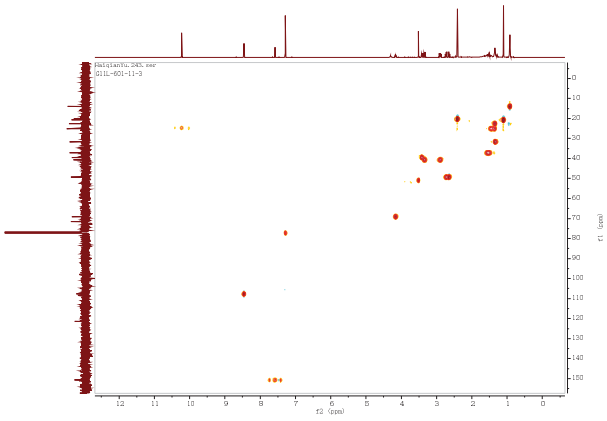

Supplemental Figure 3.3-45. The HSQC (600 MHz, $CDCl_3$) spectrum of compound 6.

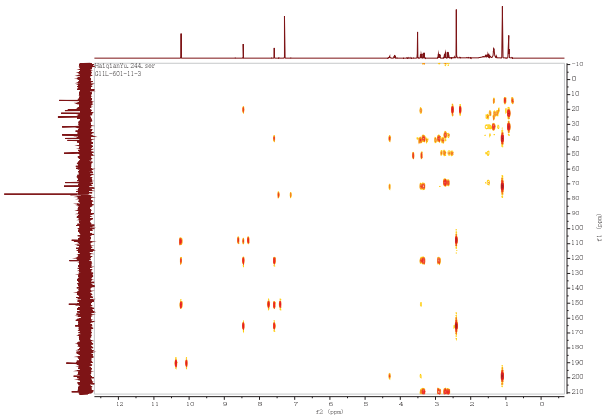

Supplemental Figure 3.3-46. The HMBC (600 MHz, $CDCl_3$) spectrum of compound 6.

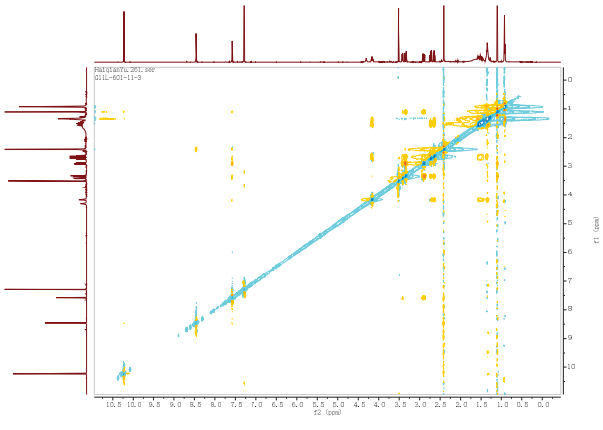

Supplemental Figure 3.3-47. The ROESY (600 MHz, $CDCl_3$) spectrum of compound 6.

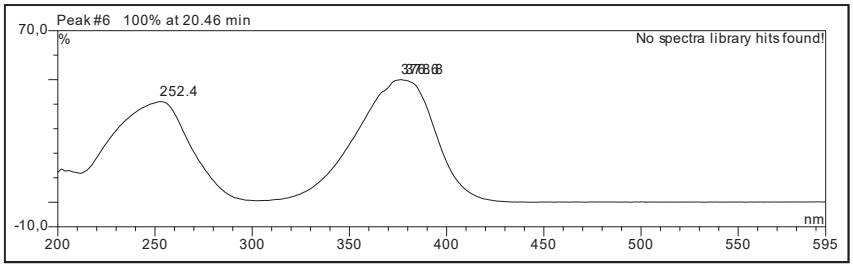

Supplemental Figure 3.3-48. The UV spectrum of compound 6.

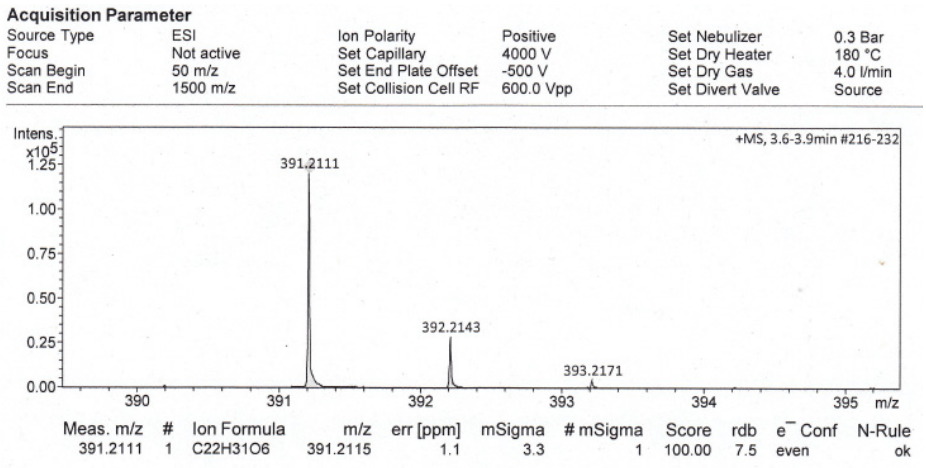

Supplemental Figure 3.3-49. The HRESIMS of compound 7.

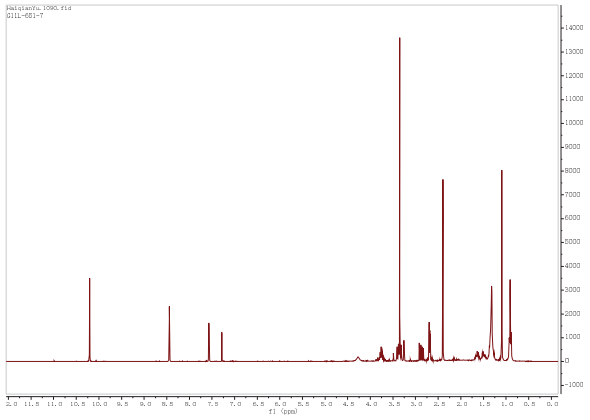

Supplemental Figure 3.3-50. The ^{1}H NMR (300 MHz, $CDCl_3$) spectrum of compound 7.

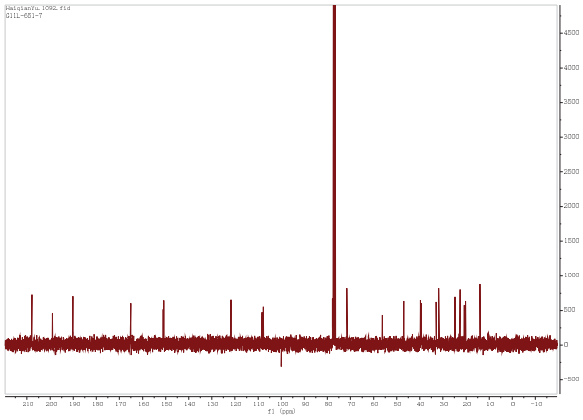

Supplemental Figure 3.3-51. The ^{13}C NMR (75 MHz, $CDCl_3$) spectrum of compound 7.

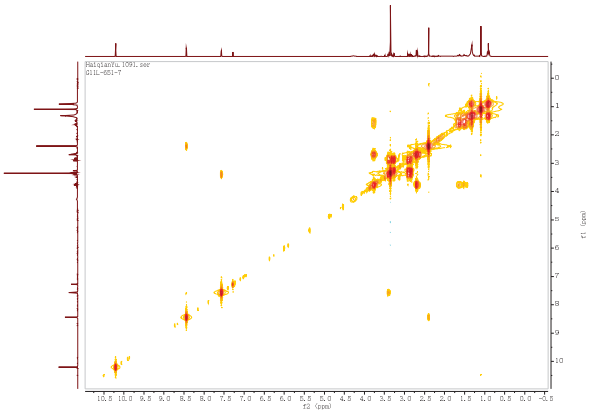

Supplemental Figure 3.3-52. The COSY (300 MHz, $CDCl_3$) spectrum of compound 7.

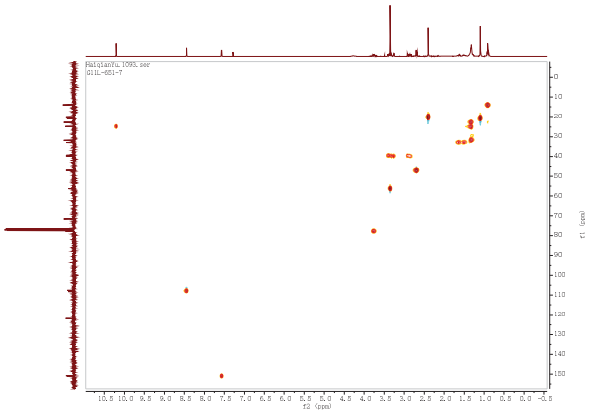

Supplemental Figure 3.3-53. The HSQC (300 MHz, $CDCl_3$) spectrum of compound 7.

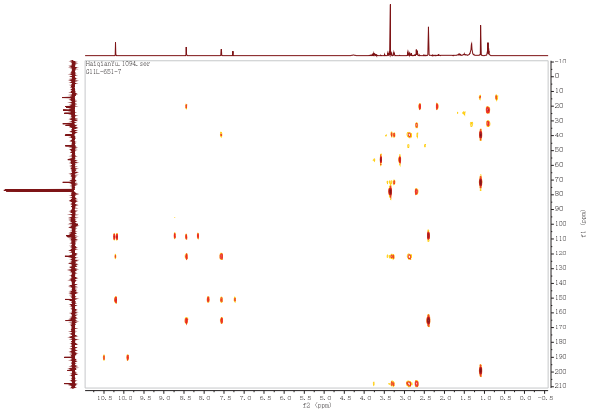

Supplemental Figure 3.3-54. The HMBC (300 MHz, $CDCl_3$) spectrum of compound 7.

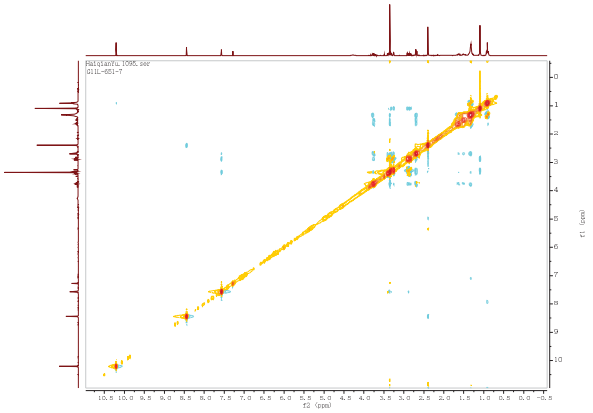

Supplemental Figure 3.3-55. The ROESY (300 MHz, $CDCl_3$) spectrum of compound 7.

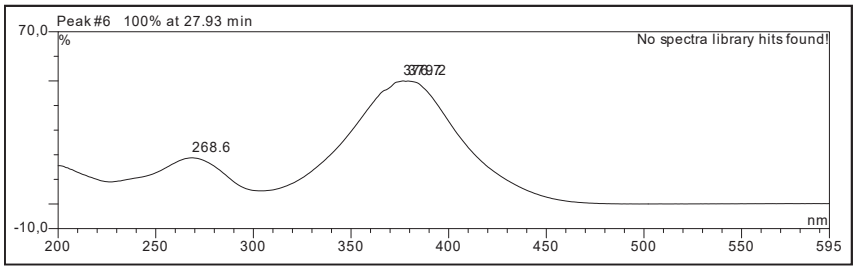

Supplemental Figure 3.3-56. The UV spectrum of compound 7.

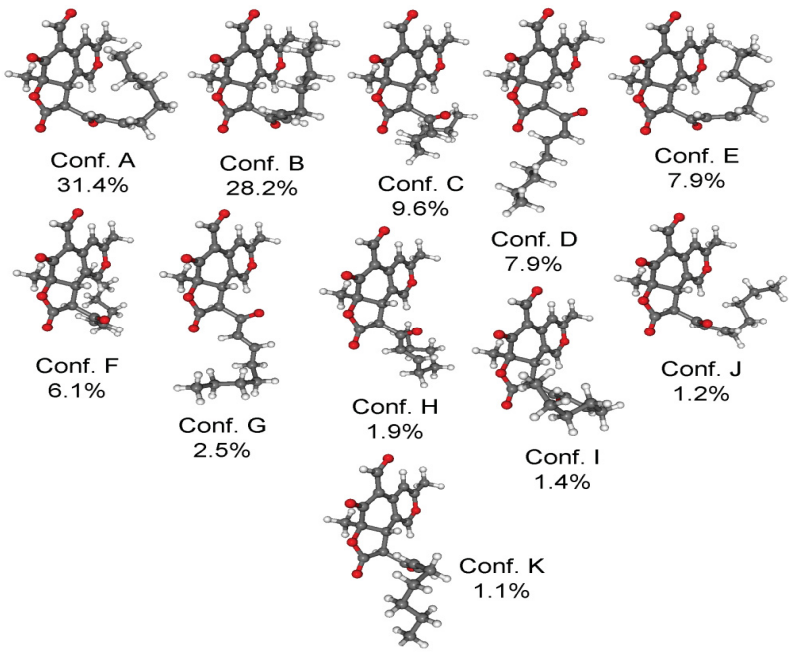

Supplemental Figure 3.3-57. Structure and population of the low-energy B97D/TZVP PCM/MeCN conformers (>1%) of (8*S*,9*R*,12*S*)-1.

Supplemental Table 3.3-1. Boltzmann populations and optical rotations of the low-energy conformers of (8*S*,9*R*,12*S*)-1 computed at various levels for the B3LYP/6-31G(d) reoptimized MMFF conformers

Conformer	Boltzmann population	B3LYP/TZVP	BH&HLYP/TZVP	PBE0/TZVP
Conf. A	69.86 %	438.48	409.24	437.21
Conf. B	21.11 %	176.36	161.57	182.60
Conf. C	8.46 %	319.58	328.65	324.36
Average	N/A	372.71	349.80	373.55

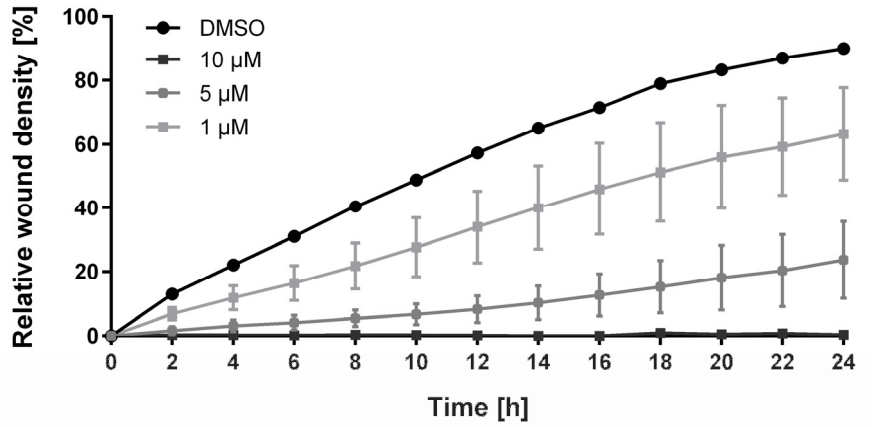

Supplemental Figure 3.3-58. Time course of tumor cell migration.

Cell migration in the presence of azaphilone (compound **1**) was evaluated at concentrations 1, 5 and 10 µM. Images were taken every two hours for a time period of 24 hours. Data represent increasing relative wound density in percentage calculated with the IncuCyte ZOOM® software. Error bars show ±SEM.

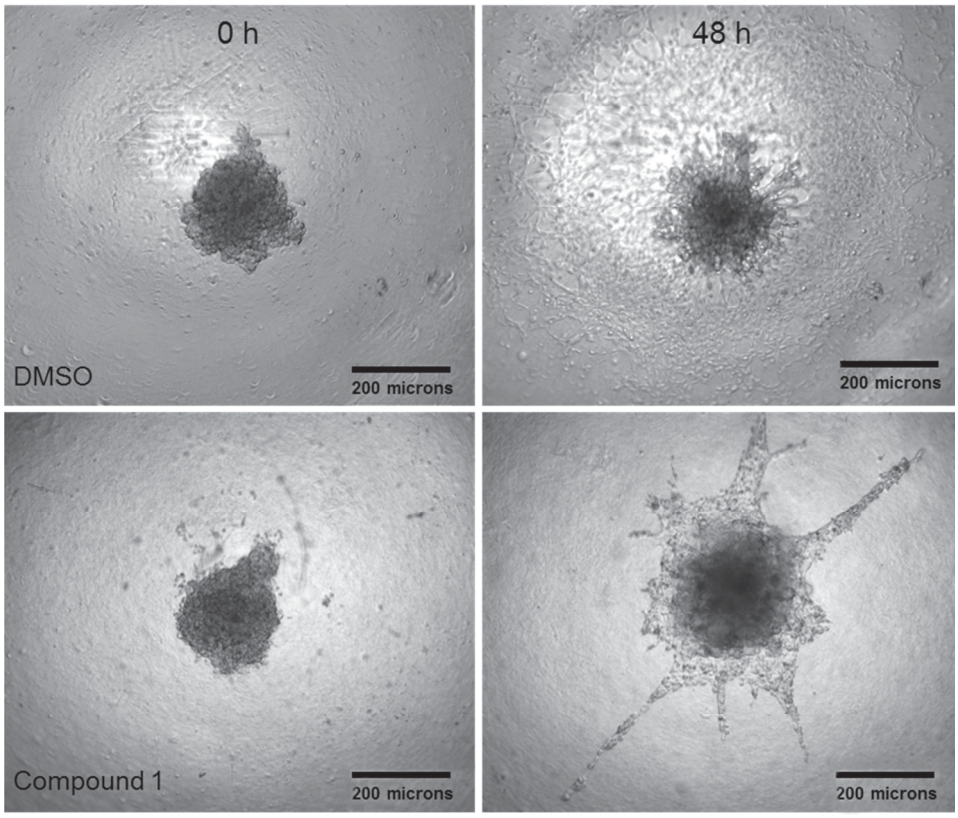

(**A**)

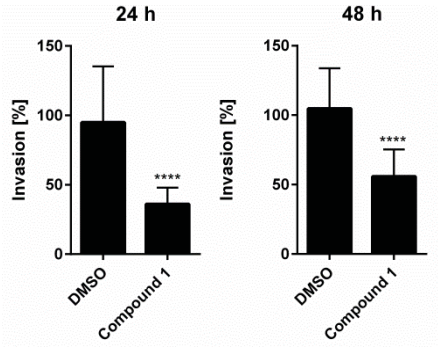

(**B**)

Supplemental Figure 3.3-59. Compound 1 inhibits invasion into the 3D extracellular matrix.

Representative images of invasion into matrigel are shown in (**A**). Spheroids were generated with 3,000 cells/well of MDA-MB-231 cells supplemented with 0.25 % matrigel in an ultra-low-attachment (ULA) plate. After 72 hours of spheroid formation, a mix of matrigel and collagen R solution (ratio of 1:1) was used for embedding the spheroids. Invasion of cells into the surrounding matrix was recorded every day for a time range of 48 hours and quantification of invasion was performed with ImageJ Fiji in (**B**). Compound **1** was tested at 5 µM. Invasion, shown in percentage, was normalized to DMSO control at the specified time points. Error bars show ±SEM. Four stars represent a significance of ρ<0.0001. Scale bars in black represent 200 microns in length.

CHEMMEDCHEM
CHEMISTRY ENABLING DRUG DISCOVERY

3.4 Synthetic Indolactam V Analogs as Inhibitors of PAR2 Induced Calcium Mobilization in Triple Negative Breast Cancer Cells

Jan Stein[1], Sonja Stahn[2], Jörg-M. Neudörfl[1], Julia Sperlich[2], Hans-Günther Schmalz[1], Nicole Teusch[2]

[1]University of Cologne, Department of Chemistry, Greinstrasse 4, D-50939 Koeln, Germany;
[2]Technische Hochschule Koeln, Bio-Pharmaceutical Chemistry & Molecular Pharmacology, Faculty of Applied Natural Sciences, Kaiser-Wilhelm-Allee, G. E39, D-51373 Leverkusen, Germany;

ABSTRACT

Human proteinase-activated receptor 2 (PAR2), a transmembrane G-Protein-coupled receptor (GPCR), represents an attractive target for a novel anti-cancer therapy as it plays a critical role in cell migration and invasion. Thus, selective PAR2 inhibitors possess a potential as anti-metastatic drugs. Knowing that the natural product teleocidin A2 is able to inhibit PAR2 in tumor cells, the goal of the present study was to elaborate structure-activity relationships and to identify potent PAR2 inhibitors with lower activity against the adverse target protein kinase C (PKC). For this purpose, an efficient gram scale total synthesis of indolactam V (i.e. the parent structure of all teleocidins) was developed and a library of derivatives was prepared. Some compounds indeed exhibited high potency as PAR2 inhibitors at low nanomolar concentrations with improved selectivity (as compared to teleocidin A2). The pseudopeptidic fragment bridging the C-3 and the C-4 positions of the indole core proved to be essential for target binding, while activity and target selectivity depends on the substituents at N-1 or C-7. The study revealed novel derivatives depicting high efficacy in PAR2 antagonism combined with increased selectivity.

INTRODUCTION

Cancer is one of the diseases with high unmet medical need raising most cases of death after cardiovascular diseases in the industrialized countries. Notably, the dissemination of cancer from the primary tumor is the main reason of cancer-related mortality and represents an

enormous clinical challenge. Among the different types of malignant tumors, breast cancer is the leading cause of cancer death in females worldwide [1].

Proteinase activated receptor 2 (PAR2), a member of the seven transmembrane G protein-coupled receptor (GPCR) superfamily, has been shown to play a major role in cancer progression. Numerous *in vitro* studies including breast [2,3], pancreatic [4] and lung adenocarcinoma [5] cells revealed a critical role of PAR2 signaling in cancer cell migration and invasion correlating with increased metastatic potential. From a clinical perspective, elevated PAR2 expression in biopsy and metastatic tissue could be linked to an increased malignancy grade and subsequently to a reduced overall survival rate [6]. Whereas initial PAR2 inhibiting compounds were mostly limited in potency or displayed agonistic properties at higher concentrations, recent medicinal chemistry approaches have led to more efficacious small molecule PAR2 antagonists [7,8]. Overall, the distinct role of PAR2 in tumor biology illustrates the need for low molecular weight PAR2 inhibitors providing the basis for the development of a novel therapeutic strategy in cancer treatment [9,10].

In the course of our previous work, we recently demonstrated that some marine natural products of the indolactam/teleocidin family exhibit significant effects as PAR2 inhibitors [2]. Prior to this, the natural products (Figure 3.4-1), which were all isolated from marine organisms, had been reported to exhibit strong biological activities including tumor-promoting effects, mainly due to the activation of protein kinase C (PKC) [11–14]. However, as a solely PKC-mediated effect cannot explain the remarkable efficacy of teleocidin on PAR2-mediated signaling, it remains elusive whether the ability to activate PKC is mechanistically linked to the inhibition of PAR2-induced signaling [2].

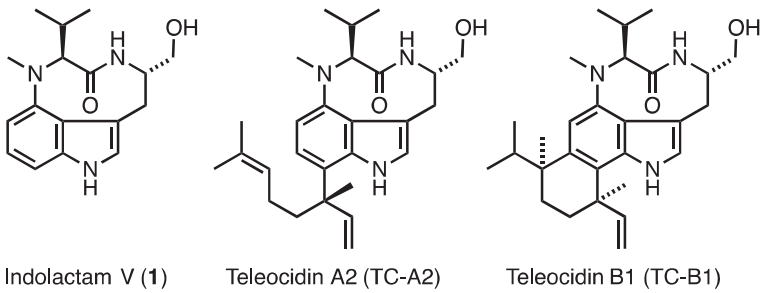

Figure 3.4-1. Structure of indolactam V (1) and teleocidins A2 and B1

Biosynthetically, the teleocidins are derived from (L)-trypto-phane via indolactam V [15–17]. All compounds of this class display a 3,4-disubstituted indole nucleus with a characteristic (L)-N-methyl-valine-containing bridge forming a 9-membered ring. Due to their powerful biological activity and their limited accessibility from natural sources, several total syntheses of indolactam V (1) [18–31] and teleocidins [32–38] have been developed, and a number of studies employing

total synthetic analogs have contributed to the profiling of indolactam V-related or -derived compounds with respect to PKC activation [13,39].

In contrast to these previous studies, the major goal of the present work was to synthesize and investigate novel indolactam V analogs with respect to their PAR2-inhibiting properties [2]. Our approach was aimed at deriving distinct structure-activity relationships (SAR) and to design derivatives depicting potent PAR2 antagonism combined with selectivity against PKC, the originally described adverse target of teleocidin A2.

RESULTS AND DISCUSSION

Synthesis

Our first task was to prepare substantial amounts (gram scale) of indolactam V (**1**) as a precondition for the planed structural variation. Careful analysis of the published syntheses of **1** [21-34] prompted us to consider the strategy of Kogan [23] and Xu [28] as most promising (Scheme 3.4-1). Key elements of this approach are the assembly of the nitro-indole derivative **4** from building blocks **5** and **6** [31] followed by conversion of the nitro group into a valinyl moiety and closure of the 9-membered ring through intramolecular peptide coupling [23].

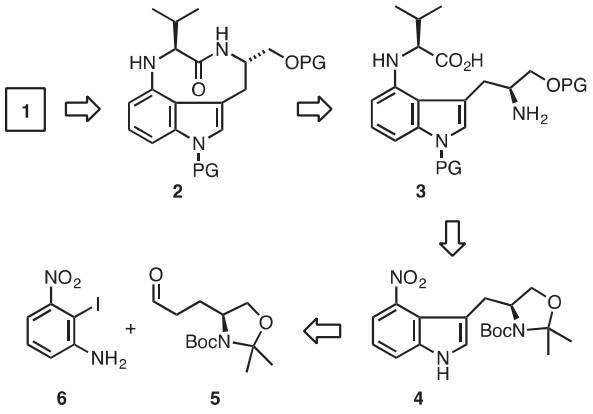

Scheme 3.4-1. Retrosynthesis of indolactam V (1) according to Kogan and Xu.

The preparation of the 4-nitro-tryptophanol derivative **4** (by Pd-catalyzed condensation of 2-iodo-3-nitroanililin **6** with the L-glutamine-derived aldehyde **5** in the presence of DABCO as a base) [28] proceeded smoothly on a multi-gram scale with 85% yield. However, our initial attempts to perform the subsequent planned steps according to the reported protocols were hampered by the instability of intermediates and low yields. We thus realized that a proper protection of the indole nitrogen appeared to be absolutely essential. After first evaluating both, tosyl and Boc, we identified the SES group (2-trimethylsilyl-ethansulfonyl) [40,41] as a superior protecting group for our purposes. In this case, all intermediates proved to be stable and readily

isolated and, even more importantly, all steps could be reproducibly performed on a multi gram scale with high yield.

As shown in Scheme 3.4-2, the resulting greatly improved synthesis of **1** commenced with the SES protection of **4** followed by reduction of the nitro group of **7** through catalytic hydrogenation. The resulting aniline **8** was then converted into the valine derivative **9** by S_N2-alkylation in virtually quantitative yield [23]. The acid-catalyzed hydrolysis of the cyclic *N,O*-acetal afforded the desired product **11** besides significant amounts of the double deprotected by-product **10** which, however, was easily re-protected with Boc_2O/NEt_3 to afford **11** in 91% combined yield from **9**. After protecting the primary alcohol functionality as a TBDPS ether, both the *N*-Boc group and the benzyl ester protecting groups, were cleaved off under standard conditions. Treatment of the resulting intermediate **14** with HATU as a coupling agent in the presence of DIPEA smoothly afforded the cyclized product **15**. In comparison with other indolactam V syntheses, the Eschweiler-Clark methylation of the secondary amino group in **15** was achieved in very high yield under appropriate conditions (CH_2O, $NaCNBH_3$, AcOH, MeCN, 0 °C) [42]. Treatment of the resulting compound **16** with TBAF finally afforded indolactam V (**1**) in high overall yield.

By means of a single crystal X-ray analysis of the hydro-tetrafluoroborate salt of **1** the relative and absolute configuration of the synthetic compound was unambiguously confirmed. The high-resolution structure (Figure 3.4-2) shows the 9-membered ring preferring a twisted conformation with a virtually planar s-*cis*-configurated peptide unit positioned almost perpendicular (orthogonal) to the plane defined by the indole ring system. This characteristic 3D structure of the indole moiety with the polar unit bridging C-3 and C-4 appears to be the essential structural motif ensuring an effective interaction (binding) with the respective protein partners.

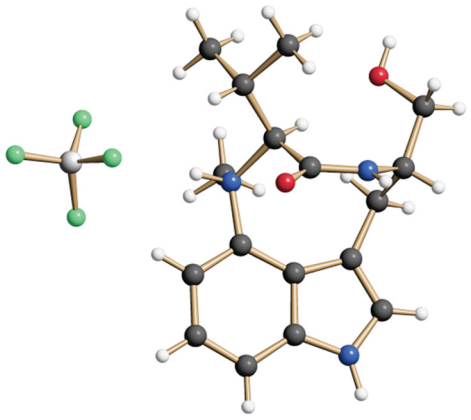

Figure 3.4-2. Structure of the hydro-tetrafluoroborate salt of indolactam V (1-HBF4) in the crystalline state.

Having successfully developed an efficient synthetic scheme, allowing us to prepare indolactam V (**1**) in gram amounts, we next turned our attention to the synthesis of various derivatives (Scheme 3.4-3) [30,43–45]. For this purpose, we preferentially used the TBS-protected compound **17a** as a safe (biologically inactive) key intermediate. In a first set of experiments we prepared a small set of N1 derivatives by simply reacting the indole **17a** with different acylating and benzylating reagents and subsequent fluoride-induced cleavage of the silyl protecting group (Scheme 3.4-3). The compounds (**20-25**) thus prepared are listed in Chart 3.4-1 together with some other indolactam V derivatives obtained in the course of the synthesis development.

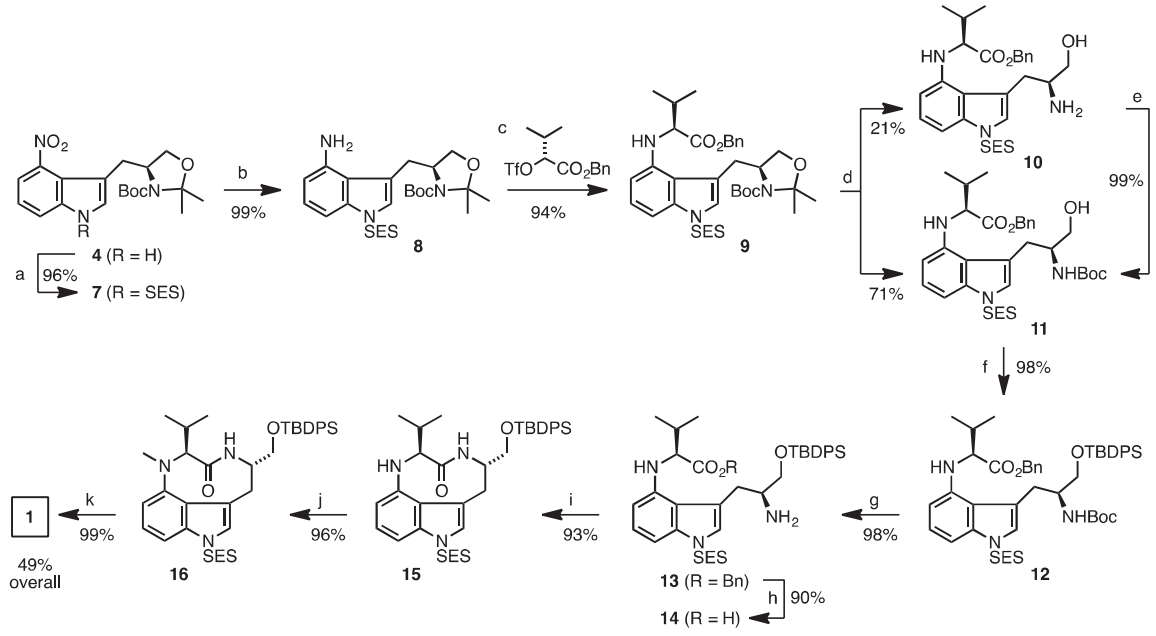

Scheme 3.4-2. Improved synthesis of indolactam V (1) performed on a gram scale.

Reagents and conditions: a) NaH, SES-Cl, THF, -20 °C, 30 min; b) Pd/C, H_2, MeOH, rt, 12 h; c) 2,6-lutidine, $C_2H_4C_{l2}$, 80 °C, 12 h; d) pTsOH.H_2O, CH_2C_{l2}, rt, 4 h; e) Boc_2O, Et_3N, MeCN, rt; f) TBDPS-Cl, imidazole, DMF, rt, 3 h; g) TFA, CH_2C_{l2}, 0 °C -> rt, 6 h; h) Pd/C, H_2, MeOH, rt, 3 h; i) HATU, DIPEA, THF, rt, 48 h; j) CH_2O, $NaCNBH_3$, AcOH, MeCN, 0 °C -> rt, 1 h; k) TBAF, THF, 0 °C to rt, 2 h. 24 h.

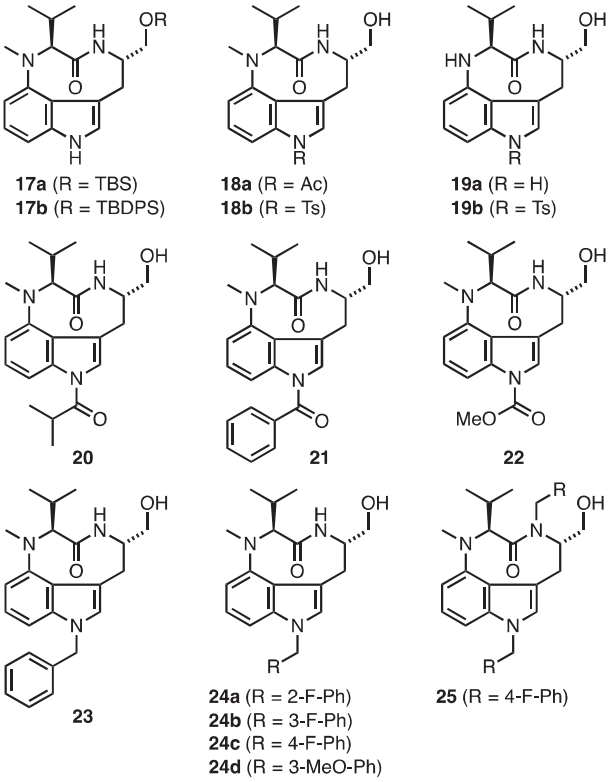

Chart 3.4-1. Various derivatives of indolactam V prepared according to Scheme 3.

As also shown in Scheme 3.4-3, a variety of C-7-substituted derivatives were synthesized starting from TBS-protected indolactam V (**17a**). Using the iodinated compound **26** [30,43–45] as a key intermediate Pd-catalyzed cross-coupling and carbonylation methods [46] were applied to introduce different substituents at C-7. As before, the silyl protecting group was cleaved off only in the final step under standard conditions (TBAF). The allylation product **27** was synthesized employing allyl-Bpin under Suzuki type conditions [47,48]. Compounds **31a**-**31e** in turn were smoothly obtained under Sonogashira conditions [49]. Two of the product alkynes (**31a** and **31b**) were hydrogenated in the presence of Pd/C to the corresponding alkanes **32a** and **32b**, respectively. Carboylative Suzuki coupling of **26** with phenyl boronic acid afforded the ketone **28**. In a related fashion, the alkoxy-carbonylated products **30a** and **30b** and the amides **30c** and **30d**, respectively, were prepared by Pd-catalyzed reaction of **26** with different alcohols and amines under CO atmosphere [50,51]. Compound **29** was obtained by carbonylative cross-coupling using phenylacetylene [52] and subsequent TBAF-induced 6-endo-dig cyclisation. The structure of **29** was again unambiguously proven by X-ray crystal structure analysis (Figure 3.4-3).

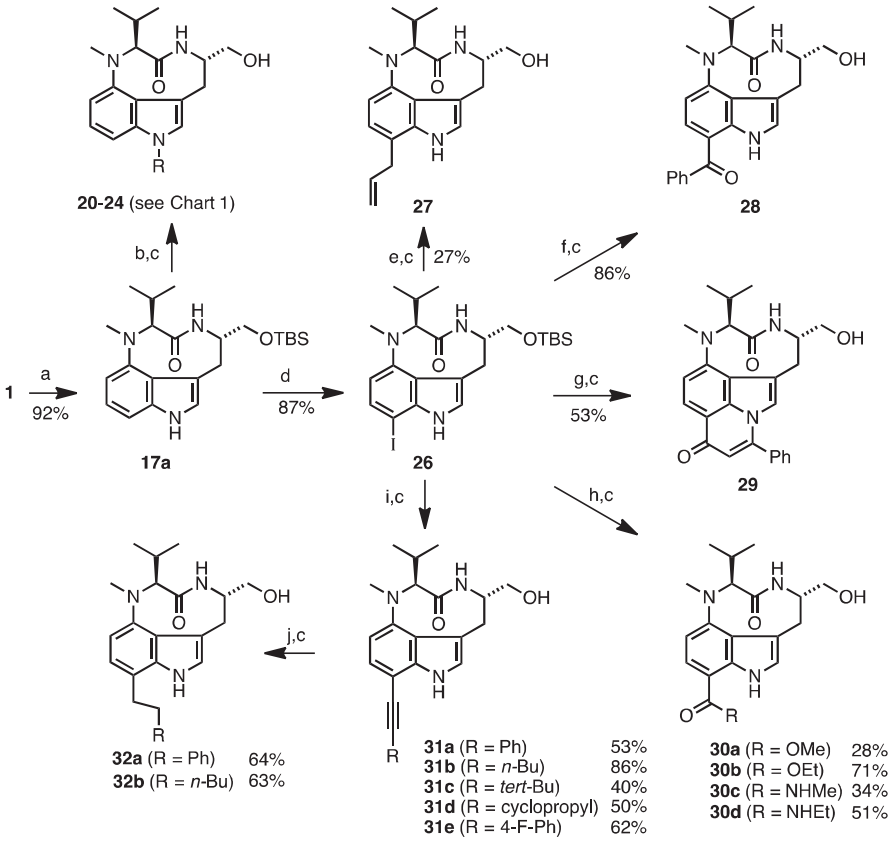

Scheme 3.4-3. Preparation of various derivatives of indolactam V (1).

Reagents and conditions: a) TBSCl, imidazole, TBAI, DMF, rt, 12 h; b) NaH, R-X, DMF, -20 °C to rt, 40 min – 12 h; c) TBAF, THF, 0 °C to rt, 2 h; d) I_2, pyridine, 1,4-dioxane, 0 °C to rt, 2.5 h; e) allyl-Bpin, cat. $Pd(PPh_3)_4$, CsF, THF, reflux, 24 h; f) $PhB(OH)_2$, CO, cat. $PdCl_2(PPh_3)_2$, 1,4-dioxane, Et_3N, 60 °C, 24 h; g) phenylacetylene, CO, cat. $PdCl_2(PPh_3)_2$, CuI, 1,4-dioxane, Et_3N, rt, 12 h; h) ROH or RNH_2, CO, cat. $PdCl_2(PPh_3)_2$, 1,4-dioxane, Et_3N, 60 °C, 12 h; i) alkyne, cat. $PdCl_2(PPh_3)_2$, CuI, 1,4-dioxane, Et_3N, rt, 12 h; j) Pd/C, H_2, rt, 5 h.

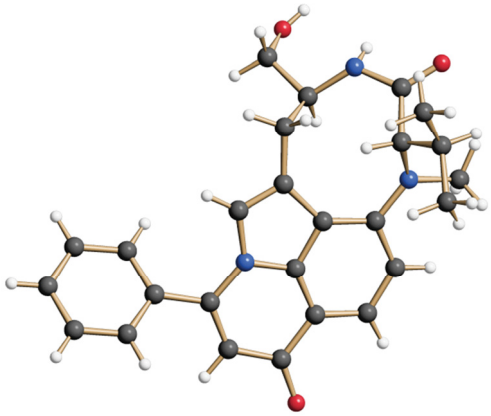

Figure 3.4-3. Structure of the cyclized indolactam V derivative 29 in the crystalline state.

Biological Investigations

The various compounds synthesized as described above were biologically evaluated with respect to (1) inhibition of PAR2-induced Ca^{2+} mobilization and (2) intracellular PKC activation.

First, physiological Ca^{2+} release induced by the PAR2 specific tethered ligand SLIGKV-NH_2 was determined in the human breast adenocarcinoma cell line MDA-MB-231 which is categorized triple negative due to the lack of expression of hormone receptors or HER2. Indolactam V derivatives were tested in the presence of the EC_{50} determined for the agonistic ligand SLIGKV-NH_2 (7.46 µM) to achieve IC_{50} values for PAR2 inhibition. The data shown in Table 3.4-1 indicate that indolactam V (**1**) itself displays a 4-fold potency loss in inhibiting PAR2 induced Ca^{2+} release (IC_{50} = 72.1 ± 4.4 nM) compared to teleocidin (IC_{50} = 18.1 ± 1.7 nM).

Changes at the pseudopeptidic bridge (N-demethylation or O-protection with a bulky silyl group) led to inactive compounds. Derivatization at the indole nitrogen caused significant effects: Small acyl substituents such as acetyl (**18a**) (IC_{50} = 26.1 ± 8.0 nM) or methoxylcarbonyl (**22**) (IC_{50} = 25.3 ± 6.3 nM) enhanced activity, as did fluorinated benzylic residues (e.g. **24c**) (IC_{50} = 24.0 ± 5.9 nM). Interestingly, substituents at C-7 of the indole nucleus (R2) also caused significant changes.

While some groups (benzoyl, alkynyl or aminocarbonyl) did not improve activity, the allylated compound **27** proved to be quite active (IC_{50} = 2.25 ± 0.39 nM). Excellent results, however, were observed for the alkoxycarbonylated indolactam V derivatives 30a and 30b, the latter inhibiting the PAR2 induced intracellular Ca^{2+} mobilization at single-digit nanomolar concentrations (IC_{50} = 1.57 ± 0.90 nM). Thus, compared to the starting compound indolactam V (**1**) the derivative **30b** displayed a 46-fold efficacy increase in inhibiting PAR2-induced intracellular signaling. Comparable concentration-dependent inhibition curves of PAR2-induced Ca^{2+} mobilization by indolactam V (1) and indolactam V analogs **18a**, **22** and **30b** in MDA-MB-231 breast cancer cells are displayed in Figure 3.4-4. Furthermore, cytotoxicity assessment of selected derivatives revealed no notable effect on cell viability (Supplemental Figure 3.4-1).

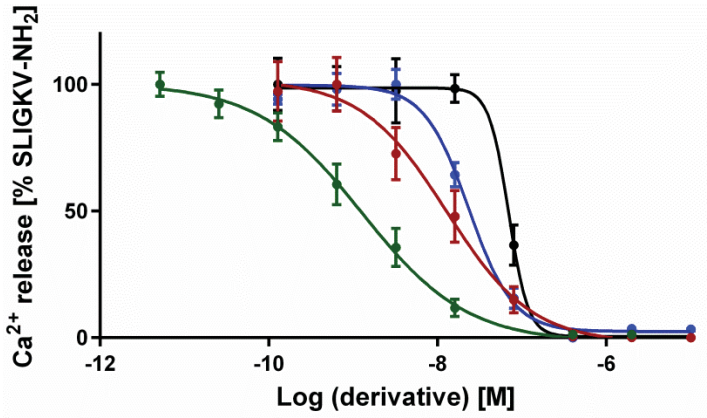

Figure 3.4-4. Concentration-dependent inhibition of PAR2 induced Ca^{2+} mobilization by indolactam V (black) and indolactam V derivative 18a (blue), 22 (red) and 30b (green) in MDA-MB-231 breast cancer cells.

Data points represent mean values ±SEM from a minimum of three independent experiments performed in triplicates and data of each experiment was normalized to PAR2 activating peptide SLIGKV-NH_2 induced Ca^{2+} release.

Intracellular PKC activation: To date, teleocidin derivatives are mainly categorized as tumor-promoting agents. Thus, within our medicinal chemistry approach aiming at targeting PAR2 with indolactame-derived compounds, a putative PKC activation represents an undesirable off-target effect. To characterize the potential of indolactam V derivatives to activate intracellular PKC, phosphorylation induction of the specific endogenous PKC substrate MARCKS was determined in the presence of the respective compounds (Figure 3.4-5). As expected, the positive control PMA (10 nM) induced a strong phosphorylation up to 3.5-fold compared to DMSO control representing a significant PKC activation. Furthermore, MARCKS was phosphorylated up to 4-fold compared to the untreated control in the presence of 25 nM teleocidin A2. In contrast to teleocidin, the level of MARCKS phosphorylation induced by indolactam V (**1**) was comparable to the level of the DMSO control (Figure 3.4-5).

Importantly, the novel indolactam V derivatives **18a** and **24c** did not activate PKC, whereas the analogs **22** and **24b** displayed moderate activation of intracellular PKC. While the respective PKC activation potential of analogs **24a**, **24d** and **27** is comparable to teleocidin, compounds **30a** and **30b** were able to phosphorylate MARCKS by a 3-fold increase compared to negative control.

Table 3.4-1. IC_{50} values of indolactam V analogues for inhibition of PAR2-induced intracellular Ca^{2+} mobilization in MDA-MB-231 breast cancer cells.

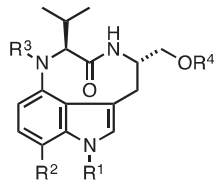	R^1	R^2	R^3	R^4	PAR2[a] IC_{50} [nM] (mean± SEM)
TC-A2	H	tert.-alkyl	Me	H	18.1 ± 1.7
1	H	H	Me	H	72.1 ± 4.4
17b	H	H	Me	TBDPS	>10000
18a	Ac	H	Me	H	26.1 ± 8.0
18b	Ts	H	Me	H	791 ± 48
19a	H	H	H	H	> 1000
19b	Ts	H	H	H	> 1000
20	i-butyryl	H	Me	H	206 ± 56
21	benzoyl	H	Me	H	116 ± 11
22	Moc	H	Me	H	25.3 ± 6.3
23	Bn	H	Me	H	78.8 ± 18.3
24a	2-F-Bn	H	Me	H	205 ± 54
24b	3-F-Bn	H	Me	H	26.3 ± 6.1
24c	4-F-Bn	H	Me	H	24.0 ± 5.9
24d	3-MeO-Bn	H	Me	H	45.1 ± 8.9
25	4-F-Bn	H	Me	H	2450 ± 430
27	H	allyl	Me	H	2.25 ± 0.39
29	H	cyclyzed	Me	H	> 2000
30a	H	CO_2Me	Me	H	6.96 ± 1.73
30b	H	CO_2Et	Me	H	1.57 ± 0.90
30c	H	CONHMe	Me	H	1994 ± 562
30d	H	CONHEt	Me	H	235 ± 29
31e	H	alkynyl	Me	H	18.3 ± 2.1

[a] Intracellular Ca^{2+} mobilization assay. PAR2 induced intracellular Ca^{2+} mobilization was induced with the determined EC_{50} concentration of the PAR2 activating peptide SLIGKV-NH_2. Data represent mean +SEM of a minimum three independent determinations performed in triplicates. Statistical analysis of specificity of single analogues was performed using an unpaired Student's t-Test.

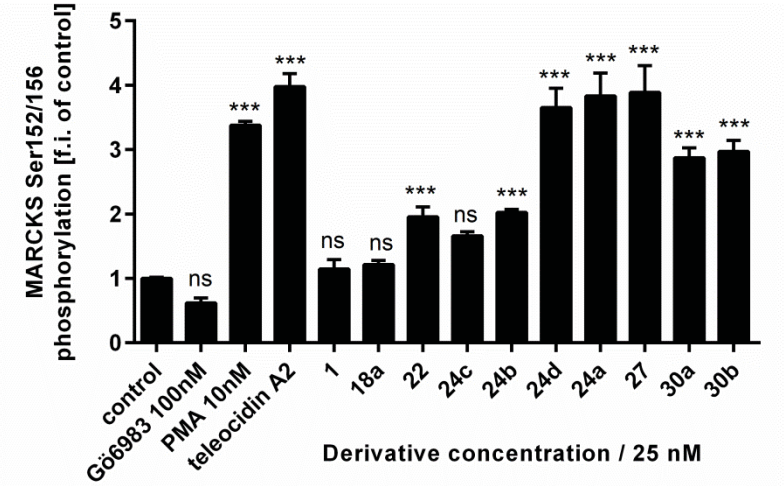

Figure 3.4-5. Phosphorylation of PKC substrate MARCKS in MDA-MB-231 cells by derivatives of indolactam V.

Cells were treated for 10 min with 25 nM of each compound. The solvent DMSO represents the control. Gö6983 is a commercially available PKC inhibitor. Data represent mean values ±SEM from three independent experiments performed in triplicates, 'ns' not statistically significant, ** ρ<0.01, *** ρ<0.001.

Moreover, PAR2 inhibition data combined with selectivity data concerning PKC activation (represented by MARCKS phosphorylation) were visualized in a two-dimensional efficacy plot (Figure 3.4-6). IC_{50} values reflecting inhibition of PAR2, our target of interest, are shown on the x-axis, whereas the fold increase in MARCKS phosphorylation, reflecting the PKC activating potential, is depicted on the y-axis. Potent derivatives (IC_{50} PAR2 <30 nM) with no or moderate (up to 2-fold compared to DMSO control) off-target activity towards PKC are depicted in green, whereas highly potent PAR2 inhibitors with more pronounced PKC activity (up to 3-fold induction of MARCKS phosphorylation) are displayed in yellow. Indolactam V (**1**) is illustrated in yellow based on its IC_{50} for PAR2 which is above 70 nM. Moreover, derivatives with unfavourable selectivity profiles comparable to teleocidin (>3-fold induction of MARCKS phosphorylation) are visualized in red.

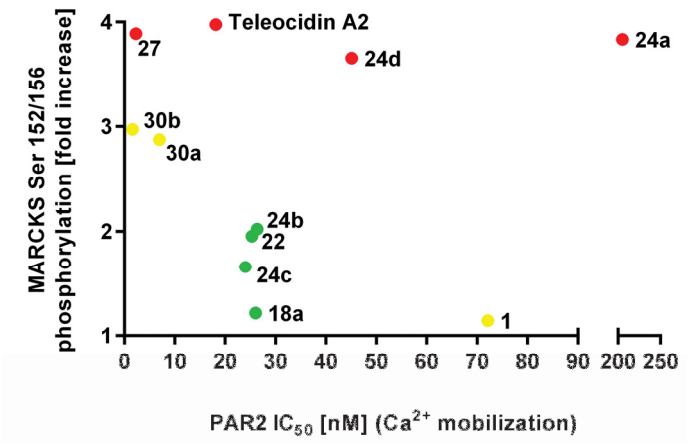

Figure 3.4-6. Scatterplot summarizing the inhibition of PAR2 induced Ca^{2+} release and the activation of PKC by selected analogues of indolactam V.

IC_{50} values versus PAR2 activating peptide SLIGKV-NH_2 are shown on the x-axis. Y-axis depicts fold increase in phosphorylation of endogenous MARCKS protein, representing PKC activation. See Table 3.4-1 for exact IC_{50} values for PAR2 inhibition.

With respect to further selectivity assessment, our previous work revealed that teleocidin markedly reduced Ca^{2+} mobilization of the Gq-coupled GPCR PAR1, however, with a 20-fold potency loss compared to PAR2 inhibition [2]. Noteworthy, in this study novel indolactam derivatives were identified confirming a clear preference for PAR2 inhibition (Supplemental Figure 3.4-2).

Finally, the effect on cancer cell migration, a notorious cause for the poor prognosis of triple negative breast cancer, was evaluated. After 24 hours of incubation of the most potent indolactam derivative **30b** (IC_{50} for PAR2 1.57 ± 0.90 nM) migration of triple negative MDA-MB-231 cells was inhibited by 25% (Figure 3.4-7).

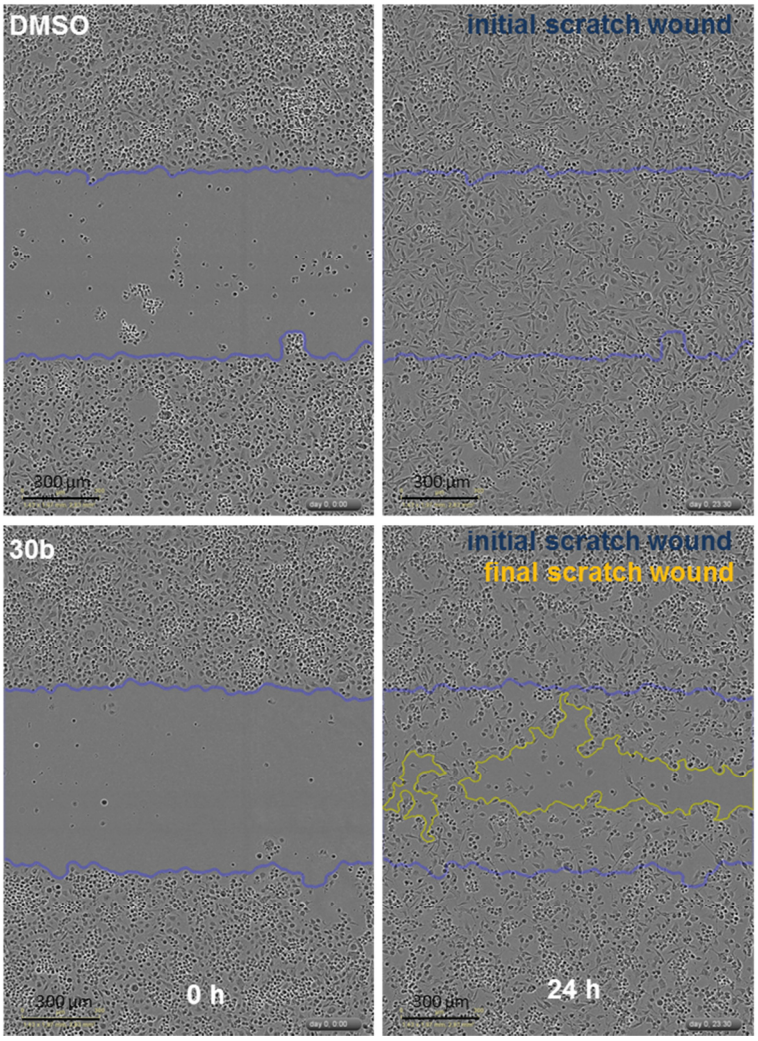

(**A**)

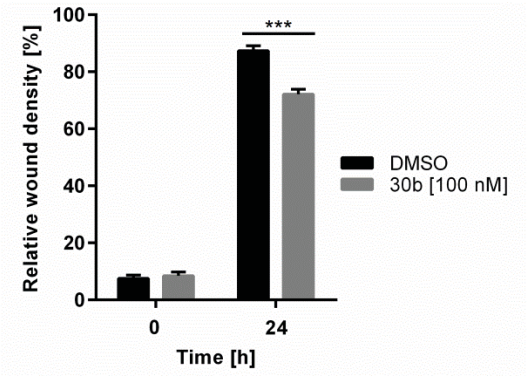

(**B**)

Figure 3.4-7. Indolactam V derivative 30b inhibits migration of triple negative breast cancer cells.

(**A**) Image of the scratch wound assay in MDA-MB-231 cells. First row depicts control cells treated with DMSO and second row shows treatment with **30b** at t=0 and t=24h, respectively. The initial scratch wound mask is marked with blue lines. Scratch wound after 24h is marked in yellow. Indolactam V derivative **30b** was applied at a concentration of 100 nM. (**B**) The quantification of migration is shown in a bar graph. X-axis shows time after inserting the initial scratch wound and y-axis depicts relative wound density. *P*-value of 0.0002 was

calculated using Sidak's multiple comparisons test. Data represent mean +SEM of quadruplicates of three independent experiments.

CONCLUSION

To investigate the potential of novel derivatives of the natural product teleocidin as inhibitors of the human proteinase-activated receptor 2 (PAR2), we have first developed (1) a powerful total synthetic access to indolactam V and (2) novel derivatization options such as carbonylative transformations of C-7-iodinated intermediates. From a small library of synthetic compounds we could then derive distinct structure-activity relationships with respect to the inhibition of PAR2. Furthermore, we found a particularly active compound (**30b**) with the potential to significantly inhibit tumor cell migration. Moreover, derivatives with IC_{50} values for PAR2 blockade in the two-digit nanomolar range, also exhibiting a good selectivity towards the tumor-promoting target PKC, have been identified. Importantly, the present study demonstrates that activation of PKC is not mandatory for inhibiting PAR2 signaling. Thus, our medicinal chemistry approach has revealed novel indolactam V derivatives depicting high efficacy and promising selectivity in PAR2 antagonism providing the basis for the development of a novel therapeutic anti-cancer strategy.

EXPERIMENTAL SECTION

Chemical Synthesis

Detailed synthetic procedures and characteristic compound data are given in the Supporting Information.

BIOLOGICAL EVALUATION

Cell Culture

Human breast adenocarcinoma MDA-MB-231 (European Collection of Cell cultures, catalog no. 92020424) was used to examine the effect of indolactam V derivatives on endogenous PAR2 and PAR1. Cells were grown in Leibovitz's L15 (Biochrom) containing 15% fetal calf serum (FCS), 2 mM glutamin, 100 units·mL^{-1} Penicillin and 100 µg·mL^{-1} Streptomycin and cultivated in humidified atmosphere at 37°C. Trypsin-free Cell Dissociation Buffer (Life Technologies) was applied for cell dissociation during passaging and seeding.

Intracellular Calcium Mobilization

Kinetic measurements of mobilization of intracellular calcium in MDA-MB-231 cells were performed in black 96-well clear bottom plates (Greiner Bio-One). Cells were seeded overnight at 2×10^4 cells per well and on the day of the experiment loaded with the indicator dye Quest Fluo-8TM AM (4 µM) (AAT Bioquest) in HBSS and 1% FCS. To examine inhibitory effects on PAR2 induced Ca^{2+} mobilization, dilution series (1:5) of derivatives in HHBS were prepared starting at concentrations of 2 µM. Wells contained HHBS, 2 mM Probenecid (AAT Bioquest) and compounds in a total volume of 100 µL. Stimulation of the named receptors was performed with the PAR2-activating peptide SLIGKV-NH_2 (Sigma-Aldrich) at its determined EC_{50} using the injector unit from Tecan Infinite M1000 Pro microplate reader after 16s of baseline measurement. Fluorescence was measured using excitation at λ= 490nm and emission at λ= 525nm. Calcium ionophore A23187 (Sigma-Aldrich) was used to generate the maximum fluorescence signal and H_2O served as a control for background fluorescence. For calculation of IC_{50}, the logarithmic concentration of the inhibitor was plotted against maximum fluorescence change in % of the A23187 induced Ca^{2+} release and using non-linear regression analysis in GraphPad Prism v. 6.07 (GraphPad Software).

Cellular Protein Kinase C (PKC) Activation

The PathScan® Phospho-MARCKS (Ser152/156) Sandwich ELISA (Cell Signaling Technology, catalog no. 7251) was used to measure the level of cellular PKC activation in MDA-MB-231 cells according to the manufacturer's information. The ELISA detects the specific endogenous phosphorylation of MARCKS at serine residues 152 and 156 by PKC as described [53]. Cells were seeded overnight at 1.8×10^6 cells in FCS-free Leibovitz's L15 culture medium to 10 cm dishes (Greiner Bio-One) and treated with the compounds at their determined IC_{50} values for inhibition of PAR2 induced Ca^{2+} release for exactly 10 min. Cell lysates of controls and compound-treated cells were generated using lysis buffer supplemented with 1 mM phenylmethanesulfonyl fluoride (PMSF). Lysate protein concentrations were determined with Bradford protein assay and adjusted to 0.3 mg mL^{-1} with sample diluent. Phosphorylated MARCKS protein was detected colorimetrically by biotinylated phospho-MARCKS antibody, horseradish peroxidase (HRP) coupled streptavidin and HRP substrate tetramethylbenzidine (TMB) using Tecan Infinite M200 Pro microplate reader.

Scratch Wound Assay

MDA-MB-231 cells were seeded at a density of 6×10^4 cells per well in an image lock 96 well plate (IncuCyte®, Essen Bioscience, Ann Arbor, USA) and incubated over night at 37° C. Scratch wound was inserted with IncuCyte® Woundmaker from Essen Bioscience and cells

were washed twice with PBS. Automatic image acquisition and analysis were done with IncuCyte® ZOOM over twenty-four hours.

Statistics

Presented data were obtained from a minimum of three independent experiments and expressed as mean ±SEM. Statistical analysis of data was held with equal sample values using one-way ANOVA followed by Dunnett's post hoc test, when groups were compared with a control and/ or comparison of mean values of only two groups, an unpaired t-test was applied. Two-way ANOVA was chosen when comparing two different groups in a grouped analysis followed by Sidak's multiple comparisons test. $P<0.05$ was chosen to announce statistically significant difference. Data analysis was done with GraphPad Prism v. 6.07 (GraphPad Software).

Supplemental Information: Figure S1: Cytotoxicity of indolactam V derivatives. Figure S2: 3D Plot summarizing the inhibition of PAR2 and PAR1 induced Ca2+ release and the activation of PKC by indolactam V derivatives (phosphorylation of PKC substrate MARCKS and scratch wound assay were performed by Julia Sperlich).

Acknowledgements: The PhD training of Sonja Stahn and Julia Sperlich was financed by the graduate program in Pharmacology and Experimental Therapeutics at the University of Cologne which is financially and scientifically supported by Bayer. We would like to thank Ina-Maria Albrecht for excellent technical assistance.

REFERENCES

1. C. P. Stewart, B. W., Wild, *World Cancer Reports* **2014**, 1–631.
2. S. Stahn, L. Thelen, I. Albrecht, J. Bitzer, T. Henkel, N. E. Teusch, *Pharmacol. Res. Perspect.* **2016**, *4*, 1–18.
3. S. Su, Y. Li, Y. Sheng, Y. Su, R. Padia, Z. Pan, Z. Dong, S. Huang, *Oncogene* **2009**, *28*, 3047–3057.
4. L. Xie, Z. Duan, C. Liu, Y. Zheng, J. Zhou, *Exp Ther Med* **2015**, *9*, 239–244.
5. C. P. Stewart, B. W., Wild, *World Cancer Reports* **2014**, 1–631.
6. S. Stahn, L. Thelen, I. Albrecht, J. Bitzer, T. Henkel, N. E. Teusch, *Pharmacol. Res. Perspect.* **2016**, *4*, 1–18.
7. S. Su, Y. Li, Y. Sheng, Y. Su, R. Padia, Z. Pan, Z. Dong, S. Huang, *Oncogene* **2009**, *28*, 3047–3057.
8. L. Xie, Z. Duan, C. Liu, Y. Zheng, J. Zhou, *Exp Ther Med* **2015**, *9*, 239–244.
9. S. Huang, Y. Li, H. Chen, J. Rong, S. Ye, *Cancer Invest.* **2013**, *31*, 578–581.
10. J. Lidfeldt, P. O. Bendahl, C. Forsare, P. Malmström, M. Fernö, M. Belting, *PLoS One*

2015, *10*, 1–12.
11. M. Yau, L. Liu, D. P. Fairlie, *J. Med. Chem.* **2013**, *56*, 7477–7497.
12. M. Yau, J. Lim, L. Liu, D. P. Fairlie, *Expert Opin. Ther. Pat.* **2016**, *26*, 471–483.
13. L. Rydén, D. Grabau, F. Schaffner, P.-E. Jönsson, W. Ruf, M. Beliting, *Int. J. Cancer* **2010**, *126*, 2330–2340.
14. S.-M. Li, P. Jiang, Y. Xiang, W.-W. Wang, Y.-C. Zhu, W.-Y. Feng, S.-D. Li, G.-Y. Yu, *Dongwuxue. Yanjiu.* **2015**, *35*, 420–425.
15. M. Takashima, H. Sakai, *Bull. Agric. Chem. Soc. Jap.* **1960**, *24*, 647–655.
16. J. H. Cardellina, F. J. Marner, R. E. Moore, *Science* **1979**, *204*, 193–195.
17. H. Fujiki, T. Sugimura, *Natl. Cancer Cent. Res. Inst.* **1987**, *49*.
18. S. F. Steinberg, *Physiol Rev.* **2008**, *88*, 1341–1378.
19. D. J. Edwards, W. H. Gerwick, *J. Am. Chem. Soc.* **2004**, *126*, 11432–11433.
20. T. Awakawa, L. Zhang, T. Wakimoto, S. Hoshino, T. Mori, T. Ito, J. Ishikawa, M. E. Tanner, I. Abe, *J. Am. Chem. Soc.* **2014**, *136*, 9910–9913.
21. K. Irie, S. Kajiyama, A. Funaki, K. Koshimizu, H. Hayashi, M. Arai, *Tetrahedron Lett.* **1990**, *31*, 101–104.
22. Y. Endo, K. Shudo, A. Itai, M. Hasegawa, Sh. Sakai, *Tetrahedron* **1986**, *42*, 5905–5924.
23. S. E. De Laszlo, S. V Ley, R. A. Porter, *J. Chem. Soc. Chem. Commun.* **1986**, *1399*, 344–346.
24. S. Nakatsuka, T. Masuda, K. Sakai, T. Goto, *Tetrahedron Lett.* **1986**, *27*, 1–4.
25. M. Mascal, C. Moody, *J. Chem. Soc. Chem. Commun.* **1988**, *8*, 589–590.
26. T. Masuda, S. Nakatsuka, T. Goto, *Agric. Biol. Chem.* **1989**, *53*, 2257–2260.
27. T. P. Kogan, T. C. Somers, M. C. Veniti, *Tetrahedron* **1990**, *46*, 6623–6632.
28. M. Mascal, C. J. Moody, A. M. Slawin, D. J. Williams, *J. Chem. Soc. Perkin Trans. 1* **1992**, *9*, 823–830.
29. M. Semmelhack, H. Rhee, *Tetrahedron Lett.* **1993**, *34*, 1395–1398.
30. J. Quick, B. Saha, P. E. Driedger, *Tetrahedron Lett.* **1994**, *35*, 8549–8552.
31. S. Bronner, A. Goetz, N. Garg, *J. Am. Chem. Soc.* **2011**, *133*, 724–732.
32. Z. Xu, F. Zhang, L. Zhang, Y. Jia, *Org. Biomol. Chem.* **2011**, *9*, 2512.
33. M. Mari, F. Bartoccini, G. Piersanti, *J. Org. Chem.* **2013**, *78*, 7727–7734.
34. N. Nathel, T. Shah, S. Bronner, N. Garg, *Chem. Sci.* **2014**, *5*, 2184–2190.
35. T. Noji, K. Okano, H. Tokuyama, *Tetrahedron* **2015**, *71*, 3833–3837.
36. H. Muratake, M. Natsume, *Tetrahedron Lett.* **1987**, *28*, 2265–2268.
37. S. Nakatsuka, T. Masuda, T. Goto, *Tetrahedron Lett.* **1987**, *28*, 3671–3674.
38. H. Muratake, K. Okabe, M. Natsume, *Tetrahedron Lett.* **1988**, *29*, 6267–6270.
39. K. Okabe, H. Muratake, M. Natsume, *Chem. Pharm. Bull.* **1989**, *37*, 563–564.
40. H. Muratake, M. Natsume, *Tetrahedron Lett.* **1991**, *47*, 8535–8544.
41. H. Muratake, K. Okabe, M. Natsume, *Tetrahedron Lett.* **1991**, *41*, 8545–8558.
42. H. Muratake, K. Okabe, M. Natsume, *Tetrahedron Lett.* **1991**, *47*, 8545–8558.
43. Y. Nakagawa, *Biosci. Biotechnol. Biochem.* **2012**, *76*, 1262–1274.
44. S. Weinreb, D. Demko, T. Lessen, *Tetrahedron Lett.* **1986**, *27*, 2099–2102.
45. S. Weinreb, C. Chase, P. Wipf, S. Venkatraman, *Org. Synth.* **1998**, *75*, DOI 10.15227/orgsyn.075.0161.
46. R. Borch, A. Hassid, *J. Org. Chem.* **1972**, *37*, 1971–1972.
47. K. Irie, R. Yanagita, K. Torii, Y. Nakagawa, *Heterocycles* **2007**, *73*, 289–302.
48. B. Meseguer, D. Alonso-Díaz, N. Griebenow, T. Herget, H. Waldmann, *Angew. Chemie Int. Ed.* **1999**, *38*, 2902–2906.
49. B. Meseguer, D. Alonso-Díaz, N. Griebenow, T. Herget, H. Waldmann, *Chemistry* **2000**, *6*, 3943–57.
50. A. Brennführer, H. Neumann, M. Beller, *Angew. Chemie - Int. Ed.* **2009**, *48*, 4114–4133.
51. N. Miyaura, A. Suzuki, *J. Chem. Soc., Chem. Commun.* **1979**, *590*, 866–867.
52. D. C. Gerbino, S. D. Mandolesi, H. G. Schmalz, J. C. Podestá, *Eur. J. Org. Chem.* **2009**, 3964–3972.
53. K. Sonogashira, Y. Tohda, N. Hagihara, *Tetrahedron Lett.* **1975**, *16*, 4467–4470.

54. [50] M. Hidai, T. Hikita, Y. Wada, Y. Fujikura, Y. Uchida, *Bull. Chem. Soc. Jpn.* **1975**, *48*, 2075–2077.
55. F. Karimi, B. Langström, *Org. Biomol. Chem.* **2003**, *1*, 541–546.
56. T. Kobayashi, M. Tanaka, *J. Chem. Soc. Chem. Commun.* **1981**, 333–334.
57. F. M. . Heemskerk, H.-C. Chen, F. L. Huang, *Biochem Biophys Res Commun.* **1993**, *190*, 236–241.

3.4.1 Supplemental Material

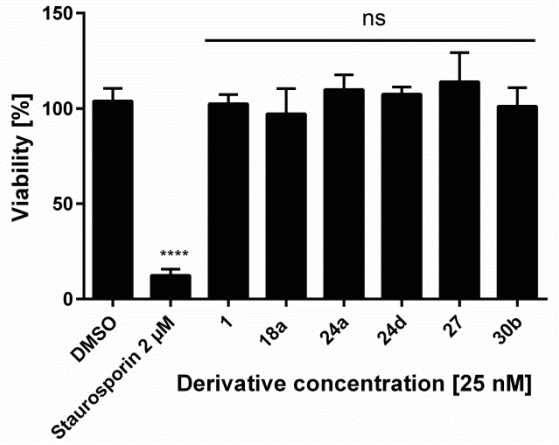

Supplemental Figure 3.4-1. Cytotoxicity of indolactam V derivatives.

Cells were treated for 48 hours with 25 nM of the displayed derivatives. Data represent mean ±SEM of three independent experiments performed in quadruplicates. Statistical analysis was calculated using one-way ANOVA.

Supplemental Method:

MDA-MB-231 breast cancer cells were cultured as described in the Experimental Section. 2.8×10^5 cells per mL were seeded in 384 well plates with the CyBio® robotic station and incubated over night at 37°C. Compounds were added at the described concentration and incubated for 48 hours. Viability of cells was measured with CellTiterGlo® kit from Promega (Madison, USA) and normalized to DMSO treated cells. Staurosporine served as positive control. ‘ns’ means not significant.

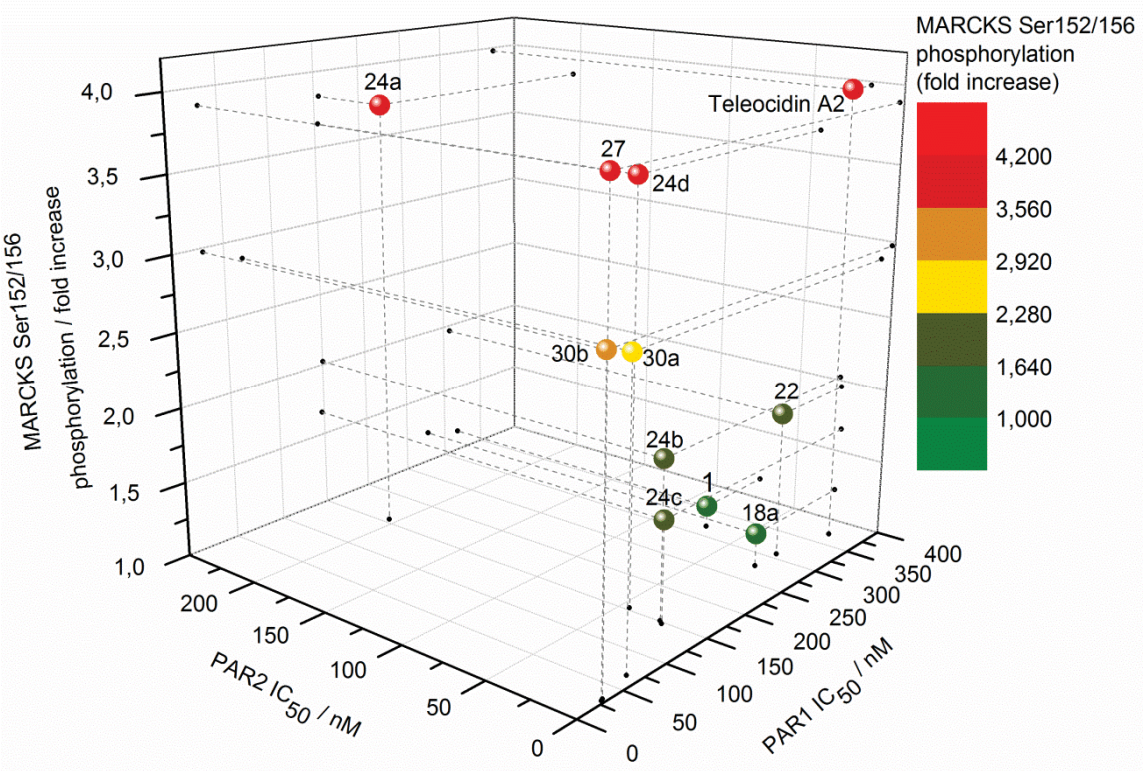

Supplemental Figure 3.4-2. 3D Plot summarizing the inhibition of PAR2 and PAR1 induced Ca2+ release and the activation of PKC by indolactam V derivatives.

IC_{50} values versus PAR2 activating peptide SLIGKV-NH2 are shown on the x-axis, IC_{50} values versus PAR1 activating peptide TFLLR-NH_2 are shown on the y-axis. Z-axis depicts phosphorylation of endogenous MARCKS protein, representing PKC activation.

Supplemental Method:

Kinetic measurements of PAR1 induced mobilization of intracellular Ca^{2+} in MDA-MB 231 cells were performed as described in the Experimental Section for PAR2. PAR1 stimulation was performed with the PAR1-activating peptide TFLLR-NH_2 (Sigma-Aldrich) at its determined EC_{50} concentration.

4 Discussion

Breast cancer is the most common cancer in women worldwide, with nearly 1.7 million new cases and 521.907 deaths in 2012 [1]. Despite the chemotherapeutic breakthrough in cancer therapy in the 1960's [228], little advances in the development of innovative and targeted therapies have been made for the breast cancer subtype triple negative breast cancer (TNBC), which is often resistant to chemotherapy. Hence, a high medical need for new selective drugs exists. TNBC-patients thus still depend on chemotherapeutics, such as paclitaxel or doxorubicin, that have no specific target in breast tumors and destroy healthy and malignant cells alike [177,229]. For non-TNBC patients, a much wider range of targeted therapy forms exist, such as the drug trastuzumab, which increases the survival rate and the chance for good prognosis after therapy much more compared to TNBC patients [12,13]. The difficulties in developing targeted TNBC therapies arise from the heterogeneity of morphological, genetic and inflammatory characteristics: features of basal-like breast tumors are combined with high inflammation and mutations in tumor suppressor genes, such as BRCA1 [5,6,10,11].

Terrestrial and marine organisms are a vast source for natural compounds inhering diverse biological and pharmacological activities which have the potential to be pharmaceutical drugs and have long been used in cancer therapy. In this study, three promising natural compounds were characterized in their potential to inhibit NF-κB signaling, PAR2-dependent calcium mobilization and characteristics of the aggressive breast cancer subtype TNBC: 1) pseudopterosin isolated from *Antillogorgia elisabethae*, 2) azaphilone isolated from *Coniella fragariae* and 3) teleocidin isolated from *Streptomyces mediocidius*. The most promising derivatives of the azaphilone and teleocidin class and pseudopterosin were evaluated on their abilities to reduce migration, invasion and proliferation of TNBC cells. The following chapters discuss these abilities with respect to being putative anti-cancer agents and their potential to target TNBC.

4.1 Pseudopterosin Inhibits NF-κB Signaling in TNBC by Agonizing the Glucocorticoid Receptor Alpha (GRα)

4.1.1 Inhibition of NF-κB and NF-κB Target Genes by Pseudopterosin

The class of pseudopterosin was first discovered in 1986 and proved to be a potent anti-inflammatory agent in *in vivo* mouse ear inflammation assays [183,186,187]. Inflammatory signals are important in the innate immune response, but chronic inflammation can lead to

cancer development. A high amount of inflammatory signals characterizes the tumor microenvironment (TME) of TNBC, triggered by constitutive activation of NF-κB signaling [35]. In chapter 3.1 and 3.2, we illuminated a novel molecular mechanism of the anti-inflammatory activity of an extract containing pseudopterosin A, B, C and D (PsA-D) in the context of TNBC and bidirectional communication of breast cancer and cancer-associated immune cells. To the best of our knowledge, only one study has investigated inhibitory abilities of pseudopterosin on cancer (non-small cell lung cancer and ER^+ breast cancer cells) showing significant cytotoxicity [185].

TNBCs are often resistant to cytotoxic chemotherapy. As an alternative approach, the inhibition of NF-κB signaling has also been shown to be an effective way to constrain TNBC: Targeting TNFα, reduces tumor growth, but does not disturb normal breast tissue [230]; inhibition of IκB phosphorylation results in reversal of epithelial-to-mesenchymal transition (EMT), decreases invasion, migration and increases apoptosis [231]; inhibition of NF-κB nuclear translocation results in reduced endogenous secretion of interleukins 6 and 8 in TNBC cells [232].

Chapters 3.1 and 3.2 showed for the first time that pseudopterosin can also inhibit the NF-κB signaling pathway in the TNBC cell line MDA-MB-231. Pseudopterosin effects were analyzed on two different TNBC cell lines and two different immune-derived cell types and revealed potent inhibitory activity of NF-κB through reduced phosphorylation of p65 as well as IκBα. This was accompanied by a reduction of the inflammatory cytokines IL-6, IL-8, MCP-1 and TNFα after stimulus as well as inhibition of endogenous cytokine secretion on both protein and mRNA level. Additionally, pseudopterosin proved to be more potent than the marketed drug indomethacin and significantly reduced the inflammatory cytokines IL-8 as well as MCP-1 also in the aggressive lung cancer cell line A549 (chapter 3.1.2). Pseudopterosin significantly blocked the invasion of cells out of spheroids and into the surrounding ECM-like matrix. The four inflammatory cytokines IL-6, IL-8, MCP-1 and TNFα are equally involved in increased invasive and migratory behavior of TNBC cells [97,117,119]. The reduction in the invasive behavior of TNBC cells may be explained by the decrease of subsequent release of IL-6, IL-8, MCP-1 and TNFα mediated by pseudopterosin in this signaling pathway. In summary, our results suggest that the downregulation of constitutive activation of NF-κB signaling correlates with the previously described anti-inflammatory abilities of pseudopterosin [183,186,187].

The bidirectional communication of cancer cells and cancer-associated immune cells in the tumor microenvironment (TME) supports tumor progression by initiating angiogenesis, proliferation and migration to other organs [31,37,38]. M2 macrophages are associated with fast proliferation and ER negativity and differentiate in the presence of TNBC conditioned medium [233]. In breast cancer tissue the amount of tumor-associated macrophages (TAMs) can reach

50% in rare cases, leading to poor prognosis [40]. TAMs communicate in paracrine manner with breast cancer cells allowing co-migration and subsequent invasion of healthy tissue [234]. In order to simulate the inter-cell communication in the TME, conditioned medium is often used as it contains secreted inflammatory cytokines and chemokines, which enhance the migration as well as the invasion of cancer cells [235,236]. Conditioned medium from monocytes, for example, contains MCP-1 and IL-8 as secreted factors which promote the migration of inflammatory breast carcinomas [237]. In this study, the cultivation of either MDA-MB-231 cells with immune-cell conditioned medium or PBMC/THP-1 monocytes with breast cancer conditioned medium increased the expression of IL-6, TNFα and MCP-1. Interestingly, pseudopterosin significantly decreased the elevated expression of IL-6 and MCP-1 in MDA-MB-231 as well as THP-1 cells and also the elevated expression of IL-6, TNFα and MCP-1 in PBMCs. I confirmed these results in a second experiment, in a co-culture of MDA-MB-231 cells with PBMCs, showing equal inhibitory activity of pseudopterosin on IL-6 and IL-8 expression. Breast cancer cells in co-culture with macrophages show an increased invasive behavior compared to mono-culture due to elevated NF-κB activation [109]. Therefore I recommend investigating the promising inhibitory potential of pseudopterosin in future studies using co-cultures of MDA-MB-231 cells with PBMCs in a 3D invasion assay and not mono-cultures.

Despite the efficiency of immunosuppressive therapies for some breast cancer types, for patients with other cancer and breast cancer types it can have deleterious effects [34]. Pseudopterosin showed potent anti-inflammatory effects reducing NF-κB, inflammatory cytokines and inhibitory abilities in the bidirectional communication of MDA-MB-231, THP-1 as well as PBMC cells. Additionally, pseudopterosin reduced the invasiveness of TNBC cells. Therefore, pseudopterosin may serve as an agent improving the efficacy of the existing immunosuppressive therapies, which demands a more in-depths evaluation of its mode if action.

4.1.2 The Mode of Action of Pseudopterosin Depends on Agonizing the Glucocorticoid Receptor Alpha (GRα)

The mechanism of action of pseudopterosin has not been identified so far, which is essential in aiming a targeted therapies based on pseudopterosin. The results presented in this thesis suggest that a reduced NF-κB signaling may be the mode of action of the anti-inflammatory abilities of pseudopterosin. In the following paragraphs, we discuss the likelihood of different interacting partners of pseudopterosin correlated with NF-κB signaling.

Xiong *et al.* (2015) suggests the mechanism of action of pseudopterosin to be downstream of the NF-κB signaling pathway. A molecular modeling of PsA with ‘nitrite oxide synthase’ (NOS)

reveals compatibility with the active pocket and NOS is up-regulated by NF-κB signaling [238,239]. Our results showed a significant reduction of NF-κB signaling independent of stimulus (LPS or TNFα), suggesting the mode of action of pseudopterosin to be downstream of TLR4 or TNFR1. NF-κB signaling blockade is associated with reduced phosphorylated 'extracellular signal-regulated kinase' (ERK) levels and reduced proliferation of cancer cells [68,123,240]. Increased expression of proliferation markers such as Ki-67 and ERK are correlated with increased proliferation of TNBC compared to non-TNBC patients, resulting in worse prognosis [241,242]. Although we confirm that pseudopterosin reduced the proliferation rate of MDA-MB-231 cells significantly, it did not modulate the phosphorylation status of ERK. Besides ERK, NF-κB modulates additional signaling pathways, including epithelial-mesenchymal transition (EMT) [44] or invasiveness [97,119]. Therefore the mechanism of action is likely to be upstream of NF-κB transcriptional activation.

The blockade and reduction of the inflammatory cytokines IL-6, IL-8, MCP-1 and TNFα mediated by pseudopterosin as described in the previous chapter, can be caused by for example 1) reduction of cytokine-producing cells; 2) inhibition of receptor signaling; 3) binding to signaling components independent of receptor (such as IKK or IκB) or 4) interference with NF-κB either by blocking the translocation into the nucleus or by blocking the binding to DNA response elements. As pseudopterosin is only moderately toxic to MDA-MB-231 cells and non-toxic to PBMCs, reduction of the cell amount as suggested in 1) cannot be explained by the inhibitory potential of pseudopterosin. However, our results of pseudopterosin inhibiting inflammatory cytokines point to a mode of action upstream of NF-κB target gene expression as described above.

The aggressiveness of breast tumors results from high amounts of inflammatory cytokines in the tumor microenvironment (TME) [35,42]. Therefore, glucocorticoid receptor alpha (GRα) signaling is utilized in the clinics due to its anti-inflammatory and immunosuppressive effects resulting in increased response rates and improved survival of breast cancer patients [122,129]. The anti-inflammatory abilities of GRα result from NF-κB blockade and subsequent downregulation of pro-inflammatory cytokines as well as upregulation of anti-inflammatory cytokines [130]. In this context, the reduction of IL-6, IL-8, MCP-1 and TNFα mediated by pseudopterosin may be explained by the activation of GRα signaling similar as described in 2). Indeed, pseudopterosin triggered GRα translocation into the nucleus similarly to the synthetic GRα ligand dexamethasone (Dex). Additionally, pseudopterosin activated a reportergene under the control of the GRα promotor and the knockdown of GRα increased cytokine expression and proliferation despite pseudopterosin treatment. In other words, the knockdown of GRα abolished the ability of pseudopterosin to decrease cytokine expression and proliferation. Although an *in*

vitro-binding study of pseudopterosin and GRα revealed only moderate IC_{50} values in the micromolar range (chapter 3.1.2), similar non-steroidal drugs to pseudopterosin are able to display a different GRα affinity and efficacy compared to Dex without causing dimerization or binding to classic GRα response elements (GREs) [243]. Alternatively, pseudopterosin may activate GRα by binding to one of the heat shock proteins (HSPs) rather than binding to GRα itself. This is similar to the anti-cancer agent tanespimycin which binds to the N-terminal domain or also cisplatin which binds to the C-terminal domain of HSP90 [244]. The inhibition of HSP70 or HSP90 contributes to reduce breast cancer cell proliferation, downregulating NF-κB, motility and invasion [245–247].

As pseudopterosin belongs to the class of terpenoids, its mechanism of action may be similar as described in 3) and 4): terpenoids modulate NF-κB signaling by activating IKK, inhibiting NF-κB-binding to DNA, phosphorylation of IκB or the translocation of NF-κB to the nucleus [248]. Even though seudopterosin may be able to act in a similar manner to the terpenoids, however, by identifying GRα as a possible interaction partner, it is unlikely that pseudopterosin modulates NF-κB signaling components similar to 3) and 4). In conclusion, the mode of action of pseudopterosin is attributed to the activation of GRα, possibly through binding to a distinct binding pocket as Dex.

Despite the anti-inflammatory characteristics of glucocorticoids (GCs), such as Dex, their clinical use is a heavily debated question due to the development of severe side effects, such as venous thromboembolism, avascular necrosis, development of chronic diseases [125,126], suppression of chemotherapy induced apoptosis [127,128] or survival of tumor cells [138]. Chapter 2.3.2 describes these contradictory effects on breast cancer progression with respect to GRα expression. A vast array of uniquely modified GRα subspecies allows diverse receptor behaviors regulating either transcriptional activation (transactivation) or transcriptional repression (transrepression). It is assumed, that the beneficial anti-inflammatory effects of GC are only mediated by repression of pro-inflammatory transcription factors, whereas unwanted metabolic side effects are attributed to the GRα transactivation [127,249]. Transactivation of GRα is defined by dimerization of the receptor followed by binding to specific sequences in the DNA – GRα positive response elements (GREs) or negative GREs (nGREs) – enabling the decondensation of the chromatin structure by coregulators [250]. In contrast, transrepression is defined as a direct interaction of GRα monomers with transcription factors such as NF-κB and subsequent negative modulation of survival-related cytokines, without binding to the DNA to regulate expression of IκB or p65/p50 [127,249]. The ability of GRα-monomers to bind directly to NF-κB thereby mediating transrepression [127,249] and the absence of nGREs in the promotor region of cytokines [135] points to pseudopterosin activating the mechanism of GRα

transrepression. Other non-steroidal drugs, which show similar capabilities compared to pseudopterosin, likewise only address the mechanism of transrepression [251]. Different ligands have been developed, that favor the activities of transrepression, without inducing the metabolic side effects of the transactivation [247,251] or specifically downregulate GRα transactivation [252]. However, the approach of developing compounds which only address the transrepession turns out to be too simplistic, because some side effects are also mediated by transrepression or even by both mechanisms [247]. N-terminal isoforms of GRα, for example, are able to act both transrepressive as well as transactivative [253]. Due to limited crystal structures of GRα bound to different GRE sequences or to full-length DNA, the understanding of different conformational changes of the receptor remains difficult [254] and further research is needed to illuminate the different mechanisms of GRα signaling.

In summary, our results show that pseudopterosin acts differently to Dex, as it did not show any modulation of ERK phosphorylation. Pseudopterosin might activate the mechanism of transrepression of GRα, thereby inhibiting NF-κB and inflammatory cytokines indirectly. This underlines the higher potency of pseudopterosin compared to Dex to reduce proliferation and to be used as anti-proliferative agent.

4.1.3 Future Perspectives

Pseudopterosin has been shown to be a potent anti-inflammatory compound in *in vivo* experiments [183,186,187] and has been assessed in phase II clinical trials as a wound-healing agent [178,255]. Aside from studies on anti-inflammation, until now, most research focused on its ability to inhibit bacterial or viral growth [185,256–258] and, to our knowledge, only one other study investigated the cytotoxicity of pseudopterosin derivatives on lung and breast cancer cells [185]. Pseudoperosin exhibited strong anti-inflammatory effects at low concentrations *in vivo*. In this work we identified the NF-κB signaling pathway as main driver for the anti-inflammatory activity with pseudopterosin showing an IC_{50} value in the micromolar range (24.4 µM). This discrepancy of potent *in vivo* anti-inflammation and reduced capabilities *in vitro* may be explained by pseudopterosin acting as a prodrug. Zhong *et al*. (2008) used a Suzuki-Miyaura cross coupling, to synthesize a pseudopterosin with a C-glycoside (PsA-OMe C-glycoside), without the possibility to cleave the sugar moiety, which results in an enhanced hydrolytic stability. As the C-glycoside analogue exhibits similar bioactivity in the mouse-ear-inflammation assay (PsA 8 µg/ear compared to C-glycoside 17 µg/ear), they conclude that pseudopterosin displays its full potential with the intact structure, not likely to be a prodrug [259]. To improve the *in vitro* pharmacological activities of pseudopterosin and to further explore its anti-inflammatory abilities, a structure-activity-relationship (SAR) analysis might help to identify a simplified derivative with improved potency on NF-κB signaling and at the same time reduce cytotoxicity

and multi-target effects. The functional optimization and toxicity evaluation is required to analyze pseudopterosin's ability to inhibit tumor growth *in vivo.* For the establishment of a xenograft model, inoculation of human MDA-MB-231 cells or a comparable breast cancer cell line in mice is suggested. After administration of an optimized pseudopterosin derivative, the tumor size and the survival of the tumor cells can be analyzed. Additionally, inhibitory abilities of pseudopterosin can be evaluated in a 3D spheroid model containing a heterogenic subpopulation of patient-derived breast cancer cells.

Cytokines are involved in distinct processes beside inflammation: MCP-1 is involved in regulating angiogenesis [121], TNFα increases expression of a multidrug resistance-related ABC transporter [110] and IL-8 is an indicator for tamoxifen resistance [93]. As pseudopterosin significantly inhibited IL-8, MCP-1 and TNFα expression in this study, a putative role in reducing multidrug resistance or reducing angiogenic processes requires further evaluation. Cytokines and chemokines are important in the inter-cell communication of tumor cells and tumor-associated immune cells and thus crucial cancer-survival factors they promote multi-drug resistance [93,110], migration, invasion [85,86], angiogenesis [97,121] and tumor growth [260,261]. Current research and applied clinical therapies therefore target cytokines with specific antibodies. In future studies, I suggest investigating further the potential of pseudopterosin to serve as anti-cancer agent in breast cancer therapy, due to its promising abilities to inhibit the expression and secretion of four different cytokines.

4.2 A new Azaphilone Derivative Inhibits NF-κB Signaling in TNBC

Fungi are a vast source of biologically active compounds and have been used extensively in the medicines against human and animal diseases, the famous penicillin G for example, was already discovered in 1929 [262]. One class of fungal-derived secondary metabolites, with a vast number of existing derivatives, is azaphilone. This class represents a collection of structurally highly variable secondary metabolites produced by a diversity of fungi including *Monascus*, *Chaetomium* [193], *Penicillium* [194], *Aspergillus*, *Bulgaria* [195] or *Talaromyces* [196]. Some azaphilones are commercialized as food colorants due to their color spectra ranging from yellow to red [193] but an increasing amount of studies investigate biological activities including anti-microbial, anti-malarial, anti-fungi, anti-virus as well as anti-inflammatory activities [206,212] and numerous more reviewed by Gao *et al*. (2013). Especially anti-cancer activities nowadays are the focus of many studies, one study analyzing a panel of 39 different cancer types [210]. To my knowledge, inhibitory effects of azaphilones in MDA-MB-231 cells, on NF-κB signaling and on migratory potential are not described, as yet. In chapter 3.3, new

naturally occurring azaphilone derivatives, extracted from *Coniella fragariae* (named coniellin A-G), were investigated on cytotoxic as well as anti-inflammatory effects. Seven derivatives were isolated, five of them showing cytotoxicity in the range of 19-22 µM and two derivatives showing no effects on MDA-MB-231 cells. Compound **1** exhibited the best inhibitory activity on NF-κB with an IC_{50} value of 4.4 µM followed by compound **7** with 11.3 µM. Compound **4** and **5** showed less potency with IC_{50} values in the range of 30-40 µM and compound **2** and **3** showed no effects. The double bond at C-14/C-15 (**1**) seems to be important for NF-κB inhibitory activities, as well as the 15*S* (**5**) compared to the 15*R* isomer (**6**) and the methyl-group at 15-OH (**7**). Compound **1** also significantly inhibited migration and invasion of MDA-MB-231 cells. Chaetomugilin I displays cytotoxic effects on the same breast cancer cell line, which compared to compound **1** (coniellin A)**,** contains no lactone ring but an additional chloride at C-5 [210]. Monascusazaphilol exhibits similar anti-inflammatory activities compared to compound **1** with strong inhibitory effects on LPS-induced TNFα release in human leukemia cells [263]. Monascin downregulates NF-κB expression and increases IκB levels in hepatic stellate cells [264]. The lactone ring in monascusazaphilol and monascin is, different to compounds **1-3,** not located on the position C-7/8 but on C-6/7. These results suggest that the location of the lactone ring is not essential for the modulation of NF-κB. The difference between the structure of monascin and monascusazaphilol is a ketone compared to a hydroxy group on C-5, suggesting the functional group is of no importance, because both compounds inhibit NF-κB signaling. However, monascin exhibits a good deal more biological activities, modulating also cyclin D1 thereby inducing cell cycle arrest, enabling an anti-inflammatory response by blocking JNK as well as ERK pathways, reducing adhesion and reactive oxygen species [265]. Additional studies are needed to determine whether the pleiotropic effects of monascin are reflected by compound **1** and monascusazaphilol as well.

The heat shock protein 90 (HSP90) is an important regulator of tumor growth, adhesion, invasion, metastasis, angiogenesis as well as apoptosis and is a potential target to inhibit tumor development and tumor progression [244]. Rubropunctatin displays moderate cytotoxicity against lung cancer with an IC_{50} value of 28 µM, but was not tested against breast cancer. Surprisingly, this azaphilone derivative shows a high binding affinity to HSP90 in the low nanomolar range and inhibits HSP90 ATPase activity [266]. SAR analysis reveals a requirement for the additional 6-internal ether, 4-carbonyl conjugated double bonds of rubropunctatin, not present in monascin, to exert anti-cancer effects, leaving the side chain with little to no influence on activity [267].

Aspergilone A [268] or longirostrerone A [269] both display cytotoxic effects against ER^+ breast cancer cells at concentrations of 25 µg/mL and 0.24 µM, respectively. Whether the additional

cyclohexanone on C-3 or the benzyl rings on C-7 of these derivatives are necessary to exert cytotoxic activity against this specific breast cancer subtype remains to be determined. Anti-inflammatory activity of monaphilols are linked to the blockade of LPS-induced NO production and anti-proliferative effects indicate an essential role for the saturated side chain on the ketone group [270]. Monascusazaphilol resembles monaphilol A and B, mainly differing in the ketone versus hydroxy group at the lactone ring as well as at C-8 and the length of the side chain 2, suggesting the functional groups and the length of the side chain to be of no importance for their activity. Sassafrin A, resembling compound **1,** inhibits NO production [204]. Helotialin A and B, resembling compound **4,** contain a carboxy group or a hydrogen at C-5 instead of an aldehyde group, respectively, displaying effects against HIV-1 replication [271]. Further studies of potential inhibitory activity of sassafrins and heliotialins against NF-κB signaling are needed to determine the correlation of the activity to the specific feature in their chemical structure.

The pyrano-quinone core that is present in some azaphilones, such as sclerotiorin, is of importance for the biological activity [212]. Anti-cancer activities and subsequent apoptosis of pancreas, lung and colorectal cancer cells after sclerotiorin treatment is associated with the modulation of important regulators in cancer progression [198,206]. However, Son *et al.* (2016) describes an azaphilone derivative, gneumsanol E, with a missing pyrano-quinone core, but cytotoxic activity with an IC_{50} value of 4.3 µM in HL-60 cells and 28 µM in mouse mammary carcinoma [212]. The effect may result from two additional double bonds at the side chain 2 [212]. The pyrano-quinone core seems to be important in the biological activities of most azaphilones, but contradicting results are described, showing a derivative with potent cytotoxic activity in mouse mammary carcinoma, missing the pyrano-quinone core.

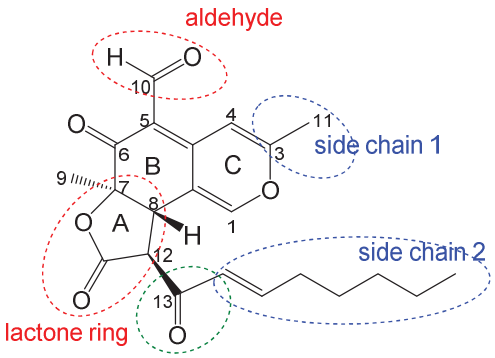

(Coniellin A)
Compound 1

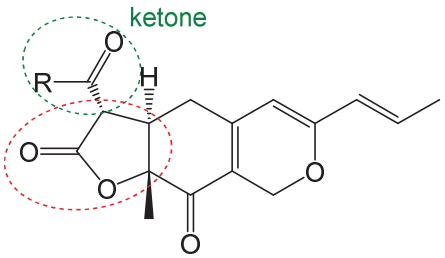

R= C_5H_{11}

Monascin

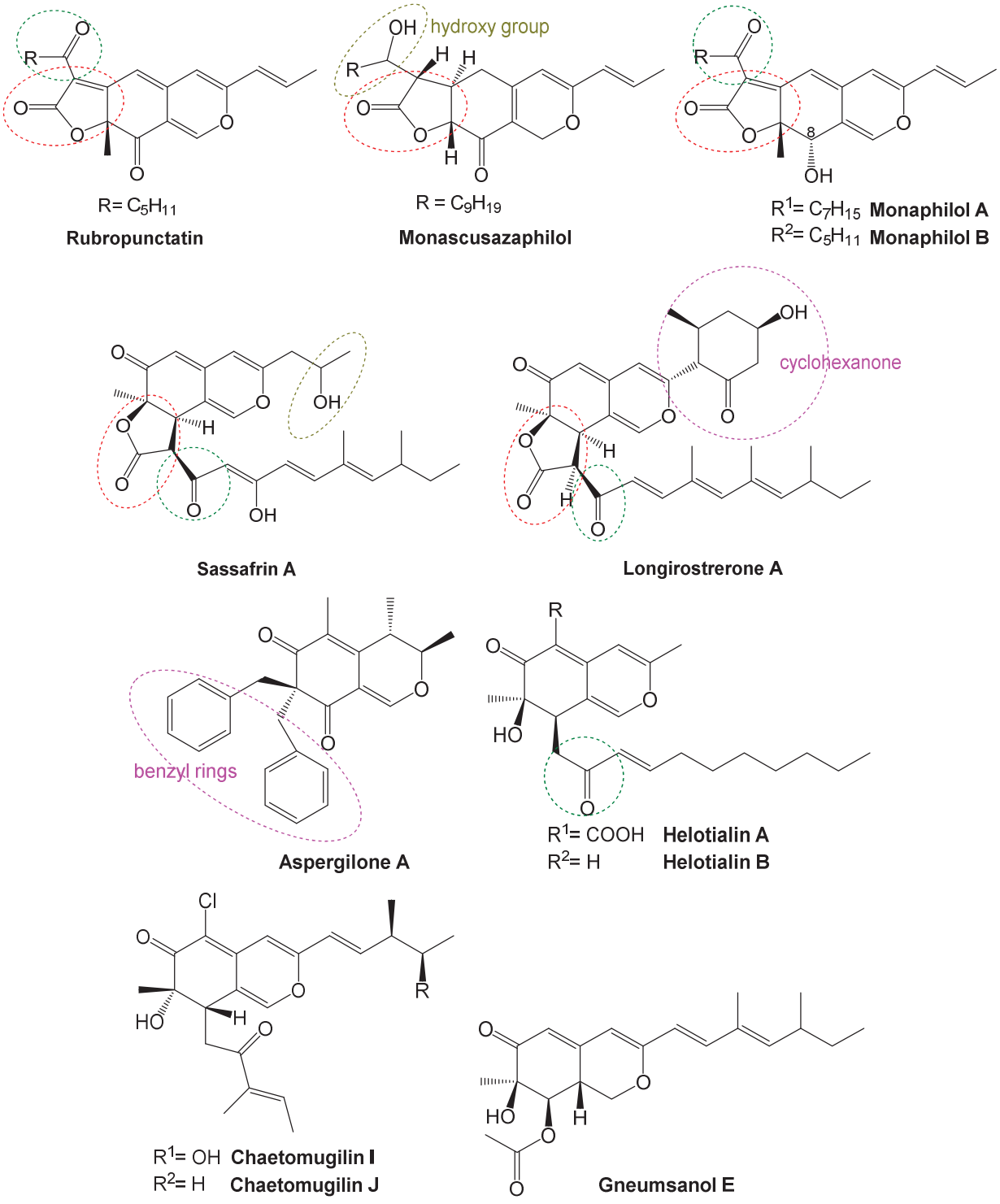

Scheme 4.2-1. Structures of azaphilone derivatives with potent biological anti-cancer related activities.

Atom numbers were adapted from Yu *et al.* (2018) and transferred accordingly to all derivatives [213]. Specific functional groups are accentuated with dashed circles and a color scheme: aldehydes and lactone rings are pictured in red, ketone groups in green, hydroxyl groups in olive, cyclohexanone and benzyl rings in magenta and side chain 1 and 2 in blue.

4.2.1 Future Perspectives

Azaphilone derivatives exhibit cytotoxicity against several different cancer cell lines such as Panc-1, A549, HL-60 [198,208,210,212] and MCF-7 [268,269,272] and can be isolated from different microorganisms including microbes, fungi as well as viruses [196,198,206,210,271]. A wide range of biological activities have been described including the induction of apoptosis [198], inhibition of HSP90 [266] as well as lipooxigenase-1 [203], downregulation of NF-κB [210] or anti-inflammatory effects [263]. Due to the high medical need of therapeutically active compounds targeting the aggressive breast cancer subtype TNBC, novel agents with specific anti-cancer properties are needed, such as the investigated natural compound pseudopterosin in chapter 3.1 and 3.2. Previous studies described inhibitory effects of azaphilones on NF-κB signaling in the context of liver damage [264], but to my knowledge, no other study further investigated a correlation of azaphilone activity on NF-κB blockade and aggressive characteristics in TNBC cells. In this study, one azaphilone derivative was identified, coniellin A isolated from *Coniella fragariae*, as the most potent derivative in inhibiting NF-κB and exhibiting anti-migratory and anti-invasive properties. Further analysis is needed to clarify whether the blockade of NF-κB by coniellin A is due to a modulation of, for example, IKK or of IκB expression. To date, no consistent SAR exists to clarify which residues on the azaphilone core structure increase or decrease anti-cancer activities or modulate regulators in cancer progression. Nevertheless, the promising results of coniellin A support further structure optimizations towards more efficacious NF-κB inhibition and lower cytotoxicity to improve the biological activity, because this is necessary conducting *in vivo* experiments.

Coniellin A showed promising inhibitory abilities addressing migration and invasion of TNBC cells in initial experiments, but additional testing to determine the mechanism of action of its inhibitory potential is necessary. A full SAR study on the length of the side chain, the location of the lactone ring or the role of the functional groups is crucial for further improvements of the chemical structure. A molecular docking using the crystal structure of the p65/p50 complex [273] can provide insights into the mechanism of action of azaphilones inhibiting NF-κB and other signaling components such as IKK or IκB.

4.3 Teleocidin Derivatives are Potent Inhibitors of PAR2-dependent Calcium Mobilization

In chapter 3.4, the third class of natural compounds, the class of teleocidins, were studied regarding inhibitory activity on TNBC characteristics. The advantage of bacteria to other organisms, for example from marine origin, is their simple and cheap cultivation methods,

guaranteeing, in most cases, the isolation of large amounts of compounds. Bacteria produce secondary metabolites with potent bioactivity also used in clinical trials in cancer chemotherapy, for example doxorubicin [229] or actinomycin D, both isolated from *Streptomyces* [274]. *Streptomyces* is the main organism producing indolactam V and teleocidins A/B and other structurally related compounds such as olivoretine and blastmycetine [215–218,221,222]. Lyngbyatoxin A is produced by a marine cyanobacterium and structurally identical to teleocidin A1 [217,220]. Natural compounds have served medicine throughout the history, however, they can also be the cause of tumor development, together with different environmental factors. Teleocidin A and B are inducers of tumor progression, due to activation of protein kinase C (PKC) [275]. PKC is known to increase proliferation of breast tumor cells and leads to increased secretion of pro-survival factors [225]. In contrast, teleocidin A2 also inhibits protease-activated receptor (PAR2)-dependent calcium mobilization in tumor cells and thus is assigned a tumor suppressor function in different tumor cells lines [169]. PAR2 increases the motility, invasion and proliferation of breast cancer cells and is associated with bad prognosis in patients [164–167].

In chapter 3.4, the potential of different indolactam V (**1**) derivatives in a structure-activity-relationship (SAR) analysis was investigated in the context of PAR2-dependent calcium mobilization. Activation of the tumor promotor PKC was analyzed using phosphorylation of the endogenous PKC substrate MARCKS and specificity to PAR2 was analyzed towards a second member of the receptor family, PAR1. The derivative **30b** showed the highest inhibitory ability against PAR2-dependent calcium mobilization with an IC_{50} value of 1.6 nM, followed by derivatives **27** and **30a** (IC_{50} value of 2.3 nM and 7.0 nM) and teleocidin A2 with an IC_{50} value of 18 nM. Indolactam V showed less potency, with an IC_{50} value of only 72 nM. The presence of a functional group on residue 2 (R2) seem to be important for the potent activity of the three derivatives, as indolactam V misses a functional groups at this position. However, the potency can be recovered by substituting R1 with an acetyl group (**18a**), methoxycarbonyl 'Moc' (**22**), 3-Fn-Bn (**24b**) or 4-Fn-Bn (**24c**) showing similar potency to teleocidin A2 in the range of 24-26 nM. Concerning the fluorinated benzyl ring, the position of the Fluor was important for the potency: in para- and meta-position, derivatives **24c** and **24b** showed activity with IC_{50} values of 24 and 26 nM, whereas in ortho-position the activity of the derivative **24a** was reduced to 200 nM. An additional fluorinated benzyl ring on position N-10 near the hydroxyl group on C-14 as in derivative **25** completely abolished its activity. Substitution on R4 reduced the potency dramatically as seen in **17b**, suggesting an essential role for the hydroxyl group on C-14. A methyl group at R3 was equally essential for PAR2 inhibition, as substitution with hydrogen resulted in the loss of potency (**19a/b**). The substitution of the acetyl group on R1 of the derivative **18a** to i-butyryl (**20**), a tosyl group (**19b**) or benzoyl (**21**), reduced the inhibitory

activity. Different functional groups on R2 are accepted, for example ethyl ester (**30b**), methyl ester (**30a**), an allyl group (**27**) or an alkynyl group (**31e**), but cyclization (**29**), N-methoxy amide (**30c**) or N-ethoxy amide (**30d**) were not tolerated at this position.

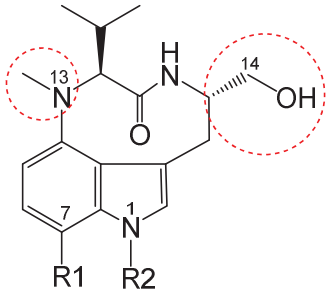

Figure 4.3-1. SAR of teleocidin/indolactam.

The free hydroxy group on C-14 and the methyl group on N-13 both are essential functional groups for the biological activity. Substitutions on N1 and C-7 with different functional groups are allowed. However, the most potent derivative contains an ethyl ester on R2 and hydrogen on R1.

PKC activation is an undesired off-target effect of the teleocidin class. Therefore, the aim was to identify a derivative with PAR2 inhibitory activity in nanomolar concentrations, but at the same time with low potency to activate PKC. A strong increase of the MARCKS phosphorylation of 4-fold after teleocidin A2 treatment confirmed its effects as described in the literature. The derivatives **30a** and **30b** showed a lower potential to phosphorylate MARKCS of only 3-fold compared to control. Indolactam V and the derivatives **18a** and **24c** displayed the least ability to phosphorylate MARCKS similar to DMSO control. Substitution of the hydrogen residues on R2 seemed to be favorable for the PKC activation, showing an increase in the ability to activate PKC, as shown by the derivatives **27**, **30a** and **30b**. The substitution of the fluorine (**24b**), in the meta-position of the benzyl ring, to a methoxy group (**24d**) also resulted in an increase in PKC activation. In summary, activation of PKC was not necessarily correlated with PAR2-dependent calcium inhibition. A reduction of PKC activation was not associated to a reduction of PAR2 inhibition.

To determine the selectivity on PAR2 inhibition, the ability to inhibit PAR1-dependent calcium mobilization was investigated: teleocidin A2 inhibited PAR1 with an IC_{50} value of 350 nM, which is a 20-fold increase compared to PAR2-dependent inhibition. In comparison, the derivatives **22, 18a** and **30a** were increased by 12-fold, 10-fold and 10-fold and **30b** showed an increase to PAR2 by 15-fold, respectively. The fluorinated benzyl ring is not favorable for PAR2 specificity as these compounds showed the lowest increase in IC_{50} values of PAR1 compared to of PAR2 inhibition: the derivatives **24c, 24d, 24a** were increased only by 6-fold, 3.5-fold and by 1.3 fold.

The teleocidin derivative **30b** was identified as a potent inhibitor of PAR2-dependent calcium mobilization with an IC_{50} value of 1.6 nM, moderate PKC activation of 3-fold increase compared to control and less specificity to PAR1-dependent calcium mobilization, with a 15-fold increase compared to PAR2. PAR2 as well as PAR1 are known to promote pro-metastatic processes [276] and especially PAR2 is correlated with VEGF and aggressive tumor types in ER^- breast cancer patients [167]. The migration of malignant cells from an existing tumor to other organs, for example developing visceral metastasis or brain metastasis [14,277], is a huge problem in the therapy of TNBC. Thus, **30b**, as the most potent derivative against PAR2 signaling, was tested on the migratory behavior of MDA-MB-231 cells, showing a significant reduction. In summary, novel teleocidin derivatives were identified, which reduce cancer-related signaling and thus, in contrast to the literature, are also potent tumor suppressive agents.

4.3.1 Future Perspectives

Until now, the research of teleocidins has focused on tumor promoting activity, mostly on PKC or other inflammatory signals [217,223,224]. In this thesis, SAR analysis revealed novel teleocidin derivatives as inhibitors of PAR2-dependent calcium mobilization with **30b** as the most potent derivative. Further improvements on the structure can reduce the abilities concerning PKC and PAR1 activation and thus provide higher specificity towards PAR2-dependent calcium release. Teleocidin A2 does not compete with the radiolabeled protease-cleaved N-terminal sequence of PAR2, suggesting another mechanism than inhibiting the N-terminus [169]. Two antagonist of PAR2 showed distinct mechanism to modulate the receptor. AZ8838 for example, binds to a pocket near the extracellular surface of PAR2, whereas AZ3451 binds to an allosteric binding site outside the helical bundle [278]. In future studies, I suggest to conduct a molecular docking with PAR2 and **30b** to help identify the binding pocket, which is responsible for the inhibitory ability similar to AZ8838 or AZ3451. Likewise a molecular docking with PAR1 may reveal the modulation site of the unspecific binding. **30b** shows no cytotoxicity in MDA-MB-231 cells at a concentration of 25 nM, stressing the need for additional studies in *in vivo* xenograft models in the future.

Vorapaxar is the only marketed drug targeting PAR1 [170]. PAR2 antagonists were not approved as yet, due to inhibitory activity only in the micromolar range and also solubility problems as a result of high molecular weight or low specificity [279]. **30b** thus may be a promising candidate for further *in vivo* studies and as a novel agent for targeted TNBC therapy.

4.4 Summary

The main objective in this thesis was to characterize three natural occurring compounds as candidates for developing targeted therapies of the aggressive breast cancer subtype triple negative. Therefore, stable reportergene cell lines to analyze modulatory abilities on different signaling pathways, multiplex immunized magnetic beads, 3D cell culture and co-cultures were established. The modulation of proliferation, invasion and migration of TNBC cells was observed using realtime imaging.

Pseudopterosin, the marine natural product isolated from *Antillogorgia elisabethae*, was able to inhibit NF-κB, significantly reduce the phosphorylation of p65, IκB as well as reduce IL-6, IL-8, MCP-1 and TNFα after stimulus as well as inhibition of endogenous cytokine secretion on both protein and mRNA level. Moreover, pseudopterosin activated the translocation of GRα into the nucleus and – in the absence of GRα – pseudopterosin was not able to reduce cytokine expression and proliferation anymore. Anti-inflammatory effects of pseudopterosin, the blockade of invasion and proliferation in TNBC cells may be explained by pseudopterosin agonizing GRα as a molecular mode of action and subsequent transrepression of NF-κB activation.

Azaphilones, a class of fungal natural compounds, show various biological activities against numerous cancer cell lines. Seven new azaphilone derivatives were identified from the fungus *Coniella fragariae.* Five derivatives exhibited cytotoxic activity against TNBC cells and two exhibited inhibitory activity against NF-κB in the low micromolar range. Coniellin A was the most promising azaphilone derivative showing significant anti-migratory and anti-invasive abilities in TNBC cells.

Teleocidin is the third natural compound investigated in this thesis and was isolated from the bacterium *Streptomyces mediocidius*. A distinct SAR for the inhibition of PAR2-dependent calcium mobilization was observed, identifying one derivative with a particular potent ability in the nanomolar range and no toxicity on TNBC cells. Additionally, this derivative showed significant inhibition of the migratory behavior of TNBC cells. Analysis of receptor specificity revealed a low ability to activate the well described “off-target” PKC and to inhibit PAR1-dependent calcium mobilization demonstrating improved abilities compared to teleocidin A2.

In summary, pseudopterosin revealed potent inhibitory abilities in NF-κB-dependent inflammatory processes and bidirectional communication of tumor cells and tumor-associated immune cells, acting as an agonist of GRα. Additionally, two novel natural product derivatives were identified with inhibitory abilities on TNBC-related signaling pathways, migration and invasion. This study has helped to improve our understanding of the mechanism of action of three natural compounds and underlines their great potential to cover the high medical need of therapeutically active agents and to develop medical drugs targeting the aggressive breast cancer subtype TNBC.

5 References

[1] Stewart BW, Wild CP. World Cancer Report 2014. 2014.

[2] Siegel R, Miller K, Jemal A. Cancer statistics, 2015. CA Cancer J Clin 2015; 65:29.

[3] Siegel RL, Miller KD, Ahmedin J. Cancer statistics, 2017. CA Cancer J Clin 2017; 67:7–30.

[4] Belova L, Delgado B, Kocherginsky M, Melhem A, Olopade O, Conzen S. Glucocorticoid receptor expression in breast cancer associates with older patient age. Breast Cancer Res Treat 2015; 116:441–447.

[5] Dawson SJ, Provenzano E, Caldas C. Triple negative breast cancers: Clinical and prognostic implications. Eur J Cancer 2009; 45:27–40.

[6] O'Reilly EA, Gubbins L, Sharma S, Tully R, Guang MHZ, Weiner-Gorzel K, McCaffrey J, Harrison M, Furlong F, Kell M, McCann A. The fate of chemoresistance in triple negative breast cancer (TNBC). BBA Clin 2015; 3:257–275.

[7] Al-Hajj M, Wicha MS, Benito-Hernandez A, Morrison SJ, Clarke MF. Prospective identification of tumorigenic breast cancer cells. Proc Natl Acad Sci 2003; 100:3983–3988.

[8] Yamamoto M, Taguchi Y, Ito-kureha T, Semba K, Yamaguchi N, Inoue J. NF-κB non-cell-autonomously regulates cancer stem cell populations in the basal-like breast cancer subtype. Nat Commun 2013; 4:1–13.

[9] Rojo F, González-Pérez A, Furriol J, Nicolau MJ, Ferrer J, Burgués O, Sabbaghi M, González-Navarrete I, Cristobal I, Serrano L, Zazo S, Madoz J, et al. Non-canonical NF-κB pathway activation predicts outcome in borderline oestrogen receptor positive breast carcinoma. Br J Cancer 2016; 115:322–331.

[10] Biswas T, Efird JT, Prasad S, James SE, Walker PR, Zagar TM. Inflammatory TNBC breast cancer: Demography and clinical outcome in a large cohort of patients with TNBC. Clin Breast Cancer 2016; 16:212–216.

[11] Kilburn LS. 'Triple negative' breast cancer: A new area for phase III breast cancer clinical trials. Clin Oncol 2008; 20:35–39.

[12] Pal SK, Childs BH, Pegram M. Triple negative breast cancer: Unmet medical needs. Breast Cancer Res Treat 2011; 125:627–636.

[13] Bauer KR, Brown M, Cress RD, Parise CA, Caggiano V. Descriptive analysis of estrogen receptor (ER)-negative, progesterone receptor (PR)-negative, and HER2-negative invasive breast cancer, the so-called triple-negative phenotype: A population-based study from the California Cancer Registry. Cancer 2007; 109:1721–1728.

[14] Wahba HA, El-Hadaad HA. Current approaches in treatment of triple-negative breast

cancer. Cancer Biol Med 2015; 12:106–16.

[15] Amos KD, Adamo B, Anders CK. Triple-negative breast cancer: An update on neoadjuvant clinical trials. Int J Breast Cancer 2012; 2012:1–7.

[16] Wang S, Yang H, Tong F, Zhang J, Yang D, Liu H, Cao Y, Liu P, Zhou P, Cheng L, Liu M, Guo J. Response to neoadjuvant therapy and disease free survival in patients with triple-negative breast cancer. Gan To Kagaku Ryoho 2009; 36:255–8.

[17] Silver DP, Richardson AL, Eklund AC, Wang ZC, Szallasi Z, Li Q, Juul N, Leong CO, Calogrias D, Buraimoh A, Fatima A, Gelman RS, et al. Efficacy of neoadjuvant cisplatin in triple-negative breast cancer. J Clin Oncol 2010; 28:1145–1153.

[18] Rouzier R, Perou CM, Symmans WF, Ibrahim N, Cristofanilli M, Anderson K, Hess KR, Stec J, Ayers M, Wagner P, Morandi P, Fan C, et al. Breast cancer molecular subtypes respond differently to preoperative chemotherapy. Clin Cancer Res 2005; 11:5678–5685.

[19] Cooper GM. The cell: A molecular approach. vol. 2. 2nd Ed. Sunderland (MA): Sinauer Associates; 2000.

[20] Geisler S, Lønning PE, Aas T, Johnsen H, Fluge O, Haugen DF, Lillehaug JR, Akslen LA, Børresen-Dale AL. Influence of TP53 gene alterations and c-erbB-2 expression on the response to treatment with doxorubicin in locally advanced breast cancer. Cancer Res 2001; 61:2505–2512.

[21] Gluz O, Liedtke C, Gottschalk N, Pusztai L, Nitz U, Harbeck N. Triple-negative breast cancer - current status and future directions. Ann Oncol 2009; 20:1913–1927.

[22] Gennari A, Sormani MP, Pronzato P, Puntoni M, Colozza M, Pfeffer U, Bruzzi P. HER2 status and efficacy of adjuvant anthracyclines in early breast cancer: A pooled analysis of randomized trials. J Natl Cancer Inst 2008; 100:14–20.

[23] Rottenberg S, Nygren AOH, Pajic M, van Leeuwen FWB, van der Heijden I, van de Wetering K, Liu X, de Visser KE, Gilhuijs KG, van Tellingen O, Schouten JP, Jonkers J, et al. Selective induction of chemotherapy resistance of mammary tumors in a conditional mouse model for hereditary breast cancer. Proc Natl Acad Sci U S A 2007; 104:12117–22.

[24] Vyas D, Deshpande K, Chaturvedi L, Gieric L, Ching K. Rapid extensive recurrence of triple negative breast cancer: Are both therapy and cancer biology the culprit? J Clin Med Res 2016; 8:162–167.

[25] Pal, Luchtenborg, Davis. The treatment and survival of patients with triple negative breast cancer in a London population. Springerplus 2014; 3:553.

[26] Place AE, Jin Huh S, Polyak K. The microenvironment in breast cancer progression: Biology and implications for treatment. Breast Cancer Res 2011; 13.

[27] Allinen M, Cai L, Brennan C, Lahti-Domenici J, Huang H, Porter D, Hu M, Chin L,

Richardson A, Schnitt S, Sellers W, Polyak K, et al. Molecular characterization of the tumor microenvironment in breast cancer. Cancer Cell 2004; 6:17–32.

[28] Hanahan D, Weinberg R a. Hallmarks of cancer: The next generation. Cell 2011; 144:646–674.

[29] Maller O, Martinson H, Schedin P. Extracellular matrix composition reveals complex and dynamic stromal-epithelial interactions in the mammary gland. J Mammary Gland Biol Neoplasia 2010; 15:301–318.

[30] Bissell MJ, Radisky D. Putting tumors in context. Nat Rev Cancer 2001; 1:46–54.

[31] Hao NB, Lü MH, Fan YH, Cao YL, Zhang ZR, Yang SM. Macrophages in tumor microenvironments and the progression of tumors. Clin Dev Immunol 2012; 2012.

[32] Toulza F, Eliaou J-F, Pinet V. Breast tumor cell soluble factors induce monocytes to produce angiogenic but not angiostatic CXC chemokines. Int J Cancer 2005; 115:429–36.

[33] Zitvogel L, Ayyoub M, Routy B, Kroemer G. Microbiome and anticancer immunosurveillance. Cell 2016; 165:276–287.

[34] Quail D, Joyce J. Microenvironmental regulation of tumor progression and metastasis. Nat Med 2013; 19:1423–1437.

[35] Whiteside TL. The tumor microenvironment and its role in promoting tumor growth. Oncogene 2008; 27:5904–12.

[36] Lewis CE, Leek R, Harris A, McGee JO. Cytokine regulation of angiogenesis in breast cancer: The role of tumor-associated macrophages. J Leukoc Biol 1995; 57:747–751.

[37] Sherman MH, Downes M, Evans RM. Nuclear receptors as modulators of the tumor microenvironment. Cancer Prev Res 2012; 5:3–10.

[38] Mohamed MM, El-Ghonaimya EA, Nouhb MA, Schneiderc RJ, Sloaned BF, El-Shinawie M. Cytokines secreted by macrophages isolated from tumor microenvironment of inflammatory breast cancer patients possess chemotactic properties. Int J Biochem Cell Biol 2014; 46:138–147.

[39] Yu T, Di G. Role of tumor microenvironment in triple-negative breast cancer and its prognostic significance. Chinese J Cancer Res 2017; 29:237–252.

[40] Pollard JW. Macrophages define the invasive microenvironment in breast cancer. J Leukoc Biol 2008; 84:623–630.

[41] Mosser DM, Edwards JP. Exploring the full spectrum of macrophage activation. Nat Rev Immunol 2008; 8:958–969.

[42] Butcher D, Alliston T, Weaver V. A tense situation: forcing tumor progression. Nat Rev Cancer 2009; 9:108–122.

[43] Shostak K, Chariot A. NF-κB, stem cells and breast cancer: the links get stronger. Breast

Cancer Res 2011; 13:214.

[44] Pires BRB, Mencalha AL, Ferreira GM, de Souza WF, Morgado-Díaz JA, Maia AM, Corrêa S, Abdelhay ESFW. NF-kappaB is involved in the regulation of EMT genes in breast cancer cells. PLoS One 2017; 12:e0169622.

[45] Sovak MA, Bellas RE, Kim DW, Zanieski GJ, Rogers AE, Traish AM. Aberrant nuclear factor-κB/Rel expression and the pathogenesis of breast cancer. J Clin Invest 1997; 100:2952–60.

[46] Badr C, Niers JM, Tjon-Kon-Fat L-A, Noske DP, Wurdinger T, Tannous B. Real-time monitoring of NF-kappaB activity in cultured cells and in animal models. Mol Imaging 2009; 8:278–290.

[47] Kawai T, Akira S. The role of pattern-recognition receptors in innate immunity: Update on Toll-like receptors. Nat Immunol 2010; 11:373–384.

[48] Ramage L. Expression of pro-inflammatory proteins in the lung epithelial cell line A549, in response to cytokine, and environmental particle exposure. Edinburgh Napier University, 2003.

[49] Blank V, Kourilsky P, Israel A, Publishers ES. NF-κB and related proteins: Rel/dorsal homologies meet ankyrin-like repeats. Elsevier Sci Publ 1992:135–140.

[50] Liu M, Sakamaki T, Casimiro MC, Willmarth N, Quong AA, Ju X, Ojeifo J, Jiao X, Yeow W-S, Sanjay Katiyar L, Shirley A, Joyce D, et al. The canonical NF-κB pathway governs mammary tumorigenesis in transgenic mice and tumor stem cell expansion. Cancer Res 2010; 70:10464–73.

[51] Ghosh S, May MJ, Kopp EB. NF-κB and Rel proteins: evolutionarily conserved mediators of immune responses. Annu Rev Immunol 1998; 16:225–260.

[52] Perkins ND. Integrating cell-signalling pathways with NF-kappaB and IKK function. Nat Rev Mol Cell Biol 2007; 8:49–62.

[53] Kawai T, Akira S. Signaling to NF-κB by Toll-like receptors. Trends Mol Med 2007; 13:460–469.

[54] Gilmore TD, Morin PJ. The IκB proteins: members of a multifunctional family. Trends Genet 1993; 9:427–433.

[55] Kretz-Remy C, Mehlen P, Mirault M-E, Arrigo A-P. Inhibition of IkappaB-alpha phosphorylation and degradation and subsequent NF-kappaB activation by glutathione peroxidase overexpression. J Cell Biol 1996; 133:1083–1093.

[56] Beg AA, Ruben SM, Scheinman RI, Haskill S, Rosen CA, Baldwin ASJ. IkappaB interacts with the nuclear localization signal of the subunits of NF-kappaB: A mechanism for cytoplasmic retention. Genes Dev 1992; 6:1899–1913.

[57] Didonato J a, Hayakawa M, Rothwarf DM, Zandi E, Karin M. A cytokine-responsive IkB

kinase that activates the transcription factor NF-κB. Nature 1997; 388:548–554.

[58] Lemaitre B, Nicolas E, Michaut L, Reichhart J, Hoffmann J a. The dorsoventral regulatory gene cassette spätzle/Toll/cactus controls the potent antifungal response in *Drosophila* adults. Cell 1996; 86:973–983.

[59] Akira S, Uematsu S, Takeuchi O. Pathogen recognition and innate immunity. Cell 2006; 124:783–801.

[60] Park BS, Lee JO. Recognition of lipopolysaccharide pattern by TLR4 complexes. Exp Mol Med 2013; 45:e66-9.

[61] Rauert-Wunderlich H, Siegmund D, Maier E, Giner T, Bargou RC, Wajant H, Stühmer T. The IKK Inhibitor Bay11-7082 induces cell death independent from inhibition of activation of NF-κB transcription factors. PLoS One 2013; 8:1–10.

[62] Yamamoto M, Sato S, Hemmi H, Hoshino K, Kaisho T, Sanjo H, Takeuchi O, Sugiyama M, Okabe M, Takeda K, Akira S. Role of adaptor TRIF in the MyD88-independent toll-like receptor signaling pathway. Science (80-) 2003; 301:640–643.

[63] Da Silva Correia J, Ulevitch RJ. MD-2 and TLR4 N-linked glycosylations are important for a functional lipopolysaccharide receptor. J Biol Chem 2002; 277:1845–1854.

[64] Kim DW, Sovak MA, Zanieski G, Nonet G, Romieu-Mourez R, Lau AW, Hafer LJ, Yaswen P, Stampfer M, Rogers AE, Russo J, Sonenshein GE. Activation of NF-κB/Rel occurs early during neoplastic transformation of mammary cells. Carcinogenesis 2000; 21:871–879.

[65] Becker-Weimann S, Xiong G, Furuta S, Han J, Kuhn I, Akavia U-D, Pe'er D, Bissell MJ, Xu R. NFκB disrupts tissue polarity in 3D by preventing integration of microenvironmental signals. Oncotarget 2013; 4:2010–2020.

[66] Inglés-Esteve J, Morales M, Dalmases A, Garcia-Carbonell R, Jené-Sanz A, López-Bigas N, Iglesias M, Ruiz-Herguido C, Rovira A, Rojo F, Albanell J, Gomis RR, et al. Inhibition of specific NF-κB activity contributes to the tumor suppressor function of 14-3-3σ in breast cancer. PLoS One 2012; 7:e38347.

[67] Biswas DK, Shi Q, Baily S, Strickland I, Ghosh S, Pardee AB, Iglehart JD. NF-κB activation in human breast cancer specimens and its role in cell proliferation and apoptosis. Proc Natl Acad Sci 2004; 101:10137–10142.

[68] Gordon AH, O'Keefe RJ, Schwarz EM, Rosier RN, Puzas JE. Nuclear factor-kappaB-dependent mechanisms in breast cancer cells regulate tumor burden and osteolysis in bone. Cancer Res 2005; 65:3209–17.

[69] Mantovani A, Allavena P, Sica A, Balkwill F. Cancer-related inflammation. Nature 2008; 454:436–444.

[70] Huber M a, Azoitei N, Baumann B, Grünert S, Sommer A, Pehamberger H, Kraut N,

Beug H, Wirth T. NF-κB is essential for epithelial- mesenchymal transition and metastasis in a model of breast cancer progression. J Clin Invest 2004; 114:569–581.

[71] Chua HL, Bhat-Nakshatri P, Clare SE, Morimiya A, Badve S, Nakshatri H. NF-κB represses E-cadherin expression and enhances epithelial to mesenchymal transition of mammary epithelial cells: Potential involvement of ZEB-1 and ZEB-2. Oncogene 2007; 26:711–724.

[72] Isogawa M, Higuchi M, Takahashi M, Oie M, Mori N, Tanaka Y, Aoyagi Y, Fujii M. Rearranged NF-κB2 gene in an adult T-cell leukemia cell line. Cancer Sci 2008; 99:792–798.

[73] Didonato J a., Mercurio F, Karin M. NF-κB and the link between inflammation and cancer. Immunol Rev 2012; 246:379–400.

[74] Yamaguchi N, Ito T, Azuma S, Ito E, Honma R, Yanagisawa Y, Nishikawa A, Kawamura M, Imai J ichi, Watanabe S, Semba K, Inoue J ichiro. Constitutive activation of nuclear factor-κB is preferentially involved in the proliferation of basal-like subtype breast cancer cell lines. Cancer Sci 2009; 100:1668–1674.

[75] Llona-Minguez S, Baiget J, Mackay SP. Small-molecule inhibitors of IκB kinase (IKK) and IKK-related kinases. Pharm Pat Anal 2013; 2:481–498.

[76] Esquivel-Velázquez M, Ostoa-Saloma P, Palacios-Arreola MI, Nava-Castro KE, Castro JI, Morales-Montor J. The role of cytokines in breast cancer development and progression. J Interf Cytokine Res 2015; 35:1–16.

[77] Negus RPM, Balkwill FR. Cytokines in tumour growth, migration and metastasis. World J Urol 1996; 14:157–165.

[78] DeNardo DG, Coussens LM. Inflammation and breast cancer. Balancing immune response: Crosstalk between adaptive and innate immune cells during breast cancer progression. Breast Cancer Res 2007; 9:1–10.

[79] E. Goldberg J, L. Schwertfeger K. Proinflammatory cytokines in breast cancer: Mechanisms of action and potential targets for therapeutics. Curr Drug Targets 2010; 11:1133–1146.

[80] Murakami M, Hibi M, Nakagawa N, Nakagawa T, Yasukawa K, Yamanishi K, Taga T, Kishimoto T. IL-6-induced homodimerization of pg130 and associated activation of a tyrosine kinase. Adv Sci 1993; 260:1808–1810.

[81] Kopf M, Baumann H, Freer G, Freudenberg MA, Lamers M, Kishimoto T, Zinkernagel R, Bluethmann H, Köhler G. Impaired immune and acute-phase responses in interleukin-6-deficient mice. Nature 1994; 368:339–42.

[82] Kishimoto T. Interleukin-6: Discovery of a pleiotropic cytokine. Arthritis Res Ther 2006; 8.

[83] Dubiński A, Zdrojewicz Z. The role of interleukin-6 in development and progression of

atherosclerosis. Pol Merkur Lek 2007; 22:291–4.

[84] Kristiansen O, Mandrup-Poulsen T. Interleukin-6 and diabetes: The good, the bad, or the indifferent? Diabetes 2005; 54:114–24.

[85] Arihiro K, Oda H, Kaneko M, Inai K. Cytokines facilitate chemotactic motility of breast carcinoma cells. Breast Cancer 2000; 7:221–230.

[86] Sullivan NJ, Sasser AK, Axel AE, Vesuna F, Raman V, Ramirez N, Oberyszyn TM, Hall BM. Interleukin-6 induces an epithelial-mesenchymal transition phenotype in human breast cancer cells. Oncogene 2009; 28:2940–2947.

[87] Sasser AK, Sullivan NJ, Studebaker AW, Hendey LF, Axel AE, Hall BM. Interleukin-6 is a potent growth factor for ER-positive human breast cancer. FASEB J 2007; 21:3763–3770.

[88] Knüpfer H, Preiß R. Significance of interleukin-6 (IL-6) in breast cancer (review). Breast Cancer Res Treat 2007; 102:129–135.

[89] Zhang G-J, Adachi I. Serum interleukin-6 levels correlate to tumor progression and prognosis in metastatic breast carcinoma. Anticancer Res 1999; 19:1427–32.

[90] Nishimura R, Nagao K, Miyayama H, Matsuda M, Baba K, Matsuoka Y, Yamashita H, Fukuda M, Mizumoto T, Hamamoto R. An analysis of serum interleukin-6 levels to predict benefits of medroxyprogesterone acetate in advanced or recurrent breast cancer. Oncology 2000; 59:166–173.

[91] Choy EHS, Isenberg DA, Garrood T, Farrow S, Ioannou Y, Bird H, Cheung N, Williams B, Hazleman B, Price R, Yoshizaki K, Nishimoto N, et al. Therapeutic benefit of blocking interleukin-6 activity with an anti-interleukin-6 receptor monoclonal antibody in rheumatoid arthritis: A randomized, double-blind, placebo-controlled, dose-escalation trial. Arthritis Rheum 2002; 46:3143–3150.

[92] Sanguinetti A, Santini D, Bonafè M, Taffurelli M, Avenia N. Interleukin-6 and pro inflammatory status in the breast tumor microenvironment. World J Surg Oncol 2015; 13:4–9.

[93] Todorović-Raković N, Milovanović J. Interleukin-8 in breast cancer progression. J Interf Cytokine Res 2013; 33:563–570.

[94] Singh RK, Gutman M, Radinsky R, Bucana CD, Fidler IJ. Expression of interleukin 8 correlates with the metastatic potential of human melanoma cells in nude mice. Cancer Res 1994; 54:3242–3247.

[95] De Larco JE, Wuertz BRK, Yee D, Rickert BL, Furcht LT. Atypical methylation of the interleukin-8 gene correlates strongly with the metastatic potential of breast carcinoma cells. Proc Natl Acad Sci U S A 2003; 100:13988–93.

[96] Rody A, Karn T, Liedtke C, Pusztai L, Ruckhaeberle E, Hanker L, Gaetje R, Solbach C,

Ahr A, Metzler D, Schmidt M, Müller V, et al. A clinically relevant gene signature in triple negative and basal-like breast cancer. Breast Cancer Res 2011; 13:R97.

[97] Lin Y, Huang R, Chen L, Li S, Shi Q, Jordan C, Huang R-P. Identification of interleukin-8 as estrogen receptor-regulated factor involved in breast cancer invasion and angiogenesis by protein arrays. Int J Cancer 2004; 109:507–515.

[98] Charafe-Jauffret E, Ginestier C, Iovino F, Wicinski J, Cervera N, Finetti P, Hur M, Diebel ME, Monville F, Brown M, Viens P, Xerri L, et al. Breast cancer cell lines contain funtional cancer stem cells with metastatic capacity and distinct molecular signature. Cancer Res 2009; 69:1302–1313.

[99] Salcedo R, Martins-green M, Gertz B. Combined administration of antibodies to human interleukin 8 and epidermal growth factor receptor results in increased antimetastatic effects on human breast carcinoma xenografts. Clin. Cancer Res. 2002; 8:2655–2665.

[100] Aggarwal BB. Signalling pathways of the TNF superfamily: A double-edged sword. Nat Rev Immunol 2003; 3:745–756.

[101] Cox GW, Melillo G, Chattopadhyay U, Mullet D, Fertel RH, Varesio L. Tumor necrosis factor-alpha-dependent production of reactive nitrogen intermediates mediates IFN-gamma plus IL-2-induced murine macrophage tumoricidal activity. J Immunol 1992; 149:3290–6.

[102] Zhou X-L, Fan W, Yang G, Yu M-X. The clinical significance of PR, ER, NF-*κ*B, and TNF-*α* in breast cancer. Dis Markers 2014; 2014:1–7.

[103] Katanov C, Lerrer S, Liubomirski Y, Leider-Trejo L, Meshel T, Bar J, Feniger-Barish R, Kamer I, Soria-Artzi G, Kahani H, Banerjee D, Ben-Baruch A. Regulation of the inflammatory profile of stromal cells in human breast cancer: Prominent roles for TNF-α and the NF-κB pathway. Stem Cell Res Ther 2015; 6:87.

[104] Balkwill F. TNF-alpha in promotion and progression of cancer. Cancer Metastasis Rev 2006; 25:409–16.

[105] Wu X, Wu MY, Jiang M, Zhi Q, Bian X, Xu MD, Gong FR, Hou J, Tao M, Shou LM, Duan W, Chen K, et al. TNF‑α sensitizes chemotherapy and radiotherapy against breast cancer cells. Cancer Cell Int 2017; 17:1–12.

[106] Miles DW, Happerfield LC, Naylor MS, Bobrow LG, Rubens RD, Balkwill FR. Expression of tumour necrosis factor (TNF alpha) and its receptors in benign and malignant breast tissue. Int J Cancer 1994; 56:777–782.

[107] Sheen-Chen SM, Chen WJ, Eng HL, Chou FF. Serum concentration of tumor necrosis factor in patients with breast cancer. Breast Cancer Res Treat 1997; 43:211–215.

[108] Cui LF, Guo XJ, Wei J, Liu FF, Fan Y, Lang RG, Gu F, Zhang XM, Fu L. Overexpression of TNF-α and TNFRII in invasive micropapillary carcinoma of the breast:

Clinicopathological correlations. Histopathology 2008; 53:381–388.

[109] Hagemann T, Wilson J, Kulbe H, Li NF, Leinster DA, Charles K, Klemm F, Pukrop T, Binder C, Balkwill FR. Macrophages induce invasiveness of epithelial cancer cells via NF-κB and JNK. J Immunol 2005; 175:1197–1205.

[110] Mosaffa F, Lage H, Afshari JT, Behravan J. Interleukin-1 beta and tumor necrosis factor-alpha increase ABCG2 expression in MCF-7 breast carcinoma cell line and its mitoxantrone-resistant derivative, MCF-7/MX. Inflamm Res 2009; 58:669–676.

[111] Tracey D, Klareskog L, Sasso EH, Salfeld JG, Tak PP. Tumor necrosis factor antagonist mechanisms of action: A comprehensive review. Pharmacol Ther 2008; 117:244–279.

[112] Madhusudan S, Foster M, Muthuramalingam SR, Braybrooke JP, Wilner S, Kaur K, Han C, Hoare S, Balkwill FR, Talbot DC, Ganesan TS, Harris AL. A phase II study of etanercept (Enbrel), a tumor necrosis factor alpha inhibitor in patients with metastatic breast cancer. Clin Cancer Res 2004; 10:6528–6534.

[113] Harrison ML, Obermueller E, Maisey NR, Hoare S, Edmonds K, Li NF, Chao D, Hall K, Lee C, Timotheadou E, Charles K, Ahern R, et al. Tumor necrosis factor α as a new target for renal cell carcinoma: Two sequential phase II trials of infliximab at standard and high dose. J Clin Oncol 2007; 25:4542–9.

[114] Yu M, Zhou X, Niu L, Lin G, Huang J, Zhou W, Gan H, Wang J. Targeting transmembrane TNF-α suppresses breast cancer growth. Cancer Res 2013; 73:4061–74.

[115] Fujimoto H, Sangai T, Ishii G, Ikehara A, Nagashima T, Miyazaki M, Ochiai A. Stromal MCP-1 in mammary tumors induces tumor-associated macrophage infiltration and contributes to tumor progression. Int J Cancer 2009; 125:1276–1284.

[116] Nesbit M, Schaider H, Miller TH, Herlyn M. Low-level monocyte chemoattractant protein-1 stimulation of monocytes leads to tumor formation in nontumorigenic melanoma cells. J Immunol 2001; 166:6483–90.

[117] Yin KB. The mesenchymal-like phenotype of the MDA-MB-231 cell line. Breast Cancer - Focusing Tumor Microenvironment, Stem cells and Metastasis. 2011:385–402.

[118] Saji H, Koike M, Yamori T, Saji S, Seiki M, Matsushima K, Toi M. Significant correlation of monocyte chemoattractant protein-1 expression with neovascularization and progression of breast carcinoma. Cancer 2001; 92:1085–91.

[119] Dutta P, Sarkissyan M, Paico K, Wu Y, Vadgama J V. MCP-1 is overexpressed in triple-negative breast cancers and drives cancer invasiveness and metastasis. Breast Cancer Res Treat 2018:1–10.

[120] Kuroda T, Kitadai Y, Tanaka S, Yang X, Mukaida N, Yoshihara M, Chayama K. Human cancer biology monocyte chemoattractant protein-1 transfection induces angiogenesis and tumorigenesis of gastric carcinoma in nude mice via macrophage recruitment. Clin

Cancer Res 2005; 11:7629–7637.

[121] Salcedo R, Ponce ML, Young HA, Wasserman K, Ward JM, Kleinman HK, Oppenheim JJ, Murphy WJ. Human endothelial cells express CCR2 and respond to MCP-1: direct role of MCP-1 in angiogenesis and tumor progression. Blood 2000; 96:34–40.

[122] Keith BD. Systematic review of the clinical effect of glucocorticoids on nonhematologic malignancy. BMC Cancer 2008; 8:84.

[123] Buxant F, Kindt N, Laurent G, Noel J, Saussez S. Antiproliferative effect of dexamethasone in the MCF-7 breast cancer cell line. Mol Med Rep 2015:4051–4054.

[124] King EM, Chivers JE, Rider CF, Minnich A, Giembycz MA, Newton R. Glucocorticoid repression of inflammatory gene expression shows differential responsiveness by transactivation- and transrepression-dependent mechanisms. PLoS One 2013; 8.

[125] Warrington TP, Bostwick JM. Psychiatric adverse effects of corticosteroids. Mayo Clin Proc 2006; 81:1361–1367.

[126] Waljee AK, Rogers MAM, Lin P, Singal AG, Stein JD, Marks RM, Ayanian JZ, Nallamothu BK. Short term use of oral corticosteroids and related harms among adults in the United States: Population based cohort study. Bmj 2017; 357:j1415.

[127] Lin KT, Wang LH. New dimension of glucocorticoids in cancer treatment. Steroids 2016; 111:84–88.

[128] Mondal SK, Jinka S, Pal K, Nelli S, Dutta SK, Wang E, Ahmad A, AlKharfy KM, Mukhopadhyay D, Banerjee R. Glucocorticoid receptor-targeted liposomal codelivery of lipophilic drug and anti-Hsp90 gene: Strategy to induce drug-sensitivity, EMT-reversal, and reduced malignancy in aggressive tumors. Mol Pharm 2016; 13:2507–2523.

[129] Lin CH, Chuang PY, You SL, Chiang CJ, Huang CS, Wang MY, Chao M, Lu YS, Cheng AL, Tang CH. Effect of glucocorticoid use on survival in patients with stage I–III breast cancer. Breast Cancer Res Treat 2018; 171:225–234.

[130] McKay LI, Cidlowski JA. Molecular control of immune/ inflammatory responses: interactions between nuclear factor-κB and steroid receptor-signaling pathways. Endocr Rev 1999; 20:435–459.

[131] Pratt WB. The role of heat shock proteins in regulating the function, folding and trafficking of the glucocorticoid receptor. J Biol Chem 1993; 268:21455–21458.

[132] Picard D, Yamamoto KR. Two signals mediate hormone-dependent nuclear localization of the glucocorticoid receptor. EMBO J 1987; 6:3333–40.

[133] Orti E, Mendel DB, Smith LI, Munck A. Agonist-dependent phosphorylation and nuclear dephosphorylation of glucocorticoid receptors in intact cells. J Biol Chem 1989; 264:9728–9731.

[134] Strömstedt PE, Poellinger L, Gustafsson JA, Carlstedt-Duke J. The glucocorticoid

receptor binds to a sequence overlapping the TATA box of the human osteocalcin promoter: A potential mechanism for negative regulation. Mol Cell Biol 1991; 11:3379–3383.

[135] Scheinman RI, Gualberto A, Jewell CM, Cidlowski JA, Baldwin AS. Characterization of mechanisms involved in transrepression of NF-kappaB by activated glucocorticoid receptors. Mol Cell Biol 1995; 15:943–53.

[136] Rosenfeld MG, Lunyak V V, Glass CK. Sensors and signals : A coactivator / corepressor / epigenetic code for integrating signal-dependent programs of transcriptional response. Genes Dev 2006; 20:1405–1428.

[137] Vilasco M, Communal L, Mourra N, Courtin A, Forgez P, Gompel A. Glucocorticoid receptor and breast cancer. Breast Cancer Res Treat 2011; 130:1–10.

[138] Conzen SD. Minireview: Nuclear receptors and breast cancer. Mol Endocrinol 2008; 22:2215–28.

[139] Alyusuf R, Wazir JF, Brahmi UP, Fakhro AR, Bakhiet M. The immunoexpression of glucocorticoid receptors in breast carcinomas, lactational change, and normal breast epithelium and its possible role in mammary carcinogenesis. Int J Breast Cancer 2017; 2017.

[140] Machuca C, Mendoza-Milla C, Córdova E, Mejía S, Covarrubias L, Ventura J, Zentella A. Dexamethasone protection from TNF-alpha-induced cell death in MCF-7 cells requires NF-kappaB and is independent from AKT. BMC Cell Biol 2006; 7:9.

[141] Pang D, Kocherginsky M, Krausz T, Kim S, Conzen SD. Dexamethasone decreases xenograft response to paclitaxel through inhibition of tumor cell apoptosis. Cancer Biol Ther 2006; 5:933–940.

[142] Pan D, Kocherginsky M, Conzen SD. Activation of the glucocorticoid receptor is associated with poor prognosis in estrogen receptor-negative breast cancer. Cancer Res 2011; 71:6360–6370.

[143] Chen Z, Lan X, Wu D, Sunkel B, Ye Z, Huang J, Liu Z, Clinton SK, Jin VX, Wang Q. Ligand-dependent genomic function of glucocorticoid receptor in triple-negative breast cancer. Nat Commun 2015; 6:8323.

[144] Schmidt S, Rainer J, Ploner C, Presul E, Riml S, Kofler R. Glucocorticoid-induced apoptosis and glucocorticoid resistance : molecular mechanisms and clinical relevance. Cell Death Differ 2004; 11:45–55.

[145] Honorat M, Mesnier A, Pietro A Di, Lin V, Cohen P, Dumontet C, Payen L. Dexamethasone down-regulates ABCG2 expression levels in breast cancer cells. Biochem Biophys Res Commun 2008; 375:308–314.

[146] Ferrand N, Stragier E, Redeuilh G, Sabbah M. Glucocorticoids induce CCN5/WISP-2

expression and attenuate invasion in oestrogen receptor-negative human breast cancer cells. Biochem J 2012; 447:71–79.

[147] Fietz ER, Keenan CR, López-Campos G, Tu Y, Johnstone CN, Harris T, Stewart AG. Glucocorticoid resistance of migration and gene expression in a daughter MDA-MB-231 breast tumour cell line selected for high metastatic potential. Sci Rep 2017; 7:1–13.

[148] Mitre-Aguilar IB, Cabrera-Quintero AJ, Zentella-Dehesa A. Genomic and non-genomic effects of glucocorticoids: Implications for breast cancer. Int J Clin Exp Pathol 2015; 8:1–10.

[149] Nauck M, Roth M, Tamm M, Eickelberg O, Wieland H, Stulz P, Perruchoud AP. Induction of vascular endothelial growth factor by platelet-activating factor and platelet-derived growth factor is downregulated by corticosteroids. Am J Respir Cell Mol Biol 1997; 16:398–406.

[150] Moutsatsou P, Papavassiliou AG. The glucocorticoid receptor signalling in breast cancer. J Cell Mol Med 2008; 12:145–63.

[151] Catteau X, Simon P, Buxant F, Noël JC. Expression of the glucocorticoid receptor in breast cancer‐associated fibroblasts. Mol Clin Biol 2016; 5:372–376.

[152] Nystedt S, Emilsson K, Wahlestedt C, Sundelin J. Molecular cloning of a potential proteinase activated receptor. Proc Natl Acad Sci 1994; 91:9208–9212.

[153] Ishihara H, Connolly A, Zeng D, Kahn M, Zheng YW, Timmons C, Tram T, Coughlin S. Protease-activated receptor 3 is a second thrombin receptor in humans. Nature 1997; 386:502-06.

[154] Xu WF, Andersen H, Whitmore TE, Presnell SR, Yee DP, Ching A, Gilbert T, Davie EW, Foster DC. Cloning and characterization of human protease-activated receptor 4. Proc Natl Acad Sci USA 1998; 95:6642–6646.

[155] Vu T-KH, Hung DT, Wheaton VI, Coughlin SR. Molecular cloning of a functional thrombin receptor reveals a novel proteolytic mechanism of receptor activation. Cell 1991; 64:1057–1068.

[156] Rothmeier AS, Ruf W. Protease-activated receptor 2 signaling in inflammation. Semin Immunopathol 2012; 34:133–149.

[157] DeFea KA, Zalevsky J, Thoma MS, Déry O, Mullins RD, Bunnett NW. B-Arrestin-dependent endocytosis of proteinase-activated receptor 2 is required for intracellular targeting of activated ERK1/2. J Cell Biol 2000; 148:1267–1281.

[158] Zoudilova M, Min J, Richards HL, Carter D, Huang T, DeFea KA. B-Arrestins scaffold cofilin with chronophin to direct localized actin filament severing and membrane protrusions downstream of protease-activated receptor-2. J Biol Chem 2010; 285:14318–14329.

[159] Yau M, Lim J, Liu L, Fairlie DP. Protease activated receptor 2 (PAR2) modulators: A patent review (2010 – 2015). Expert Opin Ther Pat 2016; 26:471–483.

[160] Kahn ML, Zheng YW, Bigornia V, Zeng D, Moff S, Farese Jr. R V, Tam C, Coughlin SR. A duel thrombin receptor system for platelet activation. Nature 1998; 394:690–694.

[161] Bucci M, Roviezzo F, Cirino G. Protease-activated receptor-2 (PAR2) in cardiovascular system. Vascul Pharmacol 2005; 43:247–253.

[162] Johansson U, Lawson C, Dabare M, Syndercombe-Court D, Newland AC, Howells GL, Macey MG. Human peripheral blood monocytes express protease receptor-2 and respond to receptor activation by production of IL-6, IL-8, and IL-1beta. J Leukoc Biol 2005; 78:967–975.

[163] Julovi SM, Xue M, Dervish S, Sambrook PN, March L, Jackson CJ. Protease activated receptor-2 mediates activated protein induced cutaneous wound healing via inhibition of p38. Am J Pathol 2011; 179:2233–2242.

[164] Su S, Li Y, Sheng Y, Su Y, Padia R, Pan Z, Dong Z, Huang S. Proteinase-activated receptor 2 expression in breast cancer and its role in breast cancer cell migration. Oncogene 2009; 28:3047–3057.

[165] Elste AP, Petersen I. Expression of proteinase-activated receptor 1-4 (PAR 1-4) in human cancer. J Mol Histol 2010; 41:89–99.

[166] Hjortoe GM, Petersen LC, Albrektsen T, Sorensen BB, Norby PL, Mandal SK, Pendurthi UR, Rao LVM. Tissue factor-factor VIIa–specific up-regulation of IL-8 expression in MDA-MB-231 cells is mediated by PAR-2 and results in increased cell migration. Blood 2004; 103:3029–37.

[167] Rydén L, Grabau D, Schaffner F, Jönsson P-E, Ruf W, Beliting M. Evidence for tissue factor phosphorylation and its correlation with protease activated receptor expression and the prognosis of primary breast cancer. Int J Cancer 2010; 126:2330–2340.

[168] Liu Y, Mueller BM. Protease-activated receptor-2 regulates vascular endothelial growth factor expression in MDA-MB-231 cells via MAPK pathways. Biochem Biophys Res Commun 2006; 344:1263–1270.

[169] Stahn S, Thelen L, Albrecht I, Bitzer J, Henkel T, Teusch NE. Teleocidin A2 inhibits human proteinase-activated receptor 2 signaling in tumor cells. Pharmacol Res Perspect 2016; 4:1–18.

[170] Chackalamannil S, Wang Y, Greenlee WJ, Hu Z, Xia Y, Ahn H, Boykow G, Hsieh Y, Palamanda J, Agans-fantuzzi J, Kurowski S, Graziano M, et al. Discovery of a novel, orally active himbacine-based thrombin receptor antagonist (SCH 530348) with potent antiplatelet activity. J Med Chem 2015; 51:3061.

[171] Boitano S, Hoffman J, Flynn AN, Asiedu MN, Tillu D V., Zhang Z, Sherwood CL, Rivas

CM, Defea KA, Vagner J, Price TJ. The novel PAR2 ligand C391 blocks multiple PAR2 signalling pathways *in vitro* and *in vivo*. Br J Pharmacol 2015; 172:4535–4545.

[172] Nijveldt R. Flavonoids : A review of probable mechanism of action and potential applications. Am J Clin Nutr 2001; 74:418–425.

[173] Zang R, Li D, Tang I-C, Wang J, Yang S-T. Cell-based assays in high-throughput screening for drug discovery. Int J Biotechnol Wellness Ind 2012; 1:31–51.

[174] Newman D., Cragg G., Snader K. Natural products as sources of new drugs over the period 1981 - 2002. J Nat Prod 2003; 66:1022–1037.

[175] Cragg GM, Newman DJ. Natural products: A continuing source of novel drug leads. Biochim Biophys Acta 2013; 1830:3670–3695.

[176] Proksch P, Edrada RA, Ebel R. Drugs from the seas - Current status and microbiological implications. Appl Microbiol Biotechnol 2002; 59:125–134.

[177] Wani MC, Kepler JA, Thompson JB, Wall ME, Levine SG. The isolation and structure of taxol, a novel antileukemic and antitumor agent from *Taxus breoifolia*. J Am Chem Soc 1970; 93:2325–2327.

[178] Mayer AMS, Glaser KB, Cuevas C, Jacobs RS, Kem W, Little RD, Mcintosh JM, Newman DJ, Potts BC, Shuster DE. The odyssey of marine pharmaceuticals : A current pipeline perspective. Trends Pharmacol Sci 2010; 31:255–265.

[179] Hirata Y, Uemura D. *Halichondrins* - antitumor polyether macrolides from a marine sponge. Pure Appl Chem 1986; 58:701–710.

[180] Calcabrini C, Catanzaro E, Bishayee A, Turrini E, Fimognari C. Marine sponge natural products with anticancer potential: An updated review. Marine Drugs 2017. 15(10): pii: E310.

[181] Stonik V A. Marine natural products : A way to new drugs. Acta Naturae 2009; 1:15–25.

[182] Berrué F, McCulloch MWB, Kerr RG. Marine diterpene glycosides. Bioorganic Med Chem 2011; 19:6702–6719.

[183] Look S a., Fenical W, Matsumoto GK, Clardy J. The pseudopterosins: A new class of antiinflammatory and analgesic diterpene pentosides from the marine sea whip *Pseudopterogorgia elisabethae* (*Octocorallia*). J Org Chem 1986; 51:5140–5145.

[184] Vassilios R, Zhongde W, Fenical W, Strobel SA, Van Duyne GD, Clardy J, Roussis V, Wu Z, Fenical W, Strobel SA, Van Duyne GD, Clardy J, et al. New antiinflammatory pseudopterosins from the marine octocoral *Pseudopterogorgia elisabethae*. J Org Chem 1990; 55:4916–4922.

[185] Rodríguez II, Shi YP, García OJ, Rodríguez AD, Mayer AMS, Sánchez J a., Ortega-Barria E, González J. New pseudopterosin and seco-pseudopterosin diterpene glycosides from two Colombian isolates of *Pseudopterogorgia elisabethae* and their

diverse biological activities. J Nat Prod 2004; 67:1672–1680.

[186] Look SA, Fenical W, Jacobs RS, Clardy J. The pseudopterosins : Anti-inflammatory and analgesic natural products from the sea whip *Pseudopterogorgia elisabethae*. Proc Natl Acad Sci 1986; 83:6238–6240.

[187] Mayer A M, Jacobson PB, Fenical W, Jacobs RS, Glaser KB. Pharmacological characterization of the pseudopterosins: Novel anti-inflammatory natural products isolated from the Caribbean soft coral, *Pseudopterogorgia elisabethae*. Elsevier Sci 1998; 62:PL401-L407.

[188] Moya CE, Jacobs RS. Pseudopterosin A inhibits phagocytosis and alters intracellular calcium turnover in a pertussis toxin sensitive site in *Tetrahymena thermophila*. Comp Biochem Physiol - C Toxicol Pharmacol 2006; 143:436–443.

[189] Caplan SL, Zheng B, Dawson-Scully K, White CA, West LM. Pseudopterosin A: Protection of synaptic function and potential as a neuromodulatory agent. Mar Drugs 2016; 14:55.

[190] Sperlich J, Kerr R, Teusch N. The marine natural product pseudopterosin blocks cytokine release of triple-negative breast cancer and monocytic leukemia cells by inhibiting NF-κB signaling. Mar Drugs 2017; 15:E262.

[191] Sperlich J, Teusch N. Pseudopterosin inhibits proliferation and 3D invasion in triple-negative breast cancer by agonizing glucocorticoid receptor alpha. Molecules 2018; 23:E1992.

[192] Zabala AO, Xu W, Chooi YH, Tang Y. Characterization of a silent azaphilone gene cluster from *Aspergillus niger* ATCC 1015 reveals a hydroxylation-mediated pyran-ring formation. Chem Biol 2012; 19:1049–1059.

[193] Yasukawa K, Takahashi M, Natori S, Kawai K, Yamazaki M, Takeuchi M, Takido M. Azaphilones inhibit tumor promotion by 12-*O*-tetra-decanoylphorbol-13-acetate in two-stage carcinogenesis in mice. Oncology 1994; 51:108–112.

[194] Mapari SAS, Thrane U, Meyer AS. Fungal polyketide azaphilone pigments as future natural food colorants? Trends Biotechnol 2010; 28:300–307.

[195] Stadler M, Anke H, Dekermendjian K, Reiss R, Witt R. Novel bioactive azaphilones from fruit bodies and mycelial cultures of the ascomycete *Bulgaria inquinans*. Nat Prod Lett 1995; 7:7–14.

[196] Gao J, Yang S, Qin J. Azaphilonoids: Chemistry and biology. Chem Rev 2013; 113:4755–4811.

[197] Chen W, Chen R, Liu Q, He Y, He K, Ding X, Kang L, Guo X, Xie N, Zhou Y, Lu Y, Cox RJ, et al. Orange, red, yellow: Biosynthesis of azaphilone pigments in *Monascus* fungi. Chem Sci 2017; 8:4917–4925.

[198] Osmanova N, Schultze W, Ayoub N. Azaphilones: A class of fungal metabolites with diverse biological activities. Phytochem Rev 2011; 10:315–342.

[199] Tabata Y, Ikegami S, Yaguchi T, Sasaki T, Hoshiko S, Sakuma S, Shin-Ya K, Seto H. Diazaphilonic acid, a new azaphilone with telomerase inhibitory activity. J Antibiot (Tokyo) 1999; 52:412–414.

[200] Akihisa T, Tokuda H, Yasukawa K, Ukiya M, Kiyota A, Sakamoto N, Suzuki T, Tanabe N, Nishino H. Azaphilones, furanoisophthalides, and amino acids from the extracts of *Monascus pilosus*-fermented rice (red-mold rice) and their chemopreventive effects. J Agric Food Chem 2005; 53:562–565.

[201] Quang DN, Hashimoto T, Stadler M, Radulovic N, Asakawa Y. Antimicrobial azaphilones from the fungus *Hypoxylon multiforme*. Planta Med 2005; 71:1058–1062.

[202] Gao SS, Li XM, Zhang Y, Li CS, Cui CM, Wang BG. Comazaphilones A-F, azaphilone derivatives from the marine sediment-derived fungus *Penicillium commune* QSD-17. J Nat Prod 2011; 74:256–261.

[203] Chidananda C, Sattur AP. Sclerotiorin, a novel inhibitor of lipoxygenase from *Penicillium frequentans*. J Agric Food Chem 2007; 55:2879–2883.

[204] Quang DN, Harinantenaina L, Nishizawa T, Hashimoto T, Kohchi C, Soma G, Asakawa Y. Inhibition of nitric oxide production in RAW 264.7 cells by azaphilones from *Xylariaceous* fungi. Biol Pharm Bull 2006; 29:34–37.

[205] Amos S, Redpath GT, Polar G, McPheson R, Schiff D, Hussaini IM. Farnesylthiosalicylic acid induces caspase activation and apoptosis in glioblastoma cells. Cell Death Differ 2006; 13:642–651.

[206] Khurana N, Sharma SB, Jafri AA, Sharma AM. Azaphilones: Their role in various biological activities. Asian J Biomed Pharm Sci 2017; 7:34–43.

[207] Kaur K, Wu X, Fields JK, Johnson DK, Lan L, Pratt M, Somoza AD, Wang CCC, Karanicolas J, Oakley BR, Xu L, De Guzman RN. The fungal natural product azaphilone-9 binds to HuR and inhibits HuR-RNA interaction *in vitro*. PLoS One 2017; 12:1–18.

[208] Li JJ, Shang XY, Li LL, Liu MT, Zheng JQ, Jin ZL. New cytotoxic azaphilones from *Monascus purpureus*-fermented rice (red yeast rice). Molecules 2010; 15:1958–1966.

[209] Yamada T, Muroga Y, Tanaka R. New azaphilones, seco-chaetomugilins A and D, produced by a marine-fish-derived *Chaetomium globosum*. Mar Drugs 2009; 7:249–257.

[210] Muroga Y, Yamada T, Numata A, Tanaka R. Chaetomugilins I-O, new potent cytotoxic metabolites from a marine-fish-derived *Chaetomium* species. Stereochemistry and biological activities. Tetrahedron 2009; 65:7580–7586.

[211] Su N-W, Lin Y-L, Lee M-H, Ho C-Y. Ankaflavin from *Monascus*-fermented red rice exhibits selective cytotoxic effect and induces cell death on HepG2 cells. J Agric Food

Chem 2005; 53:1949–1954.

[212] Son S, Ko SK, Kim JW, Lee JK, Jang M, Ryoo IJ, Hwang GJ, Kwon MC, Shin KS, Futamura Y, Hong YS, Oh H, et al. Structures and biological activities of azaphilones produced by *Penicillium sp*. KCB11A109 from a ginseng field. Phytochemistry 2016; 122:154–164.

[213] Yu H, Sperlich J, Mándi A, Kurtán T, Dai H, Teusch N, Guo Z-Y, Zou K, Liu Z, Proksch P. Azaphilone derivatives from the fungus *Coniella fragariae* inhibit NF-κB activation and reduce tumor cell migration´. J Nat Prod 2018; 81:2493–2500.

[214] Takashima M, Sakai H. A new toxic substance, teleocidin, produced by *Streptomyces*. Bull Agric Chem Soc Japan 1960; 24:647–655.

[215] Fujiki H, Sugimura T. New classes of tumor promoters: teleocidin, aplysiatoxin and palytoxin. Natl Cancer Cent Res Inst 1987; 49.

[216] Irie K, Kajiyama S, Funaki A, Koshimizu K, Hayashi H, Arai M. Biosynthesis of (-)-indolactam V, the basic ring structure of tumor promoters teleocidins. Tetrahedron Lett 1990; 31:101–104.

[217] Fujiki H, Mori M, Nakayasu M, Terada M, Sugimura T, Moore RE. Indole alkaloids: dihydroteleocidin B, teleocidin, and lyngbyatoxin A as members of a new class of tumor promoters. Proc Natl Acad Sci U S A 1981; 78:3872–3876.

[218] Mascal M, Moody CJ, Slawin AM, Williams DJ. Synthesis of (-)-Indolactam V. J Chem Soc Perkin Trans 1 1992; 9:823–830.

[219] Cardellina JH, Marner FJ, Moore RE. Seaweed dermatitis: Structure of lyngbyatoxin A. Science (80-) 1979; 204:193–195.

[220] Osborne NJT, Webb PM, Shaw GR. The toxins of *Lyngbya majuscula* and their human and ecological health effects. Environ Int 2001; 27:381–392.

[221] Horiuchi T, Fujiki H, Suganuma M, Hakii H, Nakayasu M, Hitotsuyanagi Y, Aimi N, Sakai Sh, Endo Y, Shudo K, Sugimura T. Studies on olivoretins indicate a requirement for a free hydroxyl group for teleocidin B activity. Gann 1984; 75:837–840.

[222] Irie K, Hagiwara N, Funaki A, Hayashi H, Arai M, Koshimizu K. Isolation of blastmycetin D, a possible precursor of teleocidins, from *Streptoverticillium blastmyceticum.* Agric Biol Chem 1987; 51:1733–1735.

[223] Mascal M, Moody C. Synthesis of (-)-Indolactam V. J Chem Soc Chem Commun 1988; 8:589–590.

[224] Fujiki H, Suganuma M, Ninomiya M, Yoshizawa S, Yamashita K, Takayama S, Hitotsuyanagi Y, Sakai S ichiro, Shudo K, Sugimura T. Similar, potent tumor-promoting activity of all isomers of teleocidins A and B in a two-stage carcinogenesis experiment on the skin of CD-1 mice. Cancer Res 1988; 48:4211–4214.

[225] Urtreger AJ, Kazanietz MG, Bal De Kier Joffé ED. Contribution of individual PKC isoforms to breast cancer progression. IUBMB Life 2012; 64:18–26.

[226] Imamoto A, Wang XJ, Fujiki H, Walker SE, Beltrán LM, Digiovanni J. Comparison of 12-*O*-tetradecanoylphorbol-13-acetate and teleocidin for induction of epidermal hyperplasia, activation of epidermal PKC isozymes and skin tumor promotion in SENCAR and c57bl/6 mice. Carcinogenesis 1993; 14:719–724.

[227] Meseguer B, Alonso-Díaz D, Griebenow N, Herget T, Waldmann H. Solid-phase synthesis and biological evaluation of a teleocidin library - Discovery of a selective PKCδ down regulator. Chemistry 2000; 6:3943–57.

[228] DeVita VT, Chu E. AACR Centennial Series: A history of cancer chemotherapy. Cancer Res; 2008,68:8643–8654.

[229] Arcamone F, Cassinelli G, Faktini G, Grein A, Orezzi P, Pol C, Spalla C. Adriamycin, 14-hydroxydaunomycin, a new antitumor antibiotic from *S. peucetius* var. *caesius*. Biotechnol Bioeng 1969; 11:1101–1110.

[230] Yu M, Zhou X, Niu L, Lin G, Huang J, Zhou W, Gan H, Wang J, Jiang X, Yin B, Li Z. Targeting transmembrane TNF-α suppresses breast cancer growth. Cancer Res 2013; 73:4061–4074.

[231] Arora R, Yates C, Gary BD, McClellan S, Tan M, Xi Y, Reed E, Piazza GA, Owen LB, Dean-Colomb W. Panepoxydone targets NF-κB and FOXM1 to inhibit proliferation, induce apoptosis and reverse epithelial to mesenchymal transition in breast cancer. PLoS One 2014; 9.

[232] Matsumoto G, Namekawa JI, Muta M, Nakamura T, Bando H, Tohyama K, Toi M, Umezawa K. Targeting of nuclear factor κB pathways by dehydroxymethylepoxyquinomicin, a novel inhibitor of breast carcinomas: Antitumor and antiangiogenic potential *in vivo*. Clin Cancer Res 2005; 11:1287–1293.

[233] Sousa S, Brion R, Lintunen M, Kronqvist P, Sandholm J, Mönkkönen J, Lauttia S, Tynninen O, Joensuu H, Heymann D, Määttä JA. Human breast cancer cells educate macrophages toward the M2 activation status. Breast Cancer Res 2015; 17:1–14.

[234] Wyckoff J, Wang W, Lin EY, Wang Y, Pixley F, Stanley ER, Graf T, Pollard JW, Segall J, Condeelis J. A paracrine loop between tumor cells and macrophages is required for tumor cell migration in mammary tumors. Cancer Res 2004; 64:7022–7029.

[235] Guo J, Liu C, Zhou X, Xu X, Deng L. Conditioned medium from malignant breast cancer cells induces an EMT-like phenotype and an altered n-glycan profile in normal epithelial MCF10A cells. Int J Mol Sci 2017; 18:E1528.

[236] Hwang H, Shin C, Park J, Kang E, Choi B. Human breast cancer-derived soluble factors facilitate CCL19-induced chemotaxis of human dendritic cells. Nat Publ Gr 2016; 2016:1–

12.

[237] Mohamed MM. Monocytes conditioned media stimulate fibronectin expression and spreading of inflammatory breast cancer cells in three-dimensional culture: A mechanism mediated by IL-8 signaling pathway. Cell Commun Signal 2012; 10:3.

[238] Xiong M, Guo Z, Han B, Chen M. Combating multidrug resistance in bacterial infection by targeting functional proteome with natural products. Nat Prod Res 2015; 29:1624–1629.

[239] Karin M, Greten FR. NF-kappaB: Linking inflammation and immunity to cancer development and progression. Nat Rev Immunol 2005; 5:749–59.

[240] Huang Y-C, Pan MIN, Liu N, Xiao J-G, Chen H-Q. Effects of nuclear factor-κB and ERK signaling transduction pathway inhibitors on human melanoma cell proliferation *in vitro*. Oncol Lett 2015; 10:3233–3237.

[241] Bartholomeusz C, Gonzales-Angulo A, Liu P, Hayashi N, Lluch A, Ferrer-Lozano J, Hortobagyi G. High ERK protein expression levels correlate with shorter survival in triple negative breast cancer patients. Onkol 2012; 17:1072–1081.

[242] Rakha EA, El-Sayed ME, Green AR, Lee AHS, Robertson JF, Ellis IO. Prognostic markers in triple-negative breast cancer. Cancer 2007; 109:25–32.

[243] De Bosscher K, Vanden Berghe W, Beck IM, Van Molle W, Hennuyer N, Hapgood J, Libert C, Staels B, Louw A, Haegeman G. A fully dissociated compound of plant origin for inflammatory gene repression. Proc Natl Acad Sci U S A 2005; 102:15827–15832.

[244] Wu J, Liu T, Rios Z, Mei Q, Lin X, Cao S. Heat shock proteins and cancer. Trends Pharmacol Sci 2017; 38:226–256.

[245] Nagaraju GP, Long T, Park W, Landry JC, Taliaferro-smith L, Farris AB, Diaz R, El-rayes BF. Heat shock protein 90 promotes epithelial to mesenchymal transition, invasion, and migration in colorectal cancer. Mol Carcinog 2015; 54:1147–58.

[246] Li X, Srinivasan SR, Connarn J, Ahmad A, Young ZT, Kabza AM, Zuiderweg ERP, Sun D, Gestwicki JE. Analogues of the allosteric heat shock protein 70 (Hsp70) inhibitor, MKT-077, as anti-cancer agents. ACS Med Chem Lett 2013; 4:1042–1047.

[247] Sundahl N, Bridelance J, Libert C, Bosscher K De, Beck IM. Selective glucocorticoid receptor modulation: New directions with non-steroidal scaffolds. Pharmacol & Ther 2015; 152:28–41.

[248] Heras B De, Hortelano S, de las Heras B, Hortelano S. Molecular basis of the anti-inflammatory effects of terpenoids. Inflamm Allergy Drug Targets 2009; 8:28–39.

[249] Newton R, Holden NS. Separating transrepression and transactivation: A distressing divorce for the glucocorticoid receptor? Mol Pharmacol 2007; 72:799–809.

[250] Hübner S, Dejager L, Libert C, Tuckermann JP. The glucocorticoid receptor in inflammatory processes: Transrepression is not enough. Biol Chem 2015; 396:1223–31.

[251] Schäcke H, Schottelius A, Döcke W, Strehlke P, Jaroch S, Schmees N, Rehwinkel H, Hennekes H, Asadullah K. Dissociation of transactivation from transrepression by a selective glucocorticoid receptor agonist leads to separation of therapeutic effect from side effects. PNAS 2004; 101:227–232.

[252] Petta I, Bougarne N, Vandewalle J, Dejager L, Vandevyver S, Ballegeer M, Desmet S, Thommis J, De Cauwer L, Lievens S, Libert C, Tavernier J, et al. Glucocorticoid receptor-mediated transactivation is hampered by Striatin-3, a novel interaction partner of the receptor. Sci Rep 2017; 7:1–15.

[253] Chrousos GP, Kino T. Intracellular glucocorticoid signaling: A formerly simple system turns stochastic. Sci Signal 2005; 2005:pe48-pe48.

[254] Necela BM, Cidlowski JA. A single amino acid change in the first zinc finger of the DNA binding domain of the glucocorticoid receptor regulates differential promoter selectivity. J Biol Chem 2004; 279:39279–39288.

[255] Newman DJ, Cragg GM. Marine natural products and related compounds in clinical and advanced preclinical trials. J Nat Prod 2004; 67:1216–1238.

[256] Correa H, Valenzuela AL, Ospina LF, Duque C. Anti-inflammatory effects of the gorgonian *Pseudopterogorgia elisabethae* collected at the Islands of Providencia and San Andrés (SW Caribbean). J Inflamm (Lond) 2009; 6:5.

[257] Ata A, Kerr RG, Moya CE, Jacobs RS. Identification of anti-inflammatory diterpenes from the marine gorgonian *Pseudopterogorgia elisabethae*. Tetrahedron 2003; 59:4215–4222.

[258] Ata A, Win HY, Holt D, Holloway P, Segstro EP, Jayatilake GS. New antibacterial diterpenes from *Pseudopterogorgia elisabethae*. Helv Chim Acta 2004; 87:1090–1098.

[259] Zhong W, Moya C, Jacobs RS, Little RD. Synthesis and an evaluation of the bioactivity of the C-glycoside of pseudopterosin a methyl ether. J Org Chem 2008; 73:7011–7016.

[260] Rivas MA, Carnevale RP, Proietti CJ, Rosemblit C, Beguelin W, Salatino M, Charreau EH, Frahm I, Sapia S, Brouckaert P, Elizalde P V., Schillaci R. TNFα acting on TNFR1 promotes breast cancer growth via p42/p44 MAPK, JNK, Akt and NF-κB-dependent pathways. Exp Cell Res 2008; 314:509–529.

[261] Rubio MF, Werbajh S, Cafferata EGA, Quaglino A, Coló GP, Nojek IM, Kordon EC, Nahmod VE, Costas MA. TNF-α enhances estrogen-induced cell proliferation of estrogen-dependent breast tumor cells through a complex containing nuclear factor-kappa B. Oncogene 2006; 25:1367–1377.

[262] Fleming A. On the antibacterial action of cultures of a *Penecillium*, with special reference to their use in the isolation of *B. influenzae*. Br J Exp Pathol 1929; 10:226–236.

[263] Cheng MJ, Wu M Der, Yuan GF, Su YS, Yanai H. Secondary metabolites produced by the fungus *Monascus pilosus* and their anti-inflammatory activity. Phytochem Lett 2012;

5:567–571.

[264] Cheng CF, Pan TM. Ankaflavin and monascin induce apoptosis in activated hepatic stellate cells through suppression of the Akt/NF-κB/p38 signaling pathway. J Agric Food Chem 2016; 64:9326–9334.

[265] Lin CH, Lin TH, Pan TM. Alleviation of metabolic syndrome by monascin and ankaflavin: The perspective of *Monascus* functional foods. Food Funct 2017; 8:2102–2109.

[266] Musso L, Dallavalle S, Merlini L, Bava A, Nasini G, Penco S, Giannini G, Giommarelli C, De Cesare A, Zuco V, Vesci L, Pisano C, et al. Natural and semisynthetic azaphilones as a new scaffold for Hsp90 inhibitors. Bioorganic Med Chem 2010; 18:6031–6043.

[267] Zheng Y, Xin Y, Shi X, Guo Y. Cytotoxicity of monascus pigments and their derivatives to human cancer cells. J Agric Food Chem 2010; 58:9523–9528.

[268] Shao CL, Wang CY, Wei MY, Gu YC, She ZG, Qian PY, Lin YC. Aspergilones A and B, two benzylazaphilones with an unprecedented carbon skeleton from the gorgonian-derived fungus *Aspergillus* sp. Bioorganic Med Chem Lett 2011; 21:690–693.

[269] Panthama N, Kanokmedhakul S, Kanokmedhakul K, Soytong K. Cytotoxic and antimalarial azaphilones from *Chaetomium longirostre*. J Nat Prod 2011; 74:2395–2399.

[270] Hsu YW, Hsu LC, Liang YH, Kuo YH, Pan TM. New bioactive orange pigments with yellow fluorescence from *Monascus*-fermented *dioscorea*. J Agric Food Chem 2011; 59:4512–4518.

[271] Zou X-W, Sun B-D, Chen X-L, Liu X-Z, Che Y-S. Helotialins A–C, anti-HIV metabolites from a helotialean ascomycete. Chin J Nat Med 2009; 7:140–144.

[272] Ge HM, Zhang WY, Ding G, Saparpakorn P, Song YC, Hannongbua S, Tan RX. Chaetoglobins A and B, two unusual alkaloids from endophytic *Chaetomium globosum* culture. Chem Commun 2008; 0:5978–5980.

[273] Chen FE, Huang DB, Chen YQ, Ghosh G. Crystal structure of p50/p65 heterodimer of transcription factor NF-kappaB bound to DNA. Nature 1998; 391:410–413.

[274] Demain AL, Vaishnav P. Natural products for cancer chemotherapy. Microb Biotechnol 2011; 4:687–699.

[275] Fujiki H, Sugimura T, Moore RE. New classes of environmental tumor promoters: Indole alkaloids and polyacetates. Environ Health Perspect 1983; Vol. 50:85–90.

[276] Ramachandran R, Noorbakhsh F, DeFea K, Hollenberg MD. Targeting proteinase-activated receptors: therapeutic potential and challenges. Nat Rev Drug Discov 2012; 11:69–86.

[277] Anders CK, Carey L a. Biology, metastatic patterns and treatment of patients with triple-negtive breast cancer. Clin Breast Cancer 2010; 9:S73–S81.

[278] Cheng RKY, Fiez-Vandal C, Schlenker O, Edman K, Aggeler B, Brown DG, Brown GA,

Cooke RM, Dumelin CE, Doré AS, Geschwindner S, Grebner C, et al. Structural insight into allosteric modulation of protease-activated receptor 2. Nature 2017; 545:112–115.

[279] Yau M, Liu L, Fairlie DP. Toward drugs for protease-activated receptor 2 (PAR2). J Med Chem 2013; 56:7477–7497.

Abbreviations

A

ABC..... *ATP-binding casette*

B

BRCA1 ..... *BReast CAncer 1*

C

CAFs .....*Cancer associated fibroblasts*
CM .....*conditioned medium*

D

DAPI..... *4',6-Diamidin-2-phenylindol*
Dex..... *dexamethasone*
DMSO ..... *dimethyl sulfoxide*
DNA .....*desoxyribonucleic acid*

E

ECM .....*extracellular matrix*
EGF..... *epidermal growth factor*
EMT ..... *epithelial-to-mesenchymal transition*
ER .....*estrogen receptor*
ER^- .....*estrogen-receptor negative*
ER^+..... *estrogen-receptor positiv*
ERK..... *Extracellular signal–regulated kinase*

F

FCS.....*fetal calf serum*
FITC ..... *fluorescein isothiocyanate*

G

GAPDH .....glyceraldehyde 3-phosphate dehydrogenase
GFP..... *green fluorescent protein*
GPCR..... *G protein-coupled receptor*
G-protein .....*guanine nucleotide-binding protein*
GREs ..... *glucocorticoid response elements*
GRα .....*glucocorticoid receptor alpha*

H

HER2 *human epidermal growth factor receptor-2*
HRP .....*horseradish peroxidase*
HSP .....*heat shock protein*

I

IC_{50} .....*half maximal inhibitory concentration*
IKK.. *inhibitor of κB kinase*, *inhibitor of κB kinase*
IL-6 .....*Interleukin 6*
IL-8 .....*Interleukin 8*
IκB..... *inhibitor of κB*

L

LPS .....*lipopolysaccharide*

M

M1..... *classical-activated macrophages*
M2..... *alternatively-activated macrophages*
M-CM ..... *MDA-MB-231 conditioned medium*
MCP-1 .....*monocyte chemoattractant protein 1*
Mregs..... regulatory macrophages
mRNA ..... *messenger ribonucleic acid*
MyD88 . *myeloid differentiation primary response gene 88*

N

nc siRNA.....*non-coding silencing RNA*
NF-κB *nuclear factor kappa-light-chain-enhancer of activated B-cells*
nGREs .....*negative glucocorticoid response elements*
NLS.....*nuclear localization sequence*
NOS..... *nitrite oxide synthase*
NSAID..... *non-steroidal anti-inflammatory drug*

P

PAMPs. *pathogen-associated molecular patterns*
PAR2 ..... *Proteinase-activated receptor 2*
PBMC ..... *peripheral blood mononuclear cells*
PCR ..... *polymerase chain reaction*
PKC ..... *protein kinase C*

PsA .....*pseudopterosin A*
PsA-D..... *pseudopterosins A, B, C and D*
PsE ..... *Pseudopterosin E*

R

Rac1 *Ras-related C3 botulinum toxin substrate 1*
RIP1 .....*receptor-interacting protein 1*

S

SAR.....*structure-activity-relationship*
SD ..... *standard deviation*
SEM ..... *standard error of the mean*
SES.....*2-trimethylsilyl-ethansulfonyl*
siRNA..... *silencing RNA*

T

TAM .....tumor associated macrophages
TCCF .....*cytoplasmic total corrected cell fluorescence*
THP-CM..... *THP-1 conditioned medium*
TIR.....*Toll/IL-1 receptor*
TLR.....*Toll-like receptor*
TME .....*tumor microenvironment*, *tumor microenvironment*
TNBC.....*triple negative breast cancer*
TNFR1 ..... *tumor necrosis factor α receptor 1*
TNFα.....*tumor necrosis factor alpha*
TRADD .. *TNF receptor-associated protein with a death domain*

U

ULA.....*ultra-low-attachment*

V

VEGF ..... *vascular endothelial growth factor*

Lebenslauf

Ausbildung

04/2015- 11/2018	Heinrich-Heine-Universität Düsseldorf Promotion: Pharmazie, *summa cum laude* Kooperative Promotion am Institut für Pharmazeutische Biologie und Biotechnologie mit dem Institut für Bio-Pharmazeutische Chemie & Molekulare Pharmakologie der Technischen Hochschule Köln „*Pharmacological characterization of pseudopterosin, azaphilone and teleocidin as novel drug candidates for the treatment of triple negative breast cancer* ".
10/2011- 04/2014	Karlsruher Institut für Technologie Master of Science, Biologie Masterarbeit: „*Funktionelle Analyse konservierter Module der TCF Transkriptionsfaktoren*"
10/2008- 09/2011	Karlsruher Institut für Technologie Bachelor of Science: Biologie Bachelorarbeit: „*Funktionelle Analyse der Tumorproteine AGR2 und AGR3 in Prostatakrebs*"
06/2001- 04/2008	Europa-Gymnasium Wörth Allgemeine Hochschulreife

Publikationen

10/2018	Yu, H.; **Sperlich, J**.; Mándi, A.; Kurtán, T.; Dai, H.; Teusch, N.; Liu, Z.; Proksch P. "Azaphilone Derivatives from the Fungus *Coniella fragariae* Inhibit NF-κB Activation and Reduce Tumor Cell Migration". *J. Nat. Prod*. **2018**
10/2018	Nolte J., Pöttgen L-A., **Sperlich J**., Grossert A., Kempa A., Teusch N., Schörken, U. "Glucansucrase Catalyzed Synthesis and Functional Characterization of Nordihydroguaiaretic Acid Glucosides". *Enzyme & Micr. Techn*. **2018**
08/2018	**Sperlich J.** and Teusch N. "Pseudopterosin Inhibits Proliferation and 3D Invasion in Triple Negative Breast Cancer Cells by Agonizing Glucocorticoid Receptor Alpha". *Molecules* **2018**
12/2017	Stein, J.; Stahn, S.; Neudörfl, J.-M.; **Sperlich, J.;** Schmalz, H.-G.; Teusch, N. "Synthetic Indolactam V Analogs as Inhibitors of PAR2 Induced Calcium Mobilization in Triple Negative Breast Cancer Cells". *ChemMedChem* **2017**.

07/2017	**Sperlich, J**.; Kerr, R.; Teusch, N. "The Marine Natural Product Pseudopterosin Blocks Cytokine Release of Triple-Negative Breast Cancer and Monocytic Leukemia Cells by Inhibiting NF-κB Signaling". *Mar. Drugs* **2017**

Konferenzteilnahmen und Symposien

06/2018	Dechema: 3D CellCulture 2018: "How close to '*in vivo*' can we get? Models, Applications, Translation"; Freiburg, Deutschland
09/2017	GRK2158 Symposium: Natural compounds and analogs against therapy resistant tumors and microorganisms; Düsseldorf, Deutschland; Poster: "*Pharmacological characterization of the natural products pseudopterosin and tylophorinine in the tumor microenvironment of triple negative breast cancer*"
06/2017	Cell Symposium: Cancer, Inflammation & Immunity, San Diego, U.S.; Poster: "*The natural product pseudopterosin inhibits cytokine release and bidirectional communication in the tumor microenvironment of triple negative breast cancer cells*."
12/2016	Cell Symposium: Hallmarks of Cancer, Ghent, Belgien; Poster: "*The natural product pseudopterosin inhibits bidirectional communication in the microenvironment of triple negative breast cancer*"
05/2015	Cell Symposium: Cancer, Inflammation & Immunity, Sitges, Spanien

Betreute Abschlussarbeiten

09/2018	Janina Betz, in Kooperation mit der Universität Bath, Master of Science: "*Cancer cell-fibroblast context-dependent actions of marine natural products in 2D and 3D models of human pancreatic adenocarcinoma*"
09/2018	Vanessa Mundorf, in Kooperation mit der Universität Bath, Master of Science: "*Cancer cell-fibroblast context-dependent actions of plant natural products in 2D and 3D models of human pancreatic adenocarcinoma*"
08/2017	Lars Frangenberg, Bachelor of Science: „*Pharmakologische Charakterisierung neuer Naturstoffderivate in zwei- und dreidimensionalen Tumorzellsystemen*"
08/2016	Angelika Hörst, Bachelor of Science: „*High-Throughput Screening neuer Pseudopterosin-Derivate*"
08/2016	Anne-Kathrin Wiele, Bachelor of Science: „*Aufklärung der pharmakologischen Wirkung von Pseudopterosin in der bidirektionalen Kommunikation zwischen Immun- und Tumorzellen*"
08/2015	Anastasia Nikiforov, Bachelor of Science: „*Molekulare Untersuchungen zum Tumormikromilieu metastasierender Brustkrebszellen*"
08/2015	Nicole Rüggeberg, Bachelor of Science: „*Untersuchungen zur pharmakologischen Wirkung des marinen Naturstoffs Pseudopterosin in der Immunantwort humaner Monozyten*"

Danksagung

Zum erfolgreichen Abschluss meiner Dissertation haben viele Personen beigetragen, weshalb ich im Folgenden meinen besonderen Dank ausdrücken möchte.

Zu allererst möchte ich mich bei Frau Prof. Dr. Nicole Teusch bedanken. Du hast mir die Möglichkeit gegeben, an einem spannenden Thema zu arbeiten, hast mich in meiner Ausbildung durch die Teilnahmen an Konferenzen, Seminaren und Graduiertenprogrammen unterstützt und mir bei der Anfertigung meiner Artikel maßgebend geholfen.

Herr Prof. Dr. Peter Proksch gebührt mein Dank für die Annahme als universitärer Betreuer, die Aufnahme im GRK2158 Graduiertenkolleg und die gute Zusammenarbeit in der Anfertigung eines gemeinsamen Artikels zusammen mit Haiqian Yu. Dem GRK2158 Graduiertenkolleg möchte ich danken, für die Möglichkeit mich mit Doktoranden ausführlich auszutauschen und mein Thema auf einem Symposium vorzustellen.

Ebenfalls bedanken möchte ich mich bei meinen Kooperationspartnern des Projekts „FH-Struktur“ Herr Prof. Dr. Matthias Hochgürtel, Herr Prof. Dr. Ulrich Schörken, Alexander Kempa und Johannes Nolte für die gute Zusammenarbeit. Alex, ich werde die Paperbesprechungen vermissen und deinen „hervorragenden“ Kaffee.

Ich danke dem Graduiertenprogramm „Pharmacology & Experimental Therapeutics“ der Universität zu Köln und der Bayer AG sowie dem Graduiertenzentrum der TH Köln für die interessanten Möglichkeiten zur Weiterbildung und den jährlichen Zusammentreffen.

In meiner Dissertation wurde ich tatkräftig im Labor unterstützt und möchte mich deshalb besonders bei meinen Bacheloranden/innen bedanken: Anastasia Nikiforov, Nicole Rüggeberg, Anne-Kathrin Wiele und Angelika Hörst. Ebenfalls ein großer Dank geht an Lars Frangenberg für seine Unterstützung im Projekt, dem ich gerne erneut die Wissenschaftlichkeit einer Immunfluoreszenzfärbung erkläre. Meine beiden Masterstudentinnen Janina Betz und Vanessa Mundorf gilt ein großer Dank, welche mich in England mit offenen Armen empfangen und mir den Campus sowie die Stadt liebevoll gezeigt haben.

Nun zu den Personen, die mich tagein und tagaus 3.5 Jahre lang durch dick und dünn begleitet haben: das 5.OG! Katharina, Sonja, Julia, Alessa, Johannes und Christian! Mit eurer Hilfe ging die Zeit sehr viel schneller vorbei. Viele interessante Diskussionen haben sich bei uns in der Küche zugetragen, welche ich definitiv später vermissen werde. Mit einer so tollen Truppe zusammenzuarbeiten hat unglaublich Spaß gemacht, vielen Dank für die gemeinsame Zeit!

Dem Rest der Fakultät 11 danke ich ebenfalls für die gemeinsame Zeit, vor allem Eva für die Gespräche über das Nähen oder Emily, naja du weißt schon ;)

Meine Eltern, meinen Brüdern und Schwägerinnen (Stephanie, dazu gehörst du auch) danke ich auch für das Verständnis und die Unterstützung zu jeder Zeit. Dominik, ohne dich wäre die Arbeit nicht so gut geworden. Dafür gebührt dir ein eigener Orden! Jens, du hast am meisten mit gelitten, gejubelt, hast mich aufgemuntert und mich bei allem unterstützt, bist mit mir durch dick und dünn gegangen. Ohne dich hätte ich nicht durchgehalten. DANKE!

Eidesstattliche Erklärung

Ich versichere an Eides Statt, dass die Dissertation von mir selbständig und ohne unzulässige fremde Hilfe unter Beachtung der „Grundsätze zur Sicherung guter wissenschaftlicher Praxis an der Heinrich-Heine-Universität Düsseldorf“ erstellt worden ist. Die Dissertation wurde in der vorgelegten oder in ähnlicher Form noch bei keiner anderen Fakultät eingereicht. Ich habe bisher keine erfolglosen und erfolgreichen Promotionsversuche unternommen.

Die Promotion wurde an der Technischen Hochschule Köln, Fakultät für Angewandte Naturwissenschaften in der Arbeitsgruppe „Bio-Pharmazeutische Chemie & Molekulare Pharmakologie“ unter Anleitung von Prof. Dr. Nicole Teusch durchgeführt.

Hagenbach, 07.01.2019

Julia Sperlich